# Retinoic Acid Receptor-dependent Endogenous Retinoic Acid Activity in Mouse Collecting Ducts

Wong, Yuen Fei

*Awarding institution:*
King's College London

# Retinoic Acid Receptor-dependent Endogenous Retinoic Acid Activity in Mouse Collecting Ducts

**Yuen Fei Wong**

Submitted to the King's College London in partial fulfilment of the requirements for the degree of Doctor of Philosophy

King's College London

2012

# Abstract

Retinoic acid (RA) is the main endogenous bioactive form of vitamin A that plays important role in many biological events by regulating gene expression. One of the major mechanisms via which endogenous RA regulate gene expression is through the canonical signalling, which involves binding and activation of RA receptors (RARs) by RA. It is well-acknowledged that the canonical signalling of endogenous RA is indispensable for embryonic kidney development but its role in the kidney after birth is not as well-established. It is hypothesised that the canonical signalling of endogenous RA continues to regulate gene expression in the kidney after birth. In the kidney of young and adult *RARE-hsp68-lacZ* mice, a constitutive signal of RA response element (RARE) activation was observed. The signal was largely localised to collecting duct principal cells, inner medullary collecting duct cells, and intercalated cells. In concordance with the *in vivo* observation, basal RARE activity was detected in mIMCD-3 cells, a cell line derived from mouse inner medullary collecting ducts. The RARE activity was likely a result of constitutive activation of RARs given rise by cell-autonomous synthesis of endogenous RA as the activity was suppressed by antagonists of RARs and by an inhibitor of RA synthesising enzymes. Using mIMCD-3 cells as an *in vitro* model, target genes of endogenous RA/RARs were identified using microarray at the whole genome level, and the results were validated with reverse transcription quantitative polymerase chain reaction. Gene ontology analysis on the validated genes suggests their involvement in vitamin A metabolism, as well as in some classical and novel functions of collecting ducts including kidney development.

# Declaration

I hereby declare that this thesis has been composed by myself and that it describes my own work. This thesis has not been submitted, to this or any other university, for a degree, but part of the work has been submitted for journal publication and as abstracts to nephrology conferences. A small portion of the initial preliminary work was performed by my collaborators, which was clearly indicated in the thesis.

Publications arise from this project:

- **Y. F.Wong**, P. D. Wilson, R. J. Unwin, J. T. Norman, M. Arno, B. M. Hendry, and Q. Xu. Retinoic acid receptor-dependent, cell-autonomous, endogenous retinoic acid signaling and its target genes in mouse collecting duct cells. *PLoS One*, 7(9):e457252012, September 2012.

- **Y. F. Wong**, J. B. Kopp, C. Roberts, P. J. Scambler, Y. Abe, A. C. Rankin, N. Dutt, B. M. Hendry, and Q. Xu. Endogenous retinoic acid activity in principal cells and intercalated cells of mouse collecting duct system. *PLoS One*, 6(2):e16770, Feb 2011.

Abstract submitted to conferences:

- Q. Xu, **Y. F. Wong**, P. D. Wilson, R. J. Unwin, J. T. Norman, B. M. Hendry. Target Genes of Endogenous Retinoic Acid and Retinoic Acid Receptors in Collecting Duct Cells: A Pan-Genomic View. American Society of Nephrology Annual Meeting. Nov 2011. Abstract presented as a poster.

- **Y. F. Wong**, J. B. Kopp, B. M. Hendry, Q. Xu. Endogenous Retinoic Acid Activity in the Principal Cells and Intercalated Cells of Mouse Collecting Duct System. American Society of Nephrology Annual Meeting. Nov 2010. Abstract presented as a poster.

- **Y. F. Wong**, J. B. Kopp, C. Roberts, M. Maden, P. J. Scambler, Y. Abe, A. C. Rankin, N. Dutt, M. Noor, B. M. Hendry, Q. Xu. Retinoic Acid Activity in the Collecting Duct System of Post-natal Mouse Kidney. British Renal Society/Renal Association Annual Conference. May 2010. Abstract presented as a poster.

- **Y. F. Wong**, J. B. Kopp, C. Roberts, M. Maden, P. J. Scambler, A. C. Rankin, N. Dutt, M. Noor, B. M. Hendry, Q. Xu. Physiological Retinoic Acid Activity in the Collecting Duct System of Post-natal Mouse Kidney. American Society of Nephrology Annual Meeting. Oct 2009. Abstract presented as a short communication.

- **Y. F. Wong**, J. B. Kopp, C. Roberts, M. Maden, P. J. Scambler, A. C. Rankin, N. Dutt, J. H. Wang, B. M. Hendry, Q. Xu. Endogenous Retinoids in Post-natal Mouse Kidneys. World Congress of Nephrology. May 2009. Abstract presented as a poster.

Other publications:

- Q. Xu, **Y. F. Wong**, S. Qu, Q. Kong, X. L. Zhang, X. M. Liang, Q. Hu, M. Noor, B. M. Hendry. Knowledge-based Discovery of Anti-fibrotic and pro-fibrotic activities from Chinese materia medica. *Recent Advances in Theories and Practice of Chinese Medicine*, Ed. by H. Kuang, ISBN: 978-953-307-903-5, *InTech*, 2012.

- Q. Xu, B. M. Hendry, M. Maden, H. Lu, **Y. F. Wong**, A. C. Rankin, M. Noor, J.B. Kopp. Kidneys of Alb/TGF-beta1 Transgenic Mice are Deficient in Retinoic Acid and Exogenous Retinoic Acid Shows Dose-dependent Toxicity. *Nephron Exp Nephrol*, 114(4):e127-32, 2010.

- Q. Hu, M. Noor, **Y. F. Wong**, P. J. Hylands, M.S. Simmonds, Q. Xu, D. Jiang, B. M. Hendry, Q. Xu. In vitro anti-fibrotic activities of herbal compounds and herbs. *Nephrol Dial Transplant*, 24(10):3033-41, 2009.

- **Y. F. Wong**, Q. Xu. Ablation of klotho and premature aging: is 1,25-dihydroxy-vitamin D the key middleman? *Kidney Int*, 75(11):1137-9, 2009.

# Acknowledgements

I would like to thank my supervisor Dr. Qihe Xu, an absolutely bright and ingenious man from whom I have learnt good science. I owe my deepest gratitude to Dr. Xu for his perpetual patience and guidance. I am also deeply grateful to my co-supervisor, Prof. Bruce M. Hendry, for his most invaluable advice throughout my PhD.

My warm appreciation goes to all present and past members of the Renal Group for their friendship and support, in particular Dr. A Rankin, Dr. A Cove-Smith, Dr. A Irtiza-Ali, Dr. C Sharpe, Dr. J Wang, Dr. N Hutchinson, Dr. Q Hu, and Mr. M Noor. I wish also to thank many other scientists in the Rayne Institute, for their willingness to share their knowledge and expertise with me. I also would like to convey my special thanks to our collaborators, Dr. JB Kopp, Dr. C Roberts, Dr. P Scambler, Dr. N Dutt, and Dr. M Arno for their continuous support, and not to forget Dr. SY Tham and Mr. KT Wong, without whose support I will not embark on this PhD study in the first place.

I am indebted to my parents for their unconditional and unreserved love. A big thank you to my very smart husband, who has been showering me with the most tender loving care and support (some of which are highly technical such as using Adobe Photoshop to compile the microscopic photos and LaTex to produce this very neat thesis). I am also heartily thankful to Dr. S Schnell for her ungrudging help in proofreading my thesis.

Last but not least, I would like to express my gratitude to King's College London Division of Gene and Cell Based Therapy, Department of Renal Medicine, and Graduate School, as well as Innovation China UK, Kidney Research UK, and European Union's Framework Programme, for the financial support.

# Contents

# List of Figures

# List of Tables

# List of Abbreviations

| | |
|---|---|
| Adh | Alcohol dehydrogenase |
| AF-1 | Activation function 1 |
| AF-2 | Activation function 2 |
| AGCC | Affymetrix GeneChip Command Console |
| Aldh1 | Class I I cytosolic aldehyde dehydrogenases |
| AP-1 | Activator protein 1 |
| APE 1 | Apurinic/apyrimidinic endonuclease 1 |
| AQP2 | Aquaporin 2 |
| Arat | Acyl-coA acyltransferase |
| $\beta$-gal | $\beta$-galactosidase |
| $\beta$-ME | $\beta$-mercaptoethanol |
| BSA | Bovine serum albumin |
| CARM1 | Coactivator-associated arginine methyltransferase 1 |
| CD28K | Calbindin D28K |
| 9cRA | 9-*cis* retinoic acid |
| 13cRA | 13-*cis* retinoic acid |
| 11cRal | 11-*cis* retinaldehyde |
| 11cRol | 11-*cis* retinol |
| CMV I.E | Cytomegalovirus immediate-early |
| Crabp | Cellular retinoic acid binding protein |
| Cralbp | Cellular retinaldehyde binding protein |
| Crbp | Cellular retinol binding protein |

| | |
|---|---|
| $C_T$ | Threshold cycle |
| Cyp450 | Cytochrome P450 |
| DAPI | 4,6-diamidino-2-phenylindole |
| DAVID | Database for Annotation, Visualization and Integrated Discovery |
| DBD | DNA binding domain |
| DEAB | 4-(diethylamino)benzaldehyde |
| DMSO | Dimethly sulfoxide |
| DR | Direct repeat |
| E | Embryonic day |
| E-cad | E-cadherin |
| ECM | Extra-cellular matrix |
| EDTA | Ethylenediaminetetraacetic acid |
| EGFR | Epithelial growth factor receptor |
| Fabp5 | Fatty acid binding protein 5 |
| FAM | Fluorescein amidite |
| FBS | Foetal bovine serum |
| GAG | Glycosaminoglycans |
| GDNF | Glial cell line-derived neurotrophic factor |
| GEO | Gene Expression Omnibus |
| GFP | Green fluorescent protein |
| GUDMAP | GenitoUrinary Development Molecular Anatomy Project |
| HO-1 | Hemeoxygenase-1 |
| IMCD | Inner medullary collecting duct |
| Irbp | Interphotoreceptor retinoid binding protein |
| IVT | *In vitro* transcription |
| $K_d$ | Dissociation constant |

| | |
|---|---|
| LBD | Ligand binding domain |
| LRAT | Lecithin:retinol acyltransferase |
| MDR | Medium chain dehydrogenase |
| MES | 2-(N-Morpholino)ethanesulfonic acid hydrate |
| MGB | Minor groove binder |
| N-coA1 | Nuclear receptor co-activator 1 |
| Nco-R | Nuclear receptor co-repressor |
| NFR | Non-fluorescing quencher |
| NTC | Non-template control |
| NURSA | Nuclear Receptor Signaling Atlas |
| OCT | Optimum Cutting Temperature |
| P | Passage |
| PAS | Periodic acid-Schiff |
| PBS | Phosphate-buffered saline |
| pCMV | Cytomegalovirus promoter |
| PPAR | Peroxisome proliferator-activated receptor |
| QOE | Qlucore Omics Explorer |
| RA | Retinoic acid |
| Ral | Retinaldehyde |
| Raldh | Retinaldehyde dehydrogenase |
| RAR | Retinoic acid receptor |
| RARE | Retinoic acid response element |
| Rbp | Retinol binding protein |
| Rdh | Retinol dehydrogenase |
| RLB | Reporter Lysis Buffer |
| RLU | Relative Light Unit |

| | |
|---|---|
| RMA | Robust Multichip Average |
| Rol | Retinol |
| ROR | Retinoid orphan receptor |
| RT-qPCR | Reverse transcription-quantitative polymerase chain reaction |
| RXR | Retinoic acid X receptor / rexinoid receptor |
| SAPE | Streptavidin Phycoerythrin |
| SDR | Short chain dehydrogenase |
| SMCC | Srb and Mediator protein containing complex |
| SMRT | Silencing mediator for retinoid and thyroid hormone receptors |
| SRC1 | Nuclear receptor co-activator 1 |
| Stra6 | Stimulated by retinoic acid 6 |
| SV40 | Simian virus 40 |
| SWI/SNF | Switch/sucrose non-fermenting |
| T3R | Thyroid hormone receptor |
| TdT | Deoxynucleotidyl transferase |
| TE | Tris-EDTA |
| TG | Transgenic |
| THP | Tamm-Horsfall protein |
| tRA | all-*trans* retinoic acid |
| tRal | all-*trans* retinal |
| tRol | all-*trans* retinol |
| UDG | Uracil DNA glycosylase |
| UNG | Uracil-N-glycosylase |
| VAD | Vitamin A deficient |
| V-ATPase | $H^+$-ATPase B1 |
| WT | Wild-type |

# Chapter 1

# Introduction

---

This chapter comprises three main sections. The first section is composed of a brief overview of the retinoid system, which includes the transport and metabolism of retinoids and gene expression regulation by retinoids. Data on gene knockout mice, where available, is presented to illustrate functions of genes involved in regulation of the retinoid system. Other molecules reported to be involved in crosstalk with the retinoid system signalling cascade will also be introduced. The second section covers current knowledge on the retinoid system with relevance to the kidney. Finally, the aims of this project are set out in the third section.

## 1.1 An overview of the retinoid system

Back in 1920s-1940s, knowledge on the importance of retinoids was largely derived from the symptoms observed in vitamin A deficient (VAD) patients and animals, such as xerophthalmia and night blindness [25, 26, 86], keratinisation of tissue epithelium, with and without accompanying inflammation [106, 325], infections in multiple organs [113], as well as developmental defects [323]. Therefore, vitamin A was often referred as "anti-xerophthalmic", "growth-promoting", and "anti-infective" back then [25, 113]. Notably, the regularity of developmental defects involving multiple organs had led to the introduc-

tion of the term "VAD syndromes", which can be largely prevented by maternal vitamin A supplementation [322]. Nevertheless, excessive administration of vitamin A to pregnant rats caused teratogenic effects to developing embryos, resulting in a plethora of developmental anomalies [48]. It is now clear that vitamin A is one of the many components within the retinoid system. Symptoms of vitamin A deficiency and teratogenicity are in fact due to suboptimal and over-active retinoid signalling activities, respectively.

The retinoid system comprises multiple components that govern retinoid metabolism, transport, and their activities, all of which are highly evolutionarily conserved, and act collaboratively as a coherent system to support many basic biological events [302]. In this section, the retinoid system will be introduced from five major aspects: (i) endogenous retinoids, (ii) transport of retinoids, (iii) metabolism of retinoids, (iv) regulation of gene expression by retinoids through the canonical signalling and the non-canonical signalling pathways, and (v) target genes of retinoids.

### 1.1.1 Endogenous retinoids

Early work dedicated to investigation of nutritional theories in the late $19^{th}$ and early $20^{th}$ century had led to discovery of vitamin A, the first retinoid compound described, known then as fat-soluble vital amines essential for growth [281]. Since the discovery of vitamin A, more analogs of vitamin A were discovered and subsequently synthesised.

According to the International Union of Pure and Applied Chemistry - International Union of Biochemistry (IUPAC-IUB), the term "retinoids" is defined as "*compounds consisting of four isoprenoid units joined in a head-to-tail manner; all retinoids may be formally derived from a monocyclic parent compound containing five carbon-carbon double bonds and a functional terminal group at the terminus of the acyclic portion*". The skeletal formula of retinoids is shown in Figure 1.1 [127].

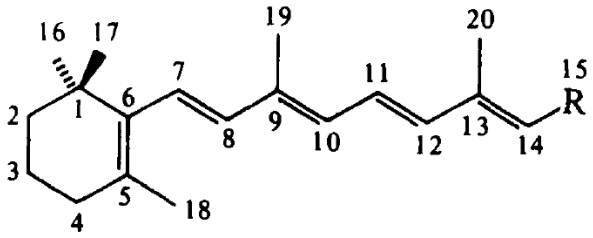


Figure 1.1: Skeletal formula of retinoids. Four isoprenoid units made up a single retinoid molecule of 20 carbons, as numbered. Figure shown here is in an all-*trans* configuration. *R* represents the functional group of retinoids, which largely determines the activity of an individual retinoid compound. Examples of common retinoid compounds are: retinol (*R*=OH), retinaldehyde (*R*=CHO) and retinoic acid (*R*=COOH) (Figure adapted from IUPAC-IUB [127]).

This thesis is focusing on naturally occurring retinoids with biological activity, i.e., vitamin A, also known as retinol (Rol), which is the parental retinoid compound, and its oxidative derivatives, retinaldehyde (Ral) and retinoic acid (RA). As one could appreciate from the skeletal formula depicting a non-polar aromatic ring and an aliphatic chain, containing only 20 carbons in total (Figure 1.1), retinoids are small lipophilic compounds, with their water solubility decreasing in the order of RA>Ral>Rol [27].

Without a natural mechanism in place for *de novo* retinoid biosynthesis, mammalian cells obtain endogenous retinoids from food primarily in the form of carotenoids, which is the retinoid precursor found in plants and egg yolks, and retinyl ester (such as retinyl stearate and retinyl palmitate), which is the storage form of retinoids in animals [302]. The processes by which dietary retinoids are absorbed then subsequently released into circulation and other tissues are highly complex events involving multiple catabolising enzymes and binding proteins of retinoids [52]. These processes are briefly summarised below:

1. Dietary carotenoids are absorbed from the intestine into enterocytes then be converted into Ral and subsequently into Rol; dietary retinyl ester is hydrolised to Rol in the intestine for absorption.

2. Newly absorbed Rol in enterocytes is esterified, predominantly by lecithin:retinol

acyltransferase (Lrat) and to a lesser extent by intestinal acyl-coA acyltransferase (Arat), into retinyl ester.

3. The newly synthesised retinyl ester is packaged into nascent chylomicron along with other dietary lipid, which is then secreted into the lymphatic system and then into the bloodstream.

4. In the circulation, chylomicron are reduced into chylomicron remnant; retinyl ester in chylomicron and chylomicron remnant are taken up by hepatocytes in liver (around 75%) and other tissues (around 25%) for storage.

5. In hepatocytes, retinyl ester is rapidly hydrolysed into Rol, which is then transferred to hepatic stellate cells where it is re-esterified, predominantly by Lrat, for storage in lipid droplets.

6. When required, retinyl ester in hepatic stellate cells will be hydrolysed into Rol and be transferred back to hepatocytes, where it will be bound by the retinol binding protein (Rbp) before being released into the bloodstream.

7. In the bloodstream, Rol-Rbp is bound by transthyretin to facilitate its transport to extra-hepatic tissues.

8. Rol taken up by the extra-hepatic tissues is then converted to Ral and RA for execution of biological function, or back to retinyl ester for storage.

The role of retinoids in maintaining a healthy visual system was one of the most actively researched areas back in 1950s. It was found that vision impairment associated with vitamin A deficiency is not a direct consequence of Rol *per se* but rather due to insufficiency of its oxidative derivative, Ral, which is required for the synthesis of rhodopsin, the retina pigment responsible for phototransduction [314]. It is now well-established that an intact retinoid cycle, constituting enzymatic inter-conversation of 11-*cis* retinaldehyde (11cRal), all-*trans* retinaldehyde (tRal), all-*trans* retinol (tRol), and 11-*cis* retinol (11cRol), is crucial for normal operation of the visual system [241].

***RA: the primary bioactive endogenous retinoids***

In 1960, researchers found that almost all symptoms of vitamin A deficiency were reversed by replenishing VAD rats with RA, except for vision impairment [64]. Since then, the role of RA has been extensively studied and it is now recognised as the primary bioactive endogenous retinoid that mediates many important biological events, such as embryonic development [67, 231], regulation of immune system [249], and cancer development [298].

All-*trans* RA (tRA) is the most widely studied isomer of RA, which is derived from tRol, the most abundant Rol isomer *in vivo* [302]. Other isomers of endogenous RA also exist and among them, 13-*cis* RA (13cRA) and 9-*cis* RA (9cRA) are the most commonly studied. The presence of various RA isomers might be a result of active isomerisation process among the RA isomers [173, 202, 343] or might be a direct oxidative conversion from the parental Rol in 13-*cis* and 9-*cis* configurations. By using a liquid chromatography tandem mass spectrometric assay with improved sensitivity, Kane et al. found tRA to be the most abundant RA isomer (in the range of 1.5 ± 0.2 to 38.1 ± 3.4 pmol/g tissue) in a wide range of mouse tissues, including adipose, brain, kidneys, liver, muscle, spleen, and testis, as well as in serum, while 9cRA was not detected [139]. Interestingly, the same group had recently reported that 9cRA was present specifically in mouse pancreas, at a level higher than tRA [138].

A few early studies had attempted to examine the potency and activities of different RA isomers, whereby the RA isomers were added to *in vitro* cell culture or administered to animals. For example, in VAD rats, 13cRA was reported to be as effective and as potent as tRA in supporting growth [343]; 13cRA and 9cRA were reported to be almost as effective as tRA in promoting HL-60 human promyelocytic leukemia cell differentiation *in vitro* [197]; topical 9cRA was found to be more potent than tRA in inducing pattern duplications in chick wing bud [301]. However, interpretation of these results are not as straight forward, because isomerisation or inactivation of the RA isomers could have

taken place during the course of preparing the reagents and upon entering the cells.

Other derivatives of RA, some of which more polar than RA, had also been isolated and examined. For example, 4-hydroxy-RA and 4-oxo-RA were reported to be bioactive albeit far less potent than RA [88]; 5,6-monoepoxy-RA was found to promote growth in VAD rats [133]. In terms of their roles in development, Thaller et al. reported the isolation of 3,4-didehydro-RA, which was found to be as potent as tRA in promoting digit duplication in chick wing bud [300], while Niederreither et al. provided genetic evidence that the oxidative metabolites of RA are not involved in mediating embryonic development in mice [230].

While the importance of other bioactive retinoid compounds cannot be ignored, RA, particularly tRA, is the most abundant isomer of endogenous RA *in vivo* and is by far the most studied retinoid compound in a multitude of experimental models. Thus, it is generally believed that tRA is the predominant and the most physiologically relevant retinoid compound in mediating most of the biological processes, except in vision.

### 1.1.2 Transport of retinoids

Given their high lipophilicity, retinoids are bound to specific binding proteins to facilitate their transport in the circulation and within the cells. In the circulation, tRol is the predominant form of retinoid compound and it is bound by Rbp; inside the cells, cellular retinol binding proteins 1, 2, and 3 (Crbp1, Crbp2, and Crbp3) bind both tRol and tRal with varied affinity, while cellular retinoic acid binding proteins 1 and 2 (Crabp1 and Crabp2) as well as fatty acid binding protein 5 (Fabp5) bind tRA, again with varied affinity [52, 280]. The focus of this section is to introduce the aforementioned binding proteins and their functions in mediating activity of RA. The cellular retinaldehyde binding protein (Cralbp) and the interphotoreceptor retinoid binding protein (Irbp), which are expressed exclusively in retina and in neural tissues [52], will not be covered here.

***Rbp and stimulated by retinoic acid (Stra6)***

Rbp is a member of the lipocalin superfamily that binds to circulating Rol [228]. Although Rbp is the only known protein that binds to and facilitate transport of circulating Rol, classical symptoms of vitamin A deficiency were not observed when Rbp gene was defected or absent. Patients with mutation of Rbp gene had very low level of circulating Rol, but were physiologically normal other than suffering from vision impairment [23]. Similarly, mice with genetic ablation of Rbp had low serum Rol level, but remained viable, fertile, and otherwise healthy; impaired retinal function was found, consistent with a lower Rol level in the eye, which were rescued with vitamin A supplementation [253]. The retinal function impairment was later found to be associated with a defect in Rol uptake into the eye rather than to low maternal retinoid supply from lactation [313].

Despite a lower basal level of circulating Rol, Rol level in the liver, kidney, spleen, and reproductive organs of 13-week-old Rbp null mutants was similar to that of the wild-type mice; hepatic retinyl ester store in Rbp null mutants was higher compared to that of wild-type mice [253]. When fed a VAD diet for one week, the Rbp null mutants suffered a rapid decline of serum Rol but hepatic Rol level remained the same, whereas hepatic Rol level in wild-type mice was reduced in compensation for reduced serum Rol [253]. Severe embryonic malformation resembling the VAD syndromes was observed only when pregnant Rbp null mutants mothers were fed a VAD diet over a prolonged period [254]. Based on these observation, the authors suggested that post-prandial and maternal supply of retinoids, i.e., retinyl ester-containing chylomicrons and cyhlomicron remnants, play a dominant role in contributing towards endogenous retinoid pool in the absence of Rbp, and that Rbp has specific function(s) in mobilisation of hepatic Rol into the circulation [253, 254].

Interestingly, circulating RA level was found to be comparable between Rbp null mutants and wild-type mice [253], and between individuals with mutated Rbp and their normal family member [23]. In another report, it was found that both hepatic and extra-hepatic

tissues can directly absorb the low circulating level of tRA, in the form of albumin-bound tRA derived from diet [157]. Thus, when Rbp was defected or absent, the intra- and extra-cellular RA equilibrium could still be somehow achieved, which might explain the lack of overt VAD syndromes.

In 2007, Kawaguchi et al. showed that Stra6 serves as a receptor of Rbp that mediates uptake of Rbp-bound Rol, which was further enhanced in the presence of intra-cellular Lrat, and proposed that the Rbp-Stra6 system constitutes an important physiological mechanism of Rol uptake in many tissues [146]. In the same year, Pasutto et al. reported that mutations of Stra6 gene in human resulted in a broad spectrum of malformations, some of which overlapped with the developmental defects observed in congenital VAD animals [244]. The severe outcomes observed in human with Stra6 gene mutation and the relatively mild defects involving only the vision system in human with Rbp mutation leads to speculation that Stra6 may have additional yet identified functions [24].

Recent reports had provided evidence of Stra6 facilitating not only Rol uptake into the cells but also export of cellular Rol [129]. In addition, Stra6 was also reported to activate transcription factors to regulate gene expression thereby inhibiting insulin responses upon associating with Rbp-bound Rol [22]. A zebrafish genetic model of Stra6 knock-down had shed light on the role of Stra6 in clearing circulating Rbp-bound Rol to prevent off-target delivery of Rol [129]. Establishment of mouse null models of Stra6 gene in the future should better define the roles of Stra6 in homeostasis of endogenous retinoids and its relationship with Rbp-bound Rol.

***Crbps***

The role of Rbp as a carrier for Rol ends when Rol enters the cell. In 1973, Bashor et al. reported the presence of a cellular protein component derived from rat lungs, liver, kidneys, testis, and intestinal mucosa, which binds Rol with high affinity, but has distinct property compared to Rbp [15], known as Crbp1. A second type of Crbp, Crbp2, was

found to be expressed predominantly in neonatal rat intestine and liver, and almost exclusively in adult rat intestine [50,237]. Both Crbp1 and Crbp2 bind Rol (tRol, 13cRol, and 9cRol) and Ral (tRal and 9cRal) but not RA [136]. An additional type of murine Crbp, Crbp3, which binds only tRol was recently reported, with high expression restricted to heart, muscle, adipose tissue, and mammary gland [312]. It is worth noting that the murine Crbp3 is not homologous to the human Crbp3 discovered in the same year [84].

Intra-cellular Rol binds with high affinity to Crbps. For instance, the dissociation constant ($K_d$) between Crbp1 and Rol is around 0.1 to 10 nM, hence it is believed that there will be little, if any, unbound Rol in the cells [223, 236]. It was proposed that holo-Crbp (Crbp bound to retinoids) have many roles other than to circumvent the low aqueous solubility of retinoids in the cells, such as sequestering retinoids from cell membrane to protect cell from membranolytic activity of retinoids, protecting retinoids from destructive enzymatic and non-enzymatic reactions, and limiting access of specific enzymes to bound-retinoids [223, 224, 236].

Crbp1 null mutants developed normally despite a lower embryonic and foetal Rol and retinyl ester store [97, 199]. A slight decrease in embryonic RA level was also noted. However, when mated with *RARβ2-lacZ* and *RARE-hsp68-lacZ* mice, which are reporter of endogenous RA activity, there was no decrease in reporter activity compared to the wild-type mice [199]. This suggests minimum impact of Crbp1 deletion on endogenous RA activity, which might explain the lack of developmental impairment. After birth, Crbp1 null mutants were healthy and had a normal intestinal retinoid uptake and esterification, but hepatic retinyl palmitate had a higher turnover rate leading to a decrease in retinoid storage in liver [97]. A lower level of Ral was also found in kidneys and lungs of adult mutant mice but no abnormalities were reported [97]. When fed a VAD diet, Crbp1 null mutants exhausted their hepatic retinyl palmitate storage six times faster than the wild-type mice and accordingly, exhibited many classical symptoms of vitamin A deficiency earlier than the wild-type mice [97].

Crbp2 null mutants also developed normally despite lower intestinal Rol uptake and lower hepatic Rol storage; when pregnant Crbp2 null mutants were fed a diet containing only marginal vitamin A, a higher neonatal lethality associated with lung and heart defects was found, which was attributed to lower maternal Rol delivery to embryos as a consequence of lower maternal hepatic Rol storage following lower intestinal uptake [71].

Crbp3 null mutants had lower retinyl ester store in the milk of lactating mother compared to that in wild-type mice [248]. When fed a high-fat diet for 20 weeks, Crbp3 null mutants had similar level of Rol and retinyl ester in the white adipose tissues and liver as that of wild-type mice, but were more resistant towards the fat accumulation in the liver [344]. The phenomenon was attributed to lower food intake and decrease in glycerol and free fatty acid efflux from adipose tissue [344].

The expression sites of Crbps and their respective knockout phenotypes suggested that Crbp1 mainly participates in regulating retinoid storage mechanism in a wide variety of tissues; Crbp2 acts as binding protein of Rol in the intestine to facilitate its intestinal absorption. On the other hand, the physiological ligand of Crbp3 remained questionable although it binds to tRol *in vitro* [52], and hence its role in retinoid transport and metabolism requires further investigations. It is noteworthy that none of the Crbp knockout mice displayed symptoms of vitamin A deficiency when fed a normal diet. Although in all the aforementioned Crbp knockout models, an up- or down-regulation of the other Crbp isoforms were observed at certain stages [71, 97, 199, 248, 344], functional redundancy among them is difficult to be justified in view of their non-direct overlapping of expression sites.

***Crabps and Fabp5***

An intra-cellular binding protein that binds specifically to RA with high affinity but not to Rol was described in the mid 1970s, first in chick embryos [275] then in rats [238], which was later named as Crabp1. The discovery of a second Crabp isoform, called Crabp2, were subsequently reported in rats [10] and in mice [99]. More recently, it was proposed that Fabp5 also serves as an intra-cellular binding protein for RA [280]. While the expression pattern of Fabp5 had not been systematically studied, expression of Crabp2 transcript was observed in a wide range of tissues, whereas expression of Crabp1 transcript was more restricted in developing mouse embryos [270].

*In vitro*, Crabp1 binds to RA with higher affinity ($K_d$ of 0.06 nM) compared to Crabp2 ($K_d$ of 0.13 nM) [63], while Fabp5 binds to RA with a $K_d$ of approximately 35 nM [280]. It was proposed that Crabps not only facilitate RA transport in the cells but shuttle RA specifically into cell nucleus [296]. The proposal was supported by the observations of Crabp1 and Crabp2 protein in nuclei of embryos and various cell types [93, 116], suggesting an active involvement of these proteins in mediating RA signalling.

Judging from the expression sites of Crabp1 transcript, which correlates well with structures susceptible towards excessive retinoid induced-teratogenicity, it was speculated that Crabp1 acts predominantly to sequester RA in order to protect these sensitive structures from being exposed to excessive RA [270]. Contrary to the speculation, Crabp1 knockout mice were indistinguishable from their wild-type counterparts during development and after birth, and when pregnant mothers were fed a low teratogenic dose of RA, both mutant and wild-type mice suffered axial skeletal malformation to a similar extent [109]. Crabp2 and Crabp1/Crabp2 double knockout mice also appeared normal, but exhibited limb outgrowth, which was not fully penetrant [77,160]. Just as null mutants of Crabps, no apparent abnormalities were noted following genetic ablation of Fabp5 [188].

While genetic null mutants did not suggest crucial involvements of Crabps and Fabp5 in

mediating RA activity, *in vitro* experiments had provided invaluable molecular insights into the roles of Crabps and Fabp5 in this regard. Boylan and Gudas showed that sense Crabp1 F9 teratocarcinoma stem cell transfectants, characterised by a higher level of functional Crabp1 protein, had a shorter intra-cellular half-life of RA and a higher rate of 4-oxo-RA production compared to wild-type cells; anti-sense Crabp1 F9 transfectants, which had reduced level of functional Crabp1, exhibited an opposite result [32]. As opposed to Crabp1, which was shown to not actively participate in mediating RA signalling [59, 308], an increase in tRA-induced reporter activity and target gene expression was found in cells expressing endogenous and transfected Crabp2, in the presence of retinoid nuclear receptors [59, 63]. Consistent with this result, a direct protein-protein interaction was observed between retinoid nuclear receptors and Crabp2 in cell nuclei [59]. Acting rather similarly as Crabp2, Fabp5 binds to RA and directs RA into cell nuclei to bind and activate peroxisome proliferator-activated receptor (PPAR) [280]. The roles of retinoid nuclear receptors and PPAR in transducing RA signalling will be presented in Sections 1.1.4 and 1.1.5.

All in all, the absence of overt defects during development and adult life in null mutants of Crabps and Fabp5, as well as the lack of evidence suggesting them to be more susceptible towards RA-induced teratogenicity, argue against their postulated functions in mediating RA signalling especially at the physiological level, except in the limbs. However, *in vitro* evidence strongly suggests their involvement in shuttling RA towards distinct molecular pathways. Until additional carrier proteins are identified or further evidence defying these postulations, it is generally accepted that Crabp1 shuttles intracellular RA to the metabolism pathways, whereas Crabp2 and Fabp5 transfer RA into cell nuclei towards the signalling pathways.

### 1.1.3 Metabolism of retinoids

Catalysed by specific enzymes, retinoids go through a series of oxidation and reduction within the cells, including a reversible inter-conversion between Rol and Ral, and an irreversible conversion of Ral into RA. Multiple isoforms of the aforementioned enzymes

had been discovered in human, rats, and mice, each of which has species-specific ontologies. In order to avoid confusion, this section is mainly focusing on enzymes derived from mice and their respective knockout phenotypes, if available.

***Inter-conversion between Rol and Ral***

The reversible conversion between Rol and Ral is mainly catalysed by enzymes of two families: (i) cytosolic alcohol dehydrogenase (Adh), a member of the medium-chain dehydrogenase/reductase superfamily, and (ii) microsomal retinol dehydrogenase (Rdh), a member of the short-chain dehydrogenase/reductase superfamily [156, 242]. Involvement of AKR1B10, a human enzyme of the aldo-keto reductase family, had also been described to catalyse the conversion of Ral back to Rol [92] but its mouse ortholog was not identified as yet [271].

Retinoids had long been identified as substrates for Adh [261]. It is now known that there are six classes of Adh (class I-VI) in mouse, of which Adh class I, III, and IV, herein referred as Adh1, Adh3, and Adh4, respectively, were reported to possess specific but somewhat overlapping functions in retinoid metabolism [119, 242]. Similarly, multiple Rdhs are known to be involved in retinoid metabolism, some of which have higher activities towards androgen than towards retinoids such as mouse Rdh7, Rdh9, and Rdh16 [242]. In mice, Rdh1 [335, 336] and Rdh10 [274] were reported to play a significant role in biosynthesis of tRA. Some of these enzymes have additional catalytic functions, e.g., Adh1 and Adh3 act as scavengers for ethanol and S-hydroxymethylglutathione, respectively [119,242], while Rdh1 has strong $3\alpha$-hydroxy and weak $17\beta$-hydroxy steroid dehydrogenase activities [335].

Adh1, Adh3, and Adh4 act mainly as oxidases (also called dehydrogenases) that convert tRol into tRal [242]; *in vitro*, mouse Adh1 and Adh4 are about 1,000x and 4,000x more active than Adh3, respectively, in generating tRal from tRol [215]. Mouse Rdh1 was found to have a preferential activity towards tRol over *cis* form of Rol [335] while

human RDH10 was found to function more efficiently as Rol dehydrogenase to produce Ral rather than acting as Ral reductase [20].

A great number of kinetic studies had been performed to determine whether Adhs or Rdhs are the predominant Rol dehydrogenases involved in biosynthesis of RA, but a general consensus has not been achieved until today due to the use of different parameters and methodologies. Specifically, while both Adhs and Rdhs follow Michaelis-Menten kinetics, enzymatic assays of Rdhs took into account the involvement of Crbp1 as binding protein of intra-cellular Rol, i.e., Crbp1-bound Rol rather than crude Rol as substrate [224, 242]. In addition, different indexes were used to describe the enzyme kinetics, i.e., $k_{cat}$, $K_m$, and $V_{max}$. Depending on the assays performed, certain indexes were deemed more apt than others in describing the enzyme activity hence precluding a direct comparison between the cytosolic Adhs and the microsomal Rdhs. It is also important to note that some of these enzymes are not fully orthologous among rat, mouse, and human [335] and hence kinetic data derived from enzymes from one species may not be applicable to another.

Genetic deletions of these enzymes were performed to further elucidate their physiological functions. Null mutants for Adh1, Adh3, Adh4, and Adh1/Adh4 were generated and were subjected to different amount of dietary vitamin A or challenged with high dose of Rol to assess rate of RA biosynthesis [57, 58, 214]. The major findings of these studies, including the phenotypes of these null mutants are summarised in Table 1.1. Based on the genetic studies, it was concluded that Adh1 likely functions to eliminate excessive Rol to prevent vitamin A toxicity, whereas Adh4 is essential for survival during vitamin A deficiency perhaps by maintaining RA supply; the functions of Adh3 overlap those of Adh1 and Adh4 [156]. It is important to note that the basal retinoid profile, especially level of RA, had not been described in the null mutants of Adhs. Therefore, the roles of Adhs in retinoid metabolism under basal condition remains to be established.

Table 1.1: Null mutants of Adh genes with associated phenotypes and retinoid homeostasis compared to sex- and age-matched wild-type animals. "Normal" indicates no difference from wild-type animals; VAD: Vitamin A deficiency.

| **Null mutants** | **Phenotype** | **Gestational VAD** | **Dietary Rol supplementation** | **RA level following high dose Rol administration** |
|---|---|---|---|---|
| Adh1$^{-/-}$ | Normal [214] | Normal [214] | Post-natal lethality [214] | Serum & liver: low [214]; kidney: low [58] |
| Adh3$^{-/-}$ | Higher post-natal lethality; growth deficiency [215] | 100% lethality at p35 [215] | Growth deficiency rescued [215] | Serum: low [215]; kidney: normal [58] |
| Adh4$^{-/-}$ | Normal [214] | 100% lethality at p15 [214]; higher stillborn rate [57] | Normal [214] | Serum & liver: normal [214]; kidney: low [57, 58] |
| Adh1$^{-/-}$/Adh4$^{-/-}$ | Normal [214] | 100% lethality at p24 [214] | Normal [214] | Serum & liver: low [214] |

Rdh1$^{-/-}$ mutants were found to develop normally and were fertile under basal condition but had a different basal retinoid profile compared to their wild-type counterparts [336]. When fed a diet with recommended amount of vitamin A (4 IU/g), a higher level of tRol was detected in mutant liver; when dietary vitamin A was reduced to 0.6 IU/g, higher level of tRol and retinyl ester were detected in liver and higher tRol was also detected in kidney (Table 1.2). In addition, expression of hepatic Cyp26a1, a gene involved in metabolism of tRA into polar metabolites, was lower in Rdh1$^{-/-}$ mutants compared to wild-type mice except when fed a diet with copious amount of vitamin A ($>$ 30 IU/g). The authors postulated the presence of an auto-compensation mechanism to spare tRA by down-regulation of Cyp26a1 in the absence of Rdh1 gene, and concluded that Rdh1 is involved in retinoid homeostasis under physiological condition [336]. Unexpectedly, when fed a VAD diet or diet containing minimum vitamin A (0.1 IU/g) for 33 weeks, Rdh1$^{-/-}$ displayed an increase in length, weight, and adiposity compared to wild-type mice, for which the mechanisms remain unresolved [224, 336].

Table 1.2: Endogenous retinoid profile in Rdh1$^{-/-}$ mice compared to paired-fed wild-type mice [336]. Endogenous tRA, tRol, and retinyl ester were assessed in serum, liver, kidneys, brain, and testis. "Normal" indicates no difference from wild-type animals; *: in serum and tissues; $^{\dagger}$: magnitude not stated clearly; ^: in tissues.

| **Dietary vitamin A** | **tRA*** | **tRol^** | **Retinyl ester^** | **Hepatic Cyp26a1** |
|---|---|---|---|---|
| 0.6 IU/g | Normal | Liver and kidney: 2-fold and 40% increase, respectively | Liver: 40% increase | 2.5-fold decrease |
| 4 IU/g | Normal | Liver: 2-fold increase | Normal | Decrease$^{\dagger}$ |
| $>$ 30 IU/g | Normal | Normal | Normal | Normal |

In an attempt to identify genes regulating embryonic development, Sandell et al. discovered a mutant mouse called *trex* that harboured a mutation in the Rdh10 gene leading to lower Rdh10 protein expression, lower tRal production, and loss of RA reporter activity with minimum residual activity in neural tube when mated to *RARE-hsp68-lacZ* reporter mice [274]. These mutants suffered developmental defects including craniofacial, limb, and organ abnormalities, beginning at embryonic day (E) 10.5, and died by approximately E13, which could be rescued by maternal RA supplementation [274]. More recently, a cross between *trex* mutant and Adh-del-mutant (with null mutations of Adh1-5) was reported, but the cross mutants exhibited a similar phenotype as *trex* mutants [156]. While the endogenous retinoid profile had not been described following a mutation in Rdh10, the embryonic lethality that was reversible with maternal RA supplementation strongly suggest it to be the predominant enzyme in biosynthesis of RA during development.

Other than the aforementioned enzymes, emerging evidence suggests the involvement of novel enzymes from the short-chain dehydrogenase/reductase family in the interconversion between Rol and Ral. For example, knockdown of Rdh1l (also known as Dhrs9) in zebrafish led to developmental defects, which were rescued by tRA treatment [220]. On the other hand, a few potential candidate enzymes has been reported to serve as reductases that convert tRal back to tRol, such as retinal reductase, RRD [166], and retSDR1 (also known as Dhrs3) [78, 117]. Mouse null mutants for these genes are either not established yet or are not being investigated in detail. Thus, their importance in maintaining a balance of Rol-Ral inter-conversion remains to be further explored. Until then, this thesis would adopt proposals that both Adhs (especially Adh3 and Adh4) as well as Rdhs (especially Rdh1 and Rdh10) are involved in the biosynthesis of RA, using Crbp1-bound and unbound Rol as substrates.

***Conversion of Ral into RA***

Conversion of Ral into RA is an irreversible oxidative process, catalysed by the class I cytosolic aldehyde dehydrogenases (Aldh1), also known as retinaldehyde dehydrogenases (Raldhs) [4, 302]. At least three Raldhs were identified to be involved in catalysing the formation of RA from Ral, namely, Aldh1a1, Aldh1a2, and Aldh1a3, also known as Raldh1, Raldh2, and Raldh3, respectively [302]. More recently, a fourth enzyme called Aldh8a1 or Raldh4, was found to also participate in this enzymatic conversion [177].

Raldh1 was the first Raldh found to oxidise Ral into RA in mouse tissues [163, 200], after which Raldh2 [339], Raldh3 [210], and Raldh4 [177] were reported. *In vitro*, Raldh1 is about 10-fold less efficient than Raldh2 and Raldh3 in converting tRal into tRA, while Raldh4 recognises predominantly 9cRal as substrate [66, 112, 177]. In addition to Ral, Raldhs recognise additional substrates, e.g., Raldh1 recognises 4-hydroxynenonal and malondialdehyde, which are break-down products of lipid hydroperoxides [4].

In 1999, Aldh1a2$^{-/-}$ mutants were established. The null mutants suffered embryonic lethality at E10.5 without undergoing body turning and presented with many developmental defects such as shortening of anterior-posterior axis, absence of limb bud, and truncated frontonasal region, which was largely but not fully rescued with maternal RA supplementation [234]. A similar phenotype was reproduced in another line of Raldh2 null mutants involving another strain [208]. Of note, a near complete loss of RA reporter activity was observed at E7.5-10.5, except for a week signal in the developing eye, when Aldh1a2$^{-/-}$ were mated to *RARE-hsp68-lacZ* and *RAR$\beta$2-lacZ* reporter mice, respectively [208, 234].

In 2003, Aldh1a3$^{-/-}$ mice were established, which were born according to Mendelian frequency but died shortly after birth due to respiratory distress; when mated to *RARE-hsp68-lacZ* reporter mice, there was a partial loss of RA reporter activity in developing eyes associated with eye development impairment, and a complete loss of RA reporter

activity in developing nose associated with severe nasal defects [69, 216]. Similar to the Aldh1a2$^{-/-}$ mice, developmental defects and post-natal lethality observed in Aldh1a3$^{-/-}$ mice were largely prevented by maternal RA supplementation [69].

Also in 2003, mouse model of Raldh1 genetic ablation was generated. Aldh1a1$^{-/-}$ mice were viable and appeared normal phenotypically [76, 198], but showed a different hepatic retinoid profile compared to wild-type mice [76]. Specifically, tRol and retinyl ester in the liver of Aldh1a1$^{-/-}$ mice were about 2-fold and 2.5-fold higher, respectively, compared to that in the liver of wild-type mice. No difference in the level of hepatic tRA was found; a lower level of hepatic tRA in Aldh1a1$^{-/-}$ mice compared to that in wild-type mice was only apparent when challenged with a single high dose of Rol [76]. An increase in incidence of cataracts was also reported in Aldh1a1$^{-/-}$ mice of 6-9 months old compared to age-matched wild-type mice, which was attributed to accumulation of toxic lipid peroxide aldehydes and free oxygen radicals leading to protein cross-linking and aggregation [161].

Following the observation of residual RA reporter activity in the developing eye of Raldh2 null mutants [235], compound null mutants of Raldhs, i.e., Aldh1a1$^{-/-}$ / Aldh1a2$^{-/-}$ mice [211], Aldh1a1$^{-/-}$ / Aldh1a3$^{-/-}$ mice [198, 216], Aldh1a2$^{-/-}$ / Aldh1a3$^{-/-}$ mice [216], and Aldh1a1$^{-/-}$ / Aldh1a2$^{-/-}$ / Aldh1a3$^{-/-}$ mice [216], were established in an attempt to further elucidate the contribution of Raldhs other than Raldh2 during eye development. Many of these compound null mutant mice were subjected to low dose RA supplementation in order to prevent mid-gestation lethality of their offsprings, and the main conclusions drawn from these reports were that both Raldh1 and Raldh3 are indeed required for eye development, and that genetic deletion of Raldh1 can be compensated by Raldh3 and vice versa.

The aforementioned genetic studies had highlighted the roles of Raldhs in biosynthesis of RA during embryonic development. Raldh2 is required for generating endoge-

nous RA during embryonic development, Raldh3 is required for nasal development, and Raldh1 and Raldh3 were needed to generate RA for eye development. The functions of these enzymes in RA biosynthesis during development were in good concordance with a diminution of reporter gene expression when the null mutants were mated to reporter mice of endogenous RA activity. After birth, Raldh1 might have additional roles in the eyes besides acting as retinaldehyde dehydrogenase, and its role in tRA biosynthesis might only be applicable when Rol is in excess. The mid-gestation lethality of Raldh2 null mutants and the early post-natal lethality of Raldh3 null mutants had precluded investigation into their contributions towards RA biosynthesis at later stages but it is well possible that there are functional redundancies among Raldh1-3, and each may play a more dominant role at certain stages and under certain conditions. The role of Raldh4 remains unknown given their low affinity towards tRal and the lack of genetic evidence suggesting its contribution towards RA biosynthesis.

Given the reversible nature of conversion between Rol and Ral, it was deemed an equilibrium will be achieved between Rol and Ral, and the irreversible conversion of Ral into RA should be the crucial step in determining the rate of RA biosynthesis [67]. However, when the involvement of Crbp1 as binding protein of intra-cellular Rol was taken into consideration, evidence from *in vitro* studies showed that conversion from Rol to Ral should be the rate limiting step [224]. Taken together, biosynthesis of RA is a complex biological process that involves multiple enzymes with potential functional redundancies. Moreover, activities of the enzymes are depending on their sites of expression, which might be dynamically regulated. To date, the roles of Raldh2, Raldh3, and Rdh10 in generating RA for embryonic and post-natal development are better acknowledged, whereas the actual physiological roles of other RA synthesising enzymes require further investigations to achieve more solid conclusions.

***Conversion of RA into polar metabolites***

The involvement of microsomal enzymes, cytochrome P450 (Cyp450), in the conversion of RA into polar metabolites was first described in 1984 [170]. Subsequent work on Cyp450 enzymes had been carried out, leading to identification and characterisation of Cyp26a1 [89,258,319,320], Cyp26b1 [186,226,321], and Cyp26c1 [294,295], in human and in mice. Although many other members of the Cyp450, e.g., Cyp2c8, Cyp3a4, Cyp3a5, and Cyp3a7, have been suggested to be involved in this reaction, it is now recognised that Cyp26a1-c1 are largely responsible in the phase I oxidation of RA into more polar metabolites, which are then glucuronidated and excreted [265].

*In vitro* experiments examining substrate specificity performed using human and mouse Cyp26a1-c1 revealed that these enzymes recognise specifically RA as substrate, but not Rol nor Ral [295, 321]. While Cyp26a1-c1 exhibited high specificity towards tRA and catalysed its metabolism into polar metabolites including 4-hydroxy-RA, 4-oxo-RA, 18-hydroxy-RA, and 5,8-epoxy-RA, Cyp26c1 also exhibited an equally high specificity towards 9cRA, yielding 4-hydroxy-9cRA and 4-oxo-9cRA [295, 321].

The generation of Cyp26a1 null mutant mice were reported by two independent groups in 2001 [1, 273]. While Cyp26a1$^{+/-}$ mice were indistinguishable from the wild-type mice, Cyp26a1$^{-/-}$ mice died before birth or within one day after birth, and exhibited symptoms recapitulating teratogenic effect of excess RA, e.g., exencephaly, spina bifida, and abnormal patterning of hindbrain and tailbud [240]. Notably, when Cyp26a1$^{-/-}$ mice were mated to *RARE-hsp68-lacZ* mice, an increase in RA reporter activity was noted not only in the sites where RA reporter activity was normally observed, but also in domains where RA reporter activity was normally absent [273]. Just as Cyp26a1$^{+/-}$ mice, heterozygous null mutants for Cyp26b1 were no different from their wild-type counterparts but Cyp26b1$^{-/-}$ died within a few hours after birth due to respiratory distress, and they exhibited truncated limbs, severe craniofacial abnormalities, and absence of germ cells (in male mice), which was again attributed to an accumulation of bioactive RA following

Cyp26b1 inactivation [187,331]. Cyp26c1$^{-/-}$ mice developed normally but when crossed with Cyp26a1$^{-/-}$ mice, the double null mutants exhibited embryonic lethality at E11-12.5 and severe malformation in the central nervous system [306].

Although there have been reports that metabolism products of RA catalysed by the Cyp26 enzymes, such as 4-oxo-RA and 4-hydroxy-RA, were bioactive, null mutants of Cyp26s exhibited phenotypes that recapitulated the classical teratogenic effects induced by RA rather than the VAD syndromes. By partially disrupting RA biosynthesis via heterozygous ablation of Raldh2 (Aldh1a2$^{+/-}$) in Cyp26a1$^{-/-}$ mice, Niederreither et al. had provided genetic evidence that argues against oxidative products of RA playing a functional role during murine development [230]. Specifically, Cyp26a1$^{-/-}$ / Aldh1a2$^{+/-}$ mice had higher post-natal survival rate compared to the early lethality of Cyp26a1 null mutants, and many developmental defects found in Cyp26a1$^{-/-}$, such as spina bifida were rescued following heterozygous disruption of Raldh2 [230]. This study supports that the phenotypes of Cyp26a1$^{-/-}$ mice were a result of RA excess, which were ameliorated by reducing RA biosynthesis, rather than due to an insufficiency of RA metabolites.

Taken together, genetic studies suggest that Cyp26a1 and Cyp26b1 are essential for embryonic development and for post-natal survival, respectively, while Cyp26c1 acts in cooperation with Cyp26a1 to reduce the sensitivity of embryo to excessive RA. In addition, Cyp26b1 may play a unique role in germ cell development. However, specific functions of these enzymes, especially in adults, are not well defined until today [265].

### 1.1.4 The canonical signalling

The canonical signalling of retinoids is the focus of this project. It involves activation of retinoid nuclear receptors by RA and subsequent mobilisation of the transcription co-regulators, leading to gene transcription modulation [264]. Target genes of RA canonical signalling are often characterised by the presence of retinoic acid response element (RARE) in their regulatory region [41]. All the key players involved in the canonical signalling are briefly introduced here.

***Retinoid nuclear receptors***

There are two families of retinoid nuclear receptors, namely, retinoic acid receptors (RARs) and retinoic acid X receptors (RXRs), which are members of the steroid nuclear receptor superfamily and act as transcription factors [41]. There are three isotypes of RARs, i.e., RAR$\alpha$, RAR$\beta$, and RAR$\gamma$, encoded by Rara, Rarb, and Rarg, respectively, and three isotypes of RXRs, i.e., RXR$\alpha$, RXR$\beta$, RXR$\gamma$, encoded by Rxra, Rxrb, and Rxrg, respectively. Each RAR and RXR isotype constitutes at least two isoforms, generated by differential promoter usage and alternative splicing [41].

In 1987, two independent groups had reported the discovery of RAR$\alpha$, which bound strongly to RA and transduced signal of RA in a dose-dependent and saturable manner, but did not respond to thyroid hormone, vitamin D, dexamethasone, or testosterone [100, 247]. Shortly after the discovery of RAR$\alpha$, two additional RAR isotypes with similar properties, namely RAR$\beta$ [33] and RAR$\gamma$ [155], were discovered. The discovery of a distinct but closely related nuclear receptor, RXR$\alpha$, was subsequently reported by Mangelsdorf et al., which responded towards RA treatment in a dose dependent manner but responded poorly towards TTNPB, a pan-RAR agonist [190]. Soon after, RXR$\beta$ and RXR$\gamma$ were discovered, and the concept of RXRs binding to RARs as heterodimers that enhance their binding to DNA leading to more efficient signal transduction was introduced [168, 333].

The amino acid sequence of an individual isotype of RAR and RXR is better conserved across species than that of the three RAR or RXR isotypes in a given species [167]. The RARs shared a similar modular structure, consisting six conserved regions designated A to F. Regions C and E that encompass DNA binding domain (DBD) and ligand binding domain (LBD), respectively, are most conserved and play the most important roles, i.e., DBD recognises specific DNA sequences and served as dimerisation interface, while LBD comprises ligand binding pockets for ligand binding, a major interface for

dimerisation, and the activation function 2 (AF-2) that is required for ligand-dependent activation [264]. The A/B region represents the N-terminal domain encompassing a ligand-independent activation function 1 (AF-1) that synergises with AF-2 to activate transcription; the D region serves mainly as a rotatable hinge between DBD and LBD; function of F region remains poorly understood but may enhance binding of transcription co-repressors in the absence of ligand and may be capable to bind specific mRNA motifs [221, 264].

RXRs adopt the same modular structure as RARs except that region F is absent [164]. Besides heterodimerising with RARs, RXRs form homodimers and homotetramers, and also serve as promiscuous binding partner for many other nuclear receptors, such as PPAR, thyroid hormone receptor (T3R), and vitamin D receptor [164]. A schematic representation of retinoid nuclear receptor heterodimers and brief description of each region are depicted in Figure 1.2.

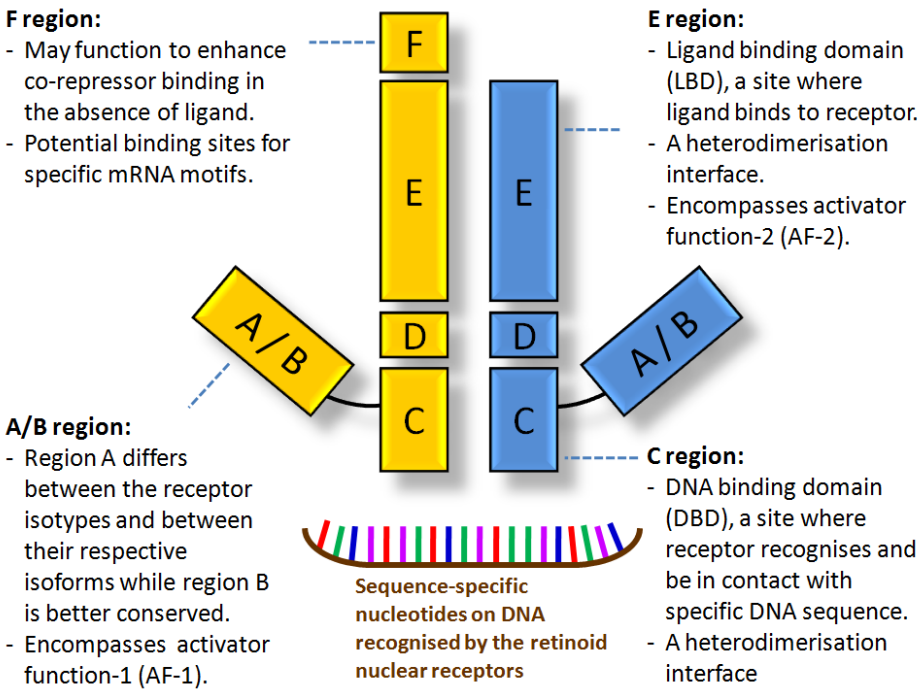


Figure 1.2: Schematic representation of retinoic acid receptor (RAR) and retinoic acid X receptor (RXR) modular structure. RAR (yellow) and RXR (blue) form heterodimers, which binds to a specific sequence called retinoic acid response element (RARE) present on retinoid target genes to modulate gene transcription activity.

In the context where RXR and RAR function as heterodimer, Forman et al. found that reporter activity can be induced by RAR ligand but not by RXR ligand [85]. By treating P19 teratocarcinoma cells and F9 cells with RAR-specific agonists and RXR-specific agonists individually and in combination, Roy et al. reported that RAR activation but not RXR activation resulted in induction of gene expression; when given in combination, a synergistic effect was observed whereby gene expression and cell differentiation were induced to a greater extent at lower doses of agonists [269]. Subsequent work proposed that binding of RAR to its ligands has to first take place before RXR can be bound by its ligand [317]. In a later study, it was reported that both RXR and RAR within the heterodimer can bind to their respective ligands independently, but their bindings elicit different responses in terms of co-regulator mobilisation [95], which will be further elucidated in the following subsection.

Several studies had investigated the endogenous ligands of RARs and RXRs. Using COS-1 African green monkey kidney fibroblast-like cells transfected with individual isotypes of mouse RARs and RXRs, Allenby et al. reported that tRA and 9cRA bound to all three isotypes of RARs with high affinity ($K_d$ of 0.2-0.4 nM for tRA and 0.2-0.7 nM for 9cRA) [3]. While the respective 3,4-didehydro form of tRA and 9cRA were also found to be as effective in receptor binding and activation [3], the role of 3,4-didehydro form of tRA as endogenous ligand of RARs was better established in avians than in rodents [260, 300]. Retinoids other than RA had also been reported to be natural ligands of RARs but the results were less definitive. For example, tRol was reported to bind and activate human RARs but was 4- to 37-fold less potent compared to tRA [259]. On the other hand, Achkar et al. reported that mouse RARs were not bound to tRol but did bind to 4-oxo-Rol [2]. Based on consistent reports derived from binding assays, transactivation assays, and its abundance detected *in vivo*, tRA is well acknowledged to be the most physiologically relevant endogenous ligand of RARs by far.

On the other hand, identification of specific endogenous ligands of RXRs remains a

great challenge until today [164]. While tRA binds to RARs with high affinity, it does not bind RXRs [3]. 9cRA binds to RXRs with high affinity ($K_d$ within 14.0-16.0 nM) and activates the receptors [3] but *in vivo*, 9cRA was only detected in the pancreas [138]. Moreover, activity of 9cRA in pancreas was found to be rapid and distinct from that of synthetic RXR agonists [138]. It is worth mentioning that some unsaturated fatty acid was reported to bind and modulate activities of RXRs, but the binding was not exclusive as the fatty acid also binds other nuclear receptors, including PPARs [164].

Null mutants of individual retinoid nuclear receptor were soon available and the roles of the receptors in transducing RA signal have been better elucidated since. $Rara^{-/-}$ mice develop normally, but exhibited testes degeneration and webbed digits, and more than 90% of the null mutant mice died before the age of two-month-old without obvious specific lethal lesions [183]. $Rarb^{-/-}$ mice were growth deficient, but were fertile and live as long as their wild-type counterparts [98, 184]. $Rarg^{-/-}$ mutant mice did not die *in utero*, but suffered congenital anomalies such as Harderian gland agenesis, tracheal cartilage malformations, and homeotic transformations along the rostral axial skeleton; a higher post-natal mortality rate was noted with less than 40% of $Rarg^{-/-}$ mutant mice surviving to 3-month-old and the surviving mice were growth deficient and sterile [182]. While null mutants of a single RAR showed few anomalies, genetic deletion of two or more RARs resulted in a plethora of developmental defects involving multiple organs with striking resemblance to VAD syndromes observed in rats with maternal vitamin A deficiency, which were comprehensively summarised in recent reviews [193, 231]. This leads to the conclusion that RARs are indeed the major players in transducing RA signalling during development and that the RARs may be functionally redundant or may be required to act in a cooperative manner.

Genetic deletion of individual Rxrs, except for Rxrg, resulted in a more severe developmental defect than that of individual Rars. Rxra heterozygotic null mutants exhibited growth deficiency, whereas Rxra homozygotic null mutants died *in utero* at E16.5, and

exhibited ocular and myocardial anomalies [142]; about 50% of Rxrb$^{-/-}$ mutant mice died *in utero* or at birth [144]; Rxrg$^{-/-}$ mutants were viable and fertile [154]. Importantly, anomalies exhibited by Rxra$^{-/-}$ mice recapitulated VAD syndromes and developmental defects of Rarb$^{-/-}$ / Rarg$^{-/-}$ double mutants, suggesting the involvement of RXR$\alpha$ in transducing RA signals [145]. Consistent with the role of RXRs as promiscuous binding partners for many nuclear receptors such as PPAR and T3R, anomalies not known to be related to vitamin A deficiency, such as defects in male reproductive organ and metabolic imbalance, were found in Rxrb$^{-/-}$ and in Rxrg$^{-/-}$ mice, respectively [35, 144, 218]. Compound null mutants of two or more RXRs had then been established to further elucidate their roles. Rxrg$^{-/-}$ / Rxra$^{-/-}$ mice exhibited similar ocular and cardiac defects as observed in Rxra$^{-/-}$ mice while Rxrg$^{-/-}$ / Rxrb$^{-/-}$ mice and Rxrg$^{-/-}$ / Rxrb$^{-/-}$ / Rxra$^{+/-}$ mice were viable despite being deficient in growth and exhibited male sterility [154]. These studies had underscored RXR$\alpha$ as the predominant RXR isotype in mediating embryonic development and that presence of a single allele is sufficient in this regard.

By establishing a battery of Rxr/Rar compound null mutants, Kastner et al. found that genetic deletion (either single or double alleles) of Rxra together with either of the individual Rar isotype resulted in a synergism of ocular and myocardial defects observed in Rxra mutants as well as other developmental defects not seen in Rxra single null mutants and the corresponding single Rar null mutants; compound null mutants of Rxrb and individual Rar isotype, as well as Rxrg and individual Rar isotype developed normally [143]. This study strongly suggests RXR$\alpha$ / RAR to be the primary functional unit in transducing RA signalling during development, consistent with the idea of retinoid receptors functioning as heterodimers. By treating the Aldh1a2$^{-/-}$ mutant mice that lack endogenous tRA with an RAR-specific agonist and an RXR-specific agonist, Mic et al. reported that activation of RARs but not RXRs is sufficient to rescue lethal defects [209], which is in good agreement with observations by Roy et al. that RAR activation is sufficient to transduce RA signalling [269]. This concept of “RXR subordination” will be further elucidated in the following subsection.

Genetic deletion of retinoid nuclear receptors had indeed highlighted the crucial roles of retinoid nuclear receptors, particularly in development. While the importance of RXR/RAR heterodimers in transducing RA activity is no longer disputed, their specific functions remained elusive and are not completely deciphered. The presence of additional abnormalities observed in compound null mutants of the receptors that are not noted in VAD animals might be due simply to the fact that some residual RA signalling might still be operational in animals with vitamin A deficiency whereas genetic deletion of retinoid receptors resulted in a total inhibition of RA canonical signalling [193]. However, the observation might also suggest additional functions of these receptors in their unliganded form. Early lethality in null mutants of retinoid nuclear receptors generated from germline mutation had also precluded further investigations into the functions of these genes, particularly during the adult stage. A few conditional knockout models were reported [193] which should allow better understanding of these receptors, especially on their roles in post-natal and adult life.

***Transcription co-regulators***

RXR/RAR-mediated regulation of gene transcription requires coordinated functions of transcription co-regulators, which bind physically to RXR/RAR heterodimer and act as "master switch" to switch the receptor heterodimers from an inactive state to an active state and *vice versa*, via multiple biochemical mechanisms [36, 104]. The transcription co-regulators make up a diverse family of proteins that function with transcription factors [36]. This section introduces their general functions in modulation of retinoid nuclear receptor silencing/activation rather than individual transcription co-regulators and their respective functions, which have been presented in recent reviews [6, 264].

The transcription co-regulators can be largely categorised into two groups, i.e., (i) transcription co-activators, and (ii) transcription co-repressors [6, 203]. Transcription co-activators, exemplified by p160 subfamily of steroid receptor co-activators such as N-

coA1 (nuclear receptor co-activator 1, also known as SRC1), CARM1 (coactivator-associated arginine methyltransferase 1) and SWI/SNF (switch/sucrose non-fermenting), bind to AF-2 on region E of retinoid nuclear receptors (Figure 1.2) in the presence of ligand. Co-activators possess activities such as histone acetyltransferase, histone methyltransferase, and ATP-dependent chromosome remodelling, which decompact chromatin into a more relaxed configuration. The co-activators are then released or degraded, giving way to the SMCC (Srb and Mediator protein containing complex), which then recruits RNA-polymerase II and general transcription factors, leading to gene transcription initiation [6, 264]. On the other hand, the transcription co-repressors, such as Nco-R (nuclear receptor co-repressor) and SMRT (silencing mediator for retinoid and thyroid hormone receptors), function to recruit big molecules with histone deacetylase activity, thereby further stabilising the compact chromatin configuration hence silencing gene transcription [6, 264].

*In vitro*, binding of transcription co-activators and transcription co-repressors to the RXR/RAR heterodimer are mutually exclusive and a single co-activator can bind to both RXR and RAR; binding of RAR to its ligand leads to dissociation of co-repressors but binding of RXR to its ligand does not [95]. Thus, RARs were deemed "permissive" in the context of RXR/RAR heterodimers, whereby liganded-RAR is sufficient to initiate transcription whereas RXR was "subordinated" to their RAR partners [16, 114].

The universal interaction of transcription co-regulators with multiple transcription factors renders genetic deletion unhelpful in learning their functions. A working model that briefly elucidates the functions of transcription co-regulators, in the context of their sequential interaction with retinoid nuclear receptors, is presented in the short summary at the end of this subsection.

***RARE***

RARE denotes a specific sequence that is present at the regulatory region of retinoid target genes, which are recognised and bound by the RXR/RAR heterodimers. The classical RARE comprises direct repeat (DR) of two hexameric motifs, (A/G)G(G/T)TCA, spaced by 1, 2 or, 5 bases, which are described as DR1, DR2, and DR5, respectively [41]. On DR2 and DR5, the RXR/RAR heterodimers bind in a polarity such that the RXR binds to the hexameric motif located at the 5' site while RAR binds at the 3' site; the polarity can reverse in the case of DR1, i.e., RAR binds to the 5' site while RXR binds to the 3' site, which switches the role of the receptors from transcription activators into transcription repressors [158]. In addition, DR1 can also be bound by RXR homodimers. More recently, Lalevee et al. had performed an *in silico* whole genome screen for DR5 RARE, and proposed that a more relaxed (A/G)G(G/T)T(C/G)A motif to be the half site of RARE, hence expanding the repertoire of classical RARE [159].

A gene cannot be defined as retinoid target gene based simply on the presence of nucleotide sequences in the regulatory region that resemble RARE. Functions of RARE are often examined in an *in vitro* setting by screening various regions of the gene promoter using reporter-based assay and by examining the physical binding of RXR/RAR to the regions determined. Point mutations of one or more nucleotides can also be performed to further confirm the functions of RARE. Using such strategies, functional RARE was identified and characterised in some members of the retinoid system, such as the Rarb gene [54, 289] and the Rbp1 gene that encodes Crbp1 [284] in the early 90s. In fact, many members of the retinoid system had subsequently been reported to contain one or more functional RARE in their regulatory region. This phenomenon reflects the presence of a self-regulatory control mechanism of the retinoid system, which will be further discussed in Section 1.1.6.

It is important to note that identification of functional RARE in a given gene is not always as straight forward. RARE determined from reporter-based assay and from DNA-protein

binding may sometimes produce artificial results, especially in cells over-expressed with RXR/RAR. Also, RARE that is responsive in a well-controlled *in vitro* setting may not be applicable to the dynamic state *in vivo*, as gene expression is often governed by more than a single regulatory factor. Another issue complicating determination of RARE is that RARE can come in far more complex arrangements other than the aforementioned classical RARE [13, 41, 159], including: (i) The hexameric motif of an RARE can have an even less rigid sequence, (A/G)G(G/T)(G/T)(G/C)A, (ii) RARE do not necessarily follow the classical spacing attributes, i.e., 1, 2, and 5, between the DR hexameric motifs, (iii) presence of RARE is not restricted to the promoter region and can also be present in the intronic regions, (iv) RARE can be present in both the coding and the non-coding DNA strands, (v) RARE can be in both forward and reversed orientation.

***A short summary of the canonical signalling***

The working model described by Bastien and Rochette-Egly [16] is presented here to summarise the canonical signalling pathway of retinoids:

1. In the absence of ligand, DBD (region C) of retinoid nuclear receptors associates with RARE at the regulatory region of retinoid target genes; transcription co-repressor complexes may be recruited to AF-2 in the LBD (region E) of the retinoid nuclear receptors if the chromatin configuration is not impeding such interaction.

2. When ligand binds to LBD (region E) resulting in a conformational change to the nuclear receptors, transcription co-repressors will be released while transcription co-activators will be recruited to AF-2 in the LBD, leading to a state of decompact nucleosome ready for transcriptional activity to take place.

3. The transcription co-activators will then dissociate or degrade hence giving way to SMCC, which facilitates the recruitment of RNA polymerase II and general transcription factors thereby initiating transcription.

The canonical signalling is a highly regulated and coordinated event, and much remains to be learnt about the canonical signalling pathway of retinoids. It is important to note that concomitant presence of RXR/RAR and transcription co-regulators in cells expressing genes that contains one or more RARE(s), are not necessarily indicative of an active retinoid canonical signalling, until proven otherwise.

### 1.1.5 The non-canonical signalling

In order to better illustrate the multiplicity of RA signalling, the non-canonical signalling of retinoids is briefly introduced here focusing on two examples.

***Binding and activation of nuclear receptors other than retinoid nuclear receptors***

Shaw et al. reported that tRA binds PPAR$\beta/\delta$ with high affinity ($K_d$ of 17 ± 3 nM for PPAR$\beta/\delta$ compared to $K_d$ of 100-200 nM for PPAR$\alpha$ and PPAR$\gamma$); tRA treatment stabilised binding of transcription co-activator SRC1 to PPAR$\beta/\delta$ and induce PPAR$\beta/\delta$ reporter activity [282]. The same group later reported that binding of RA to PPAR$\beta/\delta$ is an event strictly governed by Fabp5, whereby Fabp5-bound RA was directed to PPAR$\beta/\delta$ leading to activation of PPAR$\beta/\delta$-mediated signalling events; in the case where Crabp2 protein exceeds Fabp5 protein, binding of Crabp2 to RA dominates and Crabp2-bound RA would be channelled to RARs [280]. However, the involvement of RA in activating PPAR$\beta/\delta$ was defied by two other groups, who reported that RA does not bind to PPAR$\beta/\delta$, and does not activate PPAR$\beta/\delta$-mediated signalling [30,263]. The discrepancies remain unresolved and hence it is difficult to conclude on the relationship between RA and PPAR$\beta/\delta$ at this stage.

Besides PPAR$\beta/\delta$, tRA was also reported to bind ROR$\beta$, a member of the retinoid orphan receptors, which are ligand-dependent transcription factor. In this context, tRA functions as antagonistic ligand in a cell type-specific manner, whereby its binding antagonised transactivation of ROR$\beta$ activity in several cell types but not the others [288].

***Transrepression of activator protein 1 (AP-1) activity***

AP-1 is transcription factor complex comprising a group of structurally and functionally related members of Jun, Fos, and activating transcription factor ATF, which function as heterodimers and binds to its putative DNA response element [121]. In the beginning of 1990s, it was reported that RA suppresses gene expression by preventing binding of AP-1 to its DNA binding site, a process which requires liganded RAR but not RXR [229, 276]. Of note, the anti-AP-1 activity of retinoids can be dissociated from RAR-mediated transcriptional activation, ruling out the possibility of anti-AP-1 activity acting downstream of RA canonical signalling [43]. Many studies had since been conducted to further elucidate the transrepression activity of AP-1 by retinoids and the potential mechanisms were summarised in recent reviews [264, 329], which include: (i) suppression of Jun/Fos family member expression, (ii) direct interaction of RARs with Jun/Fos family members, (iii) disruption of dimerisation between Jun/Fos family members by RARs, and (iv) competition between RARs and AP-1 family members for common transcription co-activators. On the other hand, transrepression of retinoid canonical signalling by AP-1 was also reported [41].

Given that knowledge on crosstalk between retinoid system and AP-1 was largely derived from *in vitro* experiment and in cells over-expressing retinoid nuclear receptors, their physiological relevance remained questionable [41]. In view of the fact that AP-1 regulates cell oncogenic transformation and proliferation, the anti-proliferative effect of exogenously administered RA in tumour cells is believed to be mediated, at least in part, through its antagonisation of AP-1 activity [5].

***A short summary on the non-canonical signalling***

There are many other examples of the non-canonical signalling pathway of retinoids, all of which were summarised in recent reviews [6, 264, 302]. For example, liganded RAR can rapidly activate kinases, which in turn phosphorylate RAR hence modifying its transcriptional activity; a direct physical binding of RAR to mRNAs was found, which would

affect translation of the mRNAs depending on the presence of ligand; the involvement of Rol and Ral as signalling molecules, which leads to distinct biological events.

### 1.1.6 Target genes of RA

Many studies have examined the target genes of RA, which had provided some mechanistic insights into the biological effects of RA. It has been long appreciated that regulation of gene expression by RA is cell type-specific and context-dependent [41], i.e., while RA exerts a positive regulation on a given gene in a given cell type under certain condition, a neutral or a completely opposite regulatory effect on the same gene is well possible in another cell type under different context [12]. The cell-type specificity and context-dependency of RA regulation of gene expression can be, at least in part, explained by the following:

- The presence of multiple retinoic acid receptor isotypes, of which better conservation was found for individual isotype across multiple species than for all isotypes within a single species [167], raises the possibility of isotype-specific regulation of gene expression. It is thus possible that the varied results exerted by RA is due to the presence of different receptors and to their isotype-specific functions.

- Using mouse embryonic fibroblasts and mouse embryonic stem cells as *in vitro* models, Delacroix et al. showed that occupancy of a given RAR isotype on RA target genes differs between the two cell types [56]. Therefore, presence of same sets of retinoid nuclear receptors in two different cells would still result in distinct biological responses.

- Depending on the cell types and contexts, gene expression regulation by RA might be mediated via the canonical or the non-canonical pathways, or might be a net result of the combinatorial effects from crosstalk between the two [264].

In addition to the cell type-specificity and context-dependency, the effects of RA on gene expression regulation can be rapid and transient depending on which signalling pathways

dominate. Moreover, due to its pro-differentiative property, RA can induce fundamental phenotypical changes leading to a knock-on effect on gene expression profile. All the aforementioned had posed a great challenge in identification of genuine target genes of RA. In 2002, Balmer and Blomhoff summarised the experimental evidence available for 532 target genes of RA that were published [12]. Among them, only 27 genes (around 5%) were deemed direct target genes of RA (treatment of 1 $\mu$M of RA for 6 h or less was set as the upper limit), which were regulated through canonical signalling pathways and contain functional RARE(s); the remaining were those regulated by RA directly but mechanisms not fully elucidated or genes regulated indirectly without conclusive evidence on transcriptional regulation [12]. An important aspect worth noting is that although target genes of RA canonical signalling were rather diverse, many members of the retinoid system are themselves direct target genes of RA [12].

While many studies had focused on identifying target genes of exogenous RA, target genes of endogenous RA are less well described. Hence, it remains to be established if exogenous RA and endogenous RA share a similar set of target genes in a given cell type. Nonetheless, it is conceivable that endogenous RA also exhibits similar multiplicity and diversity as exogenous RA described earlier.

***Self-regulatory system***

As mentioned before, many members of the retinoid system are direct target genes of RA, depicting an exquisite self-regulatory and fine-tuning mechanisms to ensure the functions of retinoid system be kept in check. Specifically, many members of retinoid system contain well-characterised and functional RARE(s) in their gene regulatory region, and their expression has been shown to be regulated by RA, e.g., Rarb (DR5) [54, 289], in particular, Rarb2 and Rarb4 but not Rarb1 nor Rarb3 [205], Rara2 (DR5) [171], Rarg2 (DR5) [165], Cyp26a1 (DR5) [338], Rbp1 that encodes Crbp1 (DR2) [284], Rbp2 that encodes Crbp2 (DR1) [191], Crabp2 (DR1 and DR2) [8, 70], and Stra6 [31].

The positive regulation of RA on the RARs depicts a positive feedback mechanism to potentiate RA signalling, while up-regulation of Cyp26a1 in response to RA would promote RA catabolism as a negative feedback mechanism to prevent excessive RA. In addition, RA were also reported to down-regulate other members of the retinoid system, which do not have classical RARE, via other mechanisms, such as Raldh1 [74] and Raldh2 [233]. The non-direct negative regulation of these genes suggests a feedback mechanism to avoid aberrant RA biosynthesis leading to toxicity.

It must be reiterated that cell-specificity and context-dependency of gene expression regulation also apply to members of retinoid system including those with well-characterised RARE in their regulatory regions. For example, induction of Cyp26a1 mRNA in liver by tRA was about 20-fold more than that in kidney [338]; high dose of tRA induced rather than suppressed Raldh2 mRNA in fibrotic kidney of Alb/TGF-$\beta$1 transgenic mice [328]. It is thus crucial to always interpret "target genes" of retinoids with caution, by taking into consideration the full context, under which the gene regulation was examined.

### 1.1.7 Concluding remarks on the retinoid system

In summary, the retinoid system is highly versatile involving retinoid metabolism, transportation, and signalling. Firstly, availability of endogenous retinoids is dynamically determined by cellular uptake, as well as the expression and activity of retinoid synthesising and metabolising enzymes. Secondly, the gene expression regulatory function of retinoids, primarily RA, is governed by multiple factors, such as the binding proteins, RAR and RXR that come in multiple isotypes and isoforms, and potential crosstalk between RA with other signalling pathways. The diversity of retinoid system had lead to multiplicity of RA functions, depending on its target genes in a given cell type under specific contexts. A brief summary of retinoid system is depicted in Figure 1.3.

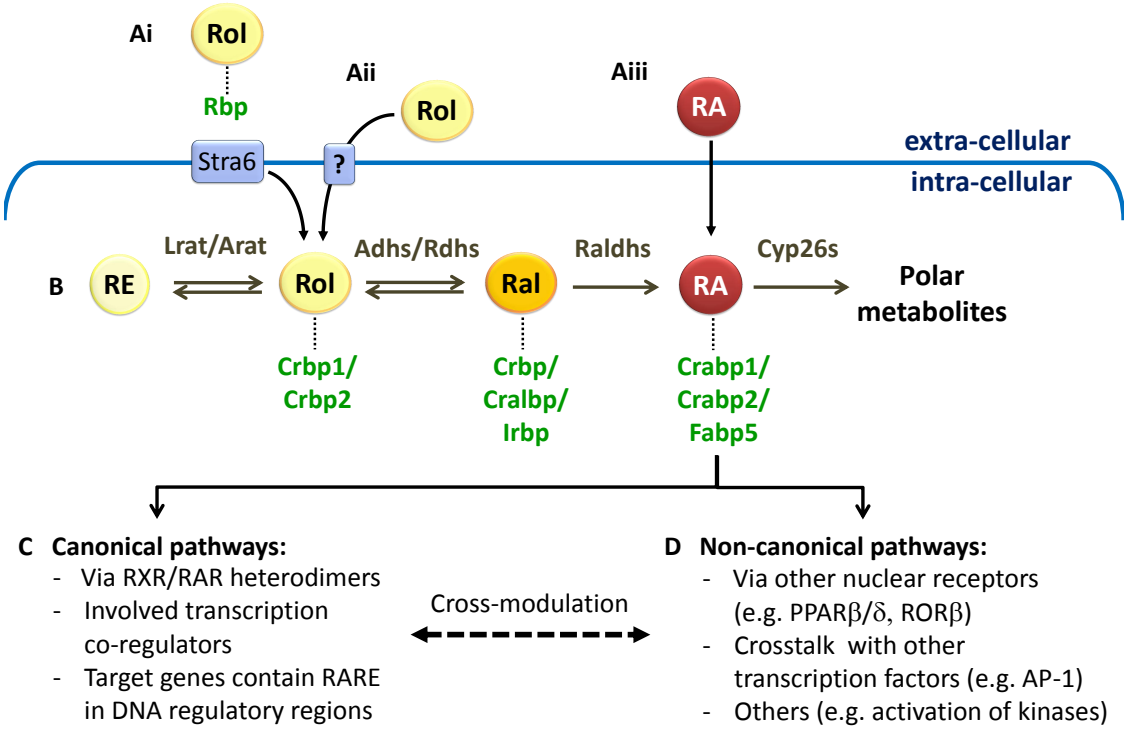


Figure 1.3: A brief overview of retinoid metabolism, transportation, and signalling. Uptake of extra-cellular Rbp bound-Rol is mediated by Stra6 (**Ai**) and perhaps via other mechanisms such as simple diffusion and yet defined mediators (**Aii**); direct uptake of extra-cellular RA into the cells is also possible (**Aiii**). In the cells, Rol is either converted, reversibly, into RE or into Ral; Ral is then converted irreversibly into RA and subsequently into polar metabolites. The retinoids were bound by various binding proteins to facilitate their intra-cellular transport, i.e., Rol is bound by Crbp1 and Crbp2, Ral is bound by Crbps, Cralbp, and Irbp, RA is bound by Crabp1, Crabp2, and Fabp5 (**B**). RA, the most physiologically relevant retinoid compound, mediates many signalling events with potential cross-modulation among them, such as the canonical signalling that typically involves the RXR/RAR heterodimers, transcription co-regulators, and the presence of RARE in the regulatory region of retinoid target genes (**C**), and the non-canonical signalling such as activation of nuclear receptors other than retinoid nuclear receptors, crosstalk with other transcription factors, and activation of kinases (**D**). Rbp: retinol binding protein; Rol: retinol; Ral: retinaldehyde; RA: retinoic acid; RE: retinyl ester; Stra6: stimulated by retinoic acid 6; Lrat: lecithin:retinol acyltransferase; Arat: acyl-coA acyltransferase; Adhs: alcohol dehydrogenases; Rdhs: retinol dehydrogenases; Raldhs: retinaldehyde dehydrogenases; Cyp26s: cytochrome P450 26 enzymes; Crbp: cellular retinol binding protein; Cralbp: cellular retinaldehyde binding protein; Irbp: interphotoreceptor retinoid binding protein; Crabp: cellular retinoic acid binding protein; Fabp5: fatty acid binding protein 5, RXR: retinoid X receptor; RAR: retinoic acid receptor; RARE: retinoic acid response element; PPAR: peroxisome-proliferator activated receptor; ROR: retinoid orphan receptor; AP-1: activator protein 1.

## 1.2 The retinoid system in kidneys

Retinoids, particularly RA and its analog, have been tested as therapeutic agents, where its anti-inflammatory, immune-modulatory, anti-proliferative, and tissue reparative roles were found to be beneficial in various experimental models of kidney diseases, as summarised in a recent review [329]. While its use appeared promising, retinoid compounds are double-edged swords whereby under certain circumstances, their use propagates disease progression and leads to severe adverse effects [328, 329].

In order to complement existing knowledge that largely revolves around the use of exogenous retinoids in experimental kidney diseases, this section presents a review on the endogenous retinoid system, which not only focuses on retinoids, but also on retinoid transport and metabolism as well as their activity in the kidney. The endogenous retinoid system is presented from two main perspectives, i.e., (i) the retinoid system in embryonic nephrogenesis and (ii) the retinoid system in the kidney after birth.

### 1.2.1 The retinoid system in embryonic nephrogenesis

As introduced earlier, a functional retinoid system is required during embryonic development, and is crucial in formation of organs undergoing branching processes such as the kidney [231]. Many studies have been performed over the last decades on the role of retinoid system in mediating nephrogenesis. Some of the most relevant studies are presented here.

#### *Vitamin A is required for nephrogenesis*

Rat foetuses with maternal vitamin A deficiency manifested VAD syndromes characterised by severe malformations of many organs, including the kidney. Developmental defects of the kidney included an abnormal and retarded nephron formation, failure of renal pelvis and calyx to undergo normal dilatation, and presence of horseshoe kidney [323]. By administering a single dose of vitamin A to pregnant rats during mid-gestational stage (from E10 to E15), kidney malformation was prevented, either partially

or completely, depending on the timing of vitamin A administration [322]. In fact, the developing kidney is highly sensitive towards vitamin A supply that even mild maternal vitamin A deficiency lead to a reduction of glomeruli number, a condition that was strictly correlated to foetal plasma Rol level [169].

***The role of retinoid nuclear receptors in nephrogenesis***

The cloning of RARs and RXRs in the late 80s and early 90s had allowed the generation of RAR and RXR null mutants (as described in Section 1.1.4), which very much facilitated studies on the roles of retinoid nuclear receptors in mediating embryonic nephrogenesis. Mendelsohn et al. had reported that while null mutants of individual RAR appeared normal, null mutants of two or more RARs suffered kidney developmental defects including kidney hypoplasia and agenesis [98, 206], a condition later reproduced in Rxra/Rara compound null mutants [143]. The compound null mutants and the associated kidney developmental abnormalities are summarised in Table 1.3.

Table 1.3: Kidney developmental defects in compound null mutants of retinoic acid receptor. *: complete penetrance.

| **Abnormalities** | **Retinoic acid receptor mutant genotypes** |
|---|---|
| Kidney hypoplasia | $Rxra^{-/-}$ / $Rara^{-/-*}$,<br>$Rara^{-/-}$ / $Rarb^{-/-*}$,<br>$Rara^{-/-}$ / $Rarb2^{-/-*}$,<br>$Rara1^{-/-}$ / $Rarb2^{-/-}$,<br>$Rara^{-/-}$ / $Rarb2^{+/-}$,<br>$Rara1^{-/-}$ / $Rarg^{-/-}$ / $Rara2^{+/-}$ |
| Kidney agenesis/aplasia | $Rxra^{-/-}$ / $Rara^{-/-}$,<br>$Rara^{-/-}$ / $Rarg^{-/-*}$ |

***Endogenous RA is the main retinoid compound in nephrogenesis***

Vilar et al. reported that adding RA to culture medium stimulated growth and differentiation of E14 rat embryonic metanephro explants in a dose-dependent manner, whereas

Rol is less effective with two magnitude difference compared to RA [310]. *In vivo* experiments had further supported RA as the key retinoid compound mediating nephrogenesis. Aldh1a2$^{-/-}$ embryos and Rdh10$^{trex/trex}$ mutant embryos, both characterised by a reduction of RA, suffered kidney development impairment [234, 274]. In a more recent publication, Rosselot et al. had confirmed Raldh2 that was expressed in the metanephric stromal cells to be the predominant RA synthesising enzyme required for nephrogenesis; during the absence of Raldh2, Raldh3 that was expressed in the ureteric bud can marginally support RA biosynthesis [267]. On the other hand, horseshoe kidney caused by an increased endogenous RA level following genetic deletion of Cyp26a1 was partially rescued by heterozygous deletion of Raldh2 to reduce endogenous RA synthesis [230].

Both *in vitro* and *in vivo* studies support the fact that RA, rather than its precursor or its polar metabolites, is the main retinoid compound mediating embryonic nephrogenesis. A fine balance of endogenous RA level is exquisitely controlled in this regard, primarily through collaborative activity of Raldh2, Raldh3, Rdh10, and Cyp26a1 enzymes. More interestingly, it was found recently that a genetic variant of ALDH1A2 in human, which is orthologous to mouse Raldh2, was associated with a higher level of umbilical cord blood RA and with a significantly higher newborn kidney volume (22% higher compared to newborns of wild-type Aldh1a2 genotype) [141]. Thus, it is very likely that endogenous RA is indeed the primary retinoid compound in mediating kidney development in rodents and in human.

***Target genes and potential mechanisms of endogenous retinoids in embryonic nephrogenesis***

Kidney morphogenesis is initiated by invasion of ureteric bud into its surrounding mesenchyme, during which signals were transduced into mesenchymal tissues; mesenchymal tissues then differentiate into nephrons and reciprocate by transducing signal back to the ureteric bud to promote branching processes [212]. Various groups had suggested

target genes of RA and the potential mechanisms, by which nephrogenesis is mediated.

One of the most established RA target gene is Ret, a proto-oncogene expressed in the ureteric buds that upon activation by its cognate ligand, glial cell line-derived neurotrophic factor (GDNF), would trigger ureteric bud branching [212]. In 1998, Moreau et al. reported that tRA up-regulated Ret mRNA expression in cultured metanephroi in a dose-dependent manner from 1 nM to 1 $\mu$M [217]. It was later found that there was a marked down-regulation of Ret in kidney of Rara$^{-/-}$ / Rarb2$^{-/-}$ mutant mice [204], and rat embryos of maternal vitamin A deficiency [17]. Of note, forced expression of Ret in the ureteric bud of Rara$^{-/-}$ / Rarb2$^{-/-}$ mutants rescued the kidney developmental defects [17].

Although it is now well accepted that Ret is the target gene of RA, via which kidney development is regulated, the exact mechanism of RA in the regulation of Ret expression remains elusive as functional RARE had not been identified in the 5'-flanking region of Ret promoter [245]. It is thus still a question whether regulation of Ret by RA is mediated via other mechanisms or mediators. It might be possible that Ret contains highly degenerative RARE rather than the well-defined classical RARE and the RARE might lie in regions other than the 5'-flanking region of gene promoter.

Based on the observation that both Rara and Rarb are expressed in the stromal cells, and that Ret is expressed in the ureteric buds, it was initially proposed that the retinoid system controlled yet defined signalling molecule(s) in the stromal cells via RAR$\alpha$/RAR$\beta$, which in turn promotes Ret expression in the ureteric buds either directly or via the surrounding metanephric mesenchyme [17, 204]. However, this proposal was recently revised following a recent publication in GenitoUrinary Development Molecular Anatomy Project (GUDMAP) consortium (http://www.gudmap.org), which reported presence of RAR$\alpha$ and RAR$\beta$ transcripts in the ureteric buds. The revised model proposes that endogenous RA binds to RARs in the ureteric buds and activates RAR-dependent signalling locally leading to Ret expression, either directly or indirectly [267].

Besides Ret, other potential RA target genes that mediate nephrogenesis had also been proposed. These include transcription factors such as the Hox genes and growth factor receptors such as epithelial growth factor receptor, EGFR [102]. More recent reports had added additional candidate genes to this list. Specifically, Vilar et al. observed a consistent down-regulation of midkine, Mdk, in E16-E20 foetal kidney of rats with maternal vitamin A deficiency, and tRA induced Mdk expression in cultured metanephroi [311]. Late-gestation lung protein 1, Lgl1, was also proposed to be another potential target gene of RA during nephrogenesis as tRA increased both Lgl1 mRNA and gene promoter reporter activity in cultured metanephric mesenchymal cells [255].

***A brief summary on the retinoid system in embryonic nephrogenesis***

A brief summary of the retinoid system in embryonic nephrogenesis is as follow:

1. Endogenous RA rather than its precursors or metabolites is the primary, if not the only, endogenous retinoid compound that mediates kidney development.

2. Rdh10, Raldh2, Raldh3 (to a lesser extent), and Cyp26a1 are believed to be the primary enzymes actively involved in the exquisite control of endogenous RA level.

3. The canonical signalling, which involves retinoid nuclear receptor-mediated signalling, is essential.

4. Endogenous RA is synthesised mainly in the stromal cells, which was then secreted to ureteric buds to bind and activate the RARs; RAR-dependent signalling in ureteric bud maintains Ret expression, either directly or indirectly.

5. Ret is by far the best characterised target gene of RA in the ureteric buds that mediates nephrogenesis although functional RARE had not been identified in the promoter region of Ret.

### 1.2.2 The retinoid system in kidneys after birth

As opposed to the well-established role of endogenous RA in nephrogenesis, relatively little is known about the role of endogenous RA in kidneys after birth. This is in part due to the early lethality following germline deletions of members of the retinoid system, precluding investigation into anomalies that may arise later during post-natal development and adulthood. However, studies that reported symptoms of post-natal vitamin A deficiency, as well as reports on the expression of members of the retinoid system and their alterations in the advent of kidney pathogenesis had provided some valuable insights into the potential roles of endogenous RA in the kidney after birth.

***Post-natal vitamin A deficiency and associated renal anomalies***

The lack of apparent histological abnormality in the kidney parenchymal tissues following post-natal vitamin A deficiency reported during mid 1920s, argues against endogenous RA playing a crucial role in maintaining renal epithelial tissue integrity [106, 325]. However, functional defects of kidney and other anomalies, including an increased susceptibility towards certain challenges, were reported as early as 1917. A summary of major experimental findings in murine models subjected to post-natal vitamin A deficiency is shown in Table 1.4.

Table 1.4: Anomalies associated with or originated from kidney of rodents fed a vitamin A deficient (VAD) diet. Shown here are major findings/observations found at a higher incidence in groups fed a VAD diet compared to control group.

| **Major findings/observations** | **Notes** | **Year** | **Reference** |
|---|---|---|---|
| Calculi of calcium phosphates and/or magnesium phosphates in kidney or bladder | Symptoms were associated to fat-soluble vitamins rather than vitamin A *per se* | 1917 | [239] |
| Calculi of calcium phosphate and oxalate in renal pelvis and bladder; calcium deposits in kidney | Calculi of phosphate were more than oxalate and their presence was higher in pelvis than in bladder | 1927 | [307] |
| Kidney infection; multiple small foci in kidney cortex | Stone was rare in kidney but was frequent in bladder | 1928 | [113] |
| Kidney pelvis filled with granular opaque mass made of desquamated cells | Calculus in renal pelvis was found in one case | 1931 | [326] |
| Urinary calculi, urinary infection, and alkalinuria | Addition of vitamin A caused disintegration of calculi | 1935 | [122] |
| Enlarged kidneys filled with white opaque mass; kidneys lost well-defined structure; renal pelvic epithelium keratinisation and calcification; acute pyelonephritis | Pathological changes in kidney were observed in 80% of mice with vitamin A deficiency | 1952 | [201] |

| Major findings/observations | Notes | Year | Reference |
|---|---|---|---|
| Superficial nodules in mitochondrial zone of proximal convoluted tubular cells | Lower renal RoI was verified; nodules were hard, greyish green, and comprised of neutral fat | 1957 | [120] |
| Kidney degeneration; focal tubular necrosis; tubular calcification and hydronephrosis in germ-free rats | Non-germ-free rats fed a VAD diet, instead of germ-free rats fed a vitamin A sufficient diet, was used as control | 1961 | [18] |
| A decrease in urinary calcium level that was restored with vitamin A supplementation | Presented within two weeks after initiating VAD diet | 1972 | [342] |
| A decrease in urine volume and glomerular filtration rate | No difference compared to control when normalised to body weight | 1976 | [189] |
| Bladder stones with or without renal stones | Calculi were formed when lactose was the source of carbohydrate | 1981 | [96] |
| Alterations in cytokeratin expression in renal pelvic epithelium | Cytokeratin alteration preceded histological abnormalities | 1992 | [101] |

| Major findings/observations | Notes | Year | Reference |
|---|---|---|---|
| Thickening of tubular and glomerular basement; an increase in TNF-$\alpha$ protein; a decrease in MMP2 and MMP9 protein; an altered composition of collagen IV at transcript and protein levels | Lower renal RoI was verified; lactating mothers were subjected to VAD diet from first day of delivery, and pups were weaned onto the same VAD diet for an additional 4 weeks | 2005 | [192] |
| Bacterial pyelonephritis with inflammation extended into medulla and cortex; urolithiasis | Observations were found in rats accidentally fed a VAD diet and thus no control group available for comparison | 2009 | [219] |
| Higher ratio of inorganic phosphate to creatinine in urine; lower inorganic phosphate uptake and lower expression of Npt2a and Npt2c in brush-border membrane vesicles derived from proximal tubules | Npt2a and Npt2c are sodium-dependent phosphate co-transporters involved in inorganic phosphate uptake from kidney | 2010 | [195] |
| Fewer number of nephrons; an increase in Apo-B100 expression and a decrease in ABCA1 expression; an increase in glomerular and interstitial TGF-$\beta$1 | Lower renal RoI was verified; Apo-B100 and ABCA1 are genes involved in lipid homeostasis; pregnant mothers were subjected to VAD diet, and offsprings were fed the similar VAD diet for 8 weeks | 2010 | [330] |

While there seems to be a large number of reports that associate post-natal vitamin A deficiency to anomalies in the kidney, these studies are not without caveats. For instance, retinoid profile in kidney was not established in some of the studies while some studies did not use appropriate control. In addition, some of these studies involved limiting vitamin A supply prior to weaning and during gestation, hence the anomalies observed may reflect a defect in pre- and post-natal kidney development. Taken together, while an association has been made, a clear cause-and-effect relationship between post-natal vitamin A deficiency and anomalies in the kidney remains to be established.

Besides reports from experimental murine models, post-natal vitamin A deficiency in farm animals and in clinical subjects had also been reported. Specifically, VAD farm animals were associated with polyuria and an increased incidence of urolithiasis [316,324]; clinical subjects with post-natal vitamin A deficiency were more susceptible towards urolithiasis [135]. Taken together, conditions such as urolithiasis that are often associated with urinary metabolite imbalance and kidney calcification, kidney/urinary infections, and renal pelvic epithelium keratinisation, are conditions most commonly reported since 1900s in rodents, farm animals, and human.

In the beginning of the millennium, several groups had started to explore the association between post-natal vitamin A deficiency and gene expression, and the potential link between the dysregulated gene expression and functional outcome. Establishing target genes of endogenous RA in the kidney should better define the role of retinoid system in the kidney after birth, and provide a better cause-and-effect link between post-natal vitamin A deficiency and the aforementioned anomalies.

***Bioactive RA in the kidney: a product of local synthesis?***

The presence of endogenous RA has been well documented in healthy murine kidney, with tRA being the most abundant isomer detected [137,139,277,286,328]. The source of renal tRA has not been investigated in detail but multiple mechanisms seem to be in-

volved in this regard. Specifically, renal uptake of retinyl ester and Rol [108,246], as well as tRA [157] were documented. Interestingly, Stra6 expression was found to be abundant in the developing mouse kidney from E12.5 and continue to be highly expressed until adulthood [31], which may facilitate uptake of RBP-bound Rol. In addition, renal proximal tubules are known to reabsorb RBP-bound Rol that was filtered through glomeruli, via endocytic receptor, Megalin [46].

The kidney also seems poised for a local biosynthesis of tRA by expressing enzymes involved in retinoid metabolism. Ang et al. reported the presence of Adh1 mRNA in adult mouse kidney, localised to the medullary rays and collecting ducts [7]. It was later found that both Adh1 and Adh3 protein [57, 58, 118], as well as Rdh1 transcript [335] were detected in adult mouse kidney but their localisation was not commented. Besides Rol dehydrogenases, Raldh1 and Raldh3 transcripts were detected in post-natal and adult kidney at a high level, concentrating in the outer medulla and inner medulla, respectively [232]; Alnouti et al. described the presence of Raldh2 and Raldh3 but not Raldh1 transcripts in adult mouse kidney [4]; Lin et al. described the expression of Raldh1 and Raldh2 proteins in the cortex and medulla, and Raldh4 protein in the cortex of adult mouse kidney [177]. As for metabolising enzymes of RA, Cyp26a1 transcript was detected at a high level in adult mouse liver, but was not detected in the kidney [45, 258]; Cyp26b1 expression was reported in rat only at birth and at post-natal day 4, localised to the cortical ureteric bud end and the associating collecting ducts [194]; expression of Cyp26c1 was not as well established in adult mouse kidney.

It is clear from the aforementioned studies that a detailed description and unequivocal consensus on the presence and localisation of enzymes involved in retinoid metabolism in the kidney after birth has not been achieved. More importantly, since kidney-specific knockout of these enzymes had not been established, their roles in determining the endogenous RA supply in the kidney under normal physiological condition remain to be established.

***RARs and RXRs in kidney***

To date, a systematic analysis examining protein expression of all known isotypes and isoforms of RAR and RXR in healthy kidney after birth is lacking. This might be due to the fact that antibodies with good selectivity and sensitivity in detecting all the RARs and RXRs are not readily available. However, according to datasets generated by the Nuclear Receptor Signaling Atlas (NURSA) consortium (www.nursa.org/10.1621/datasets.02001; last accessed on 30.07.2011), transcript of all six retinoid nuclear receptor isotypes, namely, Rara, Rarb, Rarg, Rxra, Rxrb, and Rxrg were detected in adult kidney of two strains of mice, C57Bl/6J and 129x1/SvJ (results derived from 38 mice).

***Alteration of endogenous retinoid metabolism in experimental models of kidney diseases***

An altered profile of retinoid system, including the level of tRA, expression of Raldhs and retinoid nuclear receptors, as well as a few well-established RA target genes, has been reported in a number of experimental models of kidney disease, such as puromycin-associated nephropathy [291], glomerulonephritis [176], Alb/TGF-$\beta$1 transgenic mice, a kidney fibrosis model characterised by an over-expression of transforming growth factor-$\beta$1 [328], diabetic nephropathy [286], and HIV-associated nephropathy [256]. More importantly, in cases where endogenous RA was reduced, supplementation of exogenous RA were found to halt disease progression in certain disease models [256, 291] but further worsened disease progression in other [328].

Taken together, while these reports might suggest an active participation of RA and the retinoid system in modulating disease progression, the paradoxical outcomes of exogenous RA supplementation complicate the interpretation of RA effects. Perhaps a non-specific administration of exogenous RA might not be of advantage in all cases where endogenous RA was reduced. A direct cause-and-effect relationship between disease progression and an alteration of endogenous retinoid system remains to be further eluci-

dated.

***A brief summary on the retinoid system in kidneys after birth***

The source of endogenous tRA detected in mouse kidney, whether it is a product of local biosynthesis or whether it is taken up directly from the circulation, remains unclear. Nevertheless, the presence of endogenous tRA together with all known isotypes of RARs and RXRs in healthy kidneys suggests the presence of constitutively active retinoid canonical signalling. If this is indeed the case, then the renal-associated anomalies observed during post-natal vitamin A deficiency might be at least partially explained by an attenuated RA canonical signalling, which leads to gene expression dysregulation.

## 1.3 Aims of this project

Existing evidence supports the presence of an inbuilt system in healthy murine kidneys for retinoid synthesis and metabolism, as well as the expression of retinoid nuclear receptors that are key components to support RA canonical signalling. In addition, tRA, the most physiological relevant bioactive retinoids, was reported to be present in the kidney. Thus, it is hypothesised that an RAR-dependent transcriptional activity of endogenous RA is present in the kidney after birth, to regulate gene expression.

In order to address this hypothesis, this project was designed to answer the following questions:

1. Given that all known isotypes of RARs and RXRs, as well as tRA are found in healthy kidneys, is there a direct evidence of constitutively active retinoid nuclear receptor-mediated RA canonical signalling?
2. If the canonical signalling is indeed present, does it have a temporospatial-specific pattern?
3. What are the target genes of canonical signalling of endogenous retinoids in the cell type(s) identified in (**2**)?

# Chapter 2

# General Materials and Methods

---

This chapter describes the general materials and methods used for all laboratory work. Specific protocols and procedures applicable only to specific chapters are described in the individual chapter.

## 2.1 Buffers, solutions, and reagents

All buffers, solutions, and reagents were prepared following the recipes and protocols stated below. Ultrapure water dispensed from a Maxima USF Alga machine was used for dilution and dissolution of reagents, a Metler toledo AB204-S weighing balance was used for weighing chemical reagents, a Stuart CB161 magnetic stirrer (with Fisher Brand® magnetic stir bar) and a Grant Bio PV-1 vortex mixer were used for mixing purpose, a Metler toledo 340 pH meter was used for pH measurement.

All buffers, solutions, and reagents were stored at room temperature in laboratory standard glass bottles, unless stated otherwise. Suppliers of chemical reagents are listed in Table 2.1.

### 2.1.1 Acid and alkaline solutions for pH adjustment

**1 M Hydrochloric acid**

| | |
|---|---|
| 5 M Hydrochloric acid | 20 ml |
| Ultrapure water | 80 ml |

Eighty millilitre of ultrapure water was first measured into a glass bottle, after which 20 ml of 5 M hydrochloric acid was pipetted and gently added into the water. Solution was mixed well by gentle swirling.

**0.5 M Hydrochloric acid**

| | |
|---|---|
| 1 M Hydrochloric acid | 50 ml |
| Ultrapure water | 50 ml |

Fifty millilitre of ultrapure water was first measured into a glass bottle, after which 50 ml of 1 M hydrochloric acid was pipetted and gently added into the water. Solution was mixed well by gentle swirling.

**1 M Sodium hydroxide**

| | |
|---|---|
| Sodium hydroxide | 4 g |
| Ultrapure water | To a final volume of 100 ml |

Eighty millilitre of ultrapure water was first measured into a glass bottle, after which 4 g of sodium hydroxide was weighed out and added into the water with gentle stirring on a magnetic stirrer. Ultrapure water was then added to a final volume of 100 ml after sodium hydroxide was completely dissolved.

### 2.1.2 Buffers and solutions for general use

**10x Phosphate-buffered saline (PBS), pH 7.4**

**(*1.37 M NaCl, 27 mM KCl, 81 mM $Na_2HPO_4.2H_2O$, 17.6 mM $KH_2PO_4$*)**

| | |
|---|---|
| Sodium chloride | 80 g |
| Potassium chloride | 2 g |
| Disodium hydrogen phosphate dihydrate | 14.4 g |
| Potassium dihydrogen phosphate | 2.4 g |
| Ultrapure water | To a final volume of 1 L |

Eight hundred millilitre of ultrapure water was first measured into a glass bottle, after which all reagents were weighed out and added into the water with gentle stirring on a magnetic stirrer. pH was adjusted to 7.4 using 1 M sodium hydroxide or 1 M hydrochloric acid after all reagents were completely dissolved. Ultrapure water was then added to a final volume of 1 L.

**1x PBS, pH 7.4**

**(*137 mM NaCl, 2.7 mM KCl, 8.1 mM $Na_2HPO_4.2H_2O$, 1.76 mM $KH_2PO_4$*)**

| | |
|---|---|
| 10x PBS | 200 ml |
| Ultrapure water | 1.8 L |

Two hundred millilitre of 10x PBS and 1.8 L of ultrapure water were measured into a glass bottle, and the solution was mixed well by inverting the bottle.

**0.1 % Tween® 20 in 1x PBS (0.1 % PBST)**

| | |
|---|---|
| Tween® 20 | 2 ml |
| 1x PBS | 2 L |

Two litre of 1x PBS was first measured into a glass bottle, after which 2 ml of Tween® 20 was pipetted directly into the PBS. Solution was mixed well by shaking the bottle vigorously.

**1.5 M Tris, pH 8.0**

| | |
|---|---|
| Tris | 181.71 g |
| Ultrapure water | To a final volume of 1 L |

Eight hundred millilitre of ultrapure water was first measured into a glass bottle, after which tris was weighed out and added into the water with gentle stirring on a magnetic stirrer. pH was adjusted to 8.0 using 5 M hydrochloric acid after tris was completely dissolved. Ultrapure water was then added to a final volume of 1 L.

**100 mM Ethylenediaminetetraacetic acid (EDTA), pH 8.0**

| | |
|---|---|
| EDTA disodium salt dihydrate | 1.861 g |
| Ultrapure water | To a final volume of 50 ml |

Forty millilitre of ultrapure water was first measured into a conical tube, after which 1.861 g of EDTA was weighed out and added into the water. The solution was mixed briefly by gentle vortexing. pH was adjusted to 8.0 using 1 M sodium hydroxide (a pH value of 8.0 was required for complete dissolution). Ultrapure water was then added to a final volume of 50 ml and the solution was sonicated until complete dissolution was achieved. Aliquots of 1 ml was prepared and stored at -20 °C.

### 2.1.3 Buffers and solutions for cell staining

**0.01 M Citric acid buffer, pH 6.0**

| | |
|---|---|
| Citric acid monohydrate | 2.1 g |
| Ultrapure water | To a final volume of 1.5 L |

One litre of ultrapure water was first measured into a glass bottle, after which citric acid monohydrate was weighed out and added into the water with gentle stirring on a magnetic stirrer. pH was adjusted to 6.0 using 1 M sodium hydroxide after citric acid monohydrate was completely dissolved. Ultrapure water was then added to a final volume of 1.5 L.

**Note:** After being used once for antigen retrieval, citric acid buffer was cooled to room temperature and stored in a glass bottle at room temperature. The solution was re-used

once, after which fresh buffer was prepared.

**0.1 M Glycine in 1x PBS**

| | |
|---|---|
| Glycine | 0.075 g |
| 1x PBS | 10 ml |

Ten millilitre of 1x PBS was first measured into a conical tube, after which 0.075 g of glycine was weighed out and added into the PBS. Solution was then mixed well by gentle vortexing until glycine was completely dissolved. Solution was prepared fresh before use.

**1% Bovine serum albumin (BSA) in 1x PBS**

| | |
|---|---|
| BSA | 0.1 g |
| 1x PBS | 10 ml |

Ten millilitre of 1x PBS was first measured into a conical tube, after which 0.1 g of BSA was weighed out and added into the PBS. Solution was then mixed well by gentle vortexing until BSA was completely dissolved. Solution was prepared fresh before use.

**Ice-cold 10% formalin in 1x PBS**

| | |
|---|---|
| 100% Formalin | 5 ml |
| 1x PBS | 45 ml |

Forty-five millilitre of 1x PBS was first measure into a 50 ml conical tube, after which 5 ml of 100% formalin was pipetted and added into the PBS. Solution was mixed well by inverting the conical tube and kept on ice until use.

**Note:** Handling of formalin was performed in a fumigated hood and the solution was prepared fresh before use.

**Ice-cold 5% formalin in 1x PBS**

| | |
|---|---|
| 100% Formalin | 1 ml |
| 1x PBS | 19 ml |

Nineteen millilitre of 1x PBS was first measure into a 50 ml conical tube, after which 1 ml of 100% formalin was pipetted and added into the PBS. Solution was mixed well by inverting the conical tube and kept on ice until use.

**Note:** Handling of formalin was performed in a fumigated hood and the solution was prepared fresh before use.

**5% Formalin and 0.2% glutaraldehyde in 1x PBS**

| | |
|---|---|
| 100% Formalin | 1 ml |
| 25% Glutaraldehyde | 160 $\mu$l |
| 1x PBS | To a final volume of 20 ml |

Seventeen millilitre of 1x PBS was first measure into a 50 ml conical tube, after which 1 ml of 100% formalin and 160 $\mu$l were pipetted and added into the PBS. PBS was then added to a final volume of 20 ml. Solution was mixed well by inverting the conical tube.

**Note:** Handling of formalin and glutaraldehyde was performed in a fumigated hood and the solution was prepared fresh before use.

**0.1% Triton X-100 in 1x PBS**

| | |
|---|---|
| Triton X-100 | 10 $\mu$l |
| 1x PBS | 10 ml |

Ten millilitre of 1x PBS was first measured into a conical tube, after which 10 $\mu$l of Triton X-100 was pipetted and added into the PBS. Solution was then mixed well by gentle vortexing. Solution was prepared fresh before use.

### 2.1.4 Buffers and solutions for X-gal histochemistry and cytochemistry

**X-gal dilution buffer**

**(*5 mM $K_3Fe(CN)_6$, 5 mM $K_4Fe(CN)_6.3H_2O$, 2 mM $MgCl_2$*)**

| | |
|---|---|
| Magnesium chloride | 0.01 g |
| Potassium ferricyanide cystalline | 0.08 g |
| Potassium ferrocyanide trihydrate | 0.105 g |
| 1x PBS | To a final volume of 50 ml |

Forty millilitre of 1x PBS was first measured into a conical tube, after which all reagents were weighed out and added into the PBS. Solution was mixed well by gentle vortexing. PBS was then added to a final volume of 50 ml.

**Note:** The prepared X-gal dilution buffer was then wrapped in aluminium foil and stored at 4 °C to a maximum of four weeks prior to use.

**X-gal staining solution (1 mg/ml X-gal)**

| | |
|---|---|
| X-gal stock solution (50 mg/ml) | 1 ml |
| X-gal dilution buffer | 49 ml |

Forty-nine millilitre of X-gal dilution buffer was first measured into a conical tube and pre-warmed in water bath to 37 °C before 1 ml of X-gal stock solution was added. X-gal staining solution was prepared fresh before use.

### 2.1.5 Buffers and solutions for plasmid preparation

**3 M Sodium acetate**

| | |
|---|---|
| Sodium acetate | 4.08 g |
| Ultrapure water | 10 ml |

Five millilitre of ultrapure water was first measured into a conical tube, after which sodium acetate was weighed out and added into the water. The solution was mixed well by gentle vortexing. Ultrapure water was then added to a final volume of 10 ml and was stored at 4 °C until use.

**Ice-cold 70% ethanol**

| | |
|---|---|
| 100% Ethanol | 7 ml |
| Ultrapure water | 3 ml |

Seven millilitre of 100% ethanol and 3 ml of ultrapure water were measured into a conical tube. Solution was mixed well by inverting the tube and stored at -20 °C until use.

**Tris-EDTA (TE) buffer (sterile), pH 8.0**

**(*10 mM Tris, 1 mM EDTA*)**

| | |
|---|---|
| 1.5 M Tris | 100 $\mu$l |
| 100 mM EDTA | 150 $\mu$l |
| Ultrapure water | To a final volume of 15 ml |

Fourteen millilitre of ultrapure water was first measured into a conical tube, after which 1.5 M tris and 100 mM EDTA were pipetted and added into the water. pH was adjusted to 8.0 using a few drops of 0.5 M hydrochloric acid. Solution was then filter-sterilised into a sterile conical tube using a Whatman® Puradisc™ 25 syringe filter.

Table 2.1: Suppliers of chemical reagents. ***Suppliers**: Hayman: Hayman Ltd., Essex, UK; Merck: Merck Chemicals Ltd., Nottingham, UK; Promega: Promega UK, Southampton, UK; S-A: Sigma-Aldrich Company Ltd., Dorset, UK; VWR: VWR International Ltd., Leicestershire, UK.

| **Reagents** | ***Suppliers** |
|---|---|
| Bovine serum albumin | S-A |
| Citric acid monohydrate | VWR |
| Disodium hydrogen phosphate dihydrate | VWR |
| Ethylenediaminetetraacetic acid disodium salt dihydrate | S-A |
| Ethanol | Hayman |
| 100% Formalin | S-A |
| 25% Glutaraldehyde | S-A |
| Glycine | Merck |
| Hydrochloric acid (5 M) | VWR |
| Magnesium chloride | S-A |
| Potassium chloride | VWR |
| Potassium dihydrogen phosphate | VWR |
| Potassium ferricyanide crystalline | S-A |
| Potassium ferrocyanide trihydrate | S-A |
| Sodium acetate | S-A |
| Sodium chloride | S-A |
| Sodium hydroxide | S-A |
| Tris | VWR |
| Triton X-100 | S-A |
| Tween® 20 | S-A |
| X-gal stock solution (50 mg/ml in dimethylformamide) | Promega |

## 2.2 Cell culture

The mouse inner medullary cell line, mIMCD-3, was obtained from LGC Standards, Middlesex, UK at passage (P) 11. The P11 cells were reassigned as P1 upon receipt at King's College London and were stored in liquid nitrogen tank in the original cryotube supplied by LGC Standards. In order to propagate mIMCD-3 cells for storage and future use, cells were brought out of liquid nitrogen and thawed in water bath at 37 °C. Thawed cells were then immediately plated on a 75 $cm^2$ tissue culture flask containing DMEM-F12 culture medium with penicillin (100 IU/ml), streptomycin (100 $\mu$g/ml), and amphotericin B (2.5 $\mu$g/ml), supplemented with 5% foetal bovine serum (FBS), which were pre-warmed and equilibrated with $CO_2$ for at least 15 min in a Techne incubator. Tissue culture medium, antibiotics, and FBS were from PAA Laboratories Ltd., Somerset, UK, and amphotericin B was from Invitrogen Ltd., Paisley, UK.

Cells were routinely cultured in a Techne incubator (with a setting of 37 °C and 5% $CO_2$). For passaging cells, adherent cells were first washed twice with PBS and incubated in 2 ml trypsin (0.5 mg/ml)-EDTA (0.22 mg/ml) (PAA Laboratories Ltd., UK) for 3 min at 37 °C. Complete trypsinisation was confirmed by examining the cells under microscope. Eight millilitre of culture medium was then added to the trypsinised cells and cells were titurated up and down a few times to break up cell clumps. Cells were passaged when near confluent at a ratio of 1:4 to 1:8 as recommended by LGC Standards.

In order to store cells for future use, cells were trypsinised and resuspended in culture medium as described before, after which cell number was counted using hemocytometer. Cell suspension was then centrifuged for 5 min at 328 g at 25 °C. Cell pellet was resuspended in 95% culturing medium and 5% dimethly sulfoxide (DMSO, Sigma-Aldrich Company Ltd., UK) to a final concentration of $1x10^6$ cells/ml, and 1 ml cell suspension was pipetted into each pre-labled cryotube. Cryotubes were then wrapped in multiple layers of paper towel, placed in a well-insulated polystyrene box, and kept at -80 °C overnight before being transferred into the liquid nitrogen tank. Cells at P2 and

P3 were stored. All tissue culture flasks and dishes were from Falcon (Marathon Laboratory Supplies, London, UK), and pipette tips were from Starlab (UK) Ltd., Milton Keynes, UK.

### 2.2.1 Reagents used for cell treatment

***tRA***

Stock solution of tRA (Sigma-Aldrich Company Ltd., UK) was prepared by dissolving the powder in 100% ethanol to a stock concentration of 10 mM (prepared by Dr. Q Xu). Aliquots of 40 $\mu$l 10 mM tRA solution were prepared in 500 $\mu$l microtubes, wrapped individually in aluminium foil, and sealed with Parafilm® (Starlab (UK) Ltd., UK). Aliquots were then stored at -80 °C.

Following prolonged storage at -80 °C , tRA precipitated out of ethanol forming a yellow colour precipitant. Thus, before using, aliquots of tRA were vortex-mixed briefly, and were warmed to 37 °C for about 15 min, with vortex-mixing in between, to redissolve the precipitant. Please note that prolonged vortex-mixing might increase the risk of tRA being oxidised.

***Antagonists of RARs***

Two antagonists of RARs were used in this project: (i) AGN193109, an antagonist of RAR$\alpha$, RAR$\beta$, and RAR$\gamma$ [134] (a kind gift from Allergan Pharmaceuticals, Irvine, California, USA), and (ii) BMS189453, an antagonist of RAR$\alpha$ and RAR$\gamma$, and a mixed agonist/antagonist of RAR$\beta$ [43] (a kind gift from Dr. J Corcoran at King's College London Wolfson Centre for Age Related Diseases).

Stock solution of AGN193109 was dissolved in DMSO to a concentration of 2 mM (prepared by Dr. Q Xu). Aliquots of 40 $\mu$l 2 mM AGN193109 solution were prepared in 500 $\mu$l microtubes, wrapped individually in aluminium foil, and stored at -80 °C. Stock solution of BMS189453 was dissolved in DMSO to a concentration of 1 mM (prepared

by Dr. J Corcoran). Aliquots of 40 $\mu$l 1 mM BMS189453 solution were prepared in 500 $\mu$l microtubes and stored at -80 °C (prepared by Dr. A Rankin).

***Inhibitors of RA synthesising enzymes***

Two inhibitors of retinoic acid synthesising enzymes were used in this project: (i) 4-(diethylamino)benzaldehyde (DEAB) [272], reconstituted in DMSO to a concentration of 25 mM, and (ii) tetraethylthiuram disulfide (also known as disulfiram) [75], reconstituted in DMSO to a concentration of 10 mM. Both DEAB and disulfiram were purchased from Sigma-Aldrich Company Ltd., UK. Aliquots of 40 $\mu$l 25 mM DEAB solution and 40 $\mu$l 10 mM disulfiram were prepared in 500 $\mu$l microtubes and stored at -80 °C.

## 2.3 Microscopy and digital imaging

All microscopic examinations were performed on a Nikon Eclipse TE2000-S epifluorescence microscope equipped with a mercury arc lamp and a standard RGB (FITC, G-2A, and UV-2A) filter wheel. Signal of AlexaFluor 488 (absorption max: 496 nm, emission max: 519 nm) was examined with the FITC filter, AlexaFluor 555 (absorption max: 555 nm, emission max: 565 nm) and AlexaFluor 568 (absorption max: 578 nm, emission max: 603 nm) was examined with the G-2A filter, and 4',6'-diamidino-2-phenylindole (DAPI; absorption max: 358 nm, emission max: 461 nm) was examined with the UV-2A filter.

In order to differentiate specific fluorescence signal from that given rise by non-specific staining, tissue sections or cells stained with non-immune IgG were first examined, and the exposure time was adjusted until only background signal was barely observed. Using the same exposure time, sections or cells stained with corresponding antibodies were then examined. Signals beyond the background signal on the non-immune IgG-stained sections/cells were deemed genuine signal given rise by antibody-antigen binding. Images were captured with a DXM1200F Nikon digital camera using the NIS-element software. The images were then processed and merged with Adobe® Photoshop®.

# Chapter 3

# Constitutive Retinoic Acid Response Element Activity in Mouse Kidney Collecting Ducts

---

## 3.1 Introduction

The project started off with examining the presence and temporospatial localisation of RARE activity in healthy kidney using reporter mice. This chapter describes the observation of a constitutively active RARE activity in healthy kidney and its predominant localisation in the renal collecting ducts.

Detection and localisation of RA pose great challenge to researches. Specifically, given that RA is not a nucleotide-based molecule and is non-immunogenic on its own, classical techniques such as *in situ* hybridisation and immunohistochemistry cannot be applied to detect RA. While HPLC-based assay represents the gold standard in quantifying RA, localising bioactive RA at the tissue or cellular level requires a robust and efficient method of isolating samples containing specific populations of tissues/cells, as well as a highly sensitive HPLC-based assay.

Localising RA synthesising enzymes may provide clues on site of endogenous RA pro-

duction. However, the presence of multiple synthesising enzymes of RA makes localisation of individual enzyme difficult. Moreover, there is still a big knowledge gap in the predominant enzyme(s) involve in biosynthesis of RA and the potential functional redundancy among them. In addition, since RA steady state is also governed by the Cyp26a1-c1 enzymes, their expressions have to be taken into account. Equally important is that existing evidence suggests RA can be delivered from adjacent tissues and circulation in a paracrine and autocrine manner [67, 157, 231].

There had been attempts in the past to generate antibodies recognising RA, by conjugating a larger protein to RA to confer immunogenic property to this small molecule [297, 341]. However, the antibody was found to also react towards Rol and Ral [297], as well as towards retinoid esters, $\beta$-carotene, and other polar derivatives of RA, especially the -oxo derivatives [341].

In order to get better insights on the actual sites of endogenous RA exerting its effect, it would be more meaningful to determine not only the presence of RA *per se* but also the presence of retinoid nuclear receptors. However, since there are multiple RA receptor isotypes and they function as heterodimers, examining the concomitant presence of individual receptor and RA would be arduous. More importantly, the concomitant presence of both RA and retinoid nuclear receptors does not necessarily mean that the receptors are constitutively activated by RA, unless proven otherwise.

In the early 90s, the use of transgenic mice as reporters of endogenous RA activity had been introduced by several groups. These reporter mice harbour a reporter transgene containing RARE cloned into heterologous promoters to drive the expression of bacteria derived-*lacZ* gene. For example, *RARE-TKpr-lacZ* mice, which the expression of reporter transgene was driven by the herpes simplex virus thymidine kinase promoter [11], and the *RARE-hsp68-lacZ* mice, which the expression of reporter transgene was driven by the *hsp68* minimal promoter [266]. There are also transgenic mice that the expres-

sion of reporter transgene is driven by natural RARE-containing regulatory elements in the promoter of RAR$\beta$2 [207, 262]. Expression of reporter transgene in these mice were found to largely overlap with the expression of endogenous RAR$\beta$2 [207, 262], hence representing reporter for presence and activation of RAR$\beta$2. More recently, other reporter mice of RA activity were described. In a crossed bred of *RARE-hsp68-lacZ-cre* and ROSA26R mice, cells would be permanently labelled in the presence of RA, therefore representing a more sensitive method to detect transient presence of RA activity [61]. However, the permanent labelling of the cells will not allow dynamic monitoring of RA activity. The use of DR5-luciferase reporter mice were also recently reported, which has the advantage of allowing dynamic monitoring of RA activity without the need of sacrificing animals [250].

### 3.1.1 *RARE-hsp68-lacZ* transgenic mice

The *RARE-hsp68-lacZ* transgenic mice [266], herein referred as transgenic mice, were used in this project. This model was chosen as it has been widely employed since its establishment, particularly in examining RA activity in developing embryos, some of which has been presented in Chapter 1 [69, 76, 198, 199, 208, 209, 211, 216, 230, 234, 273, 274, 306, 331]. More importantly, these mice had been used to describe endogenous RA activity in developing kidneys [235, 267] and in the thymus after birth [149].

The transgenic mice harbour a transgene that contains 32-bp oligonucleotides defining three copies of RARE derived from RAR$\beta$, which is placed upstream of a mouse *hsp68* minimal promoter that does not contain sequences determining site-specific expression [150], to drive the expression of a *lacZ* reporter gene derived from *E. coli* [266]. In cells where RXR/RAR heterodimers were activated by ligands such as RA, co-activators will be recruited to the RARE on the transgene resulting in expression of $\beta$-galactosidase ($\beta$-gal) protein encoded by the *lacZ* reporter gene. $\beta$-gal protein expression can then be determined by performing an X-gal (5-bromo-4-chloro-3-indolyl-$\beta$-D-galactopyranoside) assay (Figure 3.1) and by immunostaining.

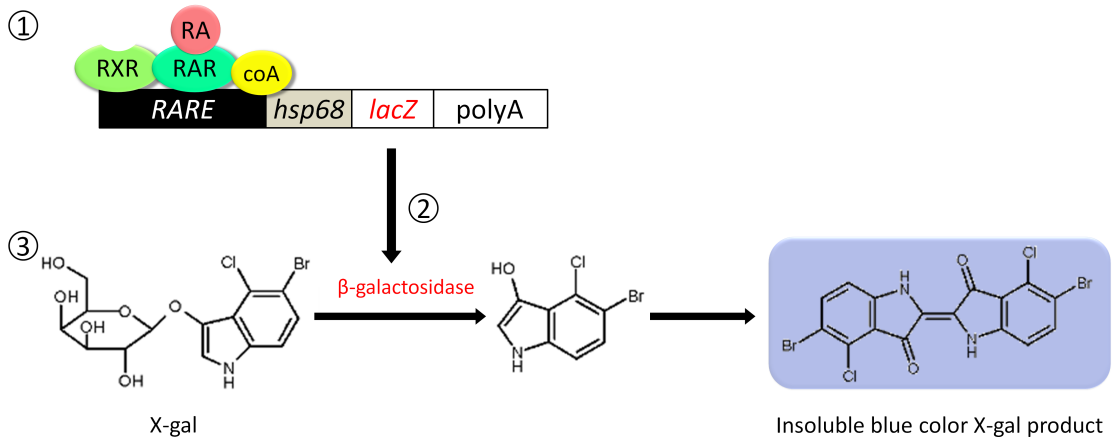


Figure 3.1: Reporter transgene activation and X-gal enzymatic reaction. In the presence of functional RXR/RAR heterodimer and their putative ligands such as RA, transcriptional co-activators will be recruited to the *RARE* (**1**), leading to activation of the *lacZ* reporter gene producing $\beta$-galactosidase protein (**2**). By performing an X-gal assay, $\beta$-galactosidase oxidised X-gal (5-bromo-4-chloro-3-indolyl-$\beta$-D-galactopyranoside) into insoluble blue X-gal product (5,5'-dibromo-4,4'-dichloro-1H,1'H-(2,2')biindolylidene-3,3'-dione) (**3**). Note that the construct of transgene is not drawn to scale and *lacZ* transgene was driven by a minimal *hsp68* promoter rather than a full *hsp68* promoter. coA: transcriptional co-activators; RA: retinoic acid; RXR: retinoic acid X receptor; RAR: retinoic acid receptor.

In view of the complexity of RA signalling involving both canonical and non-canonical pathways, "RARE activity" would be used to describe the expression of reporter transgene. In order to have better insights on the temporospatial pattern of reporter transgene activation, kidneys from 1-, 2-, 3-, 5-, and 8-week-old mice were examined; livers, known to be the major storage of retinoids, were examined alongside kidneys. When indicated, tissues from wild-type mice and transgenic mice were examined concurrently to differentiate endogenous $\beta$-gal from transgenic $\beta$-gal. X-gal signal observed in tissues of both wild-type and transgenic mice was attributed to background signal given rise by endogenous $\beta$-gal activity; X-gal signal that was detected only in tissues of transgenic mice was considered as specific induction of reporter transgene (Figure 3.2).

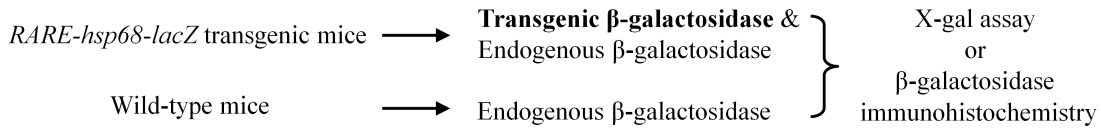


Figure 3.2: Endogenous $\beta$-galactosidase and transgenic $\beta$-galactosidase. Wild-type mice served as control to differentiate endogenous $\beta$-galactosidase from transgenic $\beta$-galactosidase.

## 3.2 Materials and methods

### 3.2.1 Animals

Both transgenic and wild-type mice were fed a standard chow and maintained at the animal facilities at Biological Services, Institute of Child Health (ICH), University College London. The transgenic mice, which were originally established on an outbred CD-1 background, had been bred onto a C57BL/6 background for at least four generations upon arrival at ICH. Animal handling, including animal housing and care, animal sacrifice, and harvest of kidneys and livers were performed by Dr. C Roberts at ICH.

### 3.2.2 Tissue preparation

Tissues from 7-16 mice in each age group were obtained. Kidneys and livers were cut transversely into halves, of which half was subjected to wholemount X-gal assay. The remaining half was divided further into two quarters, to be processed for paraffin sections and cryosections, respectively.

***Tissue preparation for cryosectioning***

Freshly harvested tissue was first submerged in 30% sucrose (Sigma-Aldrich Company Ltd., UK) in ultrapure water overnight at 4 °C, which is a dehydration step to prevent ice crystal artefact in cryosections and to minimise fracturing during cryosectioning. The tissue was then submerged in a mixture of 30% sucrose in water and Optimum Cutting Temperature (OCT) compound (VWR International Ltd., UK) at a ratio of 1:1 for 2 h at 4 °C, before being transferred into OCT compound. In order to embed tissue in OCT compound, tissue was first positioned with the cutting side facing upwards, on a piece of soft card board rested on a metal chuck. OCT compound was then slowly squeezed,

avoiding bubbles, over the tissue to cover it completely. The bottom of metal chuck was then slowly dipped into liquid nitrogen, during which OCT compound would freeze. Finally, the OCT embedded tissue was removed from the metal chuck using a blade, transferred immediately into a pre-chilled 1.5 ml cryotube, and stored at -80 °C.

A Microm HM560 cryostat machine (temperature set to -20 °C) was used to section OCT embedded tissues. The tissues were sectioned at 5 $\mu$m and were mounted on polysine® microscope slide (VWR International Ltd., UK). The sections were then air dried at room temperature for 2 min, before storing at -80 °C.

***Tissue preparation for paraffin sectioning***

Tissues were fixed and embedded in paraffin wax by the histopathology department of King's College Hospital. Briefly, freshly harvested tissues were fixed with 10% formol saline for 24-48 h, to protect tissues from proteolytic enzymes and microorganism, as well as to allow formation of cross-linking between protein thereby preserving tissue structure [125]. The tissues were then subjected to dehydration step by going through a series of graded ethanol, ending with 100% ethanol, and then through xylene before being embedded in paraffin wax.

A Reichert Jung 2030 microtome was used to section paraffin embedded tissues. The tissues were sectioned at 4 $\mu$m, and section ribbons were laid on a Raymond A Lamb mounting water bath (temperature set to 45 °C) until the creases flatten. The section ribbons were then lifted from the water bath with microscope slides and left to drip dry. Slides were placed on a Raymond A Lamb hot plate (temperature set to 80 °C) to melt the wax. The slides were then lifted off the hot plate and allowed to cool to room temperature, during which the paraffin wax solidified. The slides were stored in slide boxes at room temperature.

### 3.2.3 Detection of $\beta$-gal activity and expression

***X-gal assay on wholemount kidneys and livers and semi-quantitative scoring***

The halved tissues were fixed with PBS containing 2% paraformaldehyde and 2 mM $MgCl_2$ (pH 7.4) for 10 min, then rinsed with 2 mM $MgCl_2$ in PBS twice before incubation in X-gal staining solution in PBS (pH 7.4) containing 20 mM $K_3Fe(CN)_6$, 20 mM $K_4Fe(CN)_6.3H_2O$, 2 mM $MgCl_2$, 0.01% sodium deoxycholate, 0.02% tergitol NP-40, and 1 mg/ml X-gal substrate overnight for 16 h at 37 °C, until desired staining developed. The X-gal assay on wholemount tissues were performed by Dr. C Roberts at ICH, and microphotography was performed by Dr. Q Xu.

A total of 5-13 kidneys from transgenic mice in each age group were examined for the intensity of X-gal signal. The kidneys were first divided into two regions, i.e., (i) cortex and outer medulla, and (ii) inner medulla, following the description by Wallace et al. [315]. The intensity of the X-gal signal in renal tubules within each region was determined with naked eyes; an average score was given to renal tubules with X-gal signal within each region. A score of "1" represents the least intense signal and a score of "4" represents the most intense signal.

***X-gal assay on kidney and liver cryosections***

Kidney and liver cryosections were equilibrated to room temperature for 20 min, after which the sections were fixed briefly by submersion in ice-cold 10% formalin in PBS in a Coplin jar for 10 min. Sections were then washed with three changes of PBS with gentle rocking on a table top rocker, 5 min each wash, to remove the excess formalin solution. After fixation, the slides were submerged in X-gal staining solution (pH 7.4) in PBS (formula stated in Section 2.1.4) at 37 °C. Kidney and liver cryosections were incubated in X-gal staining solution for 7 h and 25 h, respectively. At the end of the incubation period, sections were washed with two changes of PBS that was pre-warmed to 37 °C, 5 min each wash, and rinsed briefly with ultrapure water before counter-staining.

Kidney cryosections were subjected to periodic acid-Schiff (PAS) counter-staining. The staining procedure involved incubating cryosections in 1% periodic acid solution for 15 min, followed by thorough rinsing with ultrapure water. Sections were then incubated in Schiff reagent for 15 min followed by 5 min washing in running tap water. Periodic acid selectively oxidises glucose residues, which are abundant in the brush borders of proximal tubules, into aldehyde that subsequently reacts with Schiff reagent forming purple-magenta colour. Liver cryosections were counter-stained with 0.1% nuclear fast red solution in 0.5% aluminium sulfate (Sigma-Aldrich Company Ltd., UK), which stains the nuclei red, for 20 min. After counter-staining, liver sections were rinsed briefly in ultrapure water. Both kidney and liver cryosections were then mounted directly with Glycergel® (Dako UK Ltd., Ely, UK) using cover glass.

***β-gal immunofluorescence***

A standard indirect immunofluorescence technique [213] was employed to detect $\beta$-gal. Kidney and liver paraffin sections were first dewaxed in three changes of xylene, 2 min each, and rehydrated in three changes of graded ethanol starting from 100% ethanol, 1 min each, then immersed in ultrapure water.

Due to potential masking of antigen sites by formalin cross-linking impeding their recognition by antibodies, paraffin sections were subjected to heat-induced antigen retrieval to unmask the antigenic epitopes. The slides were boiled in 0.01 M citric acid buffer (pH 6) using a domestic pressure cooker for 3 min at full pressure. Slides were then cooled to room temperature while submerged in citric acid buffer, after which they were transferred immediately into a Coplin jar containing ultrapure water, avoiding sections going dry. In order to reduce fixative induced auto-fluorescence, sections were incubated with 0.1 M glycine in PBS for 20 min, followed by 5 min PBS washing. The sections were then incubated with 1% BSA in PBS for 2 h at room temperature to reduce non-specific antibody binding. The excess BSA was tipped off the slides and a paper towel was used to wipe off residual BSA around the sections. A Dako pen (Dako UK Ltd.,

UK) was used to draw a circle around the sections to create a water-repellent barrier so that antibody can stay on the sections.

In order to establish the optimum signal to noise ratio, sections were incubated with chicken anti-$\beta$-gal IgY primary antibody (1 mg/ml) at different concentrations (dilution 1:50, 1:100, 1:200; Abcam Inc., Cambridge, UK) or non-immune chicken IgY 400 $\mu$g/ml at similar concentrations to that of the primary antibodies (dilution 1:20, 1:40, 1:80; Insight Biotechnology Ltd., Wembley, UK) as negative controls. After 1 h of incubation at room temperature, sections were washed in five changes of 0.1% PBST with gentle rocking, 5 min each wash, and incubated with goat anti-chicken secondary antibody conjugated with AlexaFluor 488 (2 mg/ml) (dilution 1:1000; Invitrogen Ltd., UK) for 1 h at room temperature. Sections were then washed in three changes of 0.1% PBST with gentle rocking. Finally, coverslip was mounted onto the sections with ProLong® Gold mounting medium (Invitrogen Ltd., UK).

After coverslipping, nail varnish was applied to four corners of the coverslip and the slides were left at room temperature on a flat surface, in an opaque box. After 24 h, nail varnish was applied around the edges of the coverslip and the slides were examined under the epifluorescence microscope. The slides were then stored in an opaque box at 4 °C and microscopy was performed within the next 48 h.

As shown in Figure 3.3, a 1:200 dilution of chicken anti-$\beta$-gal IgY (working concentration 5 $\mu$g/ml) gave an optimum signal-to-noise ratio of $\beta$-gal signal. Thus, subsequent immunostaining for $\beta$-gal was performed using 5 $\mu$g/ml chicken anti-$\beta$-gal; section stained with 5 $\mu$g/ml non-immune chicken IgY served as a negative control.

### 3.2.4 Antibodies used as markers for kidney tubules and cells

An anti-Tamm-Horsfall protein (THP) antibody was used to label the thick ascending limbs and part of the ascending thin limbs of Henle's loop; an anti-calbindin D28K (CD28K) antibody was used to label the distal convoluted tubules and connecting tubules;

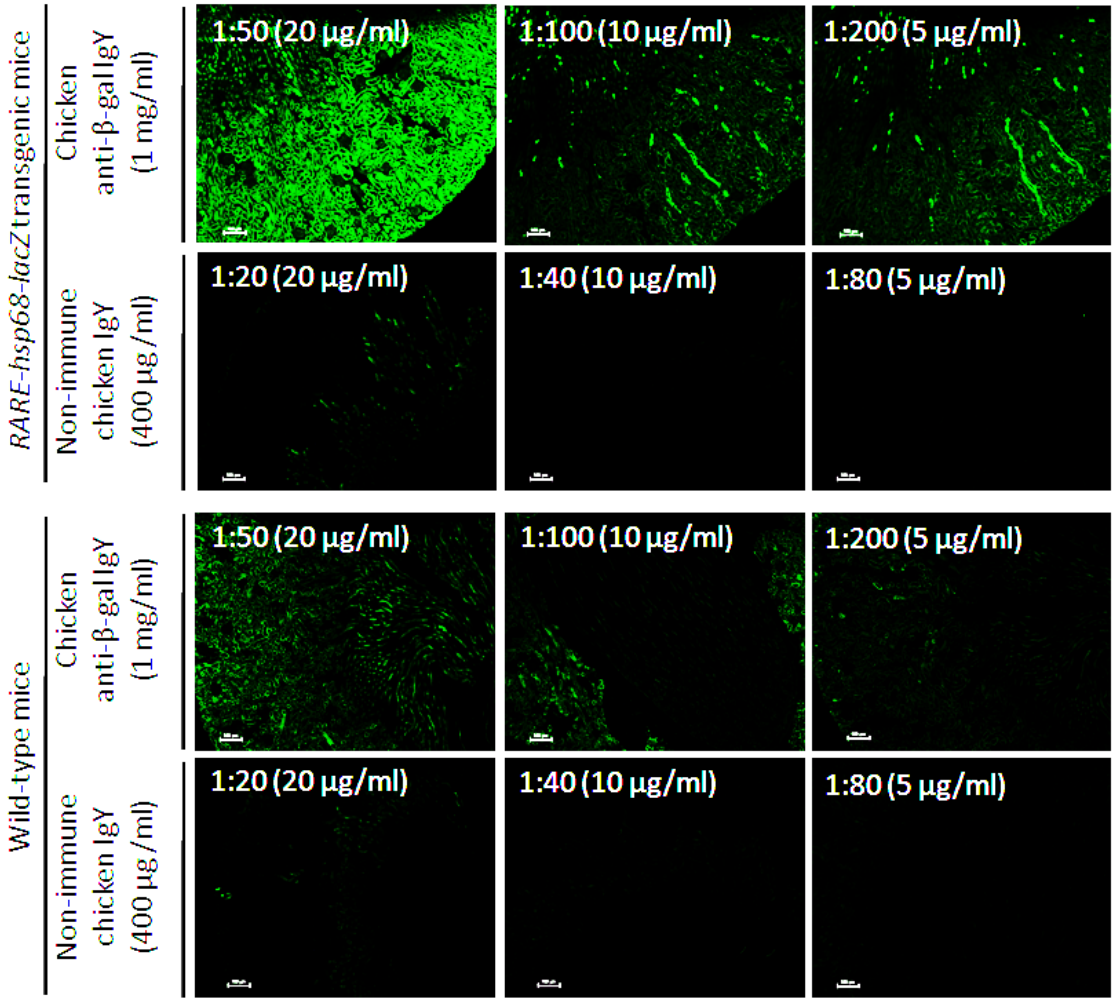


Figure 3.3: Optimisation of $\beta$-galactosidase ($\beta$-gal) antibody. In kidney sections of a 2-week-old transgenic mouse, 20 $\mu$g/ml anti-$\beta$-gal IgY gave rise to a poor signal-to-noise ratio, with a relatively high background signal that was also observed in section stained with 20 $\mu$g/ml non-immune chicken IgY. A better signal-to-noise ratio was achieved by using 10 $\mu$g/ml and 5 $\mu$g/ml anti-$\beta$-gal IgY, with the latter giving minimum signal in the wild-type mouse kidney section. Structural-specific signal was not observed in kidney section from wild-type mouse stained with equivalent concentration of antibodies. $\beta$-gal signal that was noted on kidney sections from both transgenic mouse and wild-type mouse were attributed to endogenous $\beta$-gal expression. Original magnification was 100x.

an anti-aquaporin 2 (AQP2) antibody was used to label the collecting duct principal cells and inner medullary collecting duct cells; an anti-vacuolar $H^+$-ATPase B1 (V-ATPase) antibody was used to label the intercalated cells (Figure 3.4). Anti-AQP2 antibody was from Millipore, Watford, UK. All other antibodies were from Insight Biotechnology Ltd., UK.

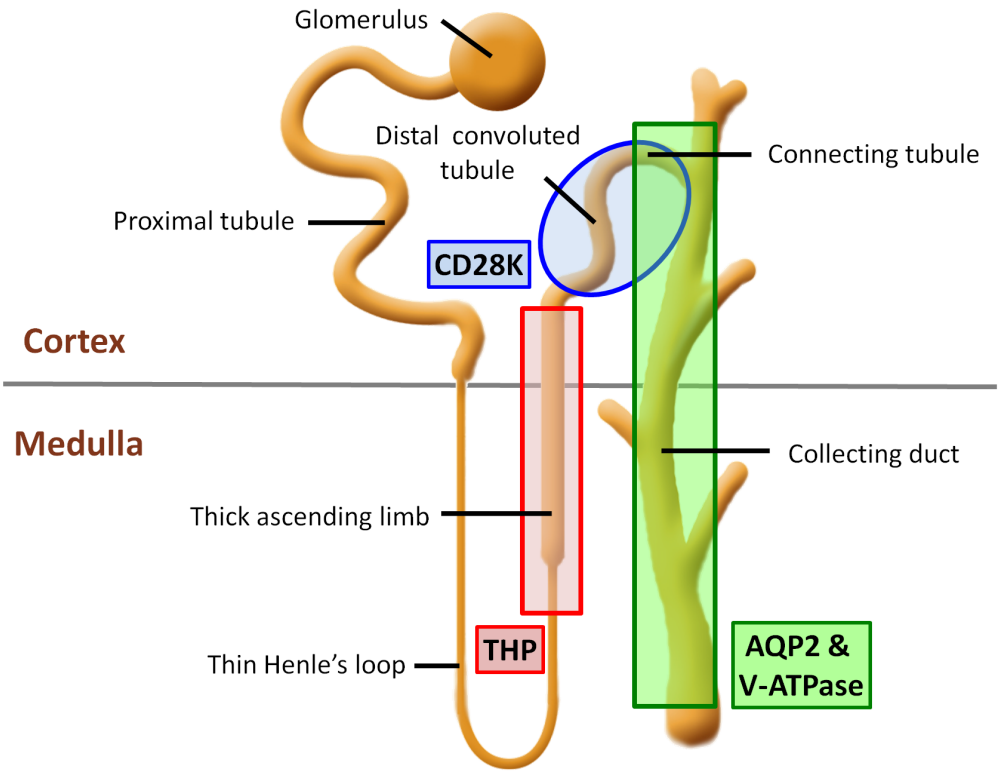


Figure 3.4: Antibodies employed as markers to identify various segments of nephron and different cell types in collecting ducts. Anti-Tamm-Horsfall protein (THP) antibody labels the thick ascending limbs and a portion of ascending thin Henle's loop (red); anti-calbindin D28K (CD28K) antibody labels the distal convoluted tubules and connecting tubules (blue); anti-aquaporin 2 (AQP2) antibody labels the collecting duct principal cells and inner medullary collecting duct cells; anti-vacuolar $H^+$-ATPase B1 (V-ATPase) antibody labels the collecting duct intercalated cells (green).

### *Optimisation of antibody concentration*

Preliminary experiments were first performed following protocol described in Section 3.2.3 by staining kidney section with individual antibody at three different dilutions (1:100, 1:200, and 1:500) to determine the optimum concentrations giving the best signal-to-noise ratio. Non-immune goat IgG and non-immune rabbit IgG (Insight Bio-

technology Ltd., UK) at concentrations similar to that of primary antibodies served as negative controls. Sections were then incubated with the corresponding anti-rabbit or anti-goat secondary antibodies conjugated with AlexaFluor 488 (2 mg/ml), AlexaFluor 555 (2 mg/ml), or AlexaFluor 568 (2 mg/ml) (dilution 1:1000, Invitrogen Ltd., UK).

The primary antibodies used to identify the specific segments/cells of kidney tubules and their optimum concentrations are summarised in Table 3.1. The microscopic images for each antibody with optimum signal-to-noise ratio and their respective negative controls are shown in Figure 3.5.

Table 3.1: Primary antibodies used as markers of specific segments/cells of kidney tubules and their optimum working concentrations.

| **Antibodies (stock concentration)** | **Segments/cells identified** | **Optimum dilution (working concentration)** |
|---|---|---|
| Rabbit anti-Tamm-Horsfall protein (THP) antibody (200 $\mu$g/ml) | Thick ascending limbs and part of the ascending thin limbs of Henle's loop | 1:100 (2 $\mu$g/ml) |
| Goat anti-calbindin D28K (CD28K) antibody (200 $\mu$g/ml) | Distal convoluted tubules and connecting tubules | 1:200 (1 $\mu$g/ml) |
| Goat anti-vacuolar $H^+$-ATPase B1 (V-ATPase) antibody (200 $\mu$g/ml) | Intercalated cells of collecting ducts | 1:500 (0.4 $\mu$g/ml) |
| Rabbit anti-aquaporin 2 (AQP2) antibody (600 $\mu$g/ml) | Principal cells and inner medullary collecting duct cells of collecting ducts | 1:150 (4 $\mu$g/ml) |

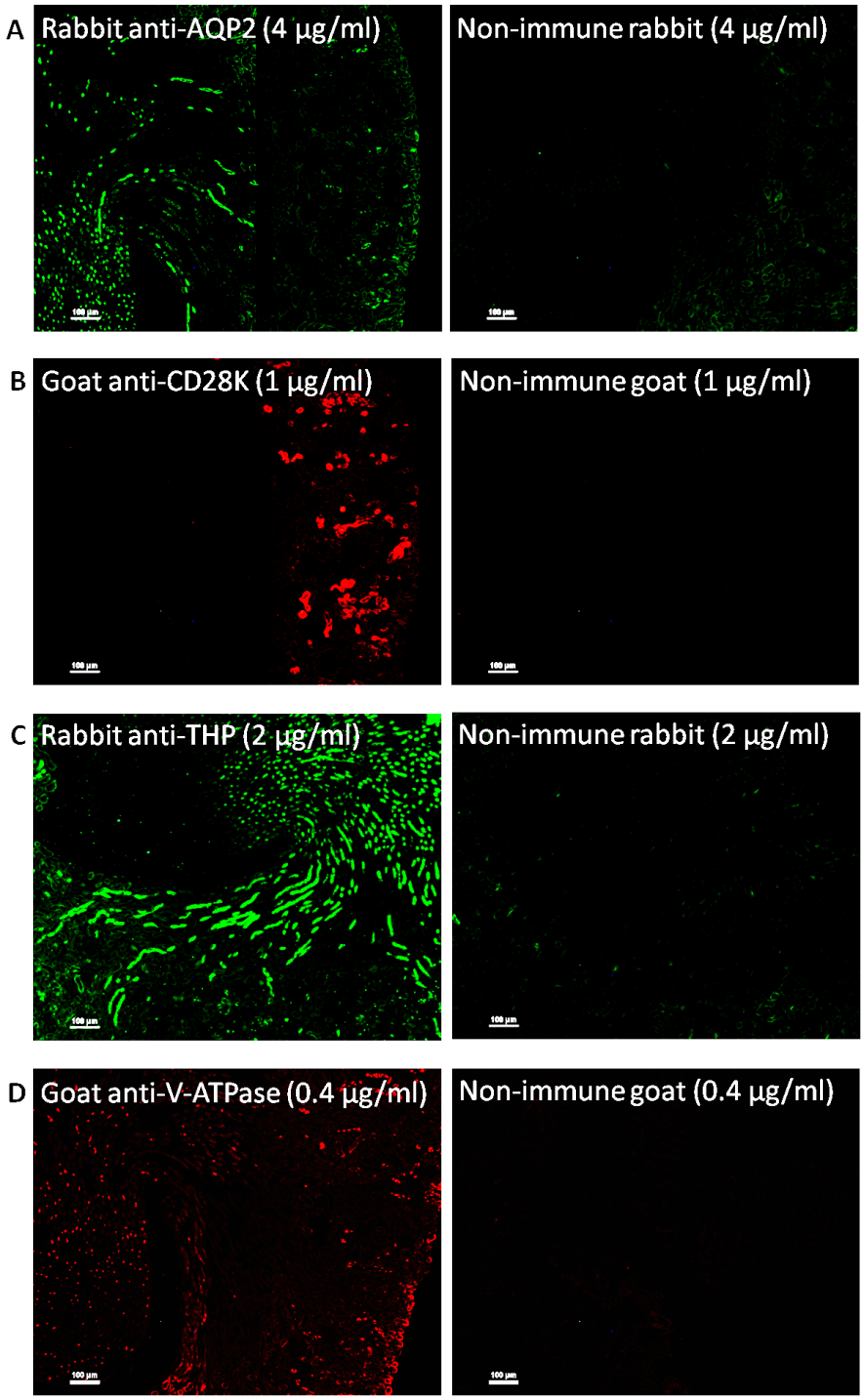


Figure 3.5: Optimum concentrations for marker antibodies. Concentrations of marker antibodies that gave optimum signal-to-noise ratio were as follow: rabbit anti-aquaporin 2 (AQP2) IgG at 4 $\mu$g/ml, goat anti-calbindin D28K (CD28K) IgG at 1 $\mu$g/ml, rabbit anti-Tamm-Horsfall protein (THP) IgG at 2 $\mu$g/ml, and goat anti-vacuolar $H^+$-ATPase B1 (V-ATPase) IgG at 0.4 $\mu$g/ml. At a similar exposure time, signal on sections stained with non-immune rabbit IgG and non-immune goat IgG was minimum, if any. Original magnification was 100x.

***Specificity of antibodies in identifying kidney tubules and cells***

In order to confirm the specificity of the antibodies serving as markers of renal tubules and cells, a double immunofluorescence staining was performed using different combinations of two of the antibodies, as follow:

1. **THP and CD28K**

   Thick ascending limbs and thin loops of Henle stain positive for THP [94]; distal convoluted tubules and connecting tubules stain positive for CD28K [94]. Thus the two immunostaining signals were expected to be mutually exclusive.

2. **CD28K and AQP2**

   In kidney cortex, distal convoluted tubules and connecting tubules stain positive for CD28K [94], although cortical collecting ducts were also reported to have weak CD28K staining [151]; principal cells of connecting tubules and collecting ducts stain positive for AQP2 [94]. Thus, distal convoluted tubules were expected to stain positive solely for CD28K, connecting tubules to stain positive for both CD28K and AQP2, whereas collecting ducts to stain positive for AQP2 and very weakly for CD28K.

3. **AQP2 and V-ATPase**

   In collecting ducts, principal cells and inner medullary collecting duct cells stain positive for AQP2 [80, 94], whereas intercalated cells stain positive for V-ATPase [82]. The principal cells and the intercalated cells were expected to be present within the cortical collecting ducts while the late portion of distal convoluted tubules were expected to have only the intercalated cells; inner medullary collecting duct cells were expected to largely stain positive for AQP2.

Kidney paraffin sections of a 2-week-old wild-type mouse were used for this purpose. Sections were first dewaxed and rehydrated as described in Section 3.2.3. Double immunofluorescence staining was performed sequentially, i.e., after incubation with 1% BSA to block non-specific binding, sections were stained with one primary antibody

followed by the corresponding fluorophore conjugated-secondary antibody; upon completion of the first cycle of immunostaining, sections were stained with the second cycle of primary and secondary antibodies. After completing the first cycle of immunostaining, the sections were examined briefly under the epifluorescence microscope to ensure successful immunostaining, before proceeding to the second cycle of immunostaining.

Whilst antigen retrieval with citric acid buffer heating and glycine incubation were performed only once before the first cycle of immunostaining, blocking non-specific binding with 1% BSA was performed before sections were incubated with primary antibodies of the first cycle and again before sections were incubated with primary antibodies of the second cycle. Washing steps were as described in Section 3.2.3. Finally, sections were incubated with DAPI (dilution 1:2000) before coverslip was mounted onto the slide.

The main procedures and steps involved in performing double immunofluorescence staining are summarised in Table 3.2.

Table 3.2: Main procedures of double immunofluorescence staining

| Procedure | Temperature | Duration |
|---|---|---|
| 1. Pressure cook section in 0.01 M citric acid buffer (pH 6) to unmask antigen-binding sites | Not Applicable (full pressure) | 3 min |
| 2. Incubate section in 0.1 M glycine to reduce fixative-induced auto-fluorescence | Room temperature | 20 min |
| 3. Rinse glycine off the section and incubate section in PBS | Room temperature | 5 min |
| 4. Incubate section in 1% BSA to reduce non-specific binding of antibody | Room temperature | 2 h |
| 5. Incubate section in primary antibody A that detects protein A | Room temperature | 1 h |
| 6. Rinse antibody off section and wash section in 0.1% PBST | Room temperature | 5 x 5 min |
| 7. Incubate section in secondary antibody conjugated to flurophore X that detects primary antibody A | Room temperature | 1 h |
| 8. Rinse antibody off section and wash section in 0.1% PBST | Room temperature | 3 x 5 min |
| 9. Incubate section in 1% BSA to reduce non-specific binding of antibody | Room temperature | 2 h |
| 10. Incubate section in primary antibody B that detects protein B | 4 °C | Overnight |
| 11. Repeat washing step “6” | | |
| 12. Incubate sections in secondary antibody conjugated to flurophore Y that detects primary antibody B | Room temperature | 1 h |
| 13. Repeat washing step “8” | | |
| 14. Counter-staining with DAPI | Room temperature | 5 min |

Primary antibodies raised in goat were selected for first round of immunostaining to avoid cross-reactivity during the second round of immunostaining. The sequence for double immunostaining is shown in Table 3.3.

Table 3.3: Double immunofluorescence sequence for characterisation of antibodies. Double immunofluorescence was performed sequentially according to the sequence below. AF: AlexaFluor.

| | **Primary Antibody** | **Secondary Antibody** |
|---|---|---|
| **THP and CD28K** | | |
| First | Goat anti-CD28K | Donkey anti-goat AF 555 |
| Second | Rabbit anti-THP | Goat anti-rabbit AF 488 |
| **CD28K and AQP2** | | |
| First | Goat anti-CD28K | Donkey anti-goat AF 555 |
| Second | Rabbit anti-AQP2 | Goat anti-rabbit AF 488 |
| **AQP2 and V-ATPase** | | |
| First | Goat anti V-ATPase | Donkey anti goat AF 555 |
| Second | Rabbit anti-AQP2 | Goat anti-rabbit AF 488 |

As shown in Figure 3.6, results of double immunofluorescence were congruent with their reported histological localisation, demonstrating their appropriateness as markers for specific segments of renal tubules and the two cell types in the collecting duct system. It was also noted that the number of V-ATPase-positive cells were higher in the kidney cortex compared to that in the medulla and only a few V-ATPase-positive cells were noted in the inner medulla, in concordance with common feature of intercalated cells in mammalian kidney [80].

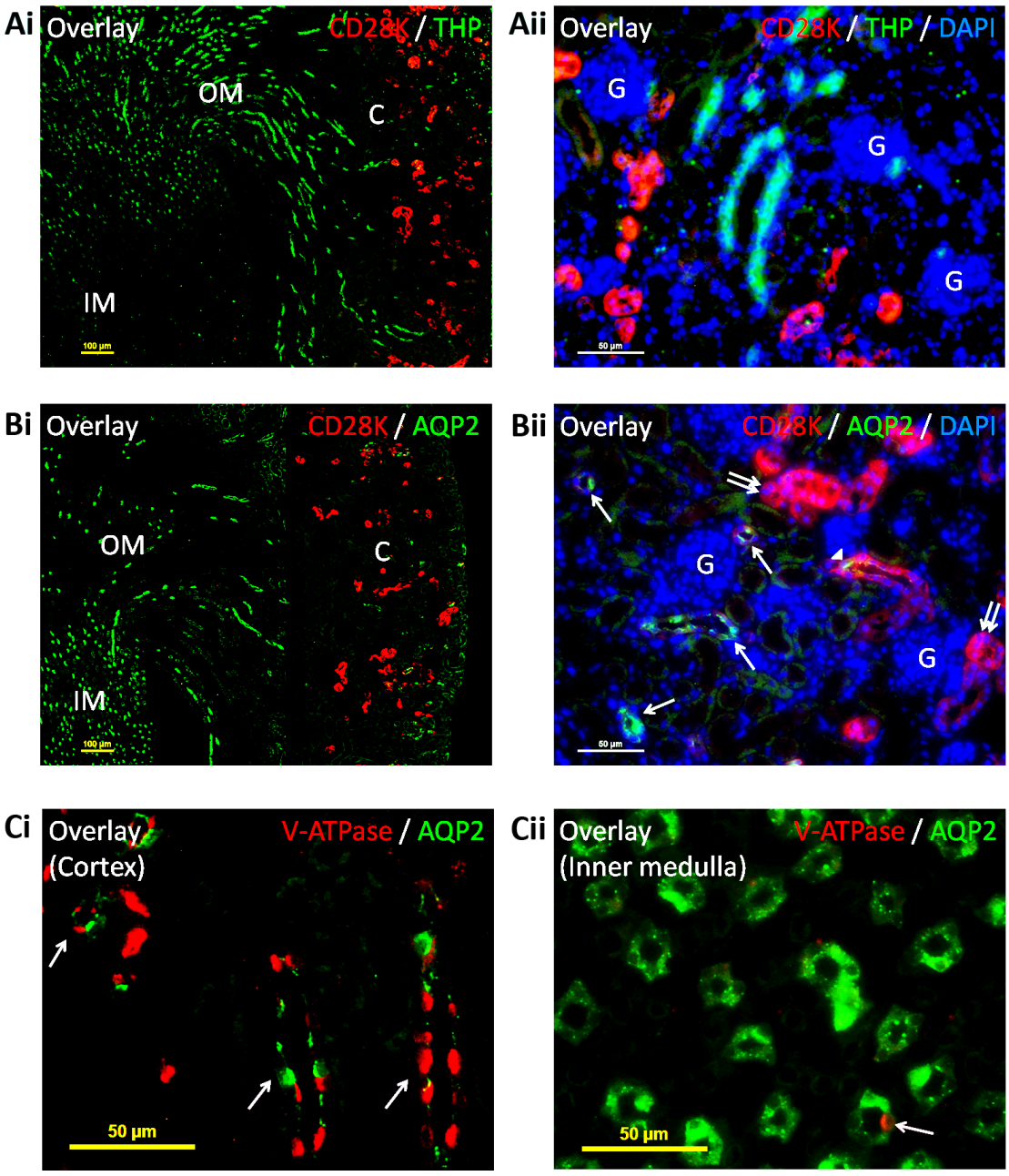


Figure 3.6: Please refer to the following page for figure legend.

Figure 3.6: Characterisation of antibodies for their specificity in labelling nephron and collecting ducts. Antibodies were used to identify thick ascending limbs, distal convoluted tubules, as well as principal cells, inner medullary collecting duct cells, and intercalated cells of collecting ducts. **Ai.** (Merged image): CD28K signal (red) was observed only in the cortex, whereas THP signal (green) was detected in both cortex and outer medulla, but not in deep inner medulla. Original magnification was 100x; **Aii.** (Merged image): CD28K (red) and THP (green) signals were mutually exclusive. Original magnification was 400x. **Bi.** (Merged image): CD28K (red) was detected only in the cortex whereas AQP2 (green) was more abundant in the outer medulla and inner medulla. Original magnification was 100x; **Bii.** (merged image): distal convoluted tubules stained exclusively and intensely for CD28K (double arrow); tubules stained positive for both CD28K and AQP2 were the connecting tubules (arrowhead) whereas those showing weak or negative CD28K but a positive AQP2 signal were the cortical collecting ducts (arrow). Original magnification was 400x. **Ci.** Principal cells that stained positive for AQP2 (green) and intercalated cells that stained positive for V-ATPase (red) co-localised to the same tubules in the cortical collecting ducts (arrow). **Cii.** In the inner medullary collecting ducts, most cells stained positive for AQP2 (green) whereas there was minimum, if any, cells that stained positive for V-ATPase (red); one cell with positive V-ATPase signal was noted (arrow), which might be an intercalated cell. Original magnification was 400x. Nuclei were visualised with DAPI (blue) counterstaining. C: cortex; OM: outer medulla; IM: inner medulla; G: glomeruli.

### 3.2.5 Localisation of $\beta$-gal

***AQP2 immunofluorescence and X-gal assay on kidney cryosection***

Following the protocol described in Section 3.2.3, cryosection was fixed briefly in formalin, then incubated in rabbit anti-AQP2 IgG for 1 h at room temperature, followed by goat anti-rabbit IgG conjugated to AlexaFluor 488 overnight at 4 °C. Upon confirming the success of immunostaining under epifluorescence microscope, cryosections were subjected to X-gal assay and then mounted with coverslip directly with ProLong® Gold mounting medium.

***Double immunofluorescence for $\beta$-gal and marker antibodies***

Double immunofluorescence was performed for $\beta$-gal and the marker antibodies sequentially, following the protocols described in Section 3.2.4. The sequence of antibody incubation is shown in Table 3.4.

Table 3.4: Double immunofluorescence sequence for localisation of $\beta$-galactosidase ($\beta$-gal). Double immunofluorescence was performed sequentially according to the sequence below. AF: AlexaFluor.

| | **Primary Antibody** | **Secondary Antibody** |
|---|---|---|
| **AQP2 and $\beta$-gal** | | |
| First | Rabbit anti-AQP2 | Goat anti-rabbit AF 568 |
| Second | Chicken anti-$\beta$-gal | Goat anti-chicken AF 488 |
| **V-ATPase and $\beta$-gal** | | |
| First | Goat anti-V-ATPase | Donkey anti-goat AF 555 |
| Second | Chicken anti-$\beta$-gal | Goat anti-chicken AF 488 |
| **CD28K and $\beta$-gal** | | |
| First | Goat anti-CD28K | Donkey anti-goat AF 555 |
| Second | Chicken anti-$\beta$-gal | Goat anti-chicken AF 488 |
| **THP and $\beta$-gal** | | |
| First | Goat anti-THP | Donkey anti-rabbit AF 568 |
| Second | Chicken anti-$\beta$-gal | Goat anti-chicken AF 488 |

### 3.2.6 Immunostaining for RAR$\beta$, RAR$\beta$2, Raldh1, and Raldh3

A double immunostaining between $\beta$-gal and RAR$\beta$, RAR$\beta$2, or Raldh3 was performed sequentially following the protocols described in Section 3.2.4. Immunostaining for $\beta$-gal protein was performed during the second cycle using the same concentration stated before; dilutions for other antibodies were as follow: rabbit anti-RAR$\beta$ antibody (1 mg/ml) (dilution 1:100; Abcam Inc., UK), rabbit anti-RAR$\beta$2 antibody (200 $\mu$g/ml) (dilution 1:100; Insight Biotechnology Ltd., UK), and goat anti-Raldh3 antibody (200 $\mu$g/ml) (dilution 1:100; Insight Biotechnology Ltd., UK).

Immunostaining for Raldh1 was performed on kidney sections from a 3-week-old mouse using a rabbit anti-Raldh1 antibody (Abcam Inc., UK); liver sections from an 8-week-old mouse was used as a positive control for the antibody, following the company's recommendation. The concentration of this antibody was not stated in the data sheets as it is a monoclonal antibody derived from tissue culture supernatant, which contains culture medium foetal calf serum. According to the company's technical support personnel, the concentration of this antibody was estimated to be around 1-3 mg/ml. Hence, for a pre-

liminary test, the concentration was assumed to be 3 mg/ml and the antibody was diluted 1:100 (working concentration: 30 $\mu$g/ml) for immunostaining. A non-immune rabbit IgG diluted to similar working concentration was used as a negative control. As shown in Figure 3.7, there was hardly any discernible Raldh1 signal in both kidney and liver sections. However, given that the actual concentration of this antibody remains questionable and that no specific signal was detected even in the liver, which was meant to serve as positive control, localisation of Raldh1 protein was not pursued any further.

In order to confirm its specificity, anti-Raldh3 antibody was pre-adsorbed to an excess amount of Raldh3 antigen (Insight Biotechnology Ltd., UK) before being incubated with section. While the section was incubated in 1% BSA to block non-specific binding, 4 $\mu$l of anti-Raldh3 antibody was mixed together with 20 $\mu$l of Raldh3 antigen in a microtube and was left at room temperature for 2 h. At the end of the incubation, the pre-adsorbed antibody was diluted with 1% BSA to a final working concentration of 2 $\mu$g/ml before being pipetted onto the section and incubated for 1 h at room temperature. The other sections were either incubated with non-pre-adsorbed anti-Raldh3 antibody or non-immune goat IgG for the same period of time.

### 3.2.7 Statistical analysis for X-gal semi-quantitative scoring

A Kruskal-Wallis one-way analysis of variance (ANOVA) test with a Dunns post-test was performed for the semi-quantitative scores of X-gal signal observed in kidney tubules using GraphPad Prism, Version 4.0. Separate comparison was made between kidney tubules within the cortex and outer medulla, and between kidney tubules within the inner medulla. A value of $p<0.05$ was taken as a statistically significant difference.

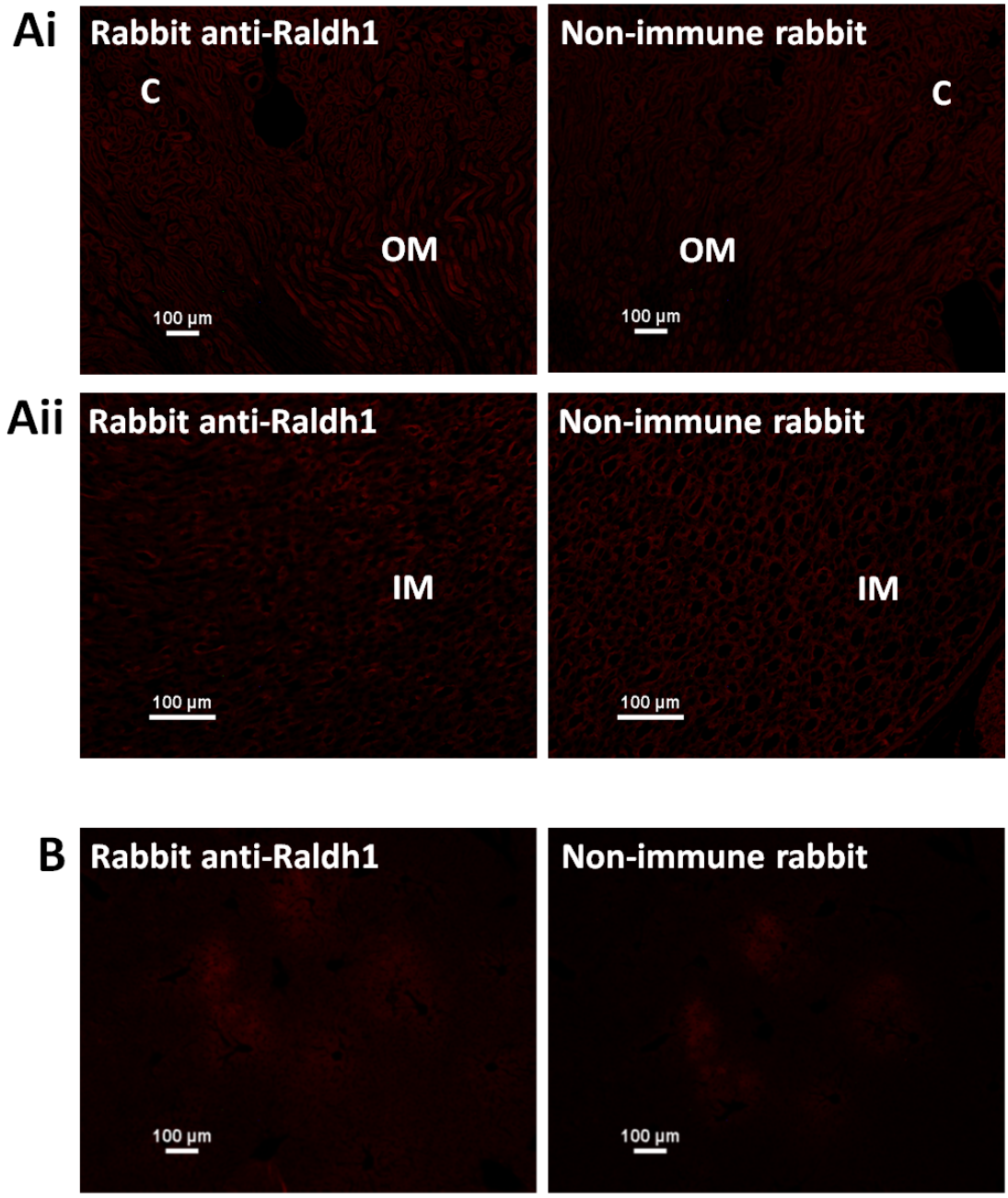


Figure 3.7: Immunostaining for retinaldehyde dehydrogenase 1 (Raldh1) in kidney and liver. In kidney sections from a 3-week-old mouse, no discernible Raldh1 immunostaining signal was observed in the cortex (C) and outer medulla (OM) (**Ai**, original magnification was 100x), as well as inner medulla (**Aii**, original magnification was 200x). No Raldh1 immunostaining signal was observed in liver section from a 8-week-old mouse either (**B**, original magnification was 100x).

## 3.3 Results

### 3.3.1 Reporter signal observed in the kidney but not in the liver

Results of X-gal assay on wholemount kidneys and livers are shown in Figure 3.8. Kidneys of 1- and 2-week-old wild-type mice had weak and ubiquitous cortical staining whereas kidney cortex of 3-, 5-, and 8-week-old wild-type mice showed no signal. In contrast, there was a conspicuous pattern of X-gal signal in kidneys of both male and female transgenic mice in all age groups. X-gal signal in the kidneys of transgenic mice was highly concentrated in the medulla, whereas in kidney cortex, X-gal signal was restricted to certain renal tubules. No specific signal was noted in livers of both wild-type mice and transgenic mice.

Following the description by Wallace et al. [315] (Figure 3.9Ai), kidney tissue was divided into two regions: (i) cortex and outer medulla region, and (ii) inner medulla region (Figure 3.9Aii). Intensity of X-gal signal in kidney tubules within each region was scored semi-quantitatively. In both regions, kidney tubules of 1-, 2-, and 3-week-old transgenic mice had a stronger intensity of X-gal signal compared to those in kidneys of 5- and 8-week-old transgenic mice (Figure 3.9B).

Results of X-gal assay on kidney cryosections were congruent with those on wholemount kidneys (Figre 3.8), whereby kidney sections of wild-type mice did not have discernible signal but a conspicuous structural-specific X-gal signal was detected in kidneys of transgenic mice. The X-gal signal was noted to be more abundant in kidneys of young mice compared to that in kidneys of older mice, in good agreement with results of wholemount X-gal assay (Figure 3.10). In addition, the signal was observed only in tubules in the renal cortex and medulla.

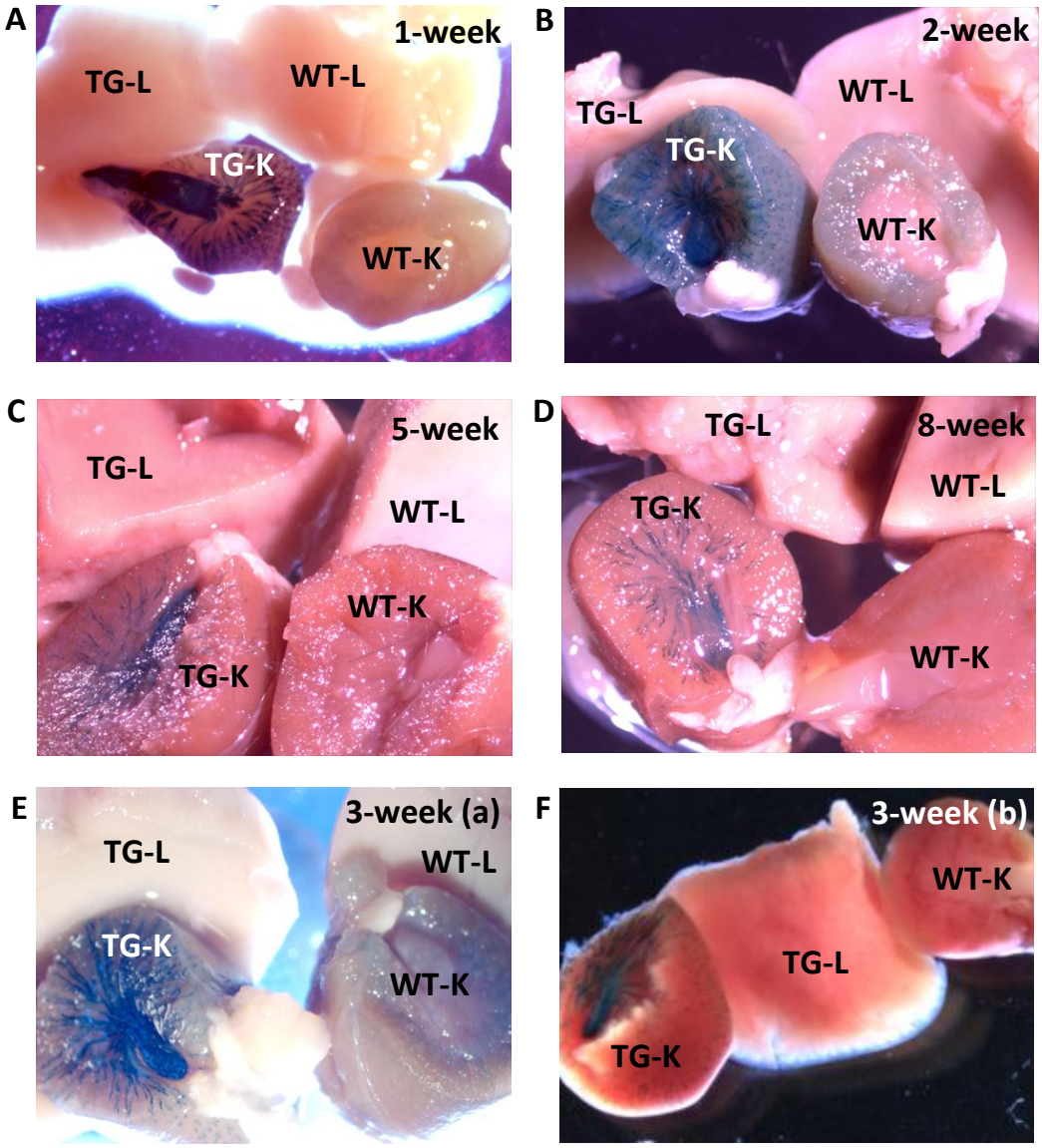


Figure 3.8: X-gal assay on wholemount kidneys and livers of transgenic (TG) and wild-type (WT) mice. Conspicuous X-gal signal (blue) was observed in kidneys of TG mice. Shown here are representative images taken from tissues of 5-13 TG mice and 1-7 WT mice from different age groups. Pictures were taken freshly after X-gal assay for 1-week (**A**), 2-week (**B**), 5-week (**C**), and 8-week (**D**) groups; tissues of the 3-week (a) (**E**) group were stained and fixed in formalin overnight before pictures were taken. Absence of endogenous X-gal signal in 3-week-old WT kidney was confirmed by repeating X-gal assay on freshly harvested and stained 3-week-old tissues (shown in 3-week (b) (**F**)), after which picture was taken immediately. TG-K and WT-K: kidney of TG and WT mice, respectively; TG-L and WT-L: liver of TG and WT mice, respectively.

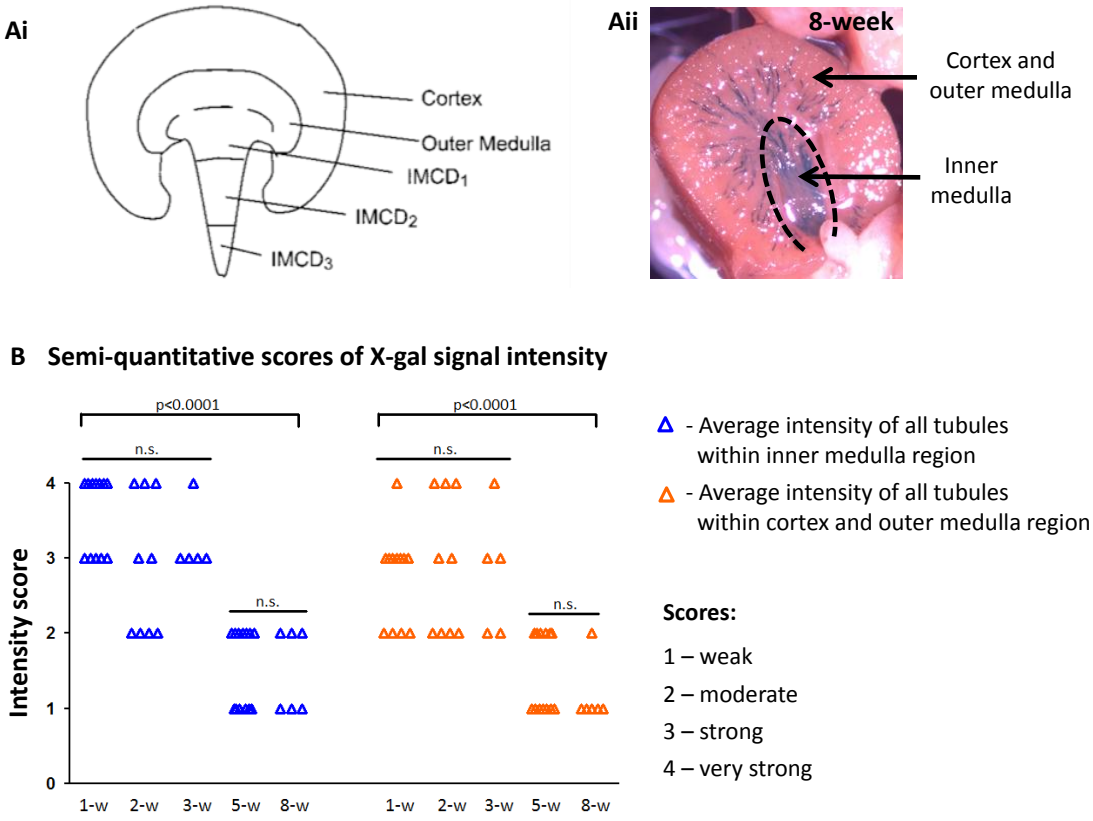


Figure 3.9: X-gal signal in different regions of kidney from transgenic mice and semi-quantitative scoring of X-gal signal intensity. Following the description by Wallace et al., who divided rat kidney into cortex, outer medulla, and three inner medulla regions (Figure adapted from [315]) (**Ai**), the transgenic mouse kidneys were divided into cortex and outer medulla region, and inner medulla region (**Aii**). **B.** Tubules with positive X-gal signal was scored semi-quantitatively on a scale of 1 to 4, with 1 representing weak signal and 4 representing very strong signal; an average score of X-gal signal intensity was given to all tubules with X-gal signal within the cortex and outer medulla region (orange triangle), and to all tubules with X-gal signal within the inner medulla region (blue triangle). Within each region, a statistical difference ($p<0.0001$) was found in the X-gal intensity among the five groups. However, no difference was found between the signal in kidney of 1-week to 3-week group, nor between those of 5-week and 8-week group. Each triangle represents signal from kidney of one transgenic mouse. 1-w, 2-w, 3-w, 5-w, and 8-w represents 1-week, 2-week, 3-week, 5-week, and 8-week-old kidneys, respectively; n=12 for 1-week, n=9 for 2-week, n=5 for 3-week, n=13 for 5-week, and n=6 for 8-week; n.s.: not statistically significant.

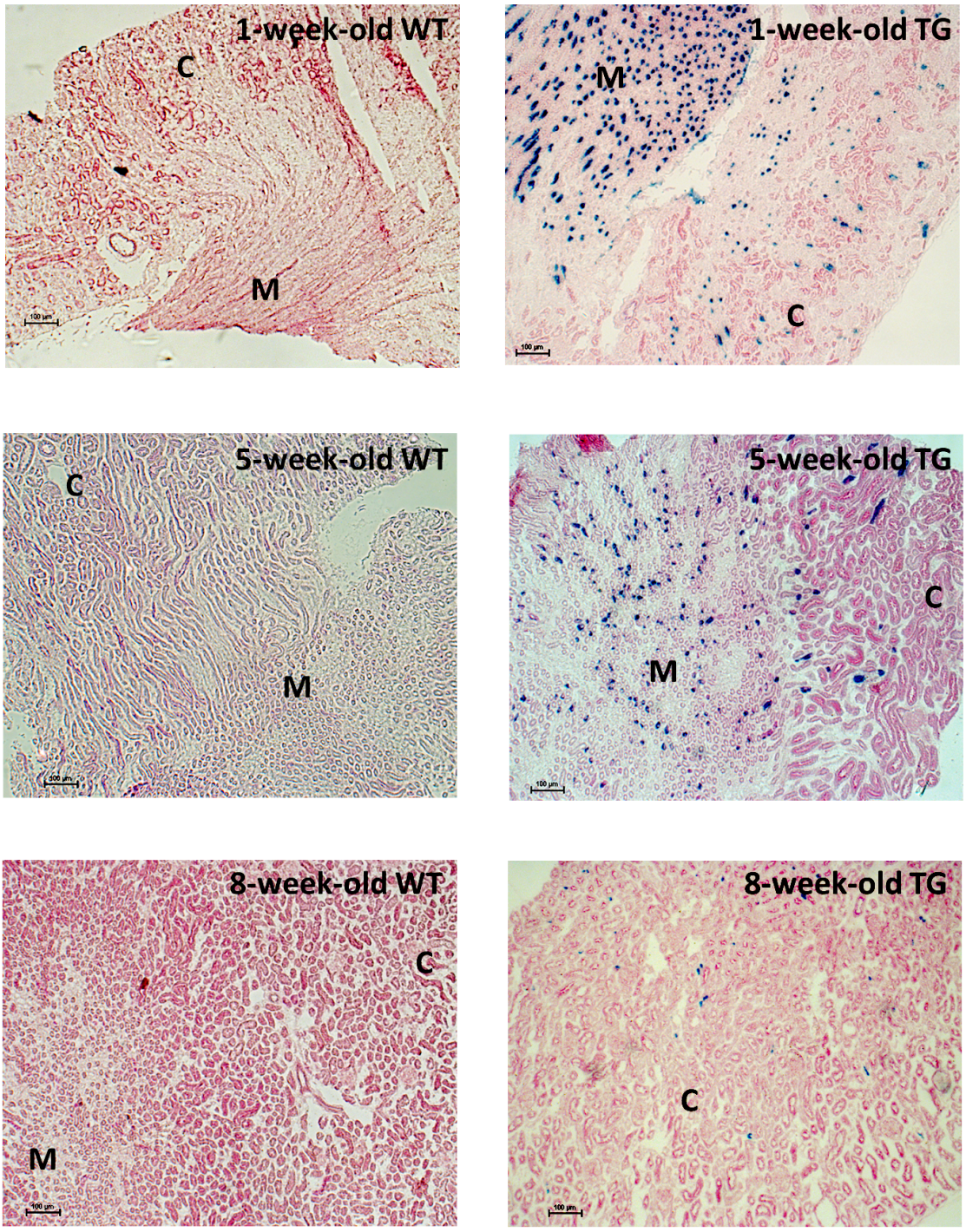


Figure 3.10: X-gal assay on kidney cryosections of transgenic (TG) and wild-type (WT) mice. X-gal signal (blue) was detected in kidneys of TG mice but not in WT mice. X-gal signal was restricted to renal tubules, and was noted to be more abundant in 1-week-old TG mice, especially in medulla, than in 5- and 8-week-old TG mice. Original magnification was 100x. C: cortex; M: medulla.

### 3.3.2 Reporter signal in a subset of kidney tubules but not in glomeruli

In all age groups, glomeruli and proximal tubules were devoid of X-gal signal; X-gal signal was present in a subset of renal tubules, in which some cells exhibited higher staining intensity than others (Figure 3.11A). The histological orientation of these tubules that were composed of large and cuboidal cells indicated that those tubules were not thin limbs of Henle's loop but were likely to be collecting ducts (with the consultation from King's College Hospital Histopathologist, Dr. N Dutt).

The tubular pattern of X-gal signal and its absence from the glomeruli were confirmed with $\beta$-gal immunohistochemistry (Figure 3.11B and Figure 3.11C).

### 3.3.3 Absence of reporter signal from the liver

In good concordance with X-gal assay on wholemount livers, no signal was observed in liver sections subjected to X-gal assay (Figure 3.12A) and to $\beta$-gal immunostaining (Figure 3.12B), suggesting the lack of reporter transgene activation in the liver. The lack of signal in liver section was not due to any experimental fault, as positive X-gal signal was observed in a kidney section stained alongside.

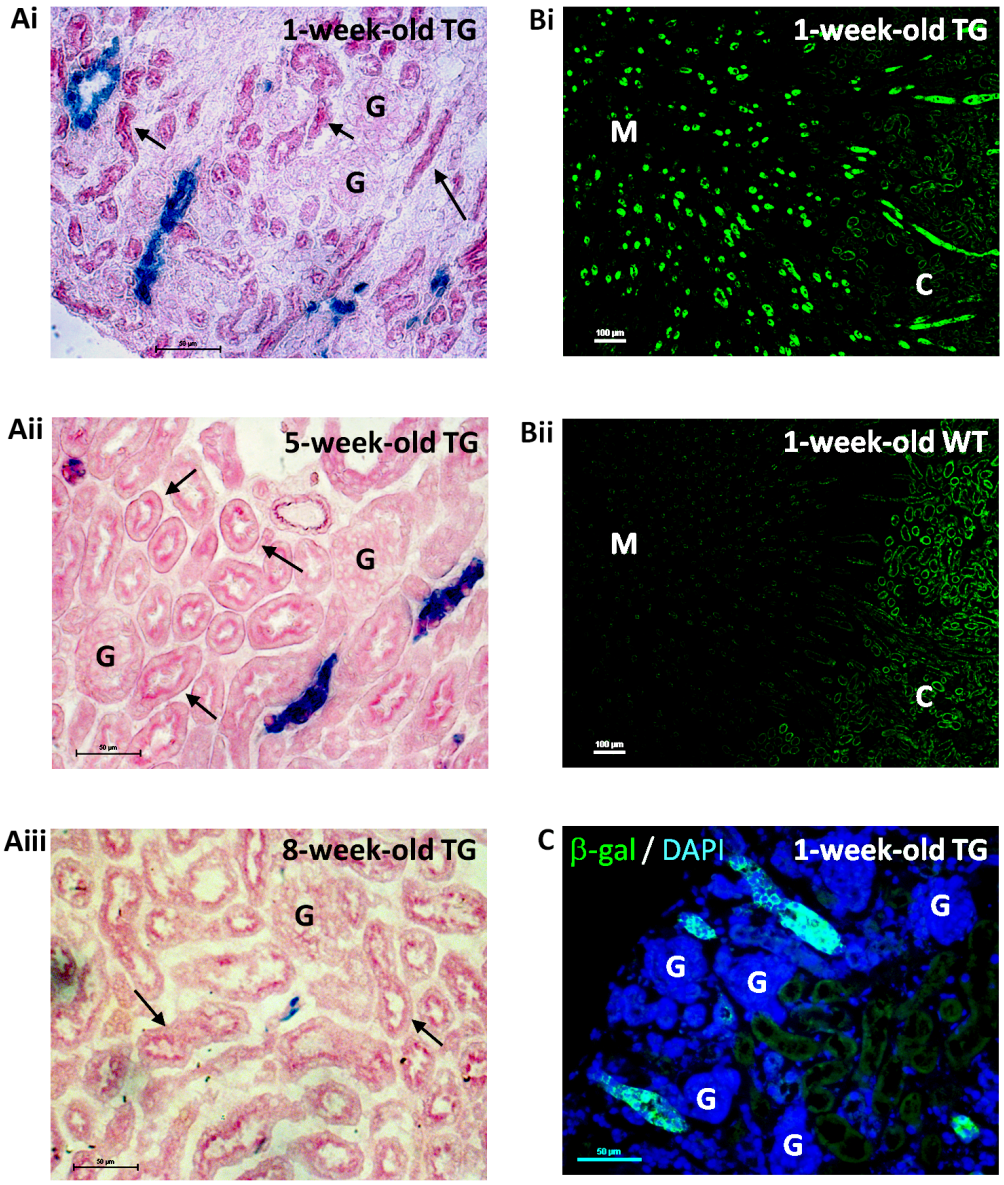


Figure 3.11: X-gal assay and $\beta$-galactosidase ($\beta$-gal) immunohistochemistry on kidney sections of transgenic (TG) and wild-type (WT) mice. X-gal signal (blue) was observed in a subset of tubules but was not observed in the proximal tubules (arrow, with distinct luminal brush border stain) nor in the glomeruli, in kidney sections of 1-week-old (**Ai**), 5-week-old (**Aii**), and 8-week-old (**Aiii**) transgenic mice. Original magnification was 400x. $\beta$-gal (green) immunostaining on kidney paraffin section of 1-week-old TG mice showed a similar tubular pattern (**Bi**). The background signal that was also noted in kidney section of 1-week-old WT mice might be attributed to endogenous $\beta$-gal (**Bii**). Original magnification was 100x. **C.** Merged image: $\beta$-gal signal (green) was observed in tubules, whereas no signal was detected in glomeruli. Nuclei were visualised with DAPI (blue) counter-staining. Original magnification was 400x. No specific signal was noted on sections incubated with non-immune IgG in place of primary antibody (data not shown). C: cortex; M: medulla; G: glomeruli.

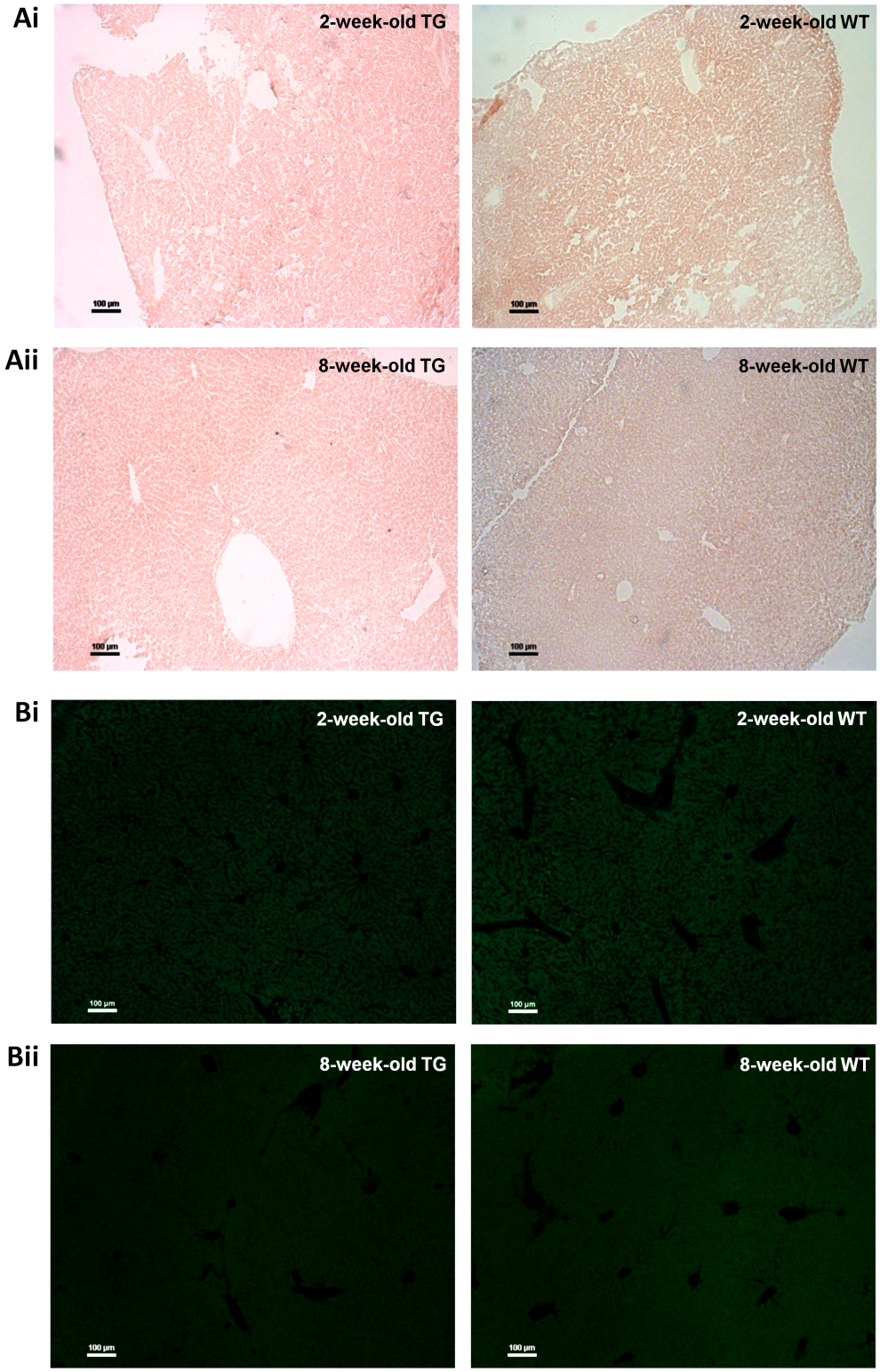


Figure 3.12: X-gal assay and $\beta$-galactosidase ($\beta$-gal) immunohistochemistry on liver sections of transgenic (TG) and wild-type (WT) mice. Reporter signal was not observed in liver sections of 2-week-old (**Ai**) and 8-week-old mice (**Aii**) subjected to X-gal assay. Similarly, signal was not observed in liver sections of 2-week-old (**Bi**) and 8-week-old mice (**Bii**) stained with anti-$\beta$-gal antibody. Original magnification was 100x.

### 3.3.4 Reporter signal in principal cells, inner medullary collecting duct cells, and intercalated cells of collecting ducts

The histological orientation and cellular morphology of tubules stained positive for X-gal and $\beta$-gal signals were suggestive of collecting ducts. Hence, initial attempt of localising reporter transgene activation was focused on examining the presence of X-gal and $\beta$-gal signals in the collecting duct.

***X-gal assay and immunostaining for AQP2***

The staining patterns of X-gal and AQP2 closely resembled each other (Figure 3.13Ai); only X-gal signal but not fluorescence signal was observed in section stained with non-immune IgG in place of anti-AQP2 IgG (Figure 3.13Aii), thus ruling out the possibility of auto-fluorescence given rise by X-gal signal. At higher magnification, X-gal and AQP2 signals co-localised to the same renal tubules (Figure 3.13B).

***Double immunostaining for AQP2 and $\beta$-gal***

In concordance with the results shown in Figure 3.13, the immunostaining pattern of $\beta$-gal and AQP2 in kidneys from young mice closely resembled each other and both signals co-localised to the same renal tubules (Figure 3.14A). At the cellular level, cells that stained positive for both $\beta$-gal and AQP2 were observed in most instances (Figure 3.14B). $\beta$-gal expression was more extensive in kidneys of young mice, evident by the presence of many cells that appeared as yellow/orange colour; in kidney of older mice, $\beta$-gal expression was less widespread, which was largely localised to cells with positive AQP2 signal in the inner medulla (Figure 3.15).

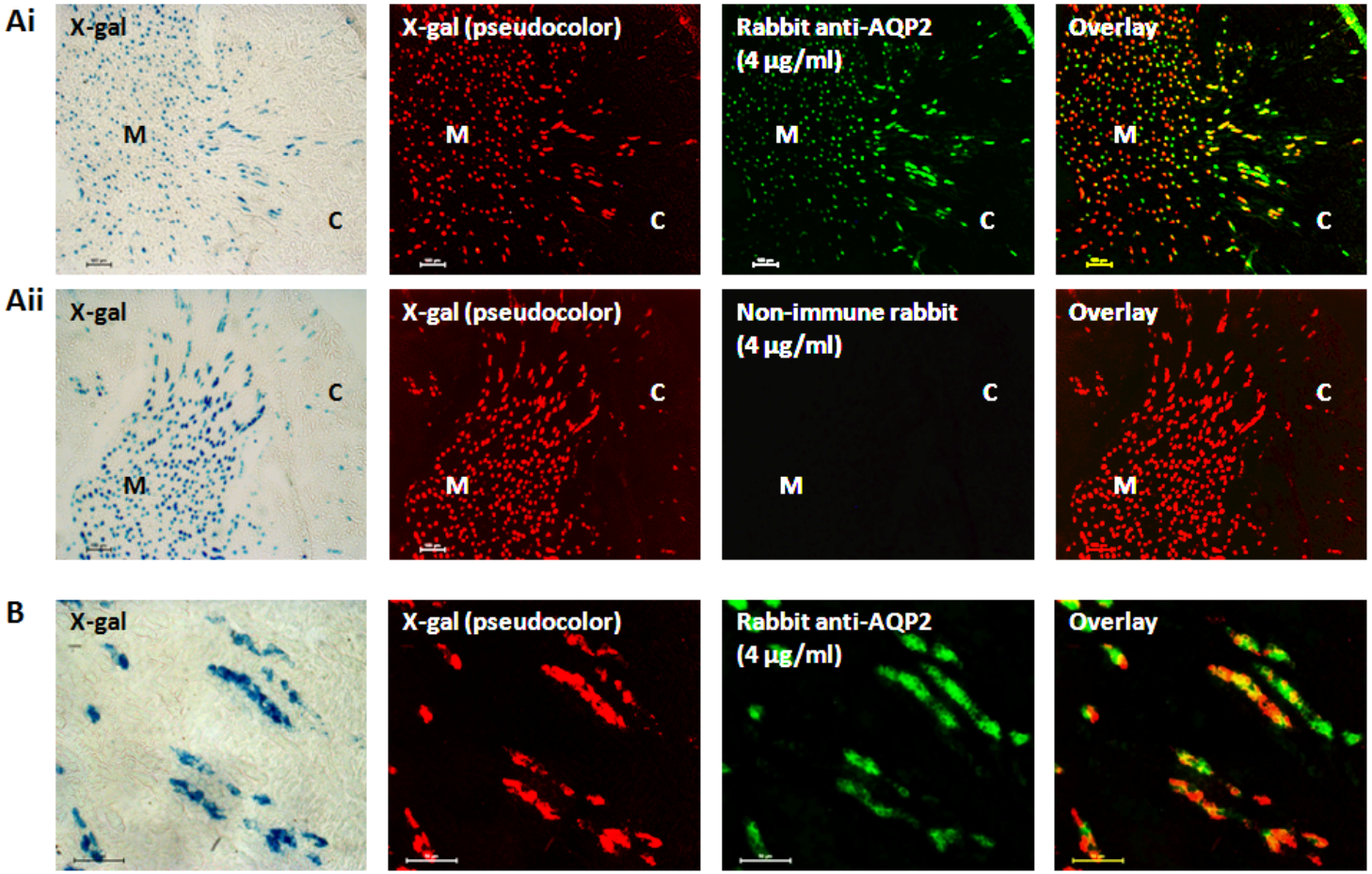


Figure 3.13: Localisation of aquaporin 2 (AQP2) and X-gal signals in renal tubules. **A** The staining pattern for AQP2 and X-gal closely resembled each other. Original magnification was 100x. C: cortex; M: medulla. **B.** AQP2 and X-gal signal co-localised to the same tubules. Original magnification was 400x. Shown are kidney sections from 1-week-old mice.

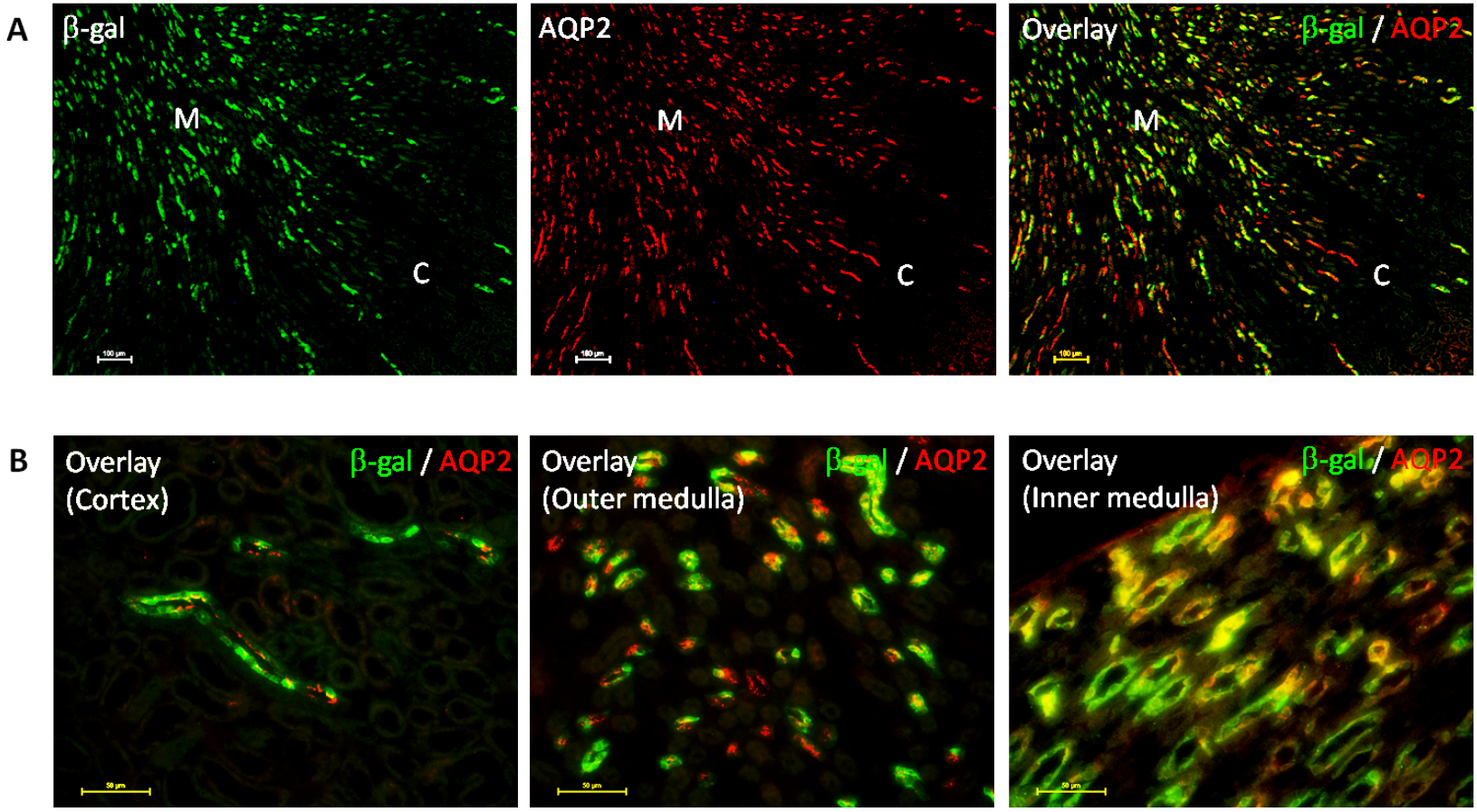


Figure 3.14: Localisation of aquaporin 2 (AQP2) and $\beta$-galactosidase ($\beta$-gal) signals in renal tubules of a young mouse. **A.** In kidneys of 2-week-old mice, $\beta$-gal (green) and AQP2 (red) signals very much resembled each other. Original magnification was 100x. C: cortex; M: medulla. **B.** Merged images: At higher magnification, co-localisation of AQP2 and $\beta$-gal signals to the same renal tubules were confirmed in cortex, outer medulla, and inner medulla. Original magnification was 400x. No specific signal was detected on sections incubated with non-immune IgGs in place of primary antibodies (data not shown).

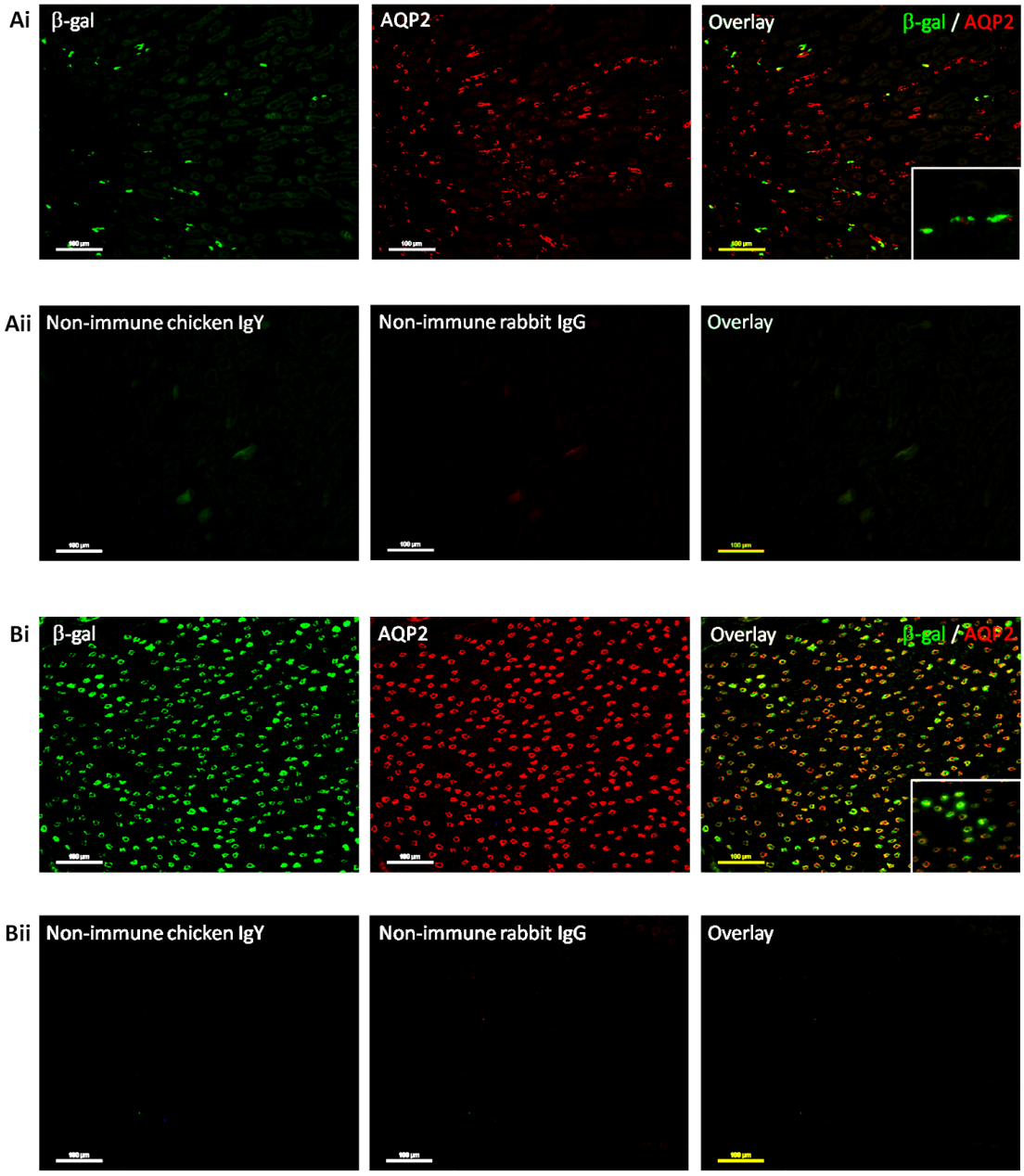


Figure 3.15: Localisation of aquaporin 2 (AQP2) and $\beta$-galactosidase ($\beta$-gal) signals in renal tubules of an adult mouse. In kidneys of 8-week-old mice, $\beta$-gal (green) signal was less abundant, which was largely localised to tubules that also stained positive for AQP2 (red). Insets showed the enlarged figure of signal co-localisation. Note that co-localisation of $\beta$-gal with AQP2 signals to the same renal tubules was more apparent in the inner medulla (**Bi**) than in the cortex (**Ai**). Original magnification was 200x. No specific signal was detected on sections incubated with non-immune IgGs in place of primary antibodies (**Aii** and **Bii**).

### *Double immunostaining for V-ATPase and β-gal*

While most β-gal-positive cells express AQP2, β-gal signal was also detected in some cells stained positive for V-ATPase (Figure 3.16).

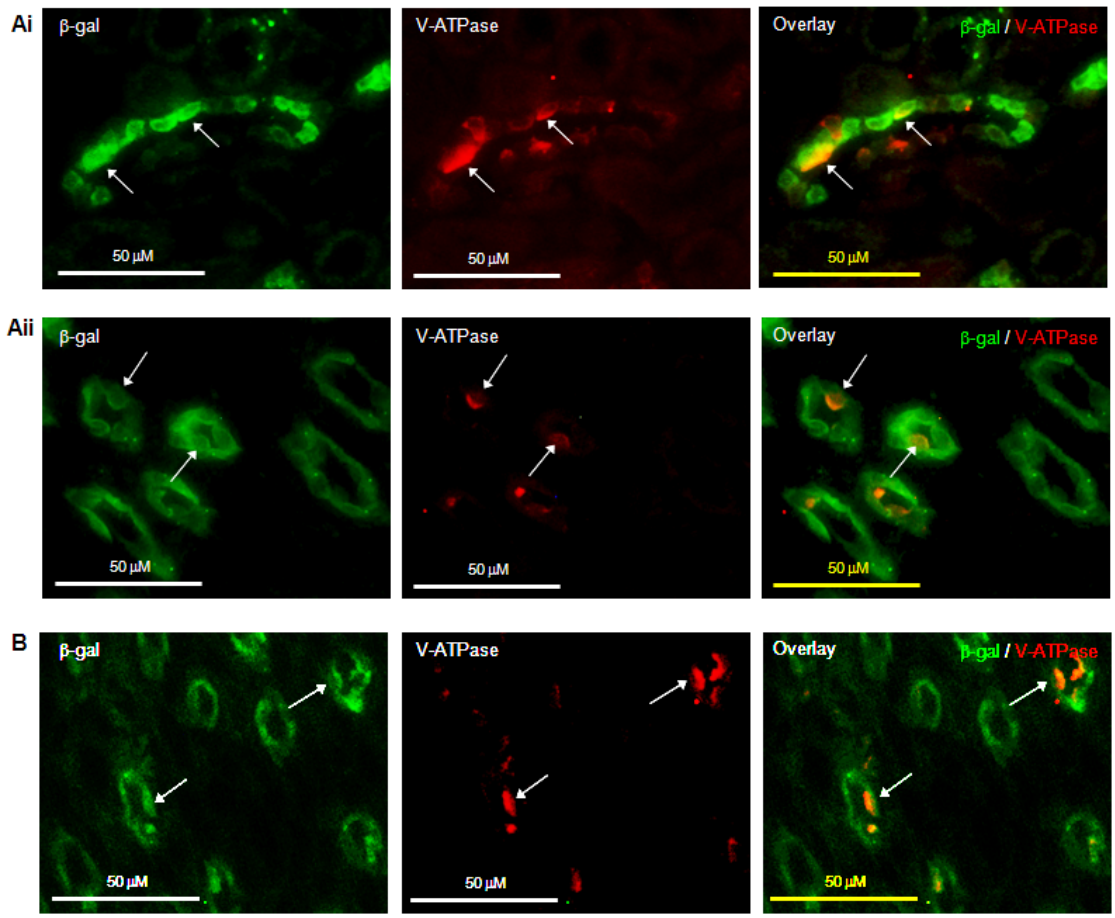


Figure 3.16: Localisation of vacuolar $H^+$-ATPase B1 (V-ATPase) and β-galactosidase (β-gal) signals in renal tubules. β-gal signal (green) was detected in some cells that stained positive for V-ATPase (red) in kidney cortex (**Ai**) and medulla (**Aii**) of 2-week-old mice, as well as in inner medulla of 8-week-old (**B**) mice. Original magnification was 400x. No specific signal was detected on sections incubated with non-immune IgGs in place of primary antibodies (data not shown).

Collectively, the observation confirms the presence of reporter transgene activation in principal cells and inner medullary collecting duct cells, which expressed AQP2, and in intercalated cells, which expressed V-ATPase. In older mice, reporter transgene activation was found to largely localised to inner medullary collecting duct cells (Figure 3.15).

### 3.3.5 Absence of reporter signal from thick ascending limbs

In kidneys of both young and adult mice, $\beta$-gal signal was not detected in THP-positive thick ascending limbs (Figure 3.17).

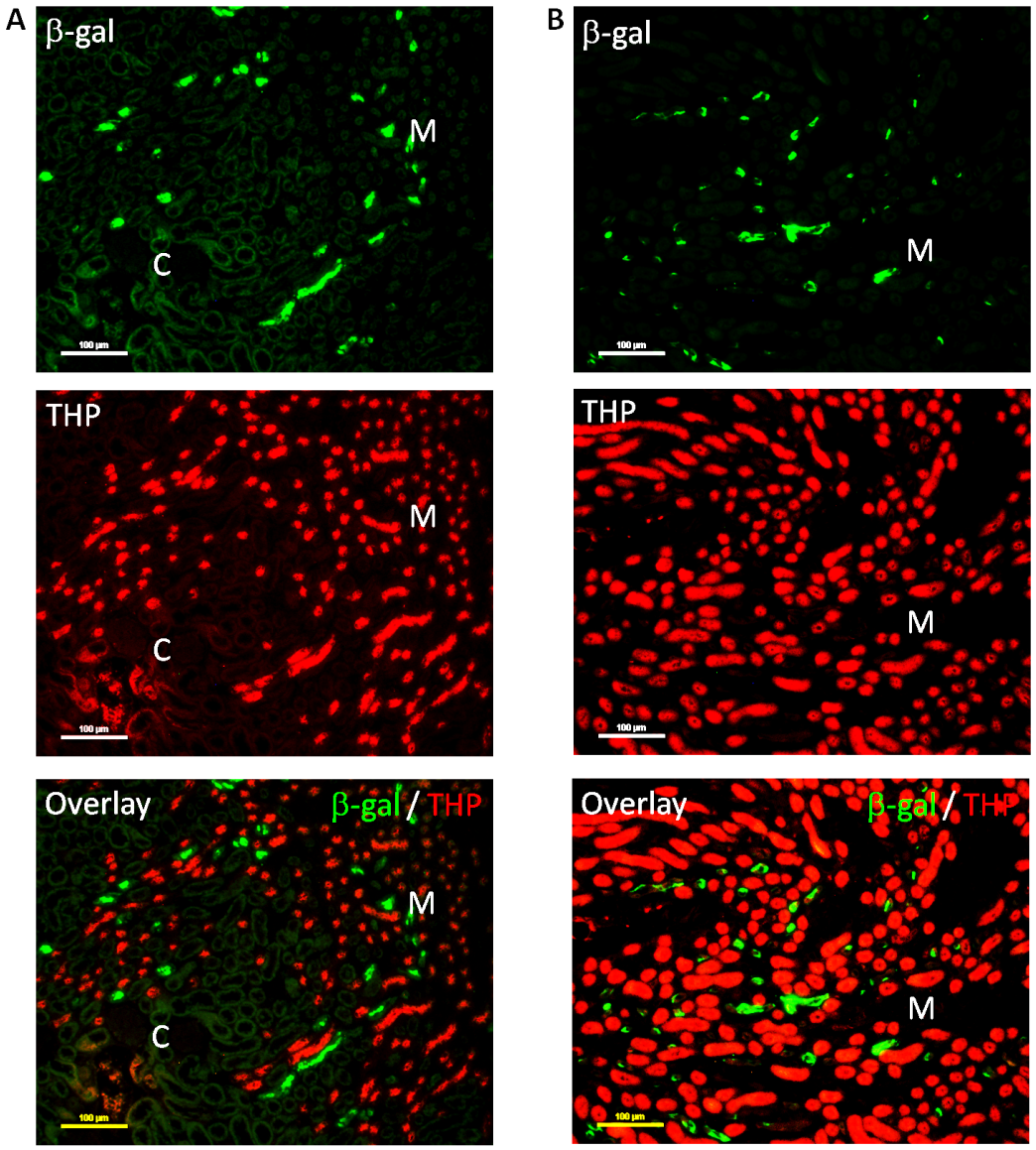


Figure 3.17: Mutually exclusive $\beta$-galactosidase ($\beta$-gal) and Tamm-Horsfall protein (THP) signals. Tubules stained positive for $\beta$-gal (green) and THP (red) were mutually exclusive in kidneys of 2-week-old (**A**) and 8-week-old (**B**) mice. Original magnification was 200x. No specific signal was detected on sections incubated with non-immune IgGs in place of primary antibodies (data not shown). C: cortex; M: medulla.

### 3.3.6 Absence of reporter signal from distal convoluted tubules

$\beta$-gal signal was not observed in tubules with intense CD28K signal, but was detected in some tubules with intermittent and relatively weak CD28K signal (Figure 3.18).

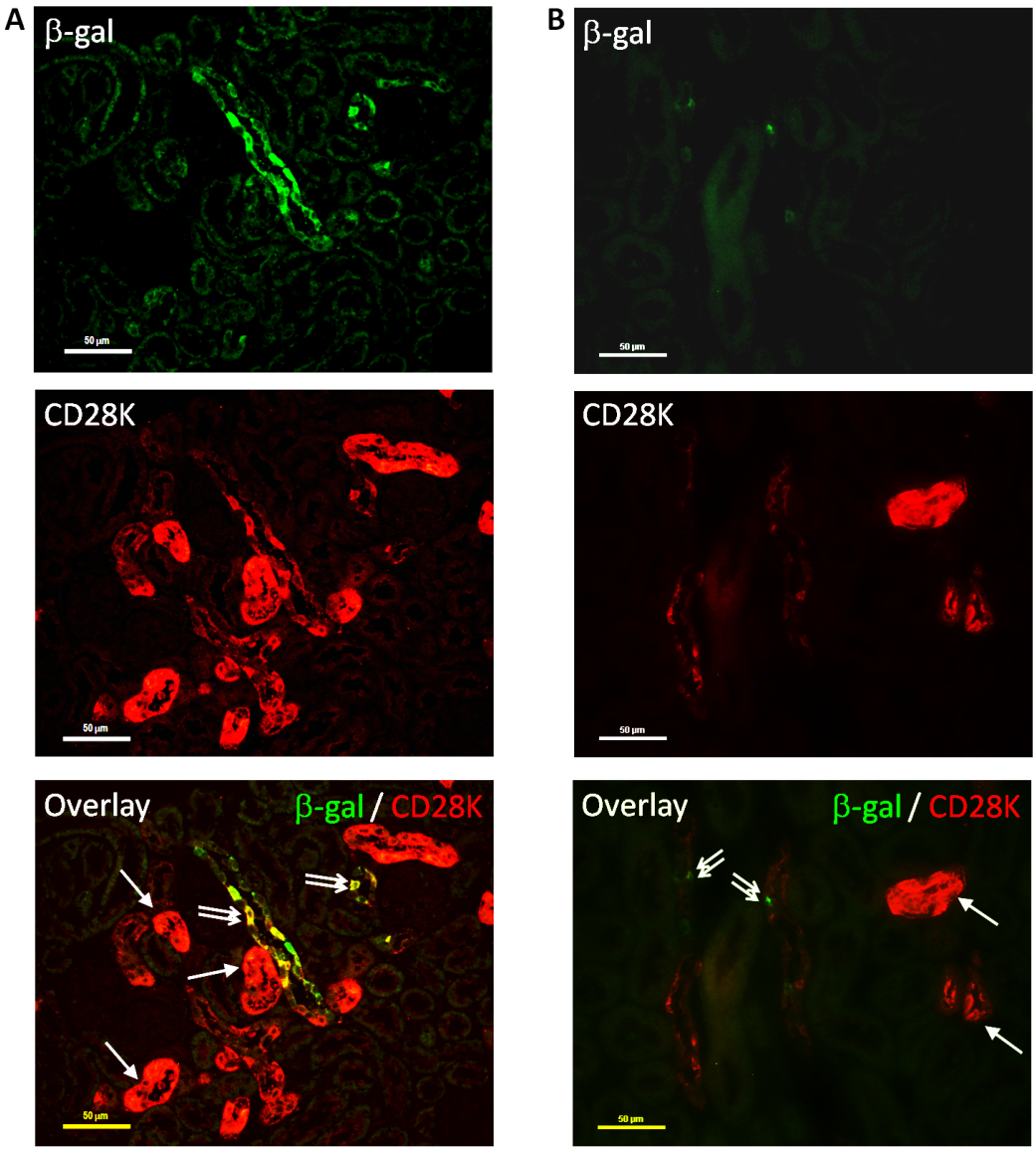


Figure 3.18: Partial overlapping of $\beta$-galactosidase ($\beta$-gal) and calbindin D28K (CD28K) signals in renal cortex. In renal cortex of 2-week-old (**A**) and 8-week-old (**B**) mice, tubules with intense CD28K signal (arrow) did not stain positive for $\beta$-gal protein. Whereas, some tubules with intermittent CD28K showed positive $\beta$-gal signal (double arrow). Original magnification was 400x. No specific signal was detected on sections incubated with non-immune IgGs in place of primary antibodies (data not shown).

The results suggest that the reporter transgene activation was absent from distal convoluted tubules with an intense CD28K signal, but was likely to be present in connecting tubules or cortical collecting ducts with intermittent CD28K signal, consistent with the presence of CD28K-negative intercalated cells in these segments [151].

### 3.3.7 Expression of Raldh3 and RAR$\beta$2 proteins in the kidney

A kidney section stained with anti-Raldh3 IgG showed predominant signal in the inner medulla region, partially overlapping with tubules stained positive for $\beta$-gal, as shown in Figure 3.19A. The specificity of anti-Raldh3 IgG was questionable as section stained with anti-Raldh3 IgG pre-adsorbed with Raldh3 antigen resulted in a similar staining pattern as section stained with anti-Raldh3 IgG (Figure 3.19B).

As shown in Figure 3.20, RAR$\beta$ protein was not detected in tubules expressing reporter transgene. Whereas, RAR$\beta$2 protein was found to be present only in a few tubules expressing reporter transgene (Figure 3.21).

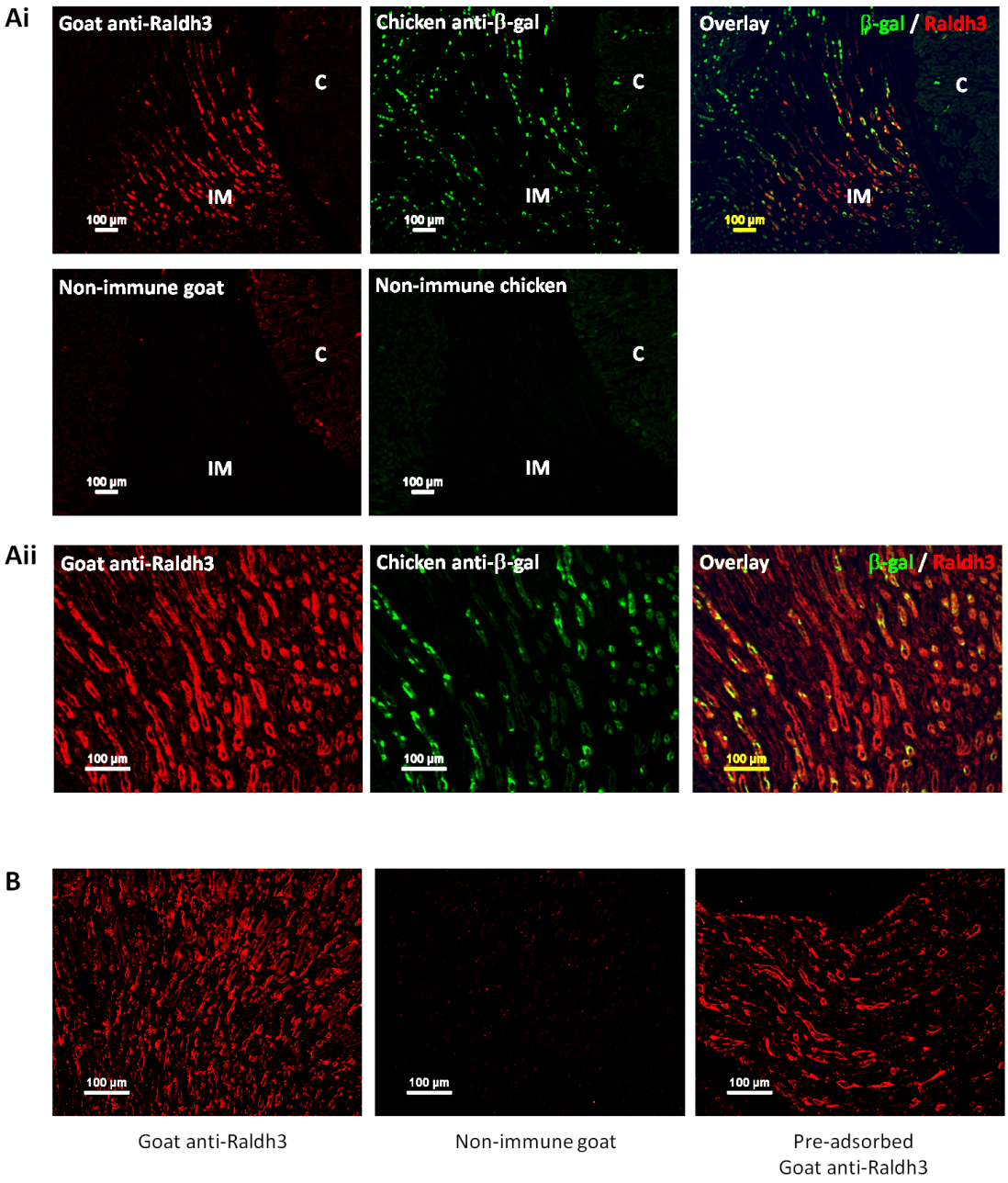


Figure 3.19: Expression of retinaldehyde dehydrogenase 3 (Raldh3) and $\beta$-galactosidase ($\beta$-gal) protein. In kidney section of a 5-week-old transgenic mouse, Raldh3 was localised predominantly to the inner medulla; no specific signal was detected on sections incubated with non-immune IgGs in place of primary antibodies (**Ai**). Original magnification was 100x. C: cortex; IM: inner medulla. At higher magnification, Raldh3 protein expression was found to be partially overlapped with $\beta$-gal protein expression (**Aii**). Original magnification was 200x. **B.** Whereas no apparent signal was observed in kidney section stained with non-immune IgG (middle panel), section stained with anti-Raldh3 IgG pre-adsorbed with Raldh3 antigen (right panel) showed a similar staining pattern as section stained with anti-Raldh3 IgG (left panel). Original magnification was 200x.

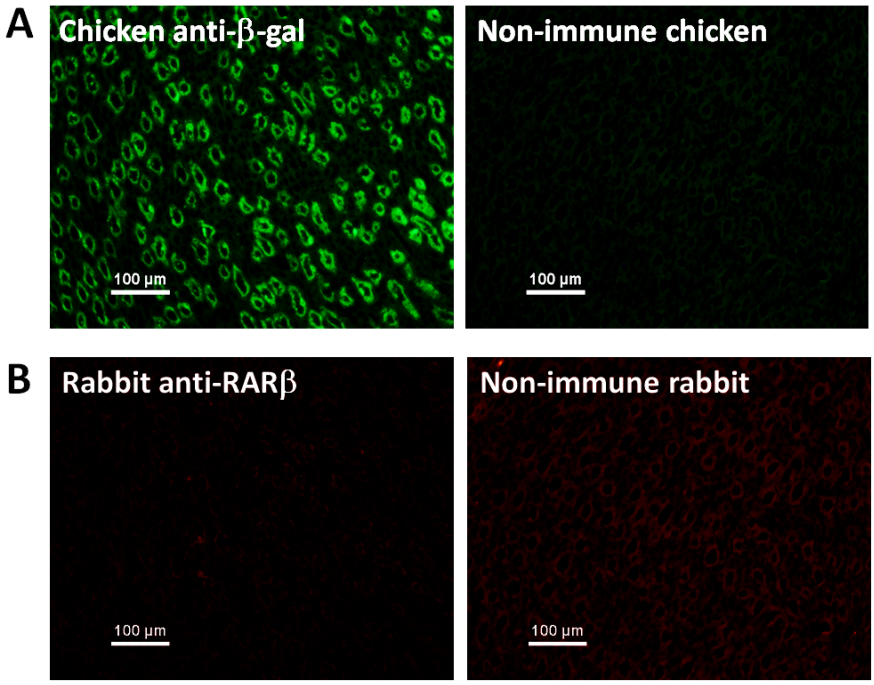


Figure 3.20: Expression of retinoic acid receptor $\beta$ (RAR$\beta$) and $\beta$-galactosidase ($\beta$-gal) protein. In kidney section of a 3-week-old transgenic mouse, expression of RAR$\beta$ (B) was not observed in tubules with positive $\beta$-gal signal (A). Original magnification was 200x.

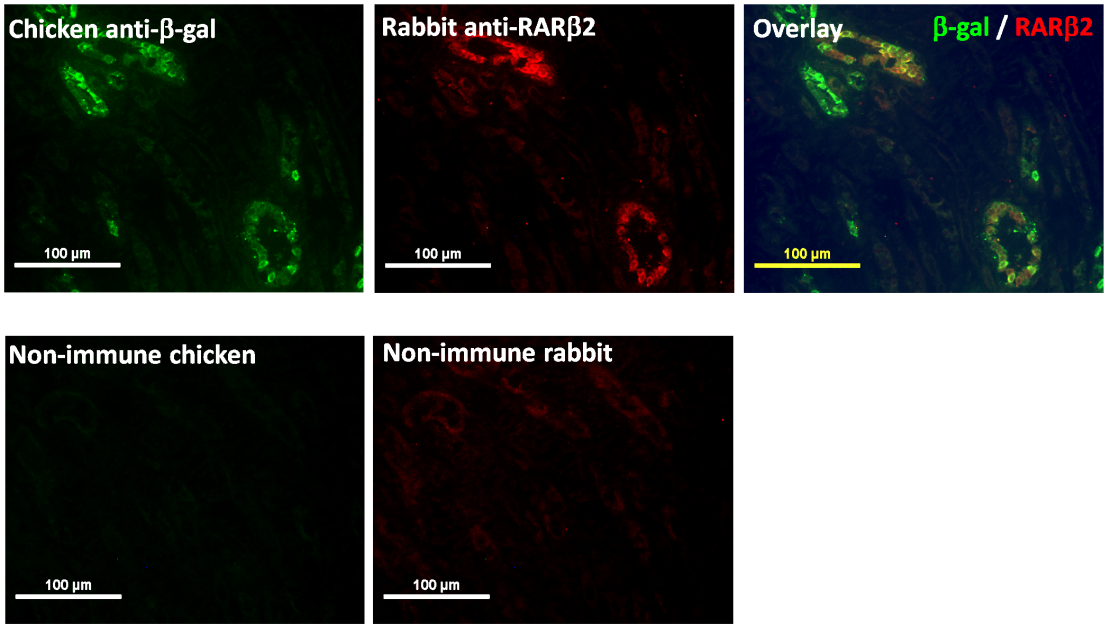


Figure 3.21: Expression of retinoic acid receptor $\beta$2 (RAR$\beta$2) and $\beta$-galactosidase ($\beta$-gal) protein. In kidney section of a 1-week-old transgenic mouse, many tubules stained positive only for $\beta$-gal, while only a few stained positive for both $\beta$-gal and RAR$\beta$2. Original magnification was 400x.

## 3.4 Discussions

### 3.4.1 Methodology used in detecting and localising reporter transgene expression

An X-gal assay was first performed on wholemount kidney and liver tissues to get a general idea on expression of reporter transgene. In order to avoid the possibility of poor penetration of X-gal into the tissues, X-gal assay was subsequently performed on kidney and liver cryosections to localise reporter transgene expression.

Although X-gal assay was a quick and convenient way of examining reporter transgene expression, it involved an enzymatic reaction that relies on functionality of the $\beta$-gal protein, which would be affected by tissue fixation [185]. Thus, X-gal assay had to be performed on cryosections that were only briefly fixed. The short fixation period did not allow precise X-gal localisation due to suboptimal histological detail. Moreover, diffusion of X-gal product to adjacent cells [266] and the inherent difficulties during sectioning that subjected tissues to multiple freeze-thaw cycles also hampered localisation of X-gal signal at the cellular level. Therefore, reporter transgene expression was further confirmed with immunostaining of $\beta$-gal protein, using an optimised concentration of antibody, performed on paraffin sections.

Localisation of reporter transgene expression was determined based on the advice from King's College hospital consultant histopathologist, Dr. N Dutt. In addition, a double immunostaining was performed for $\beta$-gal protein and a series of marker antibodies, of which their optimum concentrations and specificity were carefully examined and validated (Figure 3.6). Taken together, the expression of reporter transgene and its localisation were examined using more than one method and similar conclusions were drawn from different methodologies.

### 3.4.2 Expression of reporter transgene in the kidney but not in the liver

X-gal signal in kidneys of 1-, 2-, and 3-week-old transgenic mice was rather similar in intensity, and was higher compared to that in kidneys of 5- and 8-week-old transgenic

mice (Figure 3.8 and Figure 3.9), consistent with the pattern of immature and mature kidneys, respectively. The exact half-life of $\beta$-gal protein in these reporter mice is not known, but Rossant et al. had described a day-to-day variation (both increase and decline) of the reporter transgene activation from E7.5 until E12.5 [266], indicating a dynamic activation of reporter transgene and a relatively rapid turn-over of $\beta$-gal protein. Given that no apparent difference in the intensity of X-gal signal was observed in 1- to 3-week-old kidney and that the signal was still consistently observed in 5- and 8-week-old kidney, albeit at lower intensity, the signal was suggestive of a constant activation of reporter transgene rather than an accumulation of $\beta$-gal protein from embryonic stage.

The positive signal of reporter transgene expression observed in the kidney of transgenic mice from all age groups indicates a constitutively active RARE activity. *In vitro*, the *RARE-hsp68-lacZ* construct was activated by RA but not by thyroid hormone [266]. When metanephric kidney of *RARE-hsp68-lacZ* mice was cultured *in vitro* for 72 h without tRA, there was a complete loss of reporter transgene expression, whereas a conspicuous and intense signal continued to be present in the ureteric bud tips and trunks of wholemount kidney cultured in medium containing tRA for the same duration [267]. Administration of exogenous RA to pregnant *RARE-hsp68-lacZ* mice resulted in an elevation of reporter transgene expression in domains where reporter transgene expression was normally present, as well as in novel domains where transgene expression was not originally detected in mouse foetus [266]. Similar observation of an enhanced transgene expression was reported in mice deficient in Cyp26 when mated to *RARE-hsp68-lacZ* reporter mice [273]. Collectively, these results showed that the reporter transgene is responsive towards both exogenous and endogenous RA, as well as ruling out the possibility of site-specific silencing, at least during embryonic development. Thus, it is very likely that the constitutive RARE activity observed in the kidney of *RARE-hsp68-lacZ* transgenic mice indicated the presence of endogenous RA and activation of retinoid nuclear receptor that leads to reporter transgene expression.

On the other hand, there was no indication of reporter transgene expression in the liver. This might be due to an absence of bioactive RA or other components of retinoid system, i.e., functional RXR/RAR heterodimers and transcription co-regulators, necessary to support reporter transgene expression. Indeed, Xu et al. found that endogenous tRA was not detected in liver of 3-week-old C57BL/6 mice despite the presence of abundant tRol [328], which might explain the lack of reporter transgene expression in the liver of transgenic mice. However, absence of tRA in the liver is not unequivocal. Other groups had reported the presence of tRA in adult murine liver at a level higher than that measured in the kidney [137, 139, 277]. The discrepancy might be due to numerous variables including dietary vitamin A content, tissue preparation and retinoid extraction methods, sensitivity of assays employed, and animal strain or age difference, all of which might have an impact on tRA metabolism and detection. On the other hand, according to the NURSA database, the mRNA level of all three isotypes of "permissive" RARs, i.e., RAR$\alpha$, RAR$\beta$, and RAR$\gamma$, in the liver are at least 2-fold lower compared to those in the kidney of C57Bl/6J and 129x1/SvJ mice (www.nursa.org/10.1621/datasets.02001; last accessed on 30.07.11), which may account for the absence of reporter transgene expression in the liver. Nevertheless, presence of RARs with functional evidence had been reported in the past [60, 283]. Taken together, the presence of endogenous RA and its RAR-dependent activity in the liver is not as clear-cut at this stage and further studies are required to reconcile these discordance.

### 3.4.3 Expression of reporter transgene in the principal cells, inner medullary collecting duct cells, and intercalated cells of renal collecting ducts

The nephron, comprising the glomeruli, proximal tubules, Henle's loops, distal tubules, and connecting tubules, was originated from the metanephric mesenchyme, whereas the collecting duct is derived from ureteric bud [80]. In this project, reporter transgene expression was consistently detected in renal collecting ducts from 1-8 weeks of age, but not in glomeruli, proximal tubules, Henle's loops, and distal convoluted tubules (Figure 3.8). In rodents, AQP2-positive principal cells are found mainly in the collecting duct although some connecting tubule cells also express AQP2 protein [49]; V-ATPase-

positive cells first arise from the late portion of distal convoluted tubules [39], and are also found in the connecting tubules and collecting ducts [148]. Thus, some of the AQP2- and V-ATPase-positive cells observed in the cortical region might reside within the connecting tubules. However, it is difficult to conclude on whether the reporter transgene expression was localised to connecting tubules in the absence of a marker that specifically labels this segment [181].

Using the same reporter mice, Dr. A Yoshifusa at the National Institute of Health, Bethesda, had also detected a similar pattern of reporter transgene expression in neonatal kidneys at 1-2 days of age, whereby signal was observed in the ureteric bud tips and collecting ducts [327]. These observations closely reminisce that of Rosselot et al., who reported positive signal of reporter transgene expression in the ureteric bud tip and trunk of developing kidney at E12-E14 [267]. Hence, it is evident that the reporter transgene expression in the ureteric bud during nephrogenesis had persisted in the ureteric bud-derived collecting ducts, in principal cells, inner medullary collecting duct cells, and intercalated cells after birth.

### 3.4.4 Expression of RAR$\beta$, RAR$\beta$2, and reporter transgene

In *RARE-hsp68-lacZ*, domains of reporter transgene expression [266] closely resembled that of RAR$\beta$ transcript [62] from developmental stage E11.5 onwards, suggesting that RAR$\beta$ might be the main RAR that mediates embryonic development. It was thus speculated that reporter transgene expression observed in kidney collecting ducts might overlap with that of RAR$\beta$ and RAR$\beta$2.

In kidney of a 3-week-old transgenic mouse, RAR$\beta$ protein was not detected in tubules expressing reporter transgene (Figure3.20) while RAR$\beta$2 protein was detected only in a few collecting ducts that expressed reporter transgene in kidney of a 1-week-old mouse (Figure 3.21). The discrepancy between the immunostaining results of RAR$\beta$ and RAR$\beta$2 might be due to the age difference. The lack of RAR$\beta$ and RAR$\beta$2 immunostaining signal also raised the issues of specificity and sensitivity of these antibodies in

detecting the respective protein. However, these issues were failed to be addressed due to the lack of controls such as tissues known to express a high level of RAR$\beta$ and RAR$\beta$2, and lack of RAR$\beta$ and RAR$\beta$2 antigens that antibodies could be pre-adsorbed with.

While it remains inconclusive whether the reporter transgene activation in collecting ducts were mediated by RAR$\beta$, it is important to note that the RARE on reporter transgene, although derived from RAR$\beta$, can be activated by all three RAR isotypes, i.e., RAR$\alpha$, RAR$\beta$, and RAR$\gamma$ [266]. More studies such as kidney-specific genetic ablation of individual or compound RARs and RXRs are required to determine the mediator of reporter transgene activation.

### 3.4.5 Expression of Raldh3 and reporter transgene

Transcript of Raldh3 was reported to be present predominantly in the inner medulla of adult mouse kidney [232] but expression of Raldh3 protein in the kidney has not been reported thus far. It was found in this study that the expression pattern of Raldh3 closely resembled that of Raldh3 transcript, which was primarily in the inner medulla (Figure 3.19A). The partial overlapping between Raldh3 and reporter transgene expression might suggest both autocrine and paracrine action of Raldh3 in generation of bioactive RA to activate reporter transgene in the collecting duct. However, when kidney section was incubated with anti-Raldh3 IgG pre-adsorbed with Raldh3 antigen, a similar staining pattern as the section that was stained with anti-Raldh3 IgG alone was observed (Figure 3.19B). The situation could be due to suboptimal binding between antibody and blocking antigen hence not all antigen binding sites were blocked, or could be due to an inherent fault in either the anti-Raldh3 IgG or the Raldh3 blocking antigen. Further testing including prolonged pre-incubation of antibody and Raldh3 antigen, as well as a higher ratio of Raldh3 antigen to antibody are required to achieve a solid conclusion.

Taken together, although Raldh3 immunostaining showed a pattern similar to the Raldh3 transcript reported before, it remains inconclusive if the immunostaining signal was indeed Raldh3. Even if Raldh3 protein did indeed overlap with reporter transgene expres-

sion, further testing such as knock down of Aldh1a3 that encodes Raldh3 is required to confirm its contribution towards generating RA for reporter transgene activation.

### 3.4.6 Concluding remarks

In this study, constitutive RARE activity was observed in principal cells, inner medullary collecting duct cells, and intercalated cells, which might indicate constitutive RAR activation by endogenous RA in these cells as discussed before. Nevertheless, there is a possibility whereby the reporter transgene was activated by other elements in addition to RA. In fact, it was reported that *RARE-hsp68-lacZ* transgene could be activated by heat shock and by arsenite [150]. While the reporter mice were not exposed to either of these elements, it remains unknown if the RARE activity was given rise by other yet identified elements. However, based on the observation of reporter transgene expression in the ureteric buds of developing kidneys, which are dependent on RA [267], the RARE activity observed in the ureteric bud-derived collecting duct in this study was very likely to be mediated by a constitutive activation of RAR/RXR by endogenous RA. On the other hand, sites devoid of reporter signal could be a result of site-specific transgene silencing that might have happened during the transition from embryo to adulthood [51]. Thus, whether the lack of reporter signal in sites other than the collecting duct, such as glomeruli and proximal tubules, was due to site-specific silencing would require further confirmation.

The *RARE-hsp68-lacZ* reporter mice have been widely employed to study the role of RA activity during embryonic development but have not been extensively used at postnatal and adult stages. Thus, it would be of great interest to further characterise the reporter mice after birth, in terms of its sensitivity and specificity in reporting RAR-dependent endogenous RA activity. This can be achieved by altering the availability and level of endogenous RA in the reporter mice, e.g., by subjecting the mice to diet containing varied amount of vitamin A, or by administrating chemical reagents that inhibit RA biosynthesis or that antagonise retinoid nuclear receptors. In addition, by mating *RARE-hsp68-lacZ* mice to conditional knockout mutants of individual or compound

RARs/RXRs, as well as of retinoid synthesising and metabolising enzymes, would allow the identification of mediators of reporter transgene activation.

Collecting ducts are the final renal tubular segment that connects the renal tubules to the bladder and are the only renal tubules that spans across the whole kidney from cortex to inner medulla. It is well acknowledged that collecting ducts are made up of a heterogeneous population of cells with distinct features and functions. Classically, the principal cells are known to be regulating $Na^+$ and water reabsorption, while intercalated cells that are subdivided into at least three subtypes, i.e., $\alpha$-, $\beta$-, and non-$\alpha$- non-$\beta$-intercalated cells, are thought to be regulating acid/base balance; a third distinct cell type, designated inner medullary collecting duct cells, are present in the collecting duct of inner medullary region 2 (middle) and 3 (terminal), which possess some characteristics of both principal cells and intercalated cells, as well as mediate urea transport [73, 80]. Emerging publications are challenging the classical views on functions of collecting ducts, and have shown evidence of their novel properties, such as: (i) involvement of intercalated cells in regulation of $Na^+/K^+$ exchange and in paracrine communication with principal cells [73], (ii) defence against bacterial infection [42], (iii) regulation of tubulointerstitial inflammatory processes and fibrogenesis via Krüpel-like factor 5 [91], and (iv) epithelial-mesenchymal transition leading to fibrotic changes [37, 130].

Considering its multifaceted functions, the collecting duct is indeed highly versatile. If the reporter transgene activation indeed represents a constitutive activation of RAR/RXR by endogenous RA, it might play a role in mediating some of the known and perhaps other as yet unknown functions of collecting ducts. Finally, it must be reiterated that the presence of a constitutive activation of RAR/RXR by endogenous RA in the collecting duct does not negate the fact that other RAR-independent signalling mechanisms of RA might also be operative in the collecting duct, as well as in sites other than the collecting duct.

# Chapter 4

# Retinoic Acid Receptor-dependent Endogenous Retinoic Acid Activity in a Mouse Collecting Duct Cell Line

---

## 4.1 Introduction

While the presence of RARE activity was observed in kidney collecting ducts of *RARE-hsp68-lacZ* mice, a direct evidence of it being a result of retinoid nuclear receptor activation by endogenous RA is lacking. In order to address this issue, the presence of RARE activity was examined in an *in vitro* model of collecting duct cells. This chapter describes the presence of constitutive retinoid nuclear receptor activation by endogenous RA in a well-established collecting duct cell line.

### 4.1.1 mIMCD-3 as an *in vitro* model

Although primary cultures derived from mouse collecting ducts would be more physiologically relevant, establishment of highly enriched primary cultures of collecting duct cells that maintain high level of epithelial differentiation and collecting duct cells-specific characteristics would be laborious and technically challenging. An alternative to primary cultures is to employ cell lines derived from collecting ducts. Mouse inner

medullary collecting duct cells, mIMCD-3 cells, were chosen as a cell model for this purpose.

The mIMCD-3 cells were derived from the terminal one third of inner medullary collecting ducts of a mouse transgenic for the early region (large T antigen) of simian virus 40, Tg(SV40E)Bri/7 [257]. The original founder reported that mIMCD-3 cells retain many characteristics of the inner medullary collecting duct cells observed *in vivo*, including high transepithelial resistance, presence of amiloride-sensitive sodium channel with luminal-to-basolateral sodium flux that was blocked by both amiloride and atrial natriuretic peptide, and the ability to grow in hypertonic medium up to 900 mOsmol/kg $H_2O$ [257].

Ever since its establishment, mIMCD-3 cells have been employed as an *in vitro* model in various studies, which are highly relevant to functions and activities of collecting duct principal cells and inner medullary collecting duct cells, such as ion channel signalling [105, 285], signalling during osmotic and hypertonic stress [38], and urea signalling [47]. In addition, mIMCD-3 cells undergo branching morphogenesis when grown on 3-dimensional gel matrix [162], a unique feature of the ureteric bud cells in developing embryonic kidney. Therefore, as a starting point, mIMCD-3 cells should serve as a good *in vitro* model of collecting duct principal cells, inner medullary collecting duct cells, and ureteric bud cells, for examination of RARE activity.

## 4.2 Materials and methods

### 4.2.1 Cell culture and cell morphology

The basic maintenance and culturing of mIMCD-3 cells was described in Chapter 2, Section 2.2. Cell morphology at different passages was examined under phase contrast microscopy and microscopic photos were taken for future reference.

At low confluence, mIMCD-3 cells had slightly spindled morphology; when near confluent, mIMCD-3 cells had an uniform cuboidal morphology (Figure 4.1A). A change in cell morphology was noted by around P9-P10 (Figure 4.1B), during which the cells were growing very quickly. The phenomenon might be due to a permanently high level of uncontrolled large T antigen expression leading to cell dedifferentiation [21]. Thus, all experiments employing mIMICD-3 cells were performed within P3-P8, and cells were discarded as soon as morphological change was observed.

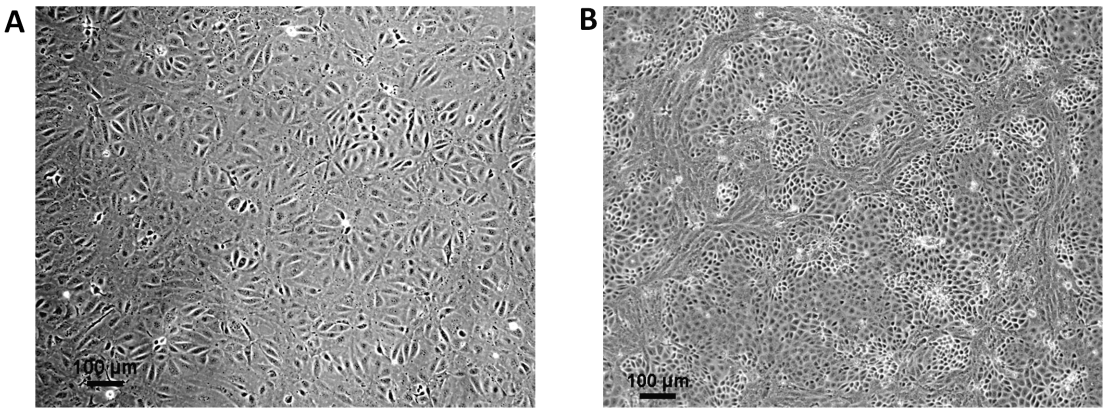


Figure 4.1: Morphology of mICMD-3 cells. The figure shows mIMCD-3 cells at P3 and P9 cultured for 48 h. At the end of 48 h, mIMCD-3 cells of P3 achieved 80% to 100% confluent and had a uniform cobblestone-like morphology with distinct cell-cell boundary (**A**). Whereas, mIMCD-3 cells of P9 were over-confluent; some cells were elongated with less apparent cell-cell boundary (**B**). Original magnification was 100x.

### 4.2.2 Immunocytochemistry for E-cadherin and AQP2

Since a detailed characterisation of mIMCD-3 cells had already been performed by the original founder of this cell line [257], a basic characterisation was performed to confirm the identity of mIMCD-3 cells. Expression of E-cadherin (E-cad), a marker of epithelial

cells, and AQP2, a marker of collecting duct principal cells and inner medullary collecting duct cells, were examined with indirect immunocytochemistry.

Cells were seeded at 6 x $10^5$ cells/35 $mm^2$ dish in 2 ml DMEM-F12 medium containing antibiotics and anti-fungal, supplemented with 5% FBS. After an overnight culture until confluent, cells were fixed with ice-cold 5% formalin for 15 min on ice, followed by washing with three changes of PBS, 5 min each wash. Cells were then permeabilised with 0.1% Triton X-100 for 3 min and washed with three changes of PBS, 5 min each wash. After fixation and permeabilisation, cells were incubated with 1% BSA for 2 h at room temperature to reduce non-specific antibody binding, followed by 1 h incubation of rabbit anti-AQP2 IgG (dilution 1:150), or mouse anti-E-cad $IgG_{2a}$ (dilution 1:50, BD Biosciences, Oxford, UK), at room temperature. Cells incubated with non-immune rabbit IgG and non-immune mouse $IgG_{2a}$ (Insight Biotechnology Ltd., UK) at the same concentrations served as negative controls for anti-AQP2 IgG and for anti-E-cad $IgG_{2a}$, respectively. Cells were then washed with three changes of PBS, 5 min each wash, and were incubated with goat anti-rabbit conjugated with AlexaFluor 488 (2 $\mu$g/ml) for AQP2 detection or goat anti-mouse conjugated with AlexaFluor 555 (2 $\mu$g/ml) for E-cad detection, for 1 h at room temperature. At the end of secondary antibody incubation, cells were washed with three changes of PBS, 5 min each wash. One millilitre of fresh PBS was then pipetted onto the cell monolayer and fluorescence microscopy was performed immediately. For all washing steps, PBS was pipetted gently onto cells from the side of dishes, after which dishes were shaken at low speed on a table top rocker.

As shown in Figure 4.2, both E-cad and AQP2 protein were detected in mIMCD-3 cells. The morphology of mIMCD-3 cells (Figure 4.1), as well as the presence of E-cad and AQP2 protein in this cell line (Figure 4.2) were consistent with it being of epithelial and of principal cell/inner medullary collecting duct cell origin.

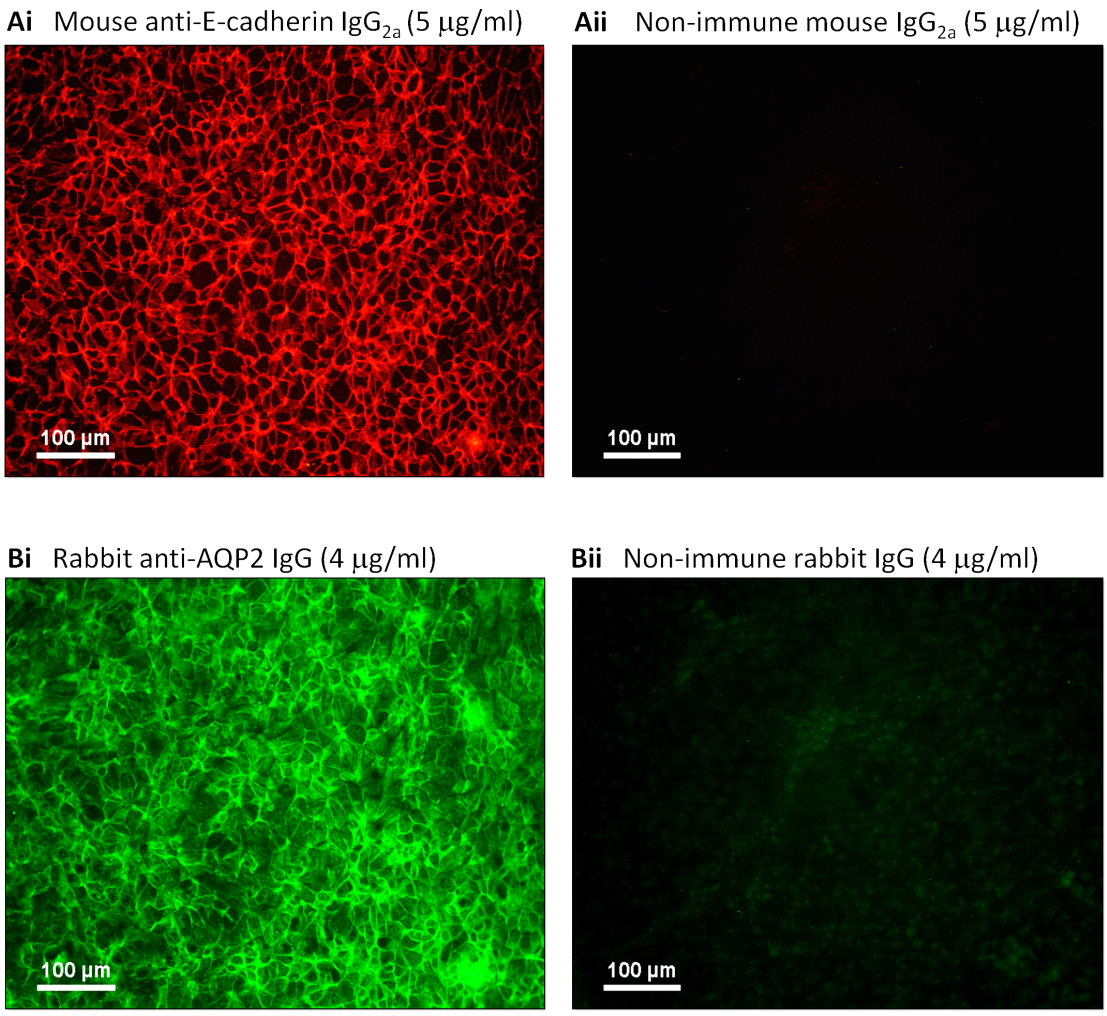


Figure 4.2: E-cadherin (E-cad) and aquaporin 2 (AQP2) protein expression in mIMCD-3 cells. **Ai.** Expression of E-cad protein was predominantly localised to cell membrane. **Bi.** Expression of AQP2 protein was more intense in cell membrane and was also noted in cell cytoplasm. No specific signal was detected in mIMCD-3 cells stained with non-immune IgGs (**Aii and Bii**). Original magnification was 100x.

### 4.2.3 Reporter assay

The presence of RARE-activity in mIMCD-3 cells was examined in reporter assay with transient transfection of RA reporter plasmid. Plasmids used are as follow:

1. **pmaxGFP in TE buffer** (Lonza Wokingham Ltd., Berkshire, UK): A plasmid that constitutively expresses green fluorescent protein (GFP) when transfected into the cells. pmaxGFP plasmid was used to assess transfection efficiency in the first instance. Map of pmaxGFP plasmid is shown in Appendix A.1.

2. **pGL3-RARE-luciferase in TE buffer** (a kind gift from Dr. T M Underhill [124] and prepared by Dr. Y Abe): A plasmid that expresses firefly luciferase in the presence of RA, functional RAR heterodimers, and transcription co-activators, similar to the principle of transgene activation in *RARE-hsp68-lacZ* transgenic mice as described in Section 3.1.1. Map of pGL3-RARE-luciferase plasmid is shown in Appendix A.2.1.

3. **pCI-$\beta$-galactosidase in $CsCl_2$** (a kind gift from Promega, Madison, USA, and prepared by Dr. Q Xu): A plasmid that constitutively expresses $\beta$-gal when transfected into the cells, and hence was co-transfected with pGL3-RARE-luciferase plasmid to serve as a control for transfection efficiency. Map of pCI-vector is shown in Appendix A.2.2.

***Plasmid DNA precipitation***

Before first use, pCI-$\beta$-galactosidase plasmid was precipitated and resuspended in sterile TE buffer. A volume of 125 $\mu$l pCI-$\beta$-galactosidase plasmid DNA was pipetted into a 1.5 ml microtube, following which 12.5 $\mu$l of 3 M sodium acetate buffer (pH 5.2) was added. The positively charged sodium ($Na^+$) acts to neutralise the negative charges on phosphate groups ($PO_3^-$) of the DNA, rendering the DNA less hydrophilic and less soluble in water. The interaction between $Na^+$ and $PO_3^-$ was further accomplished by adding 343.75 $\mu$l of ice cold 100% ethanol, which has a much lower dielectric constant, to the plasmid DNA sodium acetate mixture. The mixture was then kept at -20 °C for 2 h, after which microtube was centrifuged at 24,100 g in a Mikro 24-48R microcentrifuge for 15 min at 4 °C, with hinge of microtube facing outward. After centrifugation, supernatant was carefully decanted, after which 200 $\mu$l of ice cold 70% ethanol was pipetted into the microtube without resuspending the precipitated plasmid DNA, to wash away residual salt from DNA pellet. Microtube was again centrifuged at 24,100 g for 5 min and supernatant was removed with a 200 $\mu$l pipette, avoiding the pelleted plasmid DNA. Finally, the microtube was left in a tissue culture hood for about 15 min with the lid opened to allow evaporation of residual ethanol. Plasmid DNA pellet was then resus-

pended in 60 $\mu$l of sterile TE buffer and stored at 4 °C until use.

Supernatant was removed in a tissue culture hood throughout the procedure to ensure sterility of the plasmid DNA preparation. The final concentration of plasmid DNA was determined using a NanoDrop® ND-1000 machine, with TE buffer set as blank measurement. A ratio of ≈1.80 for A260/280 and a ratio of ≈2.0 for A260/230 were routinely obtained, confirming the purity of plasmid DNA.

***Other reagents used for transfection***

Lipofectamine™ LTX and Plus™ reagents (Invitrogen Ltd., UK) were used as transfection reagents following the company's product manual[1]. Lipofectamine™ LTX is a liposome formulation containing the polycatinoic lipid, DOSPA, and the neutral lipid, DOPE, at a ratio of 3:1 (w/w). The positive charges of the lipid will associate with the negatively charged plasmid DNA and form liposome/DNA complexes. The resulting lower net negative charges on the plasmid DNA encourages closer association between plasmid DNA and the negatively charged cell membrane, thereby facilitating transfer of plasmid DNA into the cell via endocytosis. Plus™ reagent functioned as an adjuvant that forms pre-complex with plasmid DNA to enhance DNA transfection. Opti-MEM® I Reduced Serum Medium (Invitrogen Ltd., UK) was used as a medium to dilute plasmid DNA and for formation of lipid-DNA complex.

***Examination of transfection efficiency and plasmid functionality***

Cells were seeded into a 24-well plate at 4 x $10^4$ cells/well in 500 $\mu$l of DMEM-F12 medium supplemented with 5% FBS, without antibiotics and anti-fungal. Cells were cultured overnight for 16-24 h until about 60% to 80% confluent before being transfected with 1 $\mu$g pmaxGFP plasmid. Cells were then incubated for an additional 5 h before the medium was changed to fresh DMEM-F12 medium supplemented with 1% FBS. Cells were incubated overnight before being examined under the epifluorescence microscope

[1] Invitrogen Lipofectamine™ LTX and Plus™ Reagents, edition 08/2008, P/N: 15338.pps

for presence of GFP-positive cells.

Transfection was performed in duplicates. A volume containing 1 $\mu$g of pmaxGFP plasmid DNA, 2 $\mu$l of Lipofectamine™ LTX, and 1 $\mu$l of Plus™ Reagent were prepared in 100 $\mu$l Opti-MEM® I for each well. pmaxGFP plasmid DNA was first diluted in Opti-MEM® I and mixed well, after which Plus™ reagent was added directly into the diluted plasmid DNA and incubated for 10 min at room temperature. Lipofectamine™ LTX was then added directly to the plasmid DNA-Plus™ mixture and incubated at room temperature for 30 min to allow formation of DNA-lipid complexes. Without removing the culture medium, 100 $\mu$l of DNA-lipid complexes was added directly, drop-wise, to each well, followed by gentle rocking of the plate. As a negative control for background signal, a mixture of Lipofectamine™ LTX and Plus™ reagents in Opti-MEM I prepared the same way but without plasmid DNA was added to cells in another well. By using the Matlab Image Processing Toolbox version 7.2, around 65% of the total number of cells expressed GFP (Figure 4.3). The algorithm used for image analysis is shown in Appendix A.3.

In order to determine functionality of pCI-$\beta$-galactosidase plasmid and to determine if endogenous $\beta$-gal was present in mIMCD-3 cells at a high level that would preclude its use for normalising pGL3-RARE-luciferase reporter activity, mIMCD-3 cells were transfected with 1 $\mu$g of pCI-$\beta$-galactosidase plasmid following the protocol described before for pmaxGFP plasmid transfection. At the end of transfection, cells were stained with X-gal staining solution (the same staining solution used for tissue cryosection) to determine $\beta$-gal expression. Medium was first removed and cells were washed once with PBS before being fixed in 5% formalin and 0.2% glutaraldehyde in PBS for 10 min at room temperature. Cell monolayer was then washed twice with PBS, 5 min each wash, and incubated in 150 $\mu$l of X-gal staining solution for 2 h at 37 °C with occasional rocking of the plate. At the end of 2 h incubation, X-gal solution was washed off with PBS and microscopic photos were taken immediately.

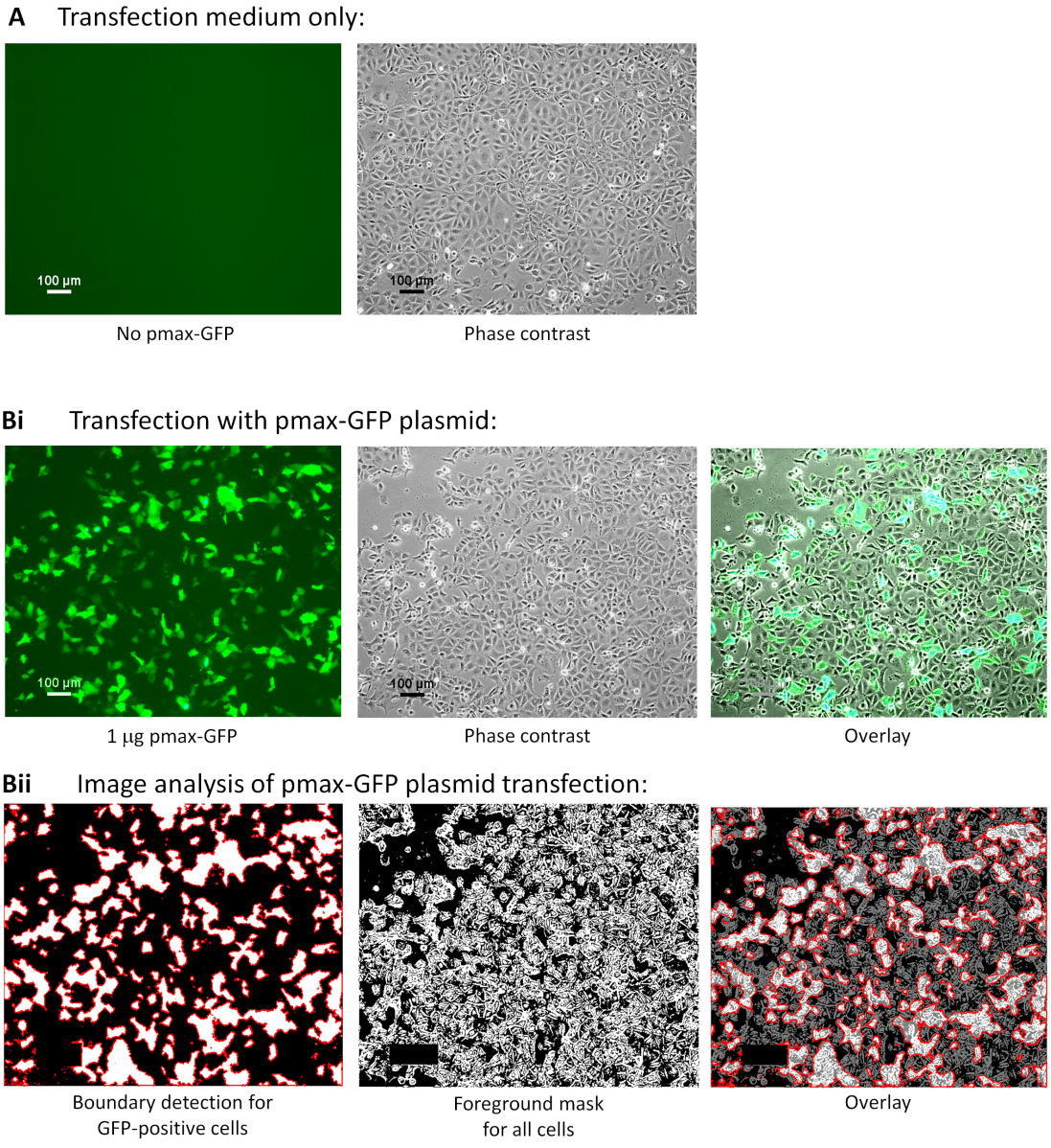


Figure 4.3: Transfection efficiency assessed from green fluorescent protein (GFP) expression. **A.** In cells where only transfection reagents were added, no GFP expression was observed. **Bi.** GFP expression was observed in cells transfected with pmaxGFP plasmid. **Bii.** Image analysis revealed that 65.25% of the total mIMCD-3 cells expressed GFP (green). Original magnification was 100x.

X-gal product was detected in transfected cells, confirming the functionality of pCI-$\beta$-galactosidase plasmid; no apparent signal was detected in non-transfected cells, indicating the absence of high endogenous $\beta$-gal (Figure 4.4). The observation suggest the presence of minimum, if any, endogenous $\beta$-gal in mIMCD-3 cells, hence permitting its use as normalisation control for transfection efficiency.

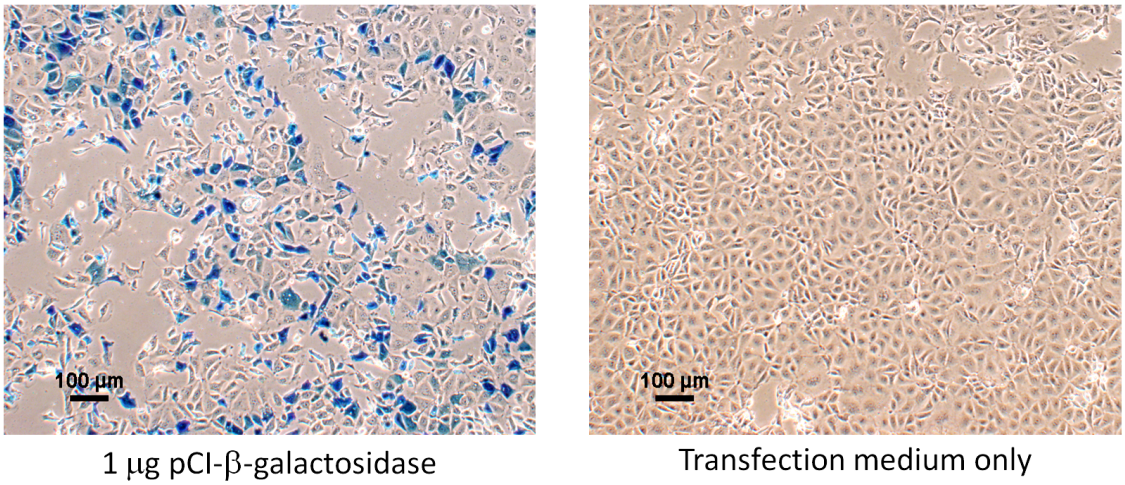


Figure 4.4: Validation of pCI-$\beta$-galactosidase plasmid as normalisation control for transfection efficiency. An intense signal of X-gal product (blue) was detected in mIMCD-3 cells transfected with pCI-$\beta$-galactosidase plasmid (left panel). No signal of X-gal product was noted in cells where only transfection reagents were added (right panel). Original magnification was 100x.

***Co-transfection of pGL3-RARE-luciferase and pCI-$\beta$-galactosidase plasmids***

Co-transfection of pGL3-RARE-luciferase and pCI-$\beta$-galactosidase plasmids were performed following the same protocol described for pmaxGFP transfection. The ratio (in $\mu$g) of pGL3-RARE-luciferase plasmid DNA : pCI-$\beta$-galactosidase plasmid DNA was 5:1, and the ratio of plasmid DNA (total of pGL3-RARE-luciferase plasmid DNA and pCI-$\beta$-galactosidase plasmid DNA in $\mu$g) : Lipofectamine™ LTX (in $\mu$l) : Plus™ Reagents (in $\mu$l) was 1:2:1. The actual amount used for transfection in individual experiment is described in Section 4.2.4.

***Cell lysis for examination of plasmid expression***

Cells were lysed in Reporter Lysis Buffer (RLB) (Promega UK, UK), which is a lysis buffer compatible with both pGL3-RARE-luciferase and pCI-$\beta$-galactosidase plasmids. Culture medium was first removed with a 1 ml pipette and the cell monolayer was carefully washed once with 600 $\mu$l of $Ca^{2+}$- and $Mg^{2+}$-free PBS per well. After removing the PBS from cell monolayer, 150 $\mu$l of 1x RLB (prepared by diluting 5x RLB with $H_2O$) was pipetted directly onto cells in each individual well. In order to ensure complete lysis, the 24-well plate containing cells in 1x RLB was kept at -80 °C for at least 2 h and then thawed at room temperature. The RLB cell lysate was then pipetted into a 1.5 ml microtube and centrifuged at 12,000 g in a Mikro 24-48R microcentrifuge for 2 min at 4 °C. The supernatant was transferred to a new 1.5 ml microtube and stored at -80 °C if not analysed immediately. Cell lysate was divided into two separate portions, to be examined for the expression of firefly luciferase and $\beta$-gal, respectively.

***Substrates for examination of plasmid expression***

Expression of firefly luciferase and $\beta$-gal was detected by production of luminescence. A Luciferase Assay System (Promega UK, UK), which contains lyophilised Luciferase Assay Substrate and Luciferase Assay Buffer, was used to examine expression of firefly luciferase following the company's technical bulletin[2]. The Luciferase Assay System contains beetle luciferin and other co-factors that are substrates for firefly luciferase, the product of *luc*$^+$ gene contained in the pGL3-RARE-luciferase plasmid. The lyophilised Luciferase Assay Substrate was first reconstituted in 10 ml of Luciferase Assay Buffer. The reconstituted Luciferase Assay Substrate was then dispensed into aliquots of 3 ml or 4 ml, and stored at -80 °C until use. The reagent was equilibrated to room temperature before use.

A Beta-Glo® Assay System (Promega UK, UK), which contains lyophilised Beta-Glo® Assay Substrate and Beta-Glo® Assay Buffer, was used to examine the expression of

[2]Luciferase Assay System Technical Bulletin, edition 03/2009, P/N: TB281

pCI-$\beta$-galactosidase plasmid, following the company's technical manual[3]. The Beta-Glo® Assay System contains 6-O-$\beta$-galactopyranosyl-luciferin that acts as a substrate for $\beta$-gal, the product of *lacZ* gene contained in the pCI-$\beta$-galactosidase plasmid, to yield D-luciferin, which was subsequently converted into oxyluciferin by firefly luciferase and other co-factors present in the assay reagent.

The basic principles of transfection and chemical reactions involved in detecting plasmid expression are illustrated in Figure 4.5.

***Detection of luminescent signal***

The luminescent signal was detected with a DTX880 multimode detector. The multimode detector was programmed to perform linear shaking at a moderate speed for 5 sec prior to reading, and to analyse the wells from left to right in a horizontal manner. The integration time was set at 1 sec for luminescence generated from both pGL3-RARE-luciferase plasmid and from pCI-$\beta$-galactosidase plasmid. Readings generated from non-transfected cells (cells treated with transfection medium without plasmid DNA) were set as background that were subtracted from all other readings generated from transfected cells. Result was expressed as Relative Light Unit (RLU), which is a ratio of light produced from pGL3-RARE-luciferase plasmid : light produced from pCI-$\beta$-galactosidase plasmid.

For the detection of light produced from pGL3-RARE-luciferase plasmid, 20 $\mu$l of cell lysate from each microtube was pipetted into individual well of an opaque black 96-well plate (Greiner Labortechnik Ltd., UK). As soon as 100 $\mu$l/well of Luciferase Assay Substrate was added to the cell lysate, light with a relatively short half-life of about 10 min will be produced, which will remain constant for about 1 min. Therefore, 100$\mu$l of Luciferase Assay Substrate was added to cell lysate in each well of a single row on the 96-well plate using multi-chamber pipette, after which reading was performed immedi-

[3]Promega Beta-Glo® Assay System Technical Manual, edition 09/2009, P/N: TM239

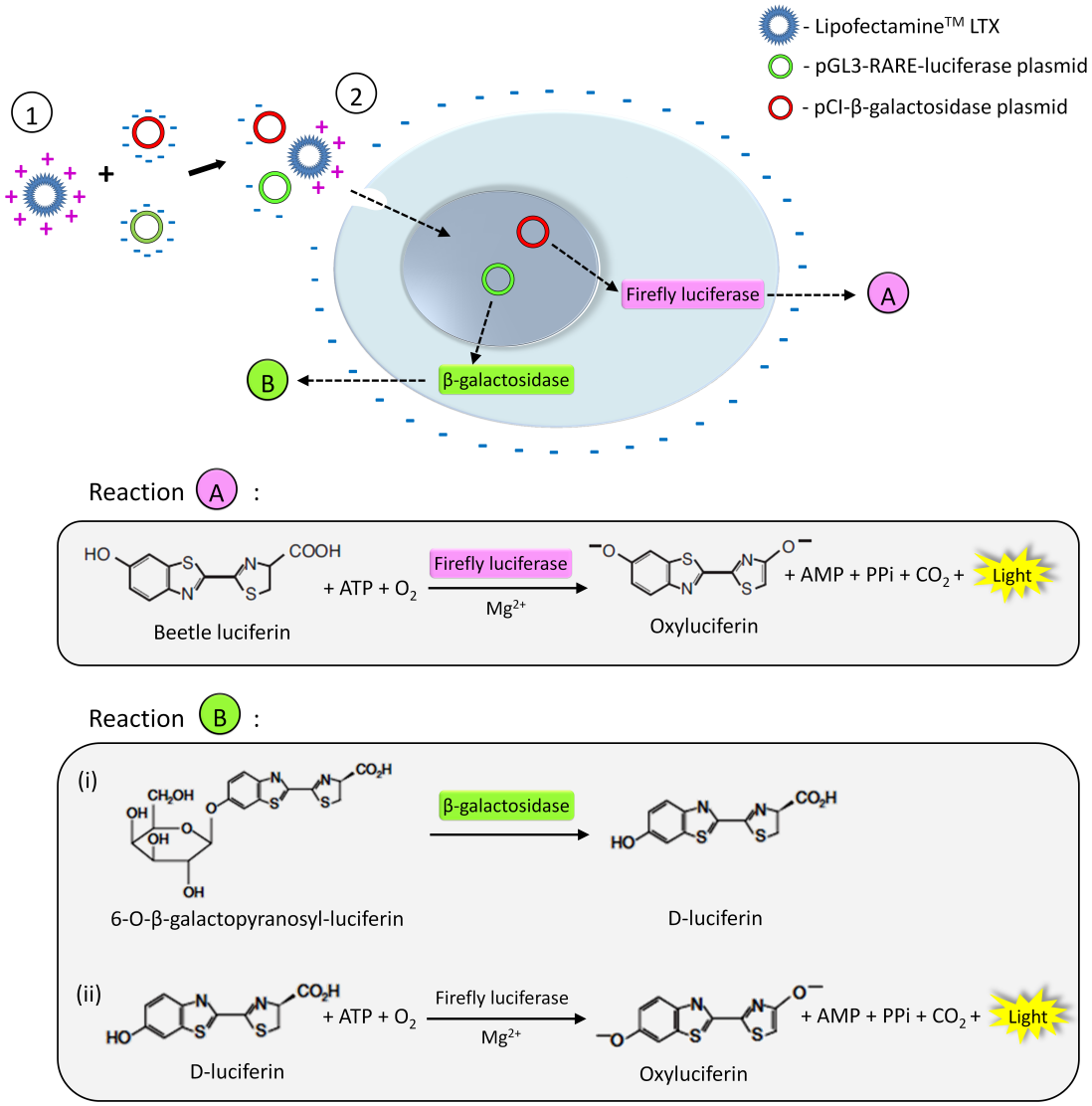


Figure 4.5: Plasmid transfection and detection. The negatively charged pGL3-RARE-luciferase and pCI-$\beta$-galactosidase plasmid DNA were first incubated with the positively charged Lipofectamine™ LTX to form complex (**1**). The lower repelling force between the negatively charged cell membrane and the DNA-Lipofectamine™ LTX complex with a lower net negative charge enhance plasmid DNA delivery into the cells (**2**). Cells were lysed and divided into two separate portions subjected to different chemical reactions: (i) Reaction A, where beetle luciferin was converted into oxyluciferin accompanied by light production catalysed by firefly luciferase (encoded by pGL3-RARE-luciferase plasmid), and (ii) Reaction B, where 6-O-$\beta$-galactopyranosyl-luciferin was converted into D-luciferin catalysed by $\beta$-gal (encoded by pCI-$\beta$-galactosidase plasmid), and subsequently into oxyluciferin accompanied by light production.

ately.

Unlike the light produced from Luciferase Assay System, light produced from Beta-Glo® Assay System has a long half-life and the signal intensity remains constant over a period of 4 h. Fifty microlitre of cell lysate from each individual microtube was pipetted into individual well of an opaque black 96-well plate, to which 50 $\mu$l/well of Beta-Glo® substrate were added. The 96-well plate was then agitated for 30 sec at moderate speed on an IKA MS1 minishaker to mix the reagents, after which it was left at room temperature covered in aluminium foil for 30 min before reading was performed.

Preliminary tests showed that luminescence generated from pCI-$\beta$-galactosidase plasmid was very high, which might saturate the detection capacity of the machine. In order to avoid saturation of luminescent signal, a serial dilution of cell lysate (from transfected cells treated with vehicle) was prepared with 1x RLB, and was analysed for luminescent signal. As shown in Figure 4.6, a near linear luminescent signal was produced by cell lysate at $10^2$x-$10^5$x dilutions. Thus, in all subsequent assays, cell lysate was diluted 1000x with 1x RLB to avoid saturation of luminescent signal.

The workflow of detecting and interpreting luminescent signal is summarised in Figure 4.7.

### 4.2.4 Experimental protocols for reporter assay

***tRA treatment in cells cultured in medium supplemented with normal FBS***

Cells were seeded into a 24-well plate at 4 x $10^4$ cells/well in 500 $\mu$l of DMEM-F12 supplemented with 5% FBS without antibiotics and anti-fungal. Cells were cultured overnight for 16-24 h until about 70% confluent before transfection was commenced. Cells were then incubated for an additional 5 h before medium was changed to fresh DMEM-F12 medium supplemented with 1% FBS with antibiotics and anti-fungal. Cells were incubated overnight before medium was again changed to fresh DMEM-F12 medium supplemented with 1% FBS containing 0.001 $\mu$M, 0.01 $\mu$M, or 0.1 $\mu$M tRA, and cultured for 24 h.

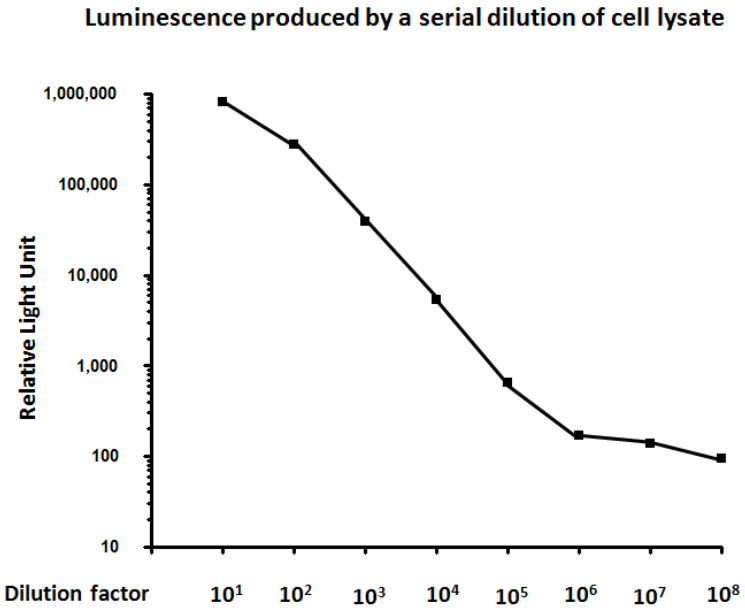


Figure 4.6: Serial dilution of Reporter Lysate Buffer cell lysate and luminescent signal. A near linear luminescent signal was achieved at $10^2$x to $10^5$x dilution of cell lysate.

For transfection, cells in each well were transfected with 0.25 $\mu$g pGL3-RARE-luciferase plasmid DNA, 0.05 $\mu$g pCI-$\beta$-galactosidase plasmid DNA, 0.6 $\mu$l Lipofectamine™ LTX, and 0.3 $\mu$l Plus™ Reagents, prepared in 100 $\mu$l of Opti-MEM® I.

***tRA treatment in cells cultured in medium supplemented with charcoal-stripped FBS***

Cells were seeded into a 24-well plate at 8 x $10^3$ cells/well in 500 $\mu$l of DMEM-F12 medium supplemented with 5% charcoal-stripped FBS (PAA laboratories Ltd., UK) to limit the supply of lipid-soluble retinoids, with antibiotics and anti-fungal. Cells were cultured for 72 h until about 70% confluent, and medium was then changed to fresh DMEM-F12 medium supplemented with 1% charcoal-stripped FBS without antibiotics and anti-fungal before transfection was commenced. Cells were incubated overnight before medium was again changed to fresh DMEM-F12 medium supplemented with 1% charcoal-stripped FBS containing 0.001 $\mu$M, 0.01 $\mu$M, or 0.1 $\mu$M tRA, and cultured for 24 h.

For transfection, cells in each well were transfected with 0.2 $\mu$g pGL3-RARE-luciferase

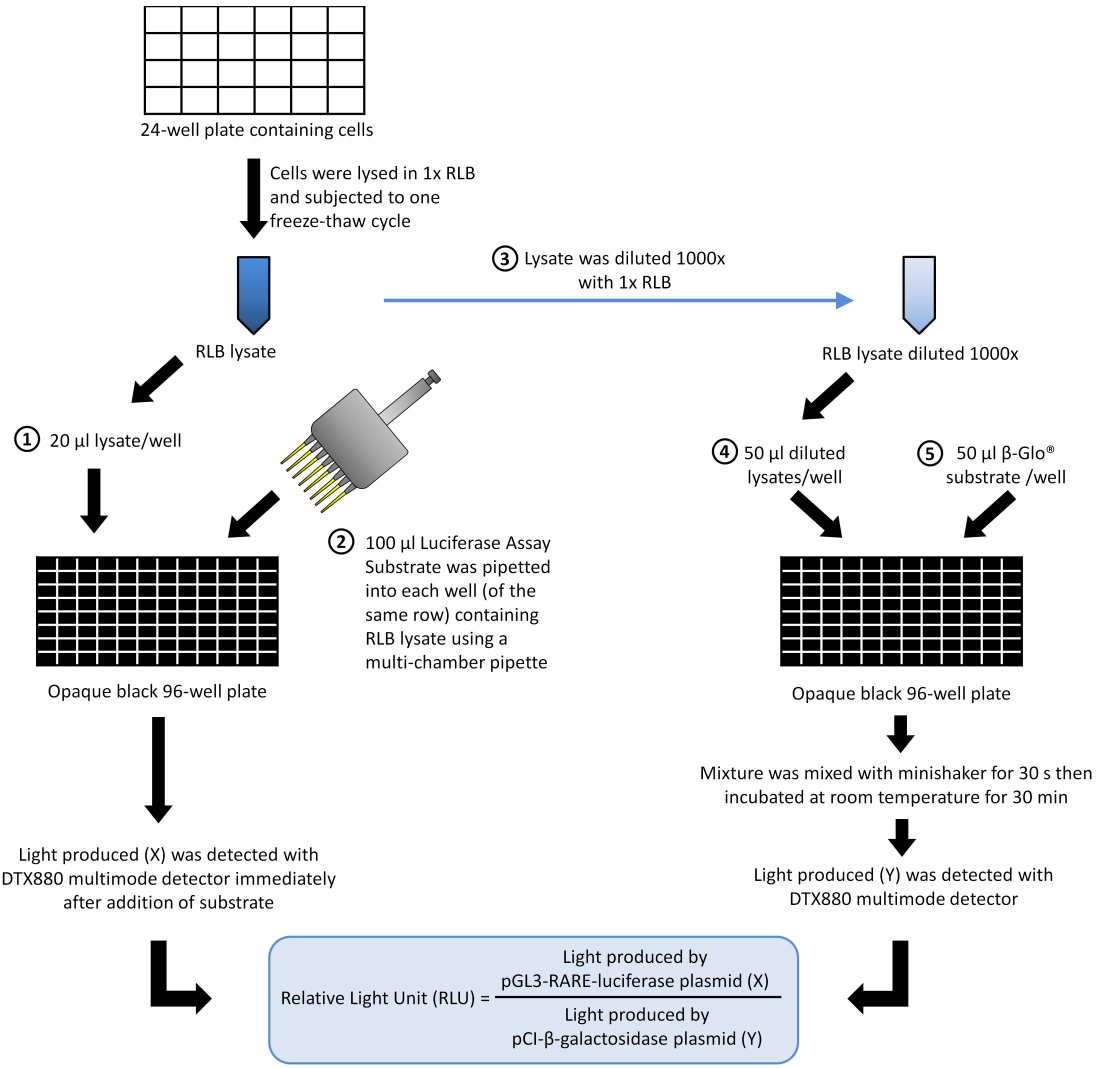


Figure 4.7: Workflow for luminescent signal detection. Cells were lysed with 1x Reporter Lysis Buffer (RLB) and subjected to one freeze-thaw cycle to ensure complete cell lysis. For the detection of light produced from pGL3-RARE-luciferase plasmid activation, 20 $\mu$l of undiluted cell lysate was pipetted into individual well of an opaque black 96-well plate (**1**). A volume of 100 $\mu$l/well of Luciferase Assay Reagent was added to wells of a single row containing cell lysate using a multi-chamber pipette (**2**). The light produced was analysed immediately after substrate addition to obtain a luminescent signal value designated "X". For the detection of light produced from pCI-$\beta$-galactosidase plasmid activation, cell lysate was first diluted 1000x with 1x RLB (**3**). The diluted cell lysate was pipetted into each well of an opaque black 96-well plate at 50 $\mu$l/well (**4**), to which 50 $\mu$l/well of Beta-Glo® substrate was added (**5**). The mixture was mixed well by shaking the 96-well plate on a minishaker for 30 sec, followed by a 30 min incubation at room temperature. The light produced was then analysed to obtain a luminescent signal value designated "Y". The Relative Light Unit (RLU) was calculated by dividing "X" by "Y".

plasmid DNA, 0.04 $\mu$g pCI-$\beta$-galactosidase plasmid DNA, 0.48 $\mu$l Lipofectamine™ LTX and 0.24 $\mu$l Plus™ Reagents, prepared in 100 $\mu$l of Opti-MEM® I.

***AGN193109 and BMS189453 treatment with and without tRA***

Cells were seeded into a 24-well plate at 4 x $10^4$ cells/well in 500 $\mu$l of DMEM-F12 medium supplemented with 5% FBS without antibiotics and anti-fungal. Cells were cultured overnight for 16-24 h until about 70% confluent before transfection was commenced. Cells were then incubated for an additional 5 h before medium was changed to fresh DMEM-F12 medium supplemented with 1% FBS with antibiotics and anti-fungal. Cells were incubated overnight before medium was again changed to fresh DMEM-F12 medium supplemented with 1% FBS containing 1 $\mu$M AGN193109 or 1 $\mu$M BMS189453, with and without 0.01 $\mu$M, 0.1 $\mu$M, or 1 $\mu$M tRA, and cultured for 24 h.

For transfection, cells in each well were transfected with 0.25 $\mu$g pGL3-RARE-luciferase plasmid DNA, 0.05 $\mu$g pCI-$\beta$-galactosidase plasmid DNA, 0.6 $\mu$l Lipofectamine™ LTX, and 0.3 $\mu$l Plus™ Reagents, prepared in 100 $\mu$l of Opti-MEM® I.

***DEAB and disulfiram treatment with and without tRA***

Cells were seeded into a 24-well plate at 2 x $10^4$ cells/well in 500 $\mu$l of DMEM-F12 medium supplemented with 5% FBS without antibiotics and anti-fungal. Cells were cultured overnight for 16-24 h, and medium was changed to fresh DMEM-F12 medium supplemented with 1% FBS, without antibiotics and anti-fungal, containing DEAB or disulfiram, or vehicle. Optimum doses for DEAB and disufiram were determined in the first instance by adding DEAB to final concentration of 1 $\mu$M, 5 $\mu$M, or 25 $\mu$M, and disulfiram to final concentrations of 0.1 $\mu$M, 1 $\mu$M, or 10 $\mu$M. Cells were then cultured for 16-24 h until about 70% confluent. Medium was changed to fresh DMEM-F12 medium supplemented with 1% FBS, without antibiotics and anti-fungal, containing DEAB or disulfiram at the aforementioned concentrations, after which transfection

was commenced. After an overnight incubation, medium was again changed to fresh DMEM-F12 medium supplemented with 1% FBS with antibiotics and anti-fungal, containing DEAB or disulfiram at the aforementioned concentrations, and cells were cultured for an additional 16-24 h, so that cells were exposed to DEAB and disulfiram for a total of 72 h.

For experiments involving aforementioned enzyme inhibitors and tRA, the protocol was similar as described above, except that during the last 24 h, medium was changed to fresh DMEM-F12 medium supplemented with 1% FBS with antibiotics and anti-fungal containing enzyme inhibitors, with and without 0.0001 $\mu$M, 0.001 $\mu$M, 0.01 $\mu$M, or 0.1 $\mu$M tRA.

For transfection, cells in each well were transfected with 0.15 $\mu$g pGL3-RARE-luciferase plasmid DNA, 0.03 $\mu$g pCI-$\beta$-galactosidase plasmid DNA, 0.36 $\mu$l Lipofectamine™ LTX, and 0.18 $\mu$l Plus™ Reagents, prepared in 100 $\mu$l of Opti-MEM® I.

***Dilutions of reagents for cell treatment and experimental replicates***

All reagents used for cell treatment were 1000x higher than the final working concentrations. The reagents were then diluted 1000x with cell culture medium to achieve the desired working concentration, immediately before adding to cells. Cells in vehicle control group were treated with ethanol and/or DMSO at a final concentration of 0.1%. Microtubes and culture plates were covered in aluminium foil whenever possible and transferring of reagents was performed quickly to minimise light exposure.

Three independent experiments, in triplicates or quadruplicates, were performed for all the reporter assays aforementioned, except for the charcoal-stripped FBS experiment, which was performed only once in triplicates.

### 4.2.5 Data normalisation and statistical analysis

Readout of reporter assay was referred as "RARE-luciferase activity". An average value of RLU was first calculated for the triplicated or quadruplicated wells in each individual experiment. The average value of RLU for vehicle-treated group was set as "1"; average values of RLU of all other treatment groups were compared to the vehicle-treated groups and expressed as "RLU fold-change".

The fold-change values derived from three independent experiments were then grouped together for statistical analysis. Due to the intrinsic asymmetric distribution of data expressed as fold-changes, fold-change values were first log-transformed, after which a Repeated Measure One-way Analysis of Variance (ANOVA) test with a Tukey post-test was performed on the log-transformed values using GraphPad Prism, Version 4.0. Please note that owing to the small sample size (n=3), the p value computed may not be precise.

## 4.3 Results

### 4.3.1 Poor inducibility of RARE-luciferase activity by exogenous RA

It was hypothesised that if mIMCD-3 cells are expressing functional RAR heterodimers and transcription co-activators, exogenous tRA would induce RARE-luciferase activity. However, although a slight trend of dose-dependent increase in RARE-luciferase activity was noted following tRA treatment at 0.001-0.1 $\mu$M, the difference was not statistically significant (Figure 4.8).

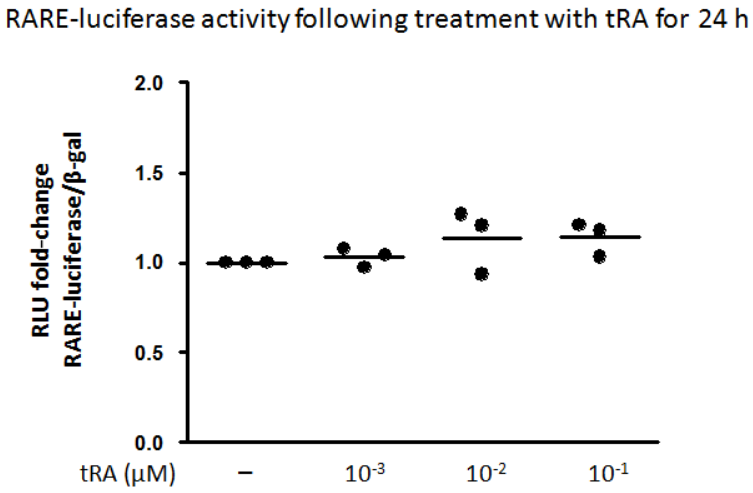


Figure 4.8: Poor inducibility of RARE-luciferase activity in mIMCD-3 cells treated with all-*trans* retinoic acid (tRA). Despite a slight dose-dependent increase of RARE-luciferase activity following 24 h of tRA treatment at the doses indicated, the difference was not statistically significant. Each dot represents mean value of triplicates or quadruplicates from a single biological experiment.

### 4.3.2 Basal RARE-luciferase activity induced by endogenous RA

Following the results of poor inducibility of RARE-luciferase activity by tRA, it was hypothesised that mIMCD-3 cells have high basal RARE-luciferase activity given rise by constitutive RAR activation. If such is the case, the transcriptional machineries might already be fully occupied therefore mIMCD-3 cells might have been "desensitised" towards exogenous tRA treatment. In order to address this hypothesis, mIMCD-3 cells were subjected to culture condition or treatments that reduced or blocked endogenous RARE-luciferase activity.

As illustrated in Figure 4.9, mIMCD-3 cells were (i) cultured in medium supplemented with charcoal-stripped FBS in place of normal FBS for 72 h to reduce retinoid supply, or (ii) treated with antagonists of RARs, AGN193109 and BMS189453, to inhibit RAR-mediated signalling, or (iii) treated with inhibitors of Raldhs, DEAB and disulfiram, to reduce cell-autonomous synthesis of RA.

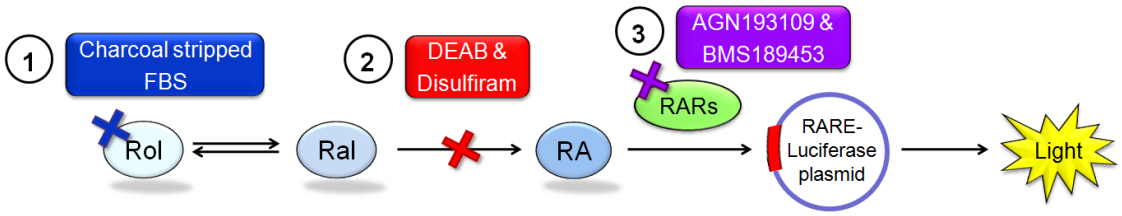


Figure 4.9: Strategies used to inhibit RARE-luciferase activity in mIMCD-3 cells. Cells were either cultured in charcoal-stripped FBS for 72 h to limit the supply of lipid-soluble retinoids, including Rol, Ral, and RA (**1**), or treated with DEAB and disulfiram to inhibit biosynthesis of RA (**2**), or treated with AGN193109 and BMS189453, to block the receptors from activating RARE-luciferase plasmid (**3**). Rol: retinol; Ral: retinal; RA: retinoic acid; RARs: functional retinoic acid receptors; RARE-luciferase plasmid: pGL3-RARE-luciferase plasmid.

***Cells cultured in medium supplemented with charcoal-stripped FBS***

Cells were treated with tRA for 24 h after 72 h of culture in medium supplemented with charcoal-stripped FBS. As shown in Figure 4.10, tRA treatment did not induce RARE-luciferase activity under such culture condition.

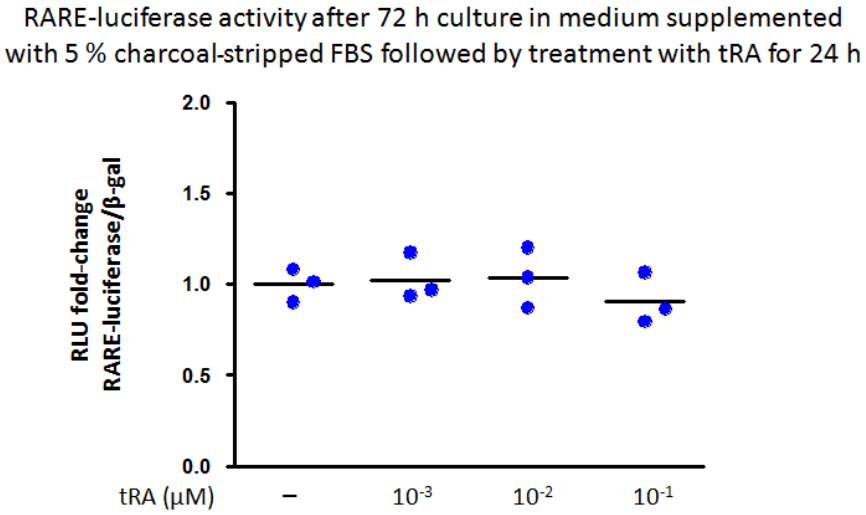


Figure 4.10: Non-inducible RARE-luciferase activity in mIMCD-3 cells cultured with charcoal-stripped foetal bovine serum (FBS) and treated with exogenous all-*trans* retinoic acid (tRA). Preliminary investigation performed in triplicates showed that 24 h tRA treatment did not induce RARE-luciferase activity in mIMCD-3 cells at the doses tested, after the cells were cultured in medium supplemented with charcoal-stripped FBS for 72 h. Results shown are triplicates from a single biological experiment.

***Cells treated with antagonists of RARs***

In cells treated with 1 $\mu$M AGN193109 or 1 $\mu$M BMS189453 for 24 h, there was a reduction of RARE-luciferase activity compared to cells treated with vehicle (Figure 4.11). When exogenous tRA was added simultaneously with the antagonists, the reduction of RARE-luciferase activity was at least partially abolished in a dose-dependent manner.

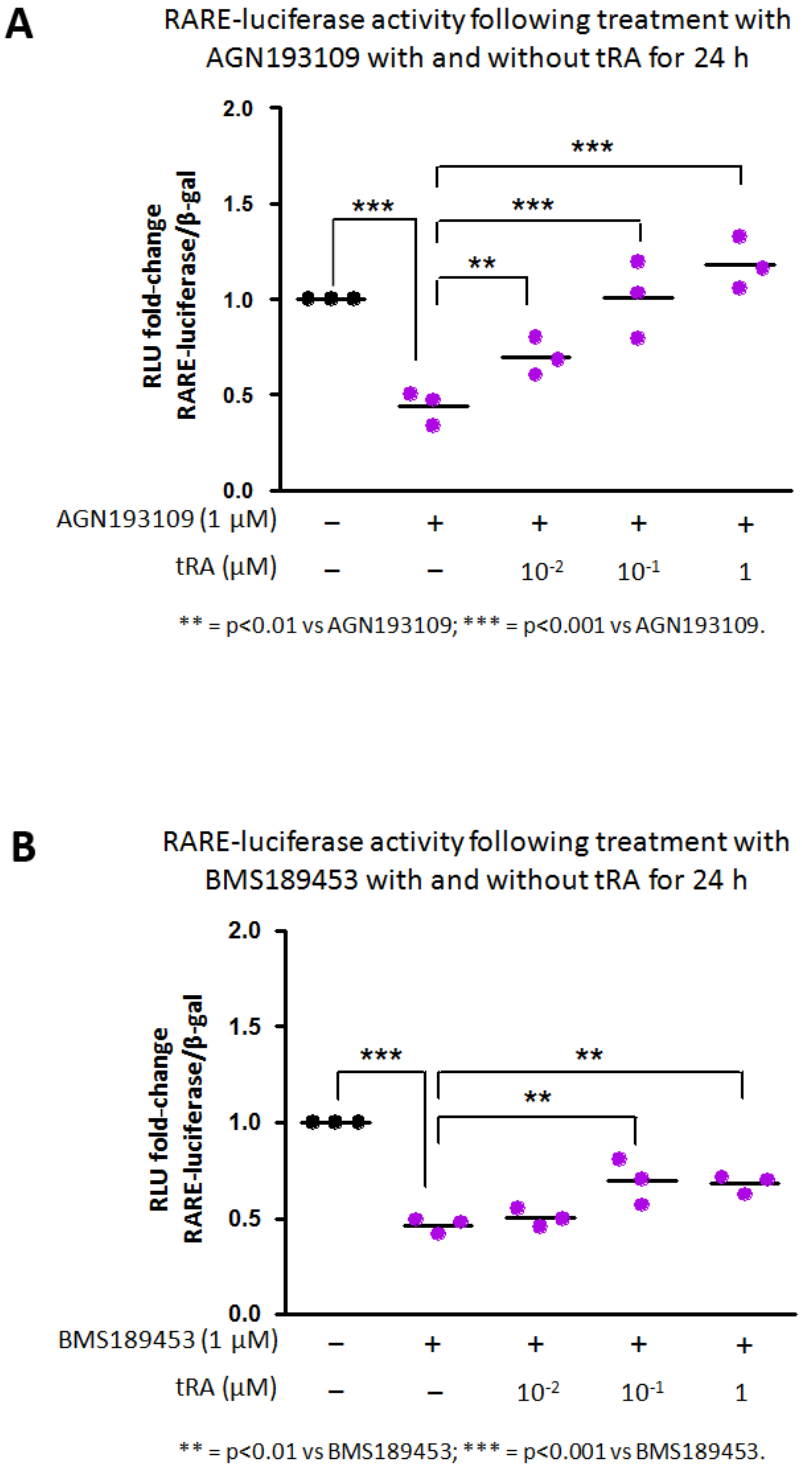


Figure 4.11: RARE-luciferase activity in mIMCD-3 cells treated with AGN193109 and BMS189453 with and without all-*trans* retinoic acid (tRA). Treating mIMCD-3 cells with 1 $\mu$M AGN193109 (**A**) or BMS189453 (**B**) for 24 h reduced the RARE-luciferase activity to about 50% of that of the vehicle control group. The reduction of basal RARE-luciferase activity by the two antagonists of RARs was at least partially abolished with simultaneous addition of exogenous tRA, in a dose-dependent manner. Each dot represents mean value of triplicates or quadruplicates from a single biological experiment.

***Cells treated with inhibitors of RA synthesising enzymes***

In cells treated with disulfiram, a reduction in cell number was observed at the lowest dose tested (0.1 $\mu$M); at 10 $\mu$M, all cells were detached. The cytotoxicity caused by disulfiram renders it unsuitable for cell treatment and hence was not used in subsequent experiments.

Treating cells with DEAB caused a dose-dependent decrease in RARE-luciferase activity (Figure 4.12), without any indication of cytotoxicity.

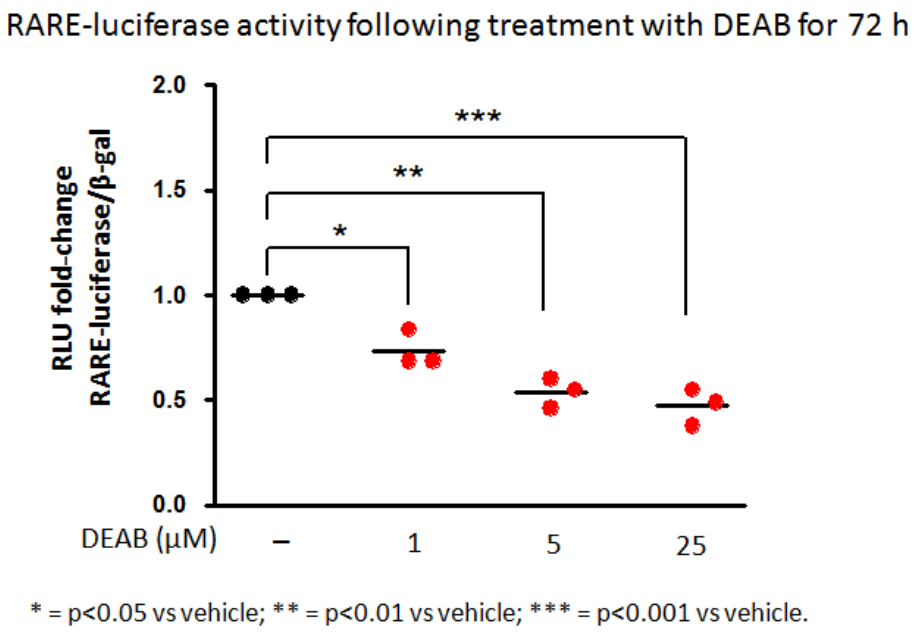


Figure 4.12: RARE-luciferase activity in mIMCD-3 cells treated with DEAB. RARE-luciferase activity was suppressed by DEAB in a dose-dependent manner after 72 h treatment. Each dot represents mean value of triplicates or quadruplicates from a single biological experiment.

The experiment involving DEAB treatment was then repeated with tRA added to the cells during the last 24 h. As shown in Figure 4.13, tRA treatment induced the RARE-luciferase activity in a dose-dependent manner, saturating at 0.001 $\mu$M.

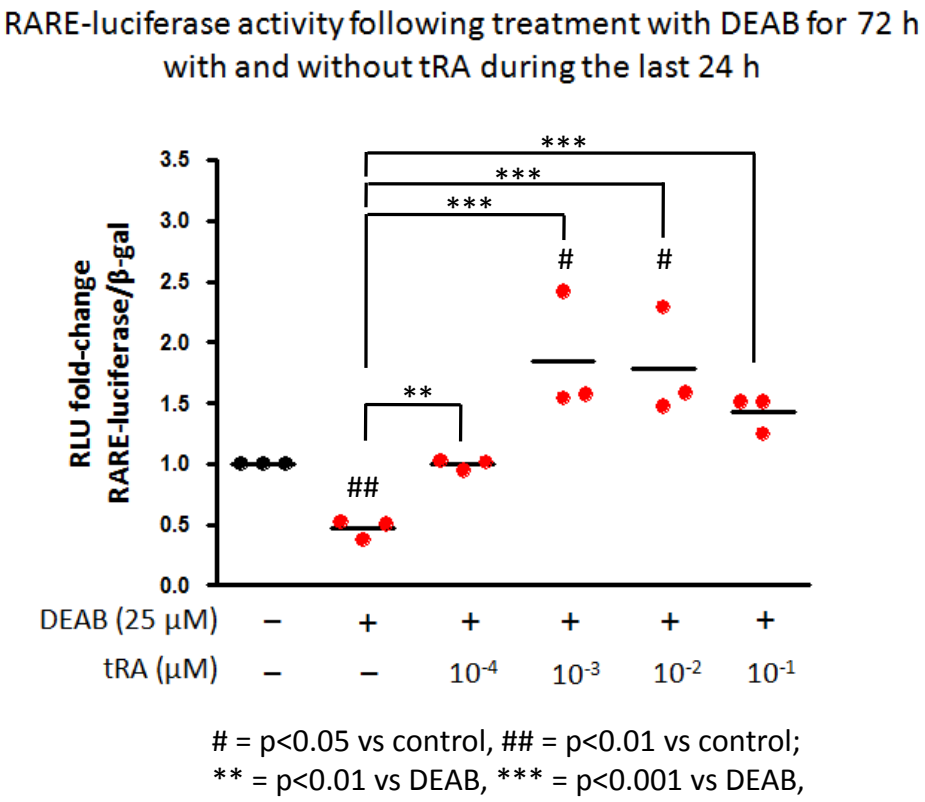


Figure 4.13: RARE-luciferase activity in mIMCD-3 cells treated with DEAB with and without all-*trans* retinoic acid (tRA). Treating cells with 25 $\mu$M DEAB resulted in a suppression of RARE-luciferase activity to about 50% of that of vehicle control group. In cells treated with 25 $\mu$M DEAB with tRA added during the last 24 h, the suppression of RARE-luciferase activity was reversed to a level similar to vehicle control group at 0.0001 $\mu$M tRA; RARE-luciferase activity was saturated by 0.001 $\mu$M tRA, which was about 1.75-fold of that of vehicle control group and about 3.5-fold of that of DEAB treated group. Each dot represents mean values of triplicates or quadruplicates from a single biological experiment.

## 4.4 Discussions

### 4.4.1 Poor inducibility of RARE-luciferase activity by exogenous tRA

When mIMCD-3 cells were treated with tRA at 0.001-0.1 $\mu$M, induction of RARE-luciferase activity was not statistically significant (Figure 4.8). The poor inducibility of RARE-luciferase activity by tRA might be due to several reasons. Firstly, given the relatively short half-life (about 3 h) of luciferase protein in mammalian cells [303], it might be possible that an increase of RARE-luciferase activity had taken place earlier on following tRA treatment, and most luciferase protein were degraded after 24 h. Secondly, there might be an inherent fault in the pGL3-RARE-luciferase plasmid that renders it unresponsive towards tRA. However, a 3-fold to 6-fold increase of RARE-luciferase activity was detected in primary cultures derived from mouse podocytes transiently transfected with the same plasmid, after a 48 h treatment of 1 $\mu$M tRA (personal communication with Dr. A Yoshifusa). The results suggest that the pGL3-RARE-luciferase plasmid is indeed functional, and detection of luciferase protein was possible even after 48 h tRA treatment. The third possibility would be that RARE-luciferase activity was already maximally induced once entered the cells therefore rendering further induction unachievable.

In cells cultured *in vitro*, supply of lipid-soluble retinoids comes solely from FBS added to the cell culture medium. In order to reduce retinoid supply to increase their sensitivity towards exogenous tRA, mIMCD-3 cells were cultured in medium supplemented with charcoal-stripped FBS in place of normal FBS for 72 h prior to tRA treatment. However, even under such culture condition, tRA treatment still failed to induce RARE-luciferase activity (Figure 4.10). This might be due to the fact that charcoal stripping is not efficient enough to remove all RA and RA precursors such as Rol that could be converted into RA upon entering the cells (personal communication with Dr. J Corcoran). In addition, if mIMCD-3 cells have a high level of intra-cellular retinoid storage, 72 h of culture in charcoal-stripped FBS-supplemented medium might not be long enough to deplete the cells of intra-cellular retinoid storage.

### 4.4.2 Suppression of RARE-luciferase activity by antagonists of RARs

While exogenous tRA failed to induce RARE-luciferase activity, treating cells with AGN193109 and BMS189453 resulted in a 50% reduction of RARE-luciferase activity compared to that of the vehicle control groups (Figure 4.11). The results indeed support the presence of basal RARE-luciferase activity in mIMCD-3 cells.

AGN193109 binds to all three isotypes of RAR, i.e., RAR$\alpha$, RAR$\beta$, and RAR$\gamma$ with high affinity ($K_d$=2-3 nM for each RAR isotype), but does not activate the RARs [134]. Instead, AGN193109 acts as an inverse agonist of RARs, which upon binding to RARs further stabilises the binding between RARs and transcription co-repressors leading to transcription repression [14]. BMS189453 has similar affinity as tRA towards all three isotypes of RARs [43]. In the absence of tRA, BMS189453 moderately transactivated RAR$\beta$ (about 30% relative to that of tRA) but had minimum, if any, agonistic effect on RAR$\alpha$ and RAR$\gamma$; in the presence of tRA, BMS189453 weakly antagonised tRA-induced transactivation mediated by RAR$\beta$ and strongly antagonised tRA-induced transactivation mediated by RAR$\alpha$ and RAR$\gamma$ [43]. In addition to its mixed agonistic/antagonistic activity on RARs, BMS189453 also possess anti-AP1 activity, similar to tRA [43]. Although activity of BMS189453 was more diverse compared to AGN193109, suppression of RARE-luciferase activity by two distinct antagonists of RARs strongly supports the presence of constant pGL3-RARE-luciferase plasmid activation mediated by ligand-activated RARs in cultured mIMCD-3 cells. Of note, neither AGN193109 nor BMS189453 binds to RXRs [43, 134], hence ruling out the possibility of these reagents inhibiting signal transduction of other nuclear receptors bound to RXRs.

While no obvious signs of cytotoxicity such as cell detachment was observed in cells treated with AGN193109 and BMS189453, it might be possible that these chemicals were mildly toxic hence lead to a reduction of RARE-luciferase activity. In addition, a suppression of RARE-luciferase activity might also be a non-specific phenomenon

rather than a result of RAR blockage. In order to rule out these possibilities, RARE-luciferase activity was examined in mIMCD-3 cells treated with the antagonists and tRA simultaneously. It was found that 0.1 $\mu$M and 1 $\mu$M of tRA completely overcame suppression of RARE-luciferase activity by 1 $\mu$M AGN193109, and partially overcame that by 1 $\mu$M BMS189453 (Figure 4.11). Although binding affinities of these antagonists and tRA to each individual RAR isotype in mIMCD-3 cells are not known, the competitive nature between these antagonists and tRA had been clearly demonstrated [43, 134]. Thus, the diminution of RARE-luciferase activity suppression confirmed the specificity of AGN193109 and BMS189453 in inhibiting pGL3-RARE-luciferase activation via RAR blockage, which was relieved by increasing doses of exogenous tRA. Although BMS189453 might have suppressed basal RARE-luciferase activity via its anti-AP-1 activity, the diminished rather than additive or synergistic effect of RARE-luciferase activity suppression by simultaneous treatment of tRA argued against AP-1 playing a role in this regard.

### 4.4.3 Suppression of RARE-luciferase activity by inhibitors of RA synthesising enzymes

The presence of a basal RARE-luciferase activity in mIMCD-3 cells suggested not only the presence of functional RARs and transcription co-activators but also bioactive RA that constantly activates the receptors. In order to investigate the source of bioactive RA, mIMCD-3 cells were treated with DEAB and disulfiram, which are inhibitors of Raldhs, to inhibit RA biosynthesis. While disulfiram treatment was cytotoxic at the doses tested precluding its use, DEAB treatment caused a dose-dependent suppression of RARE-luciferase activity (Figure 4.12).

The dose-dependent suppression of RARE-luciferase supported the presence of an active biosynthesis of RA in mIMCD-3 cells but given that DEAB inhibits all class I Aldhs [272], which includes but not limited to Raldh1-3 [4], the suppression of RARE-luciferase activity by DEAB might be a non-specific phenomenon. When exogenous

tRA was added to mIMCD-3 cells pre-treated with DEAB, RARE-luciferase activity was induced in a dose-dependent manner, and the activity was saturated at 1 nM tRA (Figure 4.13). The reversal of RARE-luciferase activity by exogenous tRA not only supports the fact that suppression of RARE-luciferase activity was a result of diminished intra-cellular RA following Raldh inhibition by DEAB, but further strengthened the presence of basal RARE-luciferase activity, in keeping with the results of RAR antagonist experiments (Figure 4.11).

Interestingly, while at least 0.1 $\mu$M tRA was required to abolish, in part or in full, the inhibitory effects of AGN193109 and BMS189453 on RARE-luciferase activity, 0.1 nM of exogenous tRA was sufficient to reverse RARE-luciferase activity back to basal level when endogenous RA was depleted from mIMCD-3 cells. Moreover, RARE-luciferase activity was maximally induced by 1 nM tRA to about 1.75-fold compared to the basal level. The relatively low dose of tRA needed to activate RARE-luciferase activity was in good concordance with low serum level of tRA, which is in nano molar ranges [139]. In *in vitro* experiments, a potent effect of RA, with an $ED_{50}$ as low as 0.01 nM, had also been described [14]. The exact mechanism of tRA inducing RARE-luciferase activity beyond basal level only when endogenous RA biosynthesis was inhibited was not clear. An enhanced cellular uptake of exogenous tRA from culture medium driven by attenuated endogenous RA supply might be a possible explanation.

### 4.4.4 Concluding remarks

In aggregate, a constitutively active RAR-dependent endogenous RA activity was present in mIMCD-3 cells, which was likely given rise by cell-autonomous synthesis of RA that constantly activates the RARs. This observation further supports that the RARE activity observed in collecting duct principal cells, inner medullary collecting duct cells, and ureteric bud cells of *RARE-hsp68-lacZ* mice might indeed be, at least in part, a result of constitutive retinoid nuclear receptor activation by endogenous RA.

Given that pan-antagonists of RARs were used and that expression of the individual isotypes of RAR and RXR had not been examined, the actual functional RARs and RXRs mediating the RARE-luciferase activity in mIMCD-3 cells remains unknown. Similarly, since DEAB inhibits the activity of all Raldh isoforms, it is not known whether RA biosynthesis in mIMCD-3 cells was attributed to a particular Raldh isoform. These issues could be addressed in the future, e.g., by using RAR and RXR isotype-specific antagonists or small interference RNA targeting specific RARs or Raldhs.

Finally, since the mIMCD-3 cell line is not a model of the collecting duct intercalated cells, it remains unknown if the intercalated cells would also demonstrate a similar pattern of constitutively active RAR-dependent endogenous RA activity. It is hoped that the reporter assay utilising RARE-reporter plasmid can be applied to intercalated cells when a good cell model of intercalated cells is available.

# Chapter 5

# Pan-genomic Study: Target Genes of Endogenous Retinoic Acid and its Receptors in mIMCD-3 Cells

---

## 5.1 Introduction

In view of the presence of constitutively active RAR-dependent endogenous RA activity in mIMCD-3 cells, the primary aim of this part of the work is to identify candidate target genes dependent on endogenous RA and RARs, herein referred as endogenous RA/RAR, in mIMCD-3 cells. Given that AGN193109 and DEAB were found to suppress RARE-luciferase activity, these inhibitors were employed in this study.

Two sets of experiment were designed as summarised in Figure 5.1. In the first set of experiment, mIMCD-3 cells were treated with AGN193109 to block RARs. In order to confirm the specificity of regulation, exogenous tRA was added simultaneously with AGN193109 in another experimental group to determine if regulation by AGN193109 were abolished or diminished. In the second set of experiment, mIMCD-3 cells were treated with DEAB to inhibit RA biosynthesis, with and without exogenous tRA.

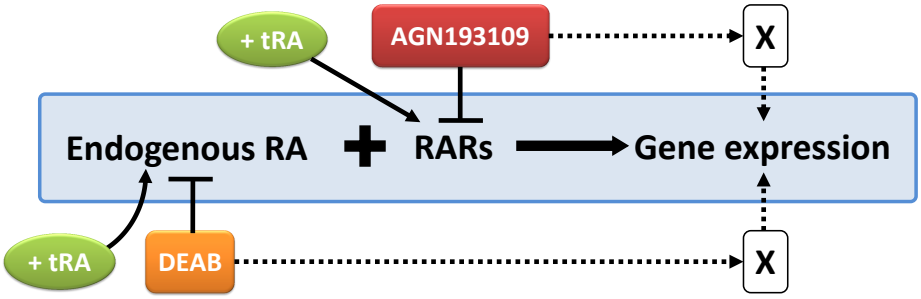


Figure 5.1: Regulation of gene expression by AGN193109 and DEAB with and without exogenous all-*trans* retinoic acid (tRA). AGN193109 and DEAB were used to inhibit endogenous RA/RAR signalling (blue box) at different stages. AGN193109 competes with endogenous RA for RARs while DEAB inhibits biosynthesis of endogenous RA. Since the effects of AGN193109 and DEAB on gene expression might be mediated via other non-specific mechanisms (X), exogenous tRA was added simultaneously to AGN193109 and DEAB to determine if the effects of AGN193109 and DEAB were abolished or diminished.

A gene was regarded as candidate target of endogenous RA/RAR if all following criteria were fulfilled: (i) regulated by AGN193109 and the regulation was abolished or diminished in the simultaneous presence of exogenous tRA, (ii) regulated by DEAB and the regulation was abolished or diminished in the simultaneous presence of exogenous tRA, (iii) the direction of regulation by AGN193109 and by DEAB was the same, i.e., either up-regulated by both or down-regulated by both.

### 5.1.1 Transcriptomic-based study for target gene examination

Various omics-based technologies, e.g., transcriptomics, proteomics, and metabolomics studies, have been introduced over the years. Given the role of RARs as transcription factors, transcriptomic-based study, i.e., microarray study covering the whole mouse genome, was deemed the most sensitive approach to identify target genes of endogenous RA/RAR in mIMCD-3 cells.

A small pilot study was first performed to examine the expression of a few genes of interest in order to verify the effectiveness of treatment as well as to guide the process of shortlisting target genes in the ensuing microarray studies. Genes were selected based on two criteria: (i) genes reported to be regulated by RA with or without known functional

RARE, and/or (ii) genes that play specific functions of special interest, in particular, water transport, defence/protection mechanism against fibrogenesis and high osmolality of the inner medullary environment, as well as kidney development.

Five genes were selected, i.e., Foxa1, Rarb, Bmp7, Wnt7b, and Pax2, which fulfil the above two criteria based on published literature. Foxa1, Rarb, Bmp7, and Wnt7b fulfil criterion (i). Specifically, Foxa1 and Rarb genes are well-known target genes of RA that contain functional DR5 RARE and are rapidly induced by RA in many cell types [12]; Bmp7 and Wnt7b had been reported to be induced by RA in human osteosarcoma cell line [243] and in adult neural stem cells [131], respectively, and a recent genome-wide *in silico* study had reported the presence of DR5 RARE in introns of these genes [159]. As for criterion (ii), Foxa1 is a transcription factor that plays an important role in maintaining water balance as Foxa1$^{-/-}$ mice suffered polyuria [19]. Bmp7 controls collecting duct proliferation and apoptosis during branching morphogenesis [251] and protects against fibrogenesis [334]. Pax2 was reported to play a crucial role in protecting collecting duct cells from high sodium chloride concentration-induced apoptosis [38]. Both Rarb and Wnt7b play an essential role in mediating early and late kidney developmental events, respectively [204, 332].

The first part of this chapter comprises the aforementioned pilot study, in which gene expression was examined by reverse transcription-quantitative polymerase chain reaction (RT-qPCR). The second part describes the microarray experiments, in which candidate target genes of endogenous RA/RAR were identified at the pan-genomic level. The third part constitutes validation of candidate target genes shortlisted from the microarray experiments with RT-qPCR.

## 5.2 Material and methods

### 5.2.1 Experimental protocols for mIMCD-3 cell treatment

***AGN193109 treatment with and without tRA***

Cells were seeded at 2 x $10^5$ cells/35 $mm^2$ dish in 2 ml DMEM-F12 medium containing antibiotics and anti-fungal supplemented with 5% FBS. After an overnight culture, medium was changed to fresh DMEM-F12 medium supplemented with 1% FBS containing antibiotics and anti-fungal. After an overnight culture, medium was again changed to fresh DMEM-F12 medium supplemented with 1% FBS containing 1 $\mu$M AGN193109, with and without 0.2 $\mu$M tRA, and cultured for 24 h. For control group, medium was changed to fresh DMEM-F12 medium supplemented with 1% FBS containing 0.1% ethanol and 0.1% DMSO, and cultured together with the treatment groups. At the end of treatment, medium was aspirated off, and culture dishes were stored in -80 °C if total RNA extraction was not performed immediately.

***DEAB treatment with and without tRA***

Cells were seeded at 1.2 x $10^5$ cells/35 $mm^2$ dish in 2 ml DMEM-F12 medium containing antibiotics and anti-fungal supplemented with 5% FBS. After an overnight culture, medium was changed to fresh DMEM-F12 medium supplemented with 1% FBS containing antibiotics and anti-fungal. After an overnight culture, medium was again changed to fresh DMEM-F12 medium supplemented with 1% FBS containing 25 $\mu$M DEAB, with and without 0.01 $\mu$M tRA, and cultured for 24 h. For control group, medium was changed to fresh DMEM-F12 medium supplemented with 1% FBS containing 0.1% ethanol and 0.1% DMSO, and cultured together with the treatment groups. At the end of treatment, medium was aspirated off, and culture dishes were stored in -80 °C if total RNA extraction was not performed immediately.

The doses of AGN193109, DEAB, and tRA used in the aforementioned experiments were selected based on the results of reporter assays in Chapter 4, Figures 4.11 and 4.13. Dilutions of reagents used in the aforementioned experiments are as described in Chap-

ter 4, Section 4.2.4. One 35 $mm^2$ dish was prepared per experimental condition in a single experiment, and three independent experiments were performed.

### 5.2.2 Examination of gene expression with RT-qPCR

***Total RNA Extraction***

Prior to RNA extraction, work bench and pipettes were cleaned with RNaseZap® (Applied Biosystems, Warrington, UK) to minimise RNase contamination. QIAshredder spin column (Qiagen Ltd., West Sussex, UK) was used to shear high molecular weight genomic DNA and other cellular components, which reduced viscosity and created a homogenous cell lysate. RNeasy® Mini Kit (Qiagen Ltd., UK) was used for RNA extraction, following the protocol provided by the company[1]. RNeasy® Mini Kit contains the following reagents and components:

- **RNeasy mini column**, which is a silica-gel-based membrane that allows binding of RNA while removing genomic DNA and other contaminants.
- **Buffer RLT**, a cell lysis buffer containing 25-50% guanidium thiocyanate as chaotropic reagent that completely denatures RNase. Before used, $\beta$-mercaptoethanol ($\beta$-ME) was added to buffer RLT at a ratio of $\beta$-ME:buffer RLT = 1:100.
- **Buffer RW1**, a washing buffer containing 2.5-10% guanidium thiocyanate and 2.5-10% ethanol that was used to wash the RNA-bound membrane.
- **Buffer RPE**, a washing buffer containing 20% ethanol that was used to wash the RNA-bound membrane. Before used, 100% ethanol was added to buffer RPE at a ratio of ethanol:buffer RPE = 4:1.

Medium was first aspirated off from culture dishes and 350 $\mu$l of RLT buffer (containing $\beta$-ME) was pipetted onto the cell monolayer directly. If culture dishes were stored at -80 °C, RLT buffer was pipetted onto cell monolayer shortly after culture dishes were taken out from the freezer. Cell lysate was then collected with cell scraper (Greiner

[1]Qiagen RNeasy® Mini Handbook, edition 04/2006, P/N: 1035969

Labortechnik Ltd., Tyne and Wear, UK) and pipetted into 1.5 ml microtube. The lysate was pipetted up and down a few times to ensure complete cell lysis before being transferred into QIAshredder spin column placed in a 2 ml collection tube, and centrifuged at 21,100 g for 2 min for homogenisation. After centrifugation was completed, one volume of 70% ethanol (prepared as described in Section 2.1.5) was added to the homogenised lysates in the collection tube and mixed well by pipetting. The mixture was then transferred to RNeasy column placed in a 2 ml collection tube and centrifuged at 8,000 g for 15 s. Total RNA bound to the membrane on RNeasy column was subjected to three washing steps in the following order:

1. 700 $\mu$l of **RW1** buffer with 15 s centrifugation at 8,000 g;
2. 500 $\mu$l of **RPE** buffer (containing ethanol) with 15 s centrifugation at 8,000 g;
3. 500 $\mu$l of **RPE** buffer (containing ethanol) with 2 min centrifugation at 8,000 g.

The RNeasy column was then transferred to a new 2 ml collection tube and centrifuged for 1 min at 21,100 g to eliminate ethanol that may be retained on the RNeasy membrane. Finally, RNeasy column was transferred to a clean 1.5 ml collection tube, following which 40 $\mu$l of RNase-free water was pipetted directly onto the RNeasy membrane. After a 1 min centrifugation at 21,100 g, the RNeasy column was discarded and the eluted total RNA was stored at -80 °C until use. A Thermo Scientific Heraeus Pico 21 centrifuge was used for all centrifugation.

***Total RNA Measurement***

Concentration and purity of total RNA were determined using a NanoDrop® ND-1000 machine (Labtech International Ltd., East Sussex, UK), with RNase-free water set as blank measurement. Presence of impurities such as protein and solvent in RNA was determined from the absorbance ratio A260/280 and A260/230. A ratio of 1.9 to 2.1 for A260/280 and a ratio of 1.8 to 2.2 for A260/230 were considered as RNA of good quality.

***Reverse transcription of RNA into cDNA***

Reverse transcription was performed using Oligo-dT primer and Omniscript® Reverse Transcription Kit (both from Qiagen Ltd., UK) following the company's protocol[2]. Omniscript® Reverse Transcription Kit contains the following reagents:

- **RT buffer** (10x stock concentration).
- **dNTP mix**, containing 5 mM of dATP, dCTP, dGTP, and dTTP, respectively.
- **Omniscript Reverse Transcriptase** (deoxynucleoside-triphosphate:DNA deoxynucleotidyltransferase (RNA-directed)), with three distinct activities: (i) RNA-dependent DNA polymerase, (ii) hybrid-dependent exoribonuclease (RNase H), and (iii) DNA-dependent DNA polymerase.

Reverse transcription reaction was set up in 1.5 ml no-stick microtube (Alpha Laboratories, Hampshire, UK) on ice, by adding 2 $\mu$g of RNA in 26 $\mu$l of RNAse-free water, 4 $\mu$l of RT buffer, 4 $\mu$l of dNTP mix, 4 $\mu$l of Oligo-dT primer, and 2 $\mu$l of Omniscript® Reverse Transcriptase. Microtube was then incubated at 37 °C for 60 min. At the end of reverse transcription, 160 $\mu$l of RNAse-free water was added to the reverse-transcribed cDNA and stored at -80 °C.

***Pilot study***

Quantitative PCR was performed using TaqMan® Gene Expression Assays and TaqMan® Universal PCR Master Mix (Applied Biosystems, UK). Each assay comes in 20x stock concentration containing two unlabelled primers (18 $\mu$M, respectively) and one TaqMan® minor groove binder (MGB) probe (5 $\mu$M). The MGB probe consists of an oligonucleotide with a fluorescein amidite (FAM) reporter dye covalently linked to its 5'-end, and a non-fluorescent quencher dye at its 3'-end. TaqMan® Universal PCR Master Mix (2x stock concentration) contains the following components:

- **AmpliTaq Gold® DNA Polymerase**, which is a thermal stable DNA polymerase that has a 5' to 3' nuclease activity but lacks a 3' to 5' exonuclease activity.

[2]Qiagen Omniscript® Reverse Transcription Handbook, edition 05/2004, P/N: 1026831

- **AmpErase® uracil-N-glycosylase (UNG)**, which prevents reamplication of carry over PCR products by removing uracil incorporated into single- or double-stranded DNA.
- **dNTPs** containing dATP, dCTP, dGTP, and dUTP.
- **ROX** dye as passive reference.
- Optimised buffer components.

Pre-validated TaqMan® Gene Expression Assays used were as follow:

1. Bmp7: Mm00432101_m1 (amplicon length: 82)
2. Foxa1: Mm00484713_m1 (amplicon length: 68)
3. Pax2: Mm01217939_m1 (amplicon length: 55)
4. Rarb: Mm01319675_mH (amplicon length: 88)
5. Wnt7b: Mm00437357_m1 (amplicon length: 88)
6. Gapdh: Mm99999915_g1 (amplicon length: 107) (used as endogenous control)

Work bench was cleaned with detergent before PCR reactions were set up. PCR reaction components, including TaqMan® Universal PCR Master Mix, TaqMan® Gene Expression Assays, and cDNA template, were first prepared in 1.5 ml no-stick microtubes and pre-mixed with finger-flicking before being pipetted into optical 384-well reaction plate (Applied Biosystems, UK). Each reaction was set up in triplicated wells and each well contains a total volume of 12.5 $\mu$l comprising 6.25 $\mu$l of TaqMan® Universal PCR Master Mix, 3.125 $\mu$l of RNase-free water, 0.625 $\mu$l of TaqMan® Gene Expression Assays, and 2.5 $\mu$l of cDNA. Gapdh TaqMan® Gene Expression Assay was set up in triplicates on each PCR plate; a non-template control, which contains same reaction components except that RNase-free water was used in place of cDNA template, was also set up in triplicates on each PCR plate. Microtubes containing PCR reaction components and cDNA mixture were kept on ice throughout the course of setting up the PCR plate.

The PCR plate was sealed well with PCR-compatible adhesive film (Alpha Laboratories, UK) to prevent evaporation of reaction components during PCR reaction. PCR plate was then centrifuged at 1,500 rounds per minute for 5 min at 15 °C before being loaded into an ABI Prism 7900 HT detection system. Condition for PCR was as follow:

1. **Stage I**: 50 °C for 2 min to activate AmpErase® UNG.
2. **Stage II**: 95 °C for 10 min to activate AmpliTaq Gold® enzyme and to inactivate AmpErase® UNG enzyme.
3. **Stage III**: 40 cycles of 95 °C for 15 s for denaturing double stranded DNA into single strands, and 60 °C for 1 min for annealing of primers and extension.

Filtered pipette tips (Starlab (UK) Ltd.) were used for RNA extraction, reverse transcription, and setting up PCR plates. The procedures and basic principles of reverse transcription and qPCR are summarised in Figure 5.2.

Expression of Gapdh was first examined to determine its suitability as endogenous control gene. As shown in Figure 5.3, Gapdh expression did not vary much following a 24 h treatment of AGN193109 and DEAB, in the absence and presence of tRA, suggesting it to be an appropriate endogenous control.

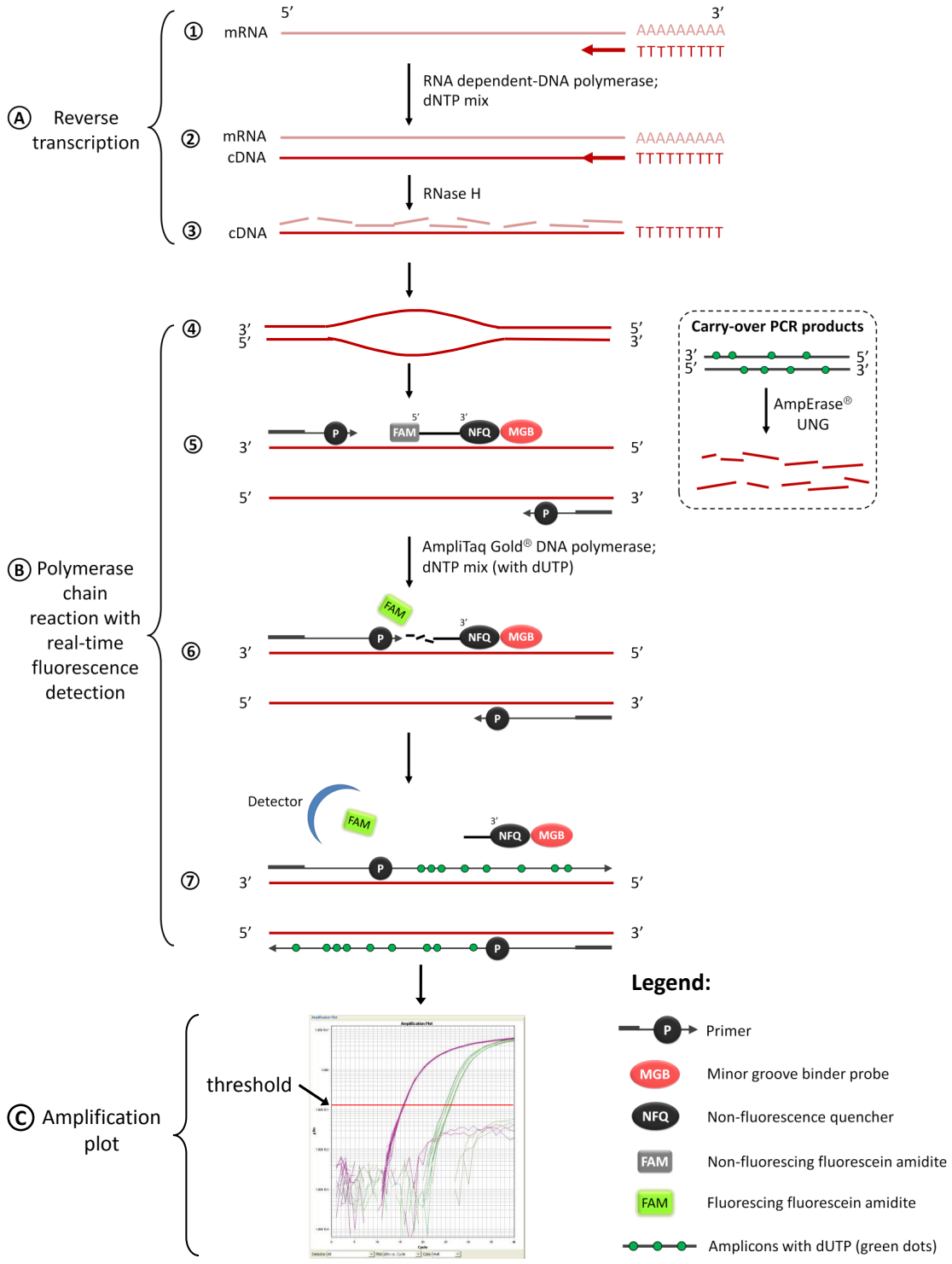


Figure 5.2: Please refer to the following page for figure legend.

Figure 5.2: Reverse transcription and quantitative polymerase chain reaction (RT-qPCR). **A.** RNA was first reversed transcribed into cDNA using Oligo-dT primers that anneal to the poly-A cap presents at the 3'-end of mRNA, in the presence of RNA dependent-DNA polymerase and dNTP mix (**1**). mRNAs hybridised to their complimentary cDNA were then degraded by RNase H (**2**), leaving only cDNA (**3**). **B.** The cDNA was then subjected to PCR with real-time fluorescence detection. AmpErase® uracil-N-glycosylase (UNG) was first activated to break down carry-over PCR products containing uracil (dotted box), after which double-stranded cDNA would de-anneal following temperature rise to 95 °C (**4**). When temperature fell to 60 °C, forward/reverse primers would anneal to complimentary target sequences, while an intact minor groove binder (MGB) probe (with low fluorescence emission due to proximity of fluorescein amidite (FAM) with a non-fluorescing quencher (NFQ)) would anneal to its complimentary sequence downstream of one of the primers (**5**). While promoting primer elongation in the presence of dNTP mix (with dUTP), the 5'-nuclease activity of AmpliTaqGold® DNA polymerase would cleave the MGB probe off separating FAM from NFQ hence emitting fluorescence signal (**6**). The fluorescence signal from FAM was then detected on a real-time basis by a detector (**7**) while the reaction (steps **4-7**) was repeated for 40 cycles, during which number of amplicons would increase exponentially. **C.** The fluorescence signal was translated into amplification plot and expressed as threshold cycle, i.e., the number of cycle required to reach the threshold level (red horizontal line).

***Analysis of relative gene expression and statistical analysis***

The results were analysed using an Applied Biosystem™ Sequence Detection System version 2.3 software. The amplification efficacy for all TaqMan® Gene Expression Assay was assumed to be close to 100%. The relative changes in gene expression was determined using the comparative threshold cycle ($C_T$) method, as described by Livak et al. [178]. The comparative $C_T$ method involves calculating the fold-change of gene expression using the formula $2^{-\Delta\Delta C_T}$, i.e., by normalising the $C_T$ of genes of interest to that of Gapdh, and the values were then normalised to a calibrator, which was the vehicle control group.

The relative mRNA expression was first calculated for individual experiment, by taking mean values of the technical triplicates for each treatment group, and expressed as fold-changes compared to vehicle control group that was set as "1". Fold-changes derived from three independent experiments were then grouped together for statistical analysis. A Repeated Measure One-way ANOVA test with a Tukey post-test was performed on log-transformed fold-change values using GraphPad Prism, Version 4.0. Please note

that owing to the small sample size (n=3), the p value computed may not be precise.

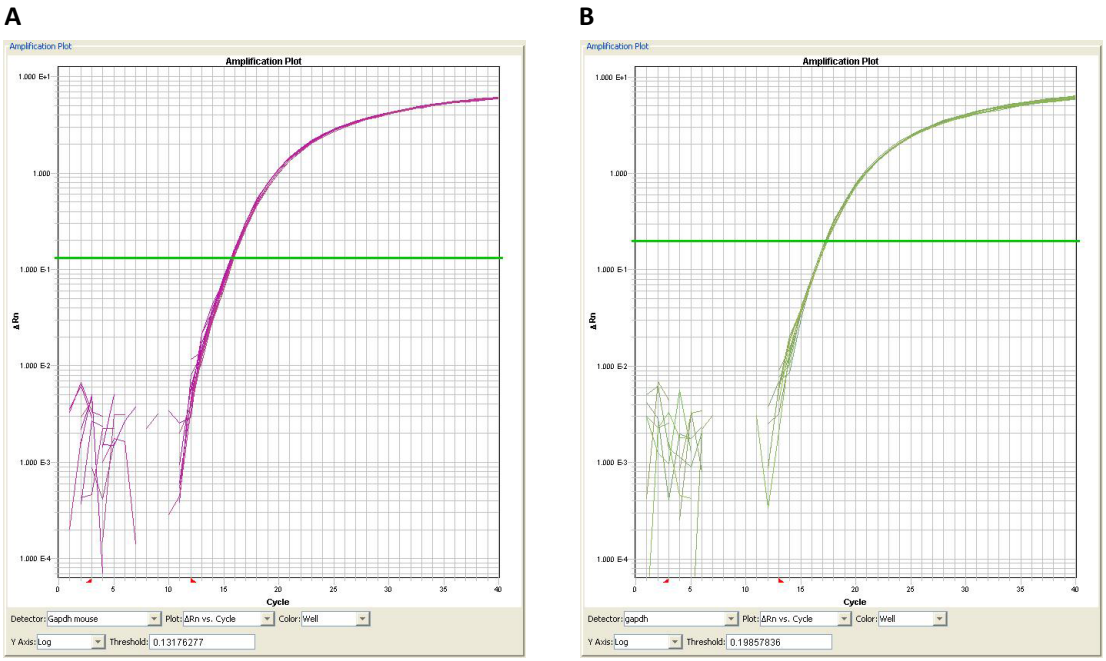


Figure 5.3: Amplification plot of Gapdh in mIMCD-3 cells treated with AGN193109 and DEAB, with and without all-*trans* retinoic acid (tRA). Expression of Gapdh did not vary much following 24 h treatment of AGN193109 with and without tRA (**A**), and of DEAB with and without tRA (**B**), evident by a tight overlapping amplification plots across all the samples. Shown here are representative amplification plots derived from technical triplicates of a single biological experiment.

### 5.2.3 Microarray experiment

Two sets of microarray experiments, i.e., AGN193109 experiment and DEAB experiment, were performed in two separate batches, each consist of samples from three independent biological replicates. The first set of microarray experiment comprises samples treated with: (i) vehicle, (ii) 1 $\mu$M AGN193109, and (iii) 1 $\mu$M AGN193109 with 0.2 $\mu$M tRA; the second set of microarray experiment comprises samples treated with: (i) vehicle, (ii) 25 $\mu$M DEAB, and (iii) 25 $\mu$M DEAB with 0.01 $\mu$M tRA.

The array used for microarray experiments was Affymetrix® GeneChip® Mouse Gene 1.0 ST Array (Affymetrix UK Ltd., High Wycombe, UK) that enables whole-genome gene-level expression examination, using sense cDNA as target. The array contains about 27 probes (of 25-mer oligonucleotides) per gene and an estimated 28,853 genes were examined.

***Quality and integrity of RNA samples***

Total RNA samples were transferred on dry ice to King's College London Genomics Centre. All subsequent work related to microarray was performed at the Genomics Centre under the supervision of Dr. E Aldecoa-Otalora Astarloa and Dr. M Arno.

The integrity of RNA samples is a critical factor that would affect the downstream procedures in microarray experiments. Thus, the integrity of RNA was first examined using an Agilent 2100 Bioanalyser and an Agilent RNA 6000 Nano Kit (Agilent Technologies, Berkshire, UK) following the company's protocol[3]. The Agilent RNA 6000 Nano Kit contains RNA Nano Chip, electrode cleaner, spin filter, and the following reagents:

1. **RNA 6000 Nano Ladder**, which contains six RNA fragments of 200, 500, 1,000, 2,000, 4,000 and 6,000 nucleotides. The ladder was pipetted into RNase-free microtubes and heat denatured for 2 min at 70 °C before used.

[3]Agilent RNA 6000 Nano Kit Guide, edition 08/2006, P/N: G2938-90034

2. **RNA 6000 Nano Gel Matrix**, a sieving polymer matrix that separates RNA fragments by their sizes, i.e., smaller RNA fragments migrate through the gel matrix faster than the larger RNA fragments. Gel matrix was prepared by pipetting 550 $\mu$l of RNA 6000 gel matrix into the top receptacle of a spin filter that comes with the kit and was centrifuged for 10 min at 1,500 g. The filtered gel was stored at 4 °C and was used within one month of preparation.

3. **RNA 6000 Nano Dye Concentrate**, which intercalates into RNA/DNA strands, allowing them to be detected by the laser in bioanalyser. Gel-dye matrix was prepared by adding 1 $\mu$l of RNA 6000 Nano dye concentrate to 65 $\mu$l of filtered gel in a RNase-free microtube. The gel-dye mix was then vortexed thoroughly and centrifuged at 13,000 g for 10 min at room temperature. The prepared gel-dye mix was concealed from light and used within one day.

4. **RNA 6000 Nano Marker**, a 25 nucleotide fragment that was run with each sample to serve as a reference compensating for possible drift effect during running.

The 16-pin electrodes of the bioanalyser were first cleaned using an electrode cleaner, filled with 350 $\mu$l of fresh RNase-free water. The water-filled electrode cleaner was placed on the receptacle of bioanalyser and the lid was closed for at least 1 min. The lid was then opened and the electrode cleaner was removed. Water was allowed to evaporate from the electrodes for about 30 sec before used.

An RNA Nano Chip, as illustrated in Figure 5.4, was first placed on a chip priming station. A volume of 9 $\mu$l gel-dye mix was drawn from the tube, avoiding the sediments at the bottom of the tube, and loaded into the bottom of the well with a mark of white colour “G” against a black colour circle. The plunger on the chip priming station was first positioned at 1 ml, and was then closed until a “click” sound was heard. The plunger was pushed downwards until it was held by the clip for a 30 sec period to disperse the gel-dye mix through the micro-channels within the chip. The clip was then released and 5 sec later, the plunger was slowly pulled back to the 1 ml position. The chip priming

station was opened and another 9 $\mu$l of gel-dye mix was loaded into both wells with the mark of black "G". A volume of 5 $\mu$l RNA 6000 Nano Marker was then loaded into the well with the ladder symbol, and each of the 12 sample wells. Subsequently, 1 $\mu$l of heat-denatured RNA sample (2 min at 70 °C) was pipetted into each sample well (1 $\mu$l of RNase-free water into wells without RNA sample), and 1 $\mu$l of RNA 6000 Nano ladder was pipetted into the ladder well. The RNA Nano Chip was vortexed for 60 sec at 2,400 rpm using an IKA® vortex mixer, before being placed onto the receptacle of bioanalyser. The lid was closed gently and samples were analysed using an Agilent Expert 2100 software.

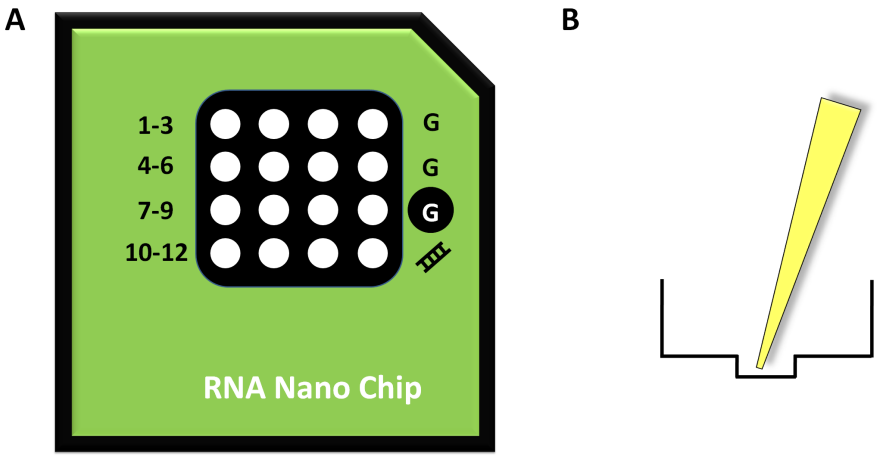


Figure 5.4: RNA Nano Chip. **A.** An RNA Nano chip, which contains micro-channels for capillary electrophoresis. Sample wells were indicated with numbers 1-12, "G" indicated wells for gel-dye mix and ladder symbol indicated well for RNA 6000 Nano ladder. Chip was not drawn to scale. **B.** Reagents and samples were loaded into the bottom of each well, as illustrated.

Following the same principle of gel electrophoresis, charged RNA or DNA molecules with a constant mass-to-charge ratio will be separated based on their sizes, except that the process took place in micro-channels fabricated within the RNA Nano Chip. As shown in Figure 5.5, all RNA samples had two sharp major peaks corresponding to the 18s and 28s ribosomal RNA, respectively, with RNA Integrity Number (RIN) [279] values ranging from 9.70 to 10.00, suggesting minimum degradation of RNA molecules.

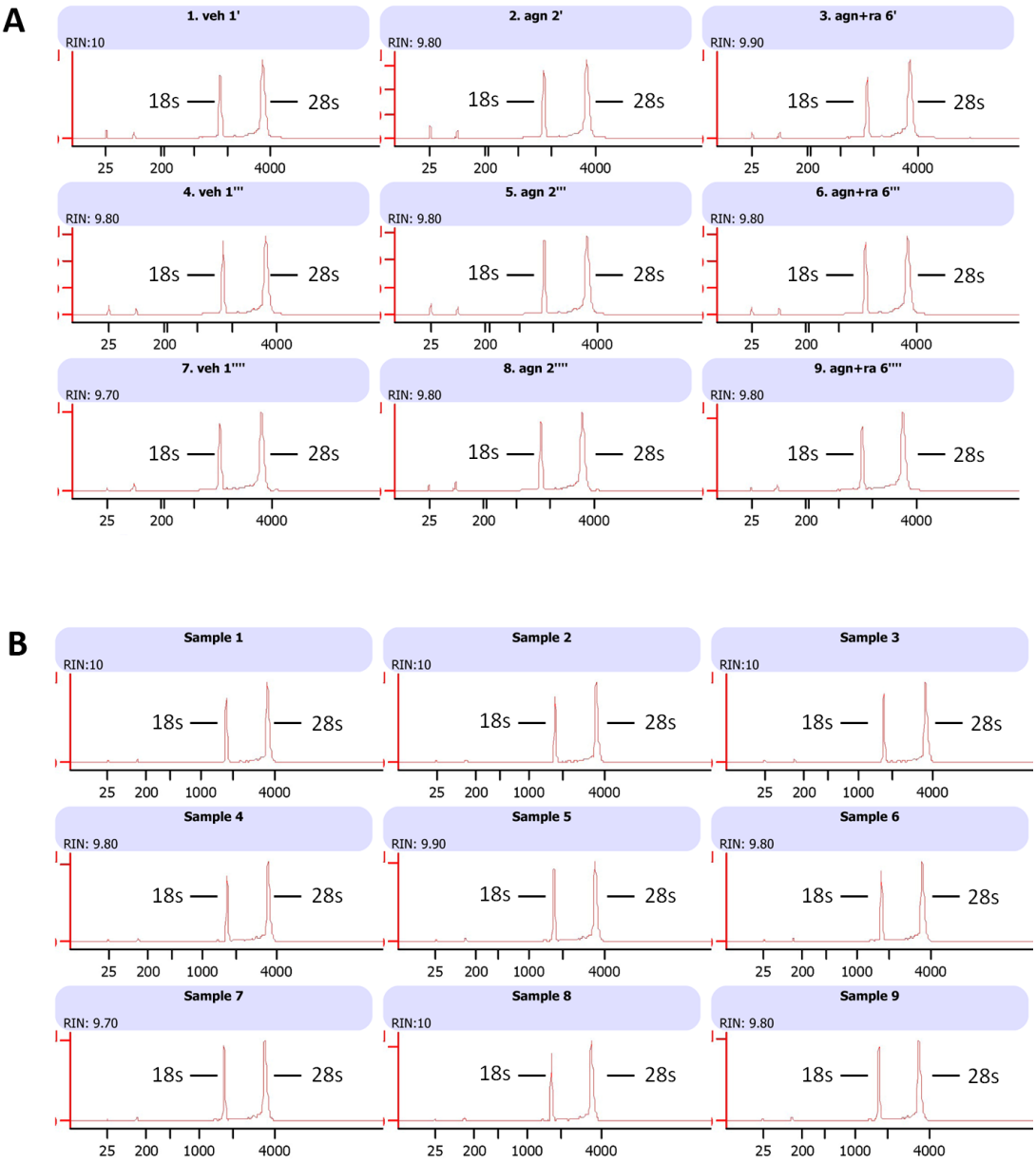


Figure 5.5: Integrity of RNA samples. Integrity of RNA samples from AGN193109 experiment (**A**) and DEAB experiment (**B**) was examined. The two sharp major peaks correspond to 18s and 28s ribosomal RNA, respectively. The high RNA Integrity Number (RIN) values, within the range of 9.70-10.00, suggest a good quality of RNA samples with minimum degradation of RNA molecules. The absence of additional peaks in between 18s and 28s RNA peaks, baseline dips, and broad peaks, also confirm the absence of genomic DNA in the RNA samples.

***Generation of sense cDNA from RNA samples***

Sense cDNA target was generated using Ambion® WT Expression Kit (Life Technologies Ltd., Paisley, UK) following the company's protocol[4]. The workflow started with synthesis of first-strand cDNA (first cycle), followed by synthesis of second-strand cDNA, synthesis of cRNA, and finally synthesis of sense cDNA (second cycle). The amount of reagents used described below is for one set of experiment containing nine samples.

All RNA samples were first normalised to the least concentrated sample with nuclease-free water. A volume containing 500 ng RNA, the maximum recommended starting material, was measured into RNase-free microtube. Nuclease-free water was added to a final volume of 3 $\mu$l, after which 2 $\mu$l of Poly-A RNA Controls was added. A volume of 5 $\mu$l First-Strand Master Mix (containing an engineered primers with a T7 promoter sequence) was then added and the mixture was mixed well with gentle finger-flicking. After a brief centrifugation, the mixture was incubated for 1 h at 25 °C, 1 h at 42 °C, then for at least 2 min at 4 °C. At the end of incubation, microtubes containing the mixture were centrifuged briefly and kept on ice.

The Poly-A RNA Controls are *in vitro* synthesised polyadenylated transcripts for the *Bacillus subtilis* genes at a staggered concentration of dap>thr>phe>lys. These genes are absent from eukaryotic samples, but would hybridise to the *Bacillus subtilis* probe sets on the array. Poly-A RNA Controls spiked into the total RNA samples would be amplified and labelled together with total RNA thus help monitoring the labelling process independently from the quality of the RNA samples. Poly-A RNA Controls were prepared by serial dilution of Poly-A RNA Control Stock and Poly-A Control Dilution Buffer (both from Affymetrix® GeneChip® Poly-A RNA Control Kit), as follow:

[4]Ambion® WT Expression Kit for Affymetrix® GeneChip® Whole Transcript (WT) Expression Arrays, edition 05/2009, P/N:4425209 Rev. B

| Poly-A RNA | Dilution buffer | Dilution |
|---|---|---|
| 2 $\mu$l (from stock) | 38 $\mu$l | 1:20 (1st dilution) |
| 2 $\mu$l (from 1st dilution) | 98 $\mu$l | 1:50 (2nd dilution) |
| 2 $\mu$l (from 2nd dilution) | 98 $\mu$l | 1:50 (3rd dilution) |
| 20 $\mu$l (from 3rd dilution) | 20 $\mu$l | 1:2 (4th dilution) |

A volume of 2 $\mu$l Poly-A RNA Controls from the 4th dilution was added to each RNA sample, mixed with gentle finger-flicking and centrifuged briefly to collect samples at the bottom of microtube. The final concentrations of Poly-A RNA Controls when added to the RNA samples were as follow:

| Poly-A RNA Spike | Final Concentrations (ratio of copy numbers) |
|---|---|
| lys | 1:100,000 |
| phe | 1:50,000 |
| thr | 1:25,000 |
| dap | 1:6,667 |

First-Strand Master Mix contained the following components and volumes per reaction:

| | |
|---|---|
| First-Strand Buffer Mix | 4 $\mu$l |
| First-Strand Enzyme Mix | 1 $\mu$l |
| **Total volume** | **5 $\mu$l** |

A total of 10 reactions was prepared at room temperature and the mixture was mixed well with gentle finger-flicking. After a brief centrifugation, 5 $\mu$l of First-Strand Master Mix was dispensed into each 5 $\mu$l of RNA sample (containing the Poly-A RNA Controls).

When the incubation was completed, second-strand cDNA was generated from the newly

synthesised first-strand cDNA by mixing Second-Strand Master Mix (containing DNA polymerase I and RNase H) to the first-strand cDNA, and incubated for 1 h at 16 °C, 10 min at 65 °C, then for at least 2 min at 4 °C. At the end of the incubation, microtubes containing the mixture were centrifuged briefly and kept on ice.

Second-Strand Master Mix contained the following components and volumes per reaction:

| | |
|---|---|
| Nuclease-free water | 32.5 $\mu$l |
| Second-Strand Buffer Mix | 12.5 $\mu$l |
| Second-Strand Enzyme Mix | 5 $\mu$l |
| **Total volume** | **50 $\mu$l** |

A total of 10 reactions was prepared on ice, and the mixture was mixed well with gentle finger-flicking. After a brief centrifugation, 50 $\mu$l of Second-Strand Master Mix was dispensed into each 10 $\mu$l of first-strand cDNA sample.

By employing the second-strand cDNA as a template, antisense cRNA was synthesised via *in vitro* transcription (IVT), which is a linear amplification step. IVT master mix (containing T7 RNA polymerase) was added to cDNA sample and was incubated for 16 h at 40 °C, then overnight at 4 °C. At the end of the incubation, the mixture was centrifuged briefly and kept on ice briefly before proceeding to the next step.

IVT Master Mix contained the following components and volumes per reaction:

| | |
|---|---|
| IVT Buffer Mix | 24 $\mu$l |
| IVT Enzyme Mix | 6 $\mu$l |
| **Total volume** | **30 $\mu$l** |

A total of 10 reactions was prepared at room temperature, and the mixture was mixed well with gentle finger-flicking. After a brief centrifugation, 30 $\mu$l of IVT Master Mix was dispensed into each 60 $\mu$l of cDNA sample.

The newly synthesised antisense cRNA was purified using nucleic acid binding beads to remove enzymes, phosphates, and unincorporated nucleotides in order to improve stability of cRNA. cRNA Binding Mix was added into cRNA sample, and mixed well with gentle pipetting.

cRNA Binding Mix contained the following components and volumes per reaction:

| | |
|---|---|
| Nucleic Acid Binding Beads | 10 $\mu$l |
| Nucleic Acid Binding Buffer Concentrate | 50 $\mu$l |
| **Total volume** | **60 $\mu$l** |

A total of 10 reactions was prepared at room temperature. Nucleic Acid Binding Beads were vortexed vigorously to ensure that the magnetic beads were fully dispersed. Nucleic Acid Binding Buffer Concentrate was pre-warmed to 45 °C to solubilise the content before used. The mixture was mixed well and 60 $\mu$l of cRNA Binding Mix was added to each 90 $\mu$l of cRNA sample. The mixture was pipetted up and down three times and transferred to individual well of a U-bottom plate, following which 60 $\mu$l of 100% isopropanol was added and mixed well by pipetting up and down three times.

The U-bottom plate was gently shaken for 2 min at 750 RPM to encourage binding of cRNA to the nucleic acid binding beads, after which it was moved to a magnetic stand and let stand for 5 min to capture the magnetic beads. The supernatant was then carefully aspirated and discarded without disrupting the magnetic beads and the plate was removed from the magnetic stand. A volume of 100 $\mu$l Nucleic Acid Wash Solution (containing ethanol) was then added to individual well containing cRNA bound-magnetic beads and mixed well with gentle pipetting. The U-bottom plate was gently shaken for 1 min at 1,200 RPM and the magnetic beads were captured on a magnetic stand and supernatant carefully discarded as in previous step. The washing step was repeated once again with 100 $\mu$l of Nucleic Acid Wash Solution, after which the U-bottom plate was shaken vigorously for 1 min at 1,350 RPM to evaporate residual ethanol from the magnetic beads.

In order to elute cRNA from the magnetic beads, 40 $\mu$l of pre-heated Elution solution (55 °C) was added to each cRNA sample and let stand for 2 min without shaking. The plate was then shaken vigorously for 3 min at 1,350 RPM to disperse the magnetic beads, after which it was moved to a magnetic stand and let stand for 5 min to capture the magnetic beads. Finally, the supernatant, now containing purified antisense cRNA, was transferred to fresh nuclease free microtubes.

The yield of purified cRNA was determined using a Nanodrop® ND-1000 and the cRNA size distribution was determined using an Agilent 2100 Bioanalyser. The cRNA yield was within the expected range, and as shown in Figure 5.6, the cRNA sizes had an expected range of 50-4,000 nucleotides.

Second-cycle sense cDNA was then generated from the purified antisense cRNA. While on ice, a volume containing 15 $\mu$g cRNA sample was measured out into a microtube, and nuclease-free water was added to a final volume of 22 $\mu$l. A volume of 2 $\mu$l random primers was added, after which the mixture was mixed well with gentle finger-flicking. After a brief centrifugation, the mixture was incubated for 5 min at 70 °C, 5 min at 25 °C, then for 2 min at 4 °C. At the end of the incubation, the mixture was centrifuged briefly and Second-cycle Master Mix (containing dNTP/dUTP mix) was added to each cRNA sample. The mixture was mixed well with gentle finger-flicking. After a brief centrifugation, the mixture was incubated for 10 min at 25 °C, 90 min at 42 °C, 10 min at 70 °C, then for at least 2 min at 4 °C. At the end of the incubation, the mixture was centrifuged briefly and kept on ice immediately.

The Second-cycle Master Mix contained the following components per reaction:

| | |
|---|---|
| Second-cycle Buffer Mix | 8 $\mu$l |
| Second-cycle Enzyme Mix | 8 $\mu$l |
| **Total volume** | **16 $\mu$l** |

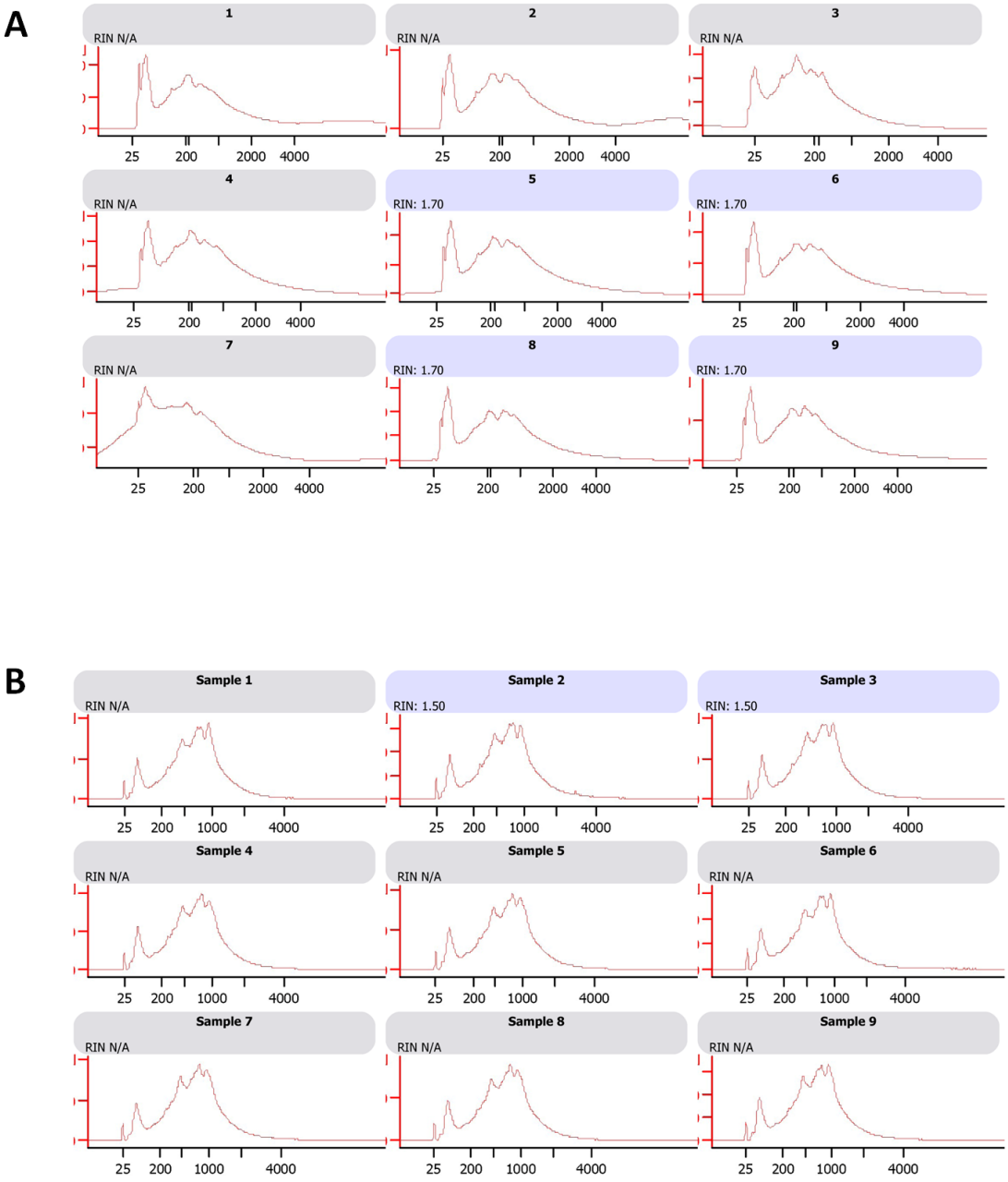


Figure 5.6: Size distribution of antisense cRNA. All samples from AGN193109 experiment (**A**) and DEAB experiment (**B**) had an expected range of size distribution from 50 to 4,000 nucleotides, with most cRNA sizes in the range of 200 to 2,000 nucleotides.

A total of 10 reactions was prepared on ice, and the mixture was mixed well with gentle finger-flicking. After a brief centrifugation, 16 $\mu$l of Second-cycle Master Mix was dispensed into each 24 $\mu$l of cDNA sample.

In order to eliminate cRNA from the second-cycle sense cDNA sample, 2 $\mu$l of RNase H was added to each 40 $\mu$l of second-cycle cDNA sample on ice and mixed well with gentle finger-flicking. After a brief centrifugation, the mixture was incubated for 45 min at 37 °C, 5 min at 95 °C, then for at least 2 min at 4 °C. Purification of sense cDNA was then performed immediately.

Purification of sense cDNA followed similar steps of antisense cRNA purification as described before. A volume of 18 $\mu$l nuclease-free water was first pipetted into each cDNA sample to achieve a final volume of 60 $\mu$l. cDNA Binding Mix was then added to each cDNA sample and mixed well with gentle pipetting.

The cDNA Binding Mix contained the following components and volumes per reaction:

| | |
|---|---|
| Nucleic Acid Binding Beads | 10 $\mu$l |
| Nucleic Acid Binding Buffer Concentrate | 50 $\mu$l |
| **Total volume** | **60 $\mu$l** |

A total of 10 reactions was prepared at room temperature. Nucleic Acid Binding Beads were vortexed vigorously to ensure the magnetic beads were fully dispersed and Nucleic Acid Binding Buffer Concentrate was pre-warmed to 45 °C to solubilise the content before used. The mixture was mixed well and 60 $\mu$l of cDNA Binding Mix was added to each 60 $\mu$l of cDNA sample. The mixture was pipetted up and down three times then transferred to individual well of a U-bottom plate, following which 120 $\mu$l of 100% ethanol was added and mixed well by pipetting up and down three times. Subsequent steps of second-cycle cDNA purification was similar to that described for cRNA purification.

Elution of cDNA from the magnetic beads was the same as for elution of cRNA except that only 30 $\mu$l of pre-heated Elution solution (55 °C) was added to each sample. The yield of purified cDNA was determined using a Nanodrop® ND-1000 and the cDNA size distribution was determined using an Agilent 2100 Bioanalyser. The cDNA yield was within the expected range, and as shown in Figure 5.7, the median size of cDNA samples was around the expected 400 nucleotides.

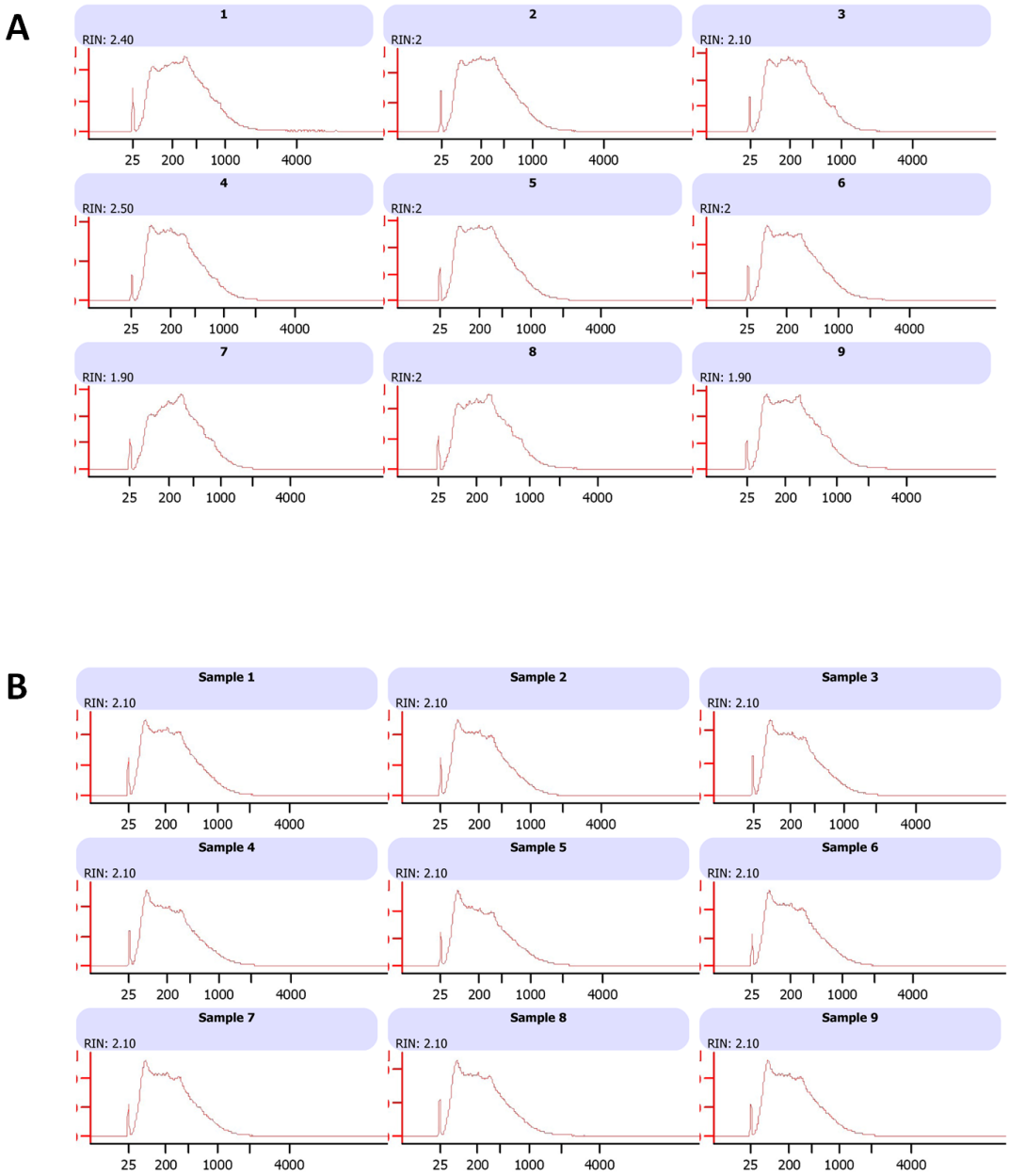


Figure 5.7: Size distribution of sense cDNA. All samples from AGN193109 experiment (**A**) and DEAB experiment (**B**) had an expected median size of 400 nucleotides.

***Sense cDNA fragmentation, terminal labelling and hybridisation cocktail preparation***

Fragmentation and terminal labelling of sense cDNA was performed using an Affymetrix® GeneChip® WT terminal Labelling Kit, while hybridisation cocktail was prepared using an Affymetrix® GeneChip® Hybridisation, Wash and Stain Kit following the manufacturer's protocol[5].

Fragmentation of sense cDNA was achieved by using uracil DNA glycosylase (UDG), an enzyme that cleaves the DNA at sites where uracil was incorporated during the second-cycle cDNA synthesis. The apurinic/apyrimidinic endonuclease 1 (APE 1) enzyme then cleaves the phosphodiester backbone where the base is missing, leaving a 3'-hydroxyl and a 5'-deoxyribose phosphate terminus.

A volume containing 5.5 $\mu$g cDNA was first measured out into a microtube, and nuclease-free water was added to a final volume of 31.2 $\mu$l. Fragmentation Master Mix was then added to each cDNA sample and mixed well with gentle finger-flicking. After a brief centrifugation, the mixture was incubated for 60 min at 37 °C, 2 min at 93 °C, then for at least 2 min at 4 °C.

The Fragmentation Master Mix contained the following components and volumes per reaction:

| | |
|---|---|
| RNase free water | 10 $\mu$l |
| 10x cDNA Fragmentation Buffer | 4.8 $\mu$l |
| UDG, 10 U/$\mu$l | 1 $\mu$l |
| APE 1, 1,000 U/$\mu$l | 1 $\mu$l |
| **Total volume** | **16.8 $\mu$l** |

A total of 10 reactions was prepared and the mixture was mixed well with gentle finger-flicking. After a brief centrifugation, 16.8 $\mu$l of Fragmentation Master Mix was dispensed into each 31.2 $\mu$l of cDNA sample.

[5] Affymetrix® GeneChip® WT Terminal Labelling and Hybridisation User Manual, P/N 702808 Rev. 4

The fragmented cDNA was labelled using deoxynucleotidyl transferase (TdT) and DNA Labelling Reagent containing Biotin Allonamide Triphosphate. A volume of 45 $\mu$l fragmented cDNA was pipetted into a nuclease-free microtube, to which Terminal Labelling Master Mix was added and mixed well with gentle finger-flicking. After a brief centrifugation, the mixture was incubated for 60 min at 37 °C, 10 min at 70 °C, then for at least 2 min at 4 °C.

The Terminal Labelling Master Mix contained the following components and volumes per reaction:

| | |
|---|---|
| 5x TdT buffer | 12 $\mu$l |
| TdT | 2 $\mu$l |
| 5 mM DNA Labelling Reagent | 1 $\mu$l |
| **Total volume** | **15 $\mu$l** |

A total of 10 reactions was prepared and the mixture was mixed thoroughly with gentle finger-flicking. After a brief centrifugation, 15 $\mu$l of Terminal Labelling Master Mix was dispensed into each 45 $\mu$l of fragmented cDNA sample.

In order to prepare the hybridisation cocktail, Hybridisation Master Mix was added to 60 $\mu$l of fragmented and labelled cDNA and mixed well with gentle finger-flicking. After a brief centrifugation, the mixture was incubated for 5 min at 99 °C, cooled to 45 °C for 5 min, then centrifuged at 21,500 g for 1 min.

Hybridisation Master Mix contained the following components and volumes per reaction:

| | |
|---|---|
| 3 nM Control Oligonucleotide B2 | 3.7 $\mu$l |
| 20x Eukaryotic Hybridisation Controls | 11 $\mu$l |
| 2x Hybridisation Mix | 110 $\mu$l |
| DMSO | 15.4 $\mu$l |
| Nuclease-free water | 19.9 $\mu$l |
| **Total volume** | **160 $\mu$l** |

The 20x Eukaryotic Hybridisation Controls were pre-heated to 65 °C for 5 min prior to use. A total of 10 reactions was prepared and the mixture was mixed thoroughly with gentle vortexing. After a brief centrifugation, 160 $\mu$l of Hybridisation Master Mix was dispensed into each 60 $\mu$l of fragmented and labelled cDNA sample.

Control Oligonecleotide B2 was used to provide alignment signals for the microarray software. Eukaryotic Hybridisation Controls contained bioB, bioC, and bioD from biotin synthesis of *E.coli*, and cre from P1 bacteriophage, at a staggered concentration (final concentrations would be 1.5 pM, 5 pM, 25 pM, and 100 pM for bioB, bioC, bioD, and cre, respectively). Given that the Eukaryotic Hybridisation Controls were spiked into hybridisation cocktail independent of RNA sample preparation, they serve as controls for sample hybridisation efficiency.

All reagents such as master mixes were prepared in nuclease-free microtubes. A MJ Research PTC-225 Peltier Thermal Cycler was used for incubation; a Jencon-PLS mini centrifuge and an Eppendorf MiniSpin centrifuge machines were used for centrifugation; a Heidolph Titramax 100 shaker was used for plate shaking.

The basic principles and workflow of sample processing for microarray experiment is illustrated in Figure 5.8.

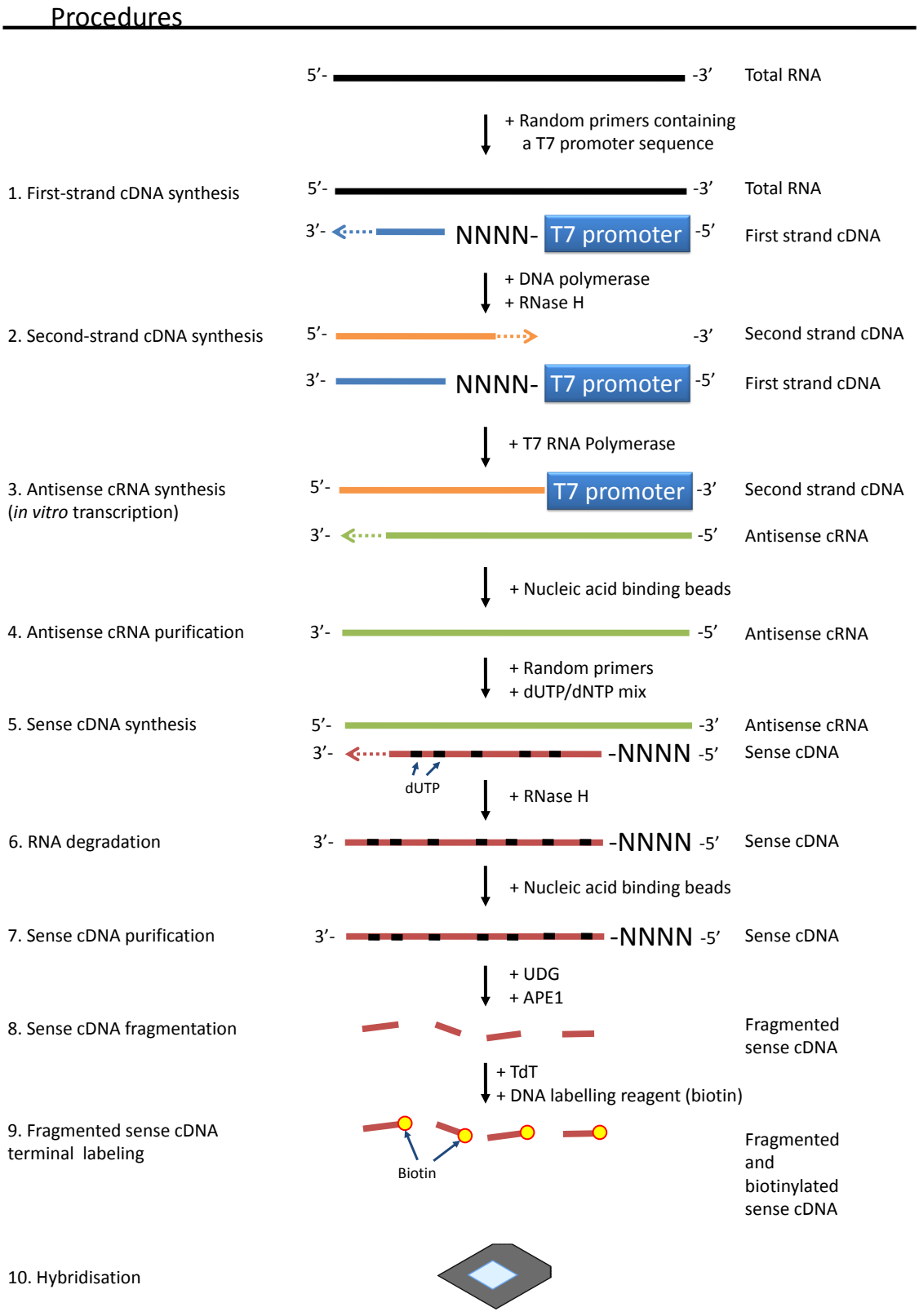


Figure 5.8: Please refer to the following page for figure legend.

Figure 5.8: Workflow of sample processing for microarray experiments. First-strand cDNA was first synthesised from total RNA using random primers containing T7 promoter sequence (**1**). Second-strand cDNA was then synthesised by DNA polymerase and RNA molecules were degraded by RNase H (**2**). By using the second-strand cDNA as a template, antisense cRNA was synthesised using T7 RNA polymerase (**3**). After a purification step (**4**), second cycle sense cDNA was synthesised with random primers and dNTP/dUTP mix (**5**). RNA molecules were then degraded by RNase H (**6**), after which the sense cDNA was purified (**7**). The purified sense cDNA was then fragmented with UDG and APE1 (**8**), after which the fragmented cDNA was labelled with biotin (**9**). Finally, the fragmented and labelled cDNA sample was hybridised to the array (**10**). UDG: uracil DNA glycosylase; APE1: apurinic/apyrimidinic endonuclease 1; TdT: deoxynucleotidyl transferase.

***Target hybridisation to microarray chip***

Array was equilibrated to room temperature and labelled with sample name. A clean pipette tip was inserted into one of the septum at the back of the cartridge to allow venting of air from the hybridisation chamber. A volume of while 80 $\mu$l hybridisation cocktail was withdrawn, avoiding the pellet at the bottom of the tube, and injected into the array through the remaining septum (Figure 5.9). The septa were then sealed using Tough-Tags® (Thistle Scientific Ltd., Glasgow, UK) and the array was incubated at 45 °C in an Affymetrix® GeneChip® Hybridisation Oven 640, rotated at 60 rpm, for 17 hours ± 1 hour.

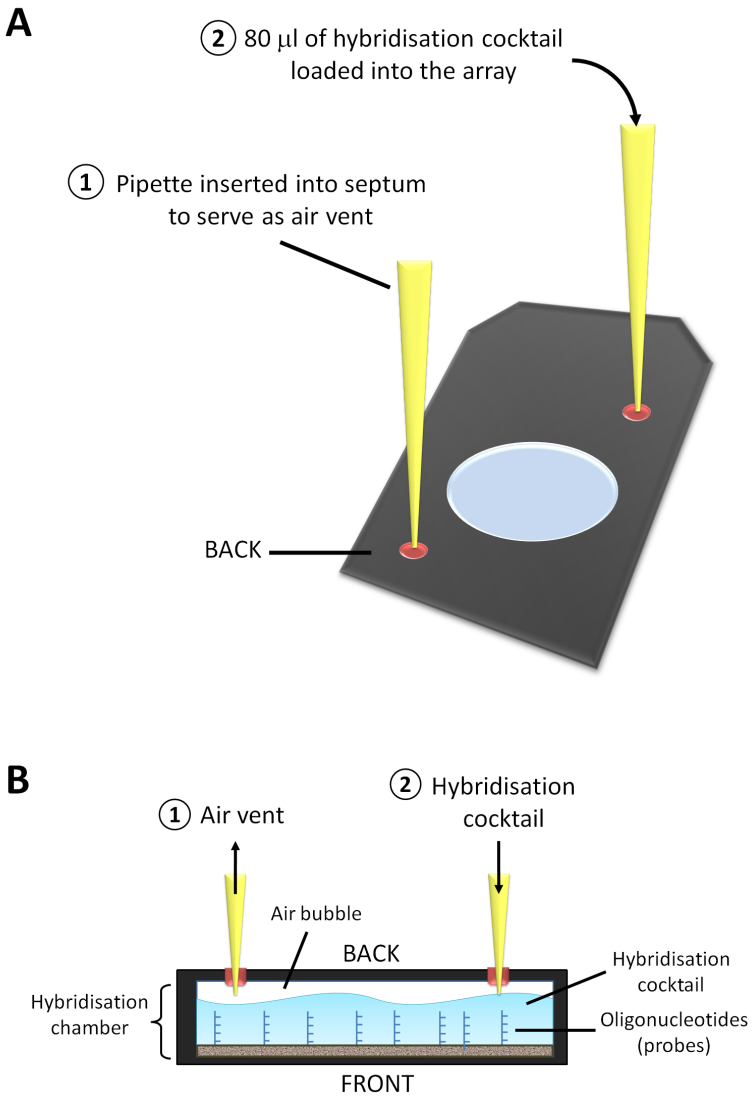


Figure 5.9: Loading of hybridisation cocktail into array cartridge. **A.** A clean pipette tip was pierced into one of the rubber septa at the back of the cartridge to serve as air vent (**1**); 80 $\mu$l of hybridisation cocktail was loaded into the hybridisation chamber of the cartridge via the remaining rubber septum (**2**). **B.** Side view of the array cartridge shows the pipette that serves as air vent (**1**), the pipette through which hybridisation cocktail was loaded (**2**), and the hybridisation cocktail in the hybridisation chamber, in contact with the array glass mounted with probes. The volume of hybridisation cocktail (80 $\mu$l) was slightly less than the capacity of the hybridisation chamber (100 $\mu$l), so that during rotation the free-floating air bubble would allow a uniform contact between the hybridisation cocktail and all portions of the array.

***Array washing and staining***

Washing and staining of the arrays were performed using an Affymetrix® GeneChip® Fluidics Station 450 machine. An experimental file was first created using an Affymetrix® GeneChip® Command Console (AGCC) Portal software. Washing and staining were executed through the AGCC Fluidics Control software following the company's protocol[6].

The prepared and pre-tested washing and staining solutions used were as follows:

- **Wash Bufer A** (non-Stringent wash buffer), containing 6x SSPE (0.9 M NaCl, 0.06 M $NaH_2PO_4$, 0.006 M EDTA) and 0.01% Tween® 20.
- **Wash Buffer B** (stringent wash buffer), containing 100 mM 2-(N-Morpholino)ethanesulfonic acid hydrate (MES), 0.1 M $Na^+$, and 0.01% Tween® 20.
- **Stain Cocktail 1**, containing 10 $\mu$g/ml Streptavidin Phycoerythrin (SAPE) and 2 mg/ml BSA in stain buffer (100 mM MES, 1 M $Na^+$, and 0.05% Tween® 20).
- **Stain Cocktail 2**, containing 3 $\mu$g/ml biotinylated anti-streptavidin, 0.1 mg/mL goat IgG, and 2 mg/ml BSA in stain buffer.
- **Array Holding Buffer**, containing 100 mM MES, 1M $Na^+$, and 0.01% Tween® 20.

Wash Buffer A, Wash Buffer B, and ultrapure water were filled into the appropriate reservoirs on the Fluidics Station. After priming the Fluidics Station, microtubes containing 600 $\mu$l of Stain Cocktail 1, 600 $\mu$l of Stain Cocktail 2, and 800 $\mu$l of Array Holding Buffer were placed into sample holders 1, 2, and 3, respectively.

After hybridisation was completed, a clean pipette tip was inserted into one of the septa at the back of the cartridge, and the hybridisation cocktail was extracted with another pipette through the remaining septum. Without removing the vent tip, 100 $\mu$l of Wash

[6]Affymetrix® GeneChip® Expression Wash, Stain and Scan User Manual for Cartridge Arrays, P/N 702731 Rev. 3

Buffer A was injected into the cartridge through another septum, and the cartridge was inserted into the washblock probe array holder on the Fluidics Station. Washing and staining of the arrays were then run using the FS450_0007 protocol[7] as stipulated in Table 5.1.

Table 5.1: FS450_0007 protocol for washing and staining

| **Procedure** | **Steps and conditions** |
|---|---|
| **Post Hyb Wash 1** | 10 cycles of 2 mixes/cycle with Wash Buffer A at 30 °C |
| **Post Hyb Wash 2** | 6 cycles of 15 mixes/cycle with Wash Buffer B at 50 °C |
| **Stain** | Stain the probe array for 5 min in Stain Cocktail 1 at 35 °C |
| **Post Stain Wash** | 10 cycles of 4 mixes/cycle with Wash Buffer A at 30 °C |
| **2nd Stain** | Stain the probe array for 5 min in Stain Cocktail 2 at 35 °C |
| **3rd Stain** | Stain the probe array for 5 minutes in Stain Cocktail 1 at 35 °C |
| **Final Wash** | 15 cycles of 4 mixes/cycle with Wash Buffer A at 35 °C |
| **Holding Buffer** | Fill the probe array with Array Holding Buffer |

After washing and staining were completed, the arrays were removed from the Fluidics Station and examined for presence of large bubbles. If bubble was trapped within the array, the Array Holding Buffer was extracted manually with a pipette and 100 $\mu$l of fresh Array Holding Buffer was injected manually into the array. The stained arrays were then kept in the dark at room temperature and scanned immediately. The basic principles of target hybridisation to array probes and the subsequent staining with SAPE and biotinylated anti-streptavidin are summarised in Figure 5.10.

[7] Affymetrix® GeneChip® WT Terminal Labelling and Hybridisation User Manual, P/N 702808 Rev. 4

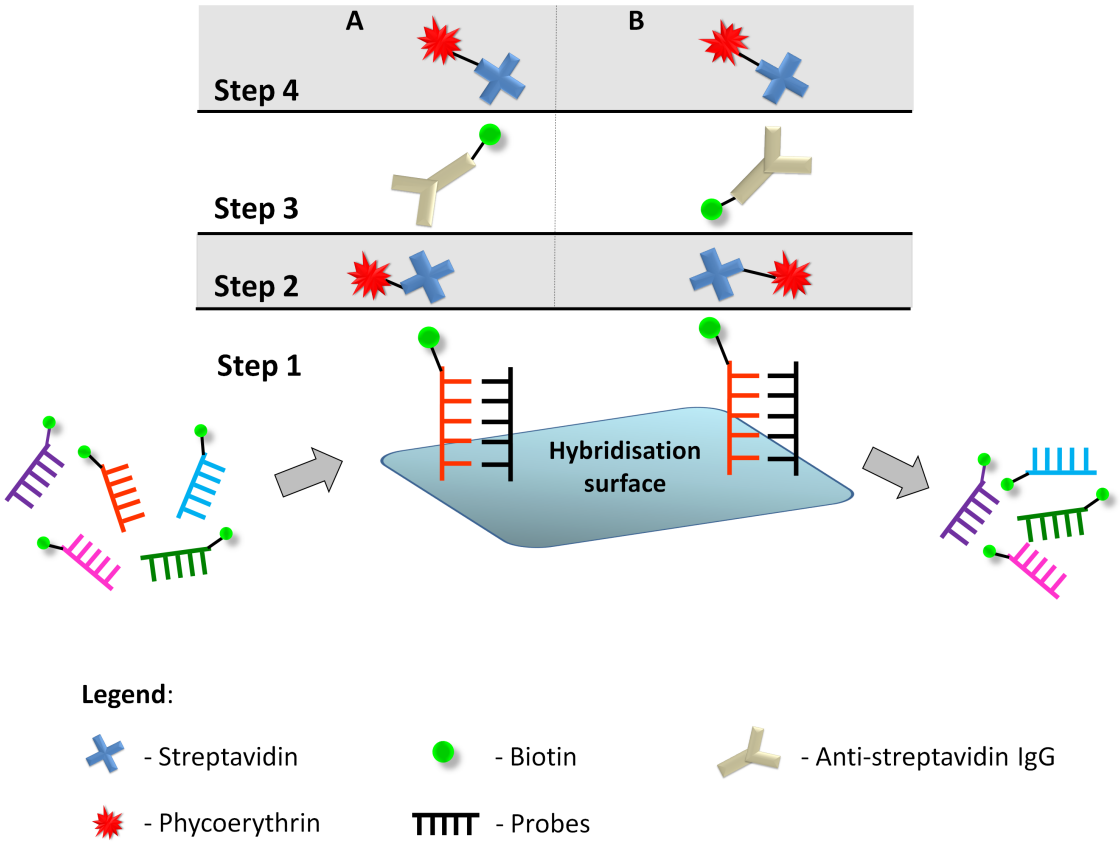


Figure 5.10: Array hybridisation and signal amplification. **Step 1:** Biotinylated cDNA targets hybridised to probes of complementary sequences by forming hydrogen bonds. A stronger bond would form between targets and probes with high number of complementary base pairs; a weak bond between targets and probes with low or no complementary base pairs would be washed off. **Step 2:** Amplification of signal was achieved by streptavidin-biotin interaction, the strongest known non-covalent bond in chemistry ($K_d = 10^{15}$ M) [107], as well as immunogenic interaction. The biotin molecules (green sphere) on the cDNA targets were bound by streptavidin (blue cross) that is conjugated to phycoerythrin (red star) (SAPE). **Step 3:** Streptavidin was either detected by anti-streptavidin IgG (**A**), or was bound by the biotin molecule conjugated to anti-streptavidin IgG (**B**). **Step 4:** SAPE was again used in this step. The biotin molecule conjugated to anti-streptavidin IgG (**A**), and the anti-streptavidin IgG itself (**B**) would be bound by streptavidin of the SAPE. Higher fluorescence signal corresponded to more copies of cDNA targets.

***Scanning of microarray chips***

Microarray cartridges were scanned using an Affymetrix® GeneChip® Scanner 3000 7G, executed via an AGCC Scan Control software, which performed auto-focus prior to scanning. The scanner was turned on for at least 10 min prior to scanning. The array cartridges were handled with gloved hands and were inserted into the scanner after gently wiping the surface with gloved fingers to get rid of dust that may interfere with scanning.

***Software used for Data Summarising, Normalisation, and Analysis***

An AGCC Expression Console™ software was used for data summarising and the default Robust Multichip Average (RMA) method was used for data normalisation [128]. A Qlucore® Omics Explorer (QOE) software was used to generate lists of genes regulated by the treatments.

***Quality check on arrays***

When the scan was completed, the image data for each array was reviewed for aberrant signal using an AGCC Viewer software. As shown in Figure 5.11, positive and negative signals were as expected, and aberrant signs, e.g., blotches of overt brightness or dimness, were not observed in all the arrays.

Prior to normalisation, the general intensity of the arrays varied greatly ,i.e., some arrays had a brighter signal in general compared to others (Figure 5.11), precluding a direct comparison. By employing RMA normalisation algorithm, a more uniform general intensity across all arrays was achieved (Figure 5.12).

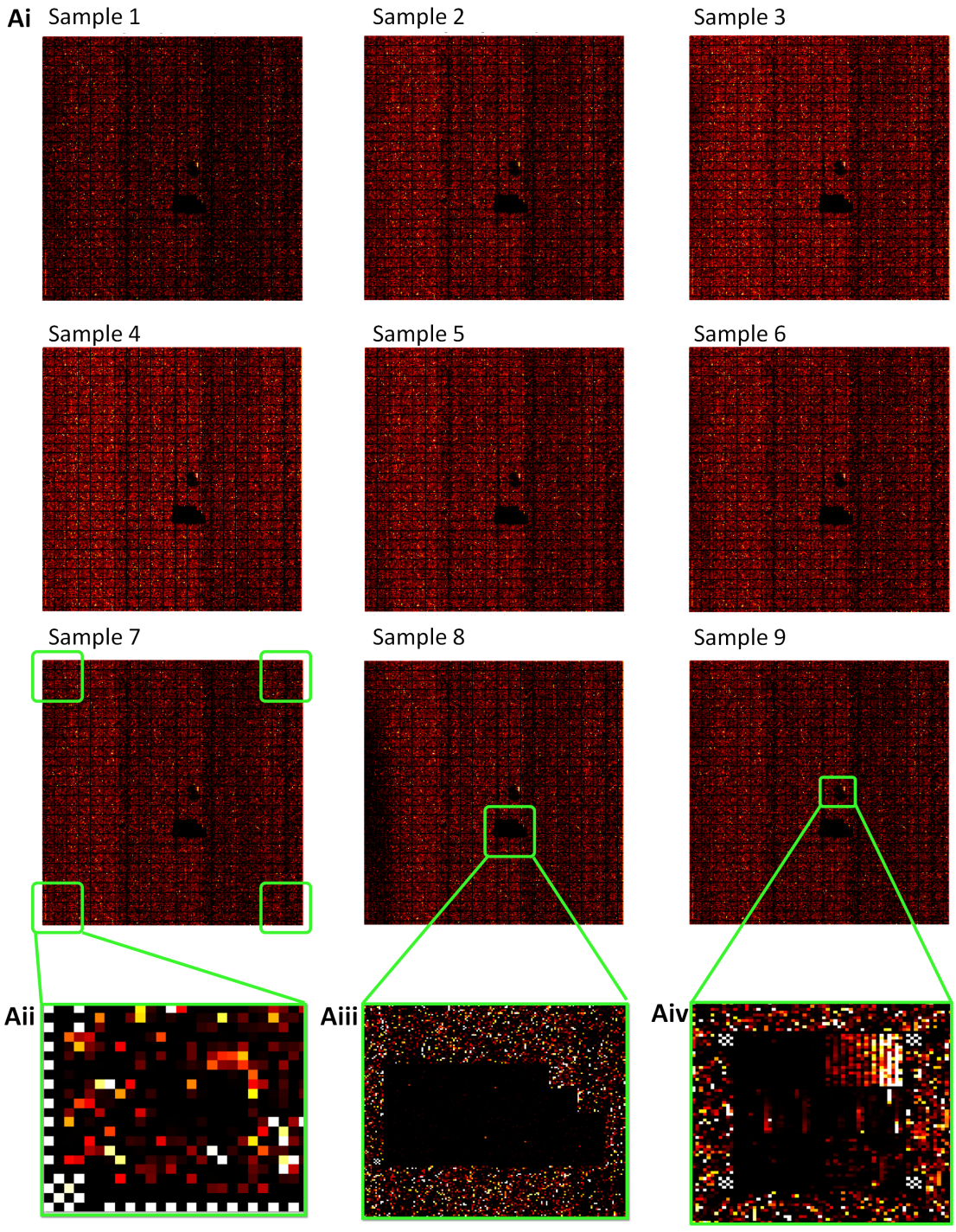


Figure 5.11: Please refer to the following page for figure legend.

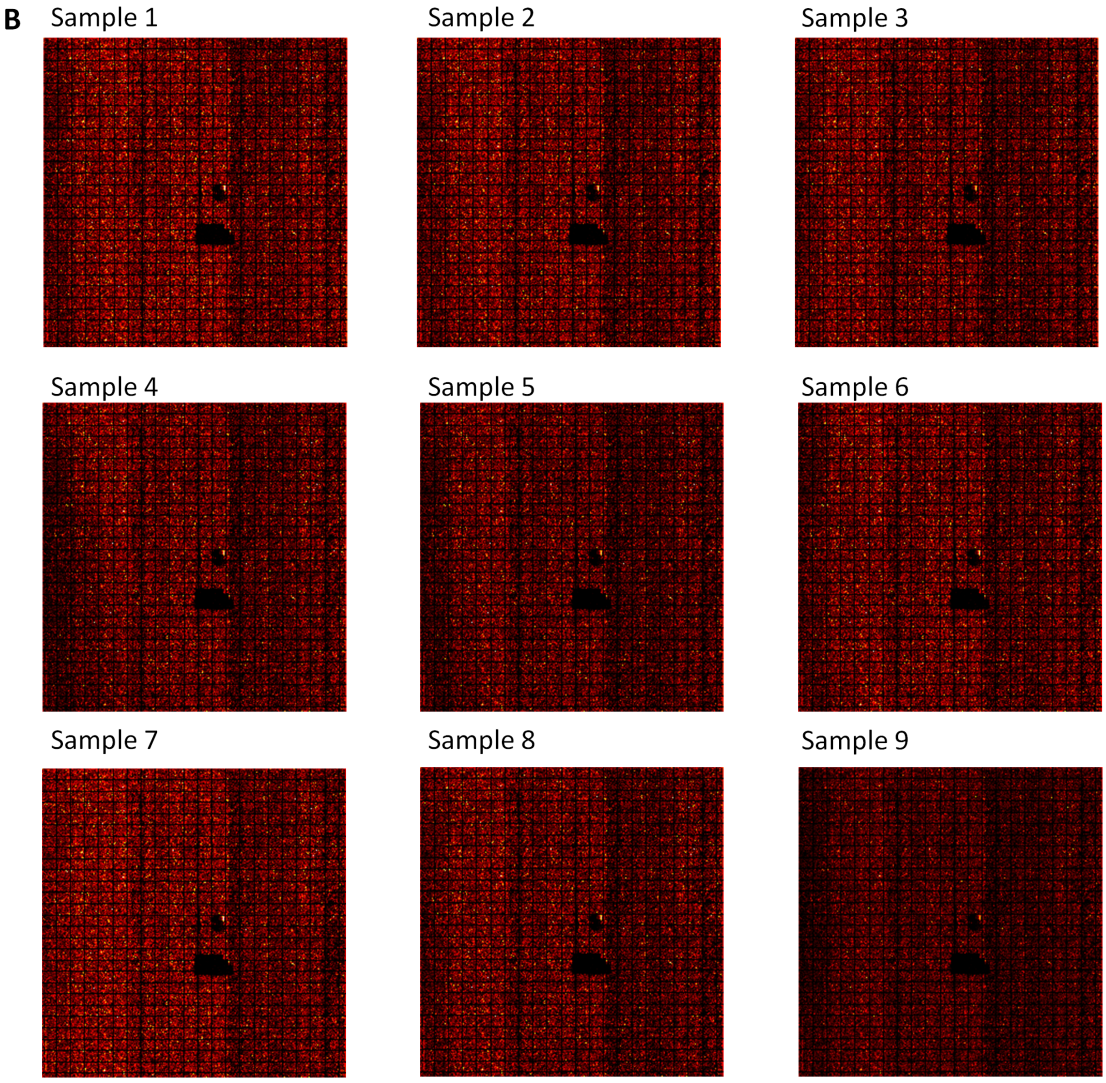


Figure 5.11: General appearance of array signal. All arrays from AGN193109 experiment (**Ai**) and from DEAB experiment (**B**) had normal hybridisation signal. The success of hybridisation was further confirmed by referring to several specific patterns given rise by hybridisation of control oligonucleotide B2 to their probes on the arrays, including the checker board pattern at the four corners and an alternating signal lining the border of each array (**Aii**), the absence of signal in the expected region containing sense probes (**Aiii**), and the square featuring a gradient of positive signal, flanked by checker board pattern at four corners (**Aiv**). Similar specific patterns were also confirmed on arrays from the DEAB experiment (**B**).

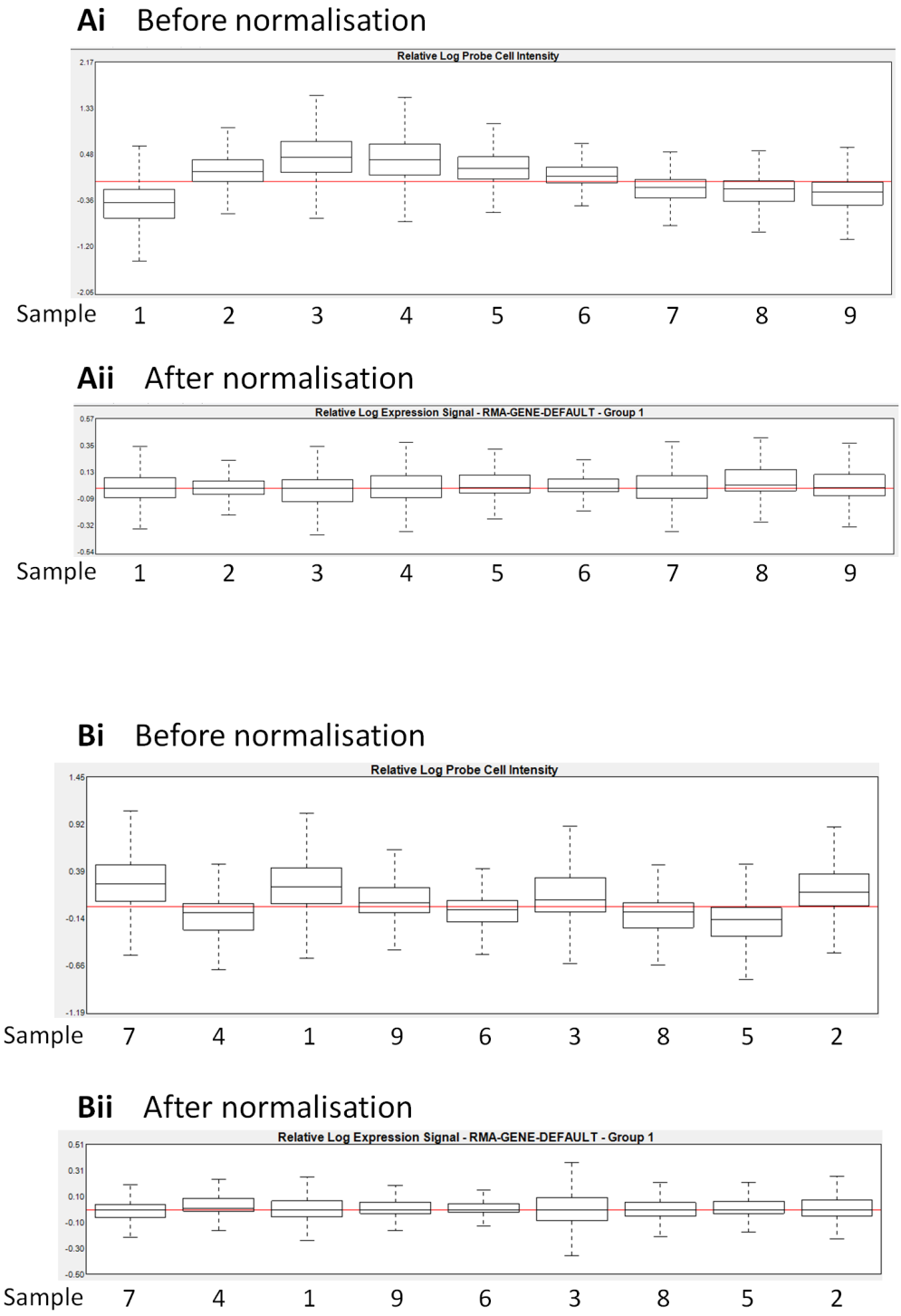


Figure 5.12: Normalisation of array intensity. Before normalisation, general intensity of arrays from AGN193109 experiment (**Ai**) and from DEAB experiment (**Bi**) varied greatly. By using a Robust Multichip Average (RMA) normalisation algorithm, a more uniform general intensity was achieved for arrays from AGN193109 experiment (**Aii**) and from DEAB experiment (**Bii**).

Additional quality check on array metrics was performed following manufacturer's recommendation[8]. Specifically, hybridisation quality was confirmed from the bacterial spikes showing an expected signal values of Cre>bioD>bioC>bioB in all samples. Poly-A RNA Controls in all samples showed signal values of thr>dap>phe>lys, which were different from the expected dap>thr>phe>lys (Figure 5.13). The situation could happen occasionally with Gene ST arrays as the Poly-A RNA Controls were originally designed for 3'-biased arrays, and it does not indicate failed labelling (personal communication with Dr. L Dupont, Affymetrix technical support supervisor). More importantly, similar pattern of the poly-A RNA controls was observed in all the samples.

Two additional metrics, i.e., (i) "pos_vs_neg_auc" and (ii) "all_probe_set_rle_mean", were also examined to further confirm sample quality. "pos_vs_neg_auc" metric is a measure of area under the curve for the receiver operating characteristic plot comparing signal values of positive controls to negative controls; a typical range of pos_vs_neg_auc"is between 0.8-0.9, with a value of 1.0 being perfect. "all_probe_set_rle_mean" metric is the mean of signal differences for each probe set compared to the median signal value of the probe set in the study; a typical range is between 0.1-0.23 and a big value indicates outlier array. As shown in Table 5.2, pos_vs_neg_auc for all arrays had a value of $\geq$0.9, and all_probeset_rle_mean for all arrays were $\leq$0.17, indicating absence of obvious outliers.

Pearson's correlation plot was generated to assess correlation between the biological replicates. As shown in Figure 5.14, samples within the same batch of experiment correlated better with each other, compared to samples treated with the same reagents in different batches of experiment. This suggested the presence of "batch effect", whereby culturing or treating different batches of cells on separate occasions are having a larger effect on transcript expression compared to that given rise by the actual treatment.

[8]Affymetrix® QC Metrics for Exon and Gene Design Expression Arrays-A summary based on the Affymetrix® Quality Assessment of Exon and Gene Arrays White Paper, edition 2008, P/N 702670 Rev. 1

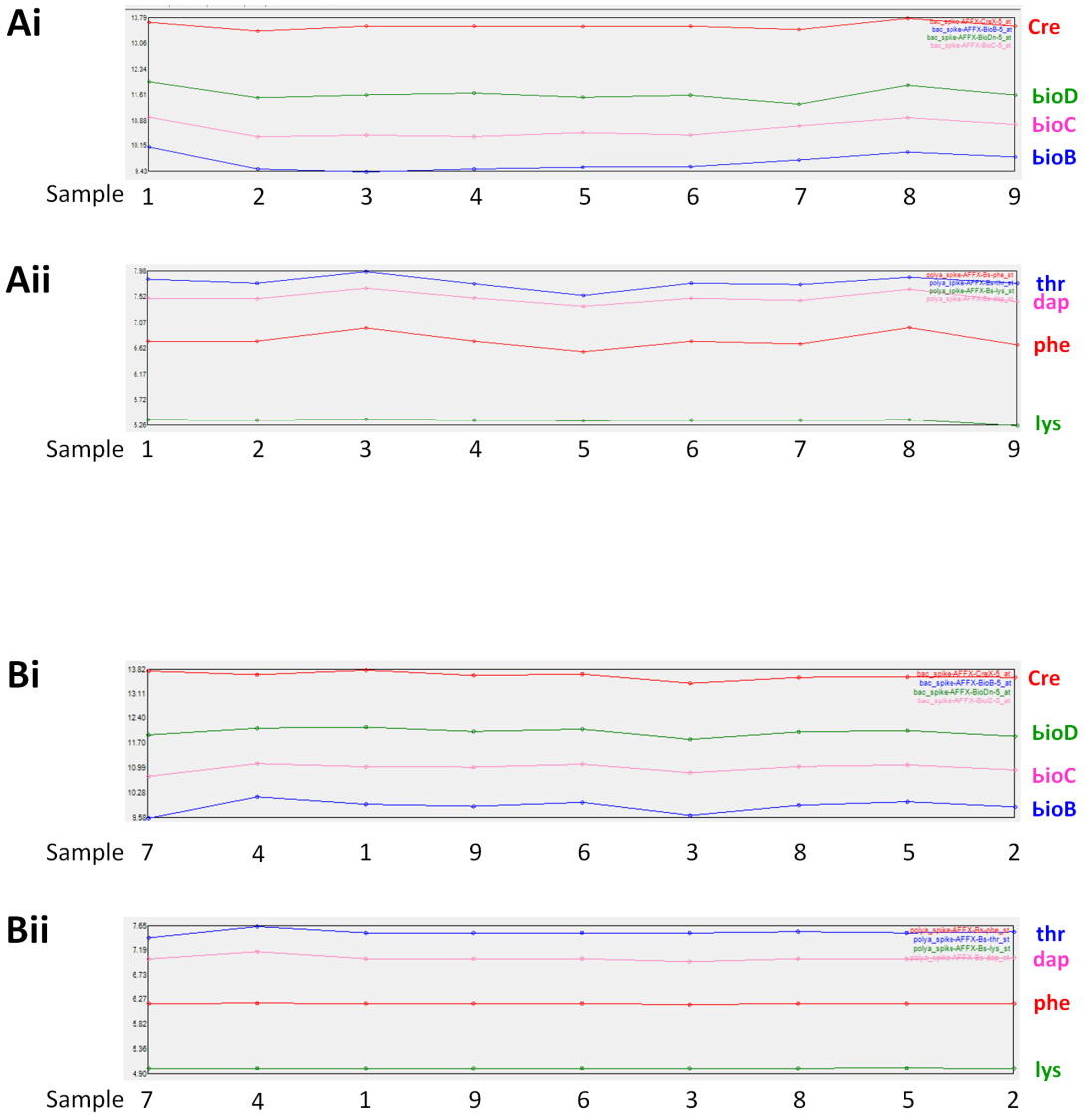


Figure 5.13: Bacterial spikes and Poly-A RNA Controls. Signal of bacterial spikes in arrays from AGN193109 experiment(**Ai**) and DEAB experiment(**Bi**) showed the expected values of Cre>bioD>bioC>bioB. Poly-A RNA Controls in arrays from AGN193109 experiment(**Aii**) and DEAB experiment(**Bii**) showed signal values of thr>dap>phe>lys.

Table 5.2: Sample quality: pos_vs_neg_auc metric and all_probe_set_rle_mean metric.

**AGN193109 experiment**

| Samples | pos_vs_neg_auc | all_probe_set_rle_mean |
|---|---|---|
| 1_VEH | 0.924494 | 0.148752 |
| 2_AGN193109 | 0.917751 | 0.104283 |
| 3_AGN193109 + tRA | 0.924471 | 0.154551 |
| 4_VEH | 0.912801 | 0.150857 |
| 5_AGN193109 | 0.914848 | 0.117575 |
| 6_AGN193109 + tRA | 0.914030 | 0.102842 |
| 7_VEH | 0.924404 | 0.161783 |
| 8_AGN193109 | 0.918907 | 0.150542 |
| 9_AGN193109 + tRA | 0.919005 | 0.146593 |

**DEAB experiment**

| Samples | pos_vs_neg_auc | all_probe_set_rle_mean |
|---|---|---|
| VEH_7 | 0.925370 | 0.097598 |
| VEH_4 | 0.927529 | 0.097436 |
| VEH_1 | 0.920282 | 0.112337 |
| DEAB + tRA_9 | 0.926551 | 0.091955 |
| DEAB + tRA_6 | 0.924961 | 0.079631 |
| DEAB + tRA_3 | 0.921759 | 0.139806 |
| DEAB_8 | 0.924260 | 0.099301 |
| DEAB_5 | 0.922637 | 0.094552 |
| DEAB_2 | 0.920006 | 0.104863 |

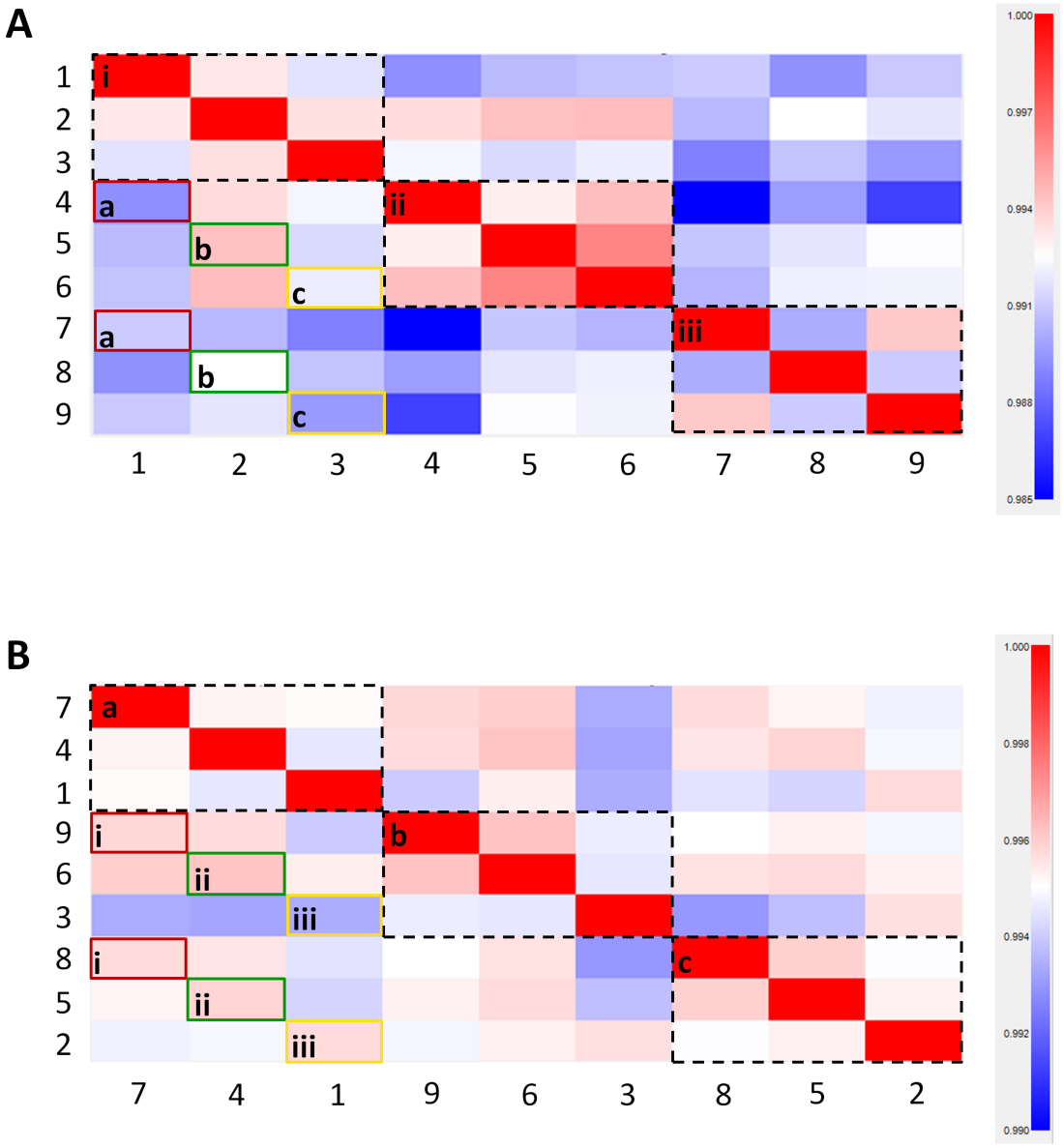


Figure 5.14: Pearson's correlation plot for array comparisons. **A.** In AGN193109 experiment, a better correlation was found among samples of the same batch (samples 1-3, 4-6, and 7-9 in dotted box labelled "i", "ii", and "iii", respectively), compared to samples treated with the same reagent on separate occasions, i.e., samples 1, 4, and 7 (in brown bracket labelled "a"), samples 2, 5, and 8 (in green bracket labelled "b"), and samples 3, 6, and 9 (in yellow bracket labelled "c"). **B.** Similarly, in DEAB experiment, a better correlation was found among samples of the same batch, i.e., samples 7-9 (in brown bracket labelled "i"), samples 4-6 (in green bracket labelled "ii"), and samples 1-3 (in yellow bracket labelled "iii"), whereas biological replicates of three independent experiments had a slightly poorer correlation (samples 1, 4, and 7 in dotted box labelled "a", samples 2, 5, and 8 in dotted box labelled "b", and samples 3, 6, and 9 in samples labelled "c").

### 5.2.4 Validation of candidate target genes shortlisted from microarray experiments with RT-qPCR

The same total RNA samples used for microarray experiment were used to validate regulation of target genes shortlisted from microarray experiments with RT-qPCR as described in Section 5.2.2. The Taqman® Gene Expression Assays used for validation of target genes are listed below:

1. Clca4: Mm00519742_ m1 (amplicon length: 68)
2. Cpm: Mm01250796_ m1 (amplicon length: 63)
3. Csn3: Mm02581554_ m1 (amplicon length: 99)
4. Dhrs3: Mm00488080_ m1 (amplicon length: 84)
5. Dusp1: Mm00457274_ g1 (amplicon length: 65)
6. Ebf1: Mm00432948_ m1 (amplicon length: 59)
7. Foxj1: Mm00807215_ m1 (amplicon length: 98)
8. Galns: Mm00489576_ m1 (amplicon length: 80)
9. Hrsp12: Mm00476177_ m1 (amplicon length: 73)
10. Itga2: Mm00434371_ m1 (amplicon length: 63)
11. Klhdc7a: Mm00557861_ s1 (amplicon length: 117)
12. Lcn2: Mm01324470_ m1 (amplicon length: 84)
13. Muc20: Mm00524818_ m1 (amplicon length: 65)
14. Npr3: Mm00435329_ m1 (amplicon length: 63)
15. Ppbp: Mm00470163_ m1 (amplicon length: 62)
16. Slc37a1: Mm00461949_ m1 (amplicon length: 78)

17. Sorcs2: Mm00473050_ m1 (amplicon length: 64)

18. Sprr1a: Mm01962902_ s1 (amplicon length: 94)

19. Tgm2: Mm00436987_ m1 (amplicon length: 72)

20. Tinag: Mm00496471_ m1 (amplicon length: 78)

21. Tinagl1: Mm00469812_ m1 (amplicon length: 57)

22. Tns1: Mm00452886_ m1 (amplicon length: 91)

23. Upk3b: Mm00558406_ m1 (amplicon length: 89)

24. 9930023K05Rik: Mm00554061_ m1 (amplicon length: 110)

25. 2310007B03Rik: Mm00549644_ m1 (amplicon length: 73)

### 5.2.5 Gene ontology analysis and transcriptomic database comparison

Gene ontology analysis was performed using two independent bioinformatic tools, i.e., **D**atabase for **A**nnotation, **V**isualization and **I**ntegrated **D**iscovery (DAVID) (http://david.abcc.ncifcrf.gov/) [126] and GeneGO MetaCore$^{TM}$ (http://www.genego.com/metacore.php) for the validated genes shortlisted from microarray studies as well as for Bmp7 and Foxa1 genes found to be significantly regulated by AGN193109 and DEAB in the pilot study. Since mIMCD-3 is an SV-40 transformed cell line, its gene expression profile might differ slightly from that of primary cells. Thus, expression of the validated genes was compared to the transcriptomic databases derived from native ureteric bud cells and matured inner medullary collecting duct (IMCD) cells available through National Center for Biotechnology Information (NCBI) Gene Expression Omnibus (GEO).

## 5.3 Results

### 5.3.1 Pilot study

As shown in Figure 5.15Ai and Aii, Bmp7 and Foxa1 mRNA expression was suppressed by AGN193109; the suppression was at least partially abolished when exogenous tRA was added simultaneously. On the other hand, mRNA expression of Wnt7b and Pax2 were not suppressed by AGN193109 (Figure 5.15Aiii and Aiv); in the simultaneous presence of 0.2 $\mu$M tRA, mRNA expression of Wnt7b gene was higher than the vehicle control group (Figure 5.15Aiv), which might indicate an RAR-independent regulation of Wnt7b gene by tRA. Rarb expression in mIMCD-3 cells was relatively low with a high $C_T$ value, which was rather close to the non-template control, as shown in Appendix B.1. The low expression of Rarb would have precluded a fair comparison between treatments and hence was not pursued further. Thus, among the five genes examined, Bmp7 and Foxa1 were found to be regulated by RARs.

In order to further confirm if Bmp7 and Foxa1 were also regulated by endogenous RA, their expression was examined following DEAB treatment. It was found that both Bmp7 and Foxa1 mRNA expression was also suppressed by DEAB; the suppression was at least partially abolished in the simultaneous presence of 0.01 $\mu$M tRA (Figure 5.15B). Taken together, Bmp7 and Foxa1 were identified as target genes of endogenous RA/RAR in mIMCD-3 cells in the pilot study.

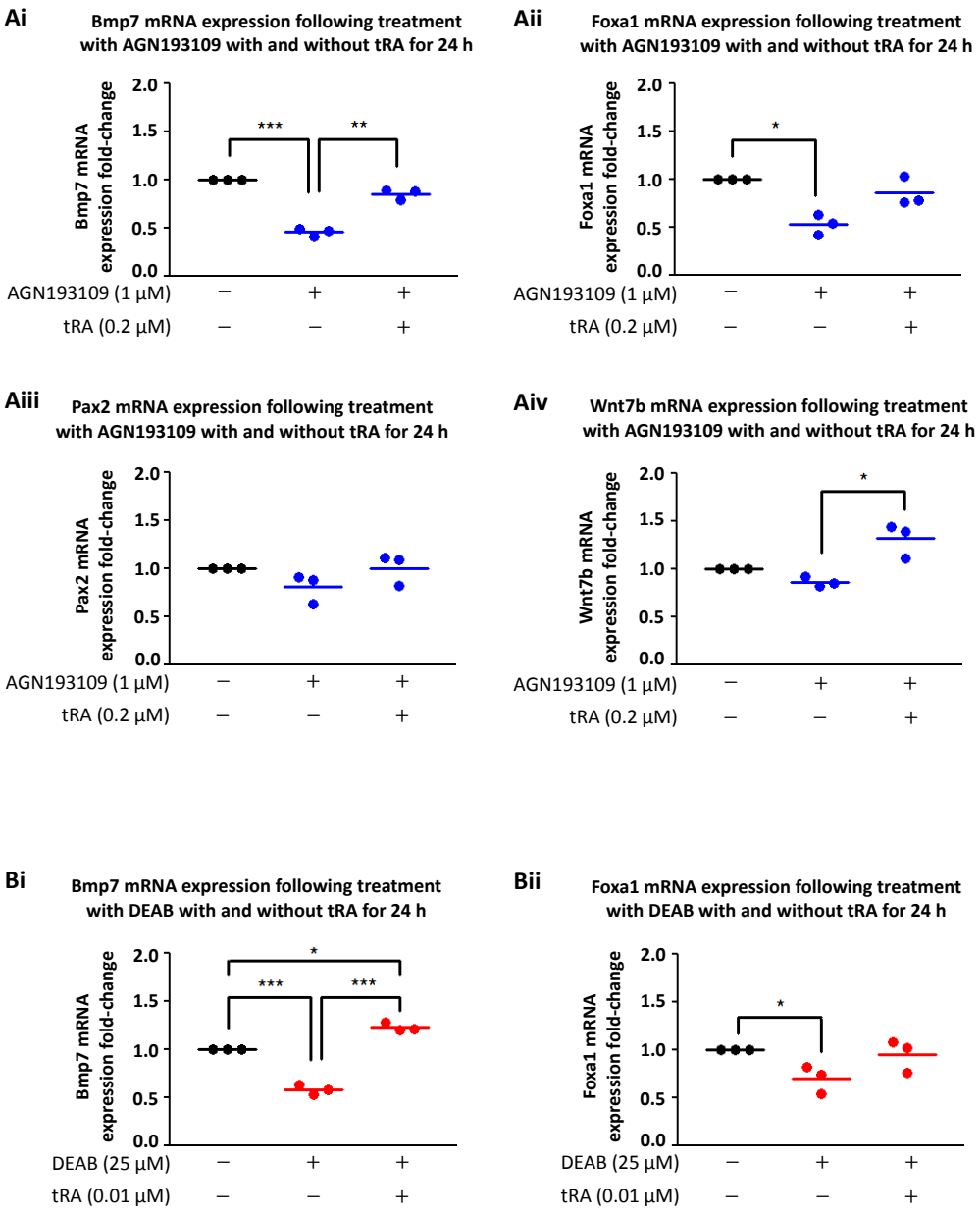


Figure 5.15: Regulation of Bmp7, Foxa1, Pax2, and Wnt7b genes by AGN193109 and DEAB with and without all-*trans* retinoic acid (tRA). mRNA expression of Bmp7 (**Ai**) and Foxa1 (**Aii**) was suppressed by AGN193109; the suppression was at least partially abolished in the presence of 0.2 $\mu$M tRA. **Aiii.** Pax2 mRNA expression was not regulated by the treatments. **Aiv.** Wnt7b mRNA expression was not suppressed by AGN193109 treatment but an induction beyond basal level was noted in the presence of 0.2 $\mu$M tRA. **Bi.** Bmp7 mRNA was suppressed by DEAB, and the suppression was reversed to a level higher than basal level in the presence of 0.01 $\mu$M tRA. **Bii.** Expression of Foxa1 mRNA was suppressed by DEAB, and the suppression was partially abolished in the presence of 0.01 $\mu$M tRA. Each dot represents mean values of three technical replicates from a single biological experiment. $*$, $**$, and $***$: $p<0.05$, $p<0.01$, and $p<0.001$, respectively.

### 5.3.2 Microarray experiment

***Candidate target genes***

A common criteria used in microarray experiment to select genes most significantly regulated by a given treatment is the q value, also known as false discovery rate threshold, of less than 0.05. When $q<0.05$ was used as a cut-off, neither Foxa1 nor Bmp7 made the shortlist although a statistically significant change was found in the pilot study, which was likely due to the low n number (n=3). Thus, instead of using $q<0.05$ as a cut-off, Foxa1 gene was selected as the cut-off threshold to generate a list of genes that were significantly regulated to an extent at least as great as that of Foxa1.

A multi-group comparison was performed using QOE software to detect differences between vehicle, AGN193109-only, and AGN193109+tRA groups in the first set of experiment, and between vehicle, DEAB-only, and DEAB+tRA groups in the second set of experiment. The total entries were first filtered by variance to eliminate the non-regulated genes using the in-built "Filter by variance" slider to the smallest possible q value for Foxa1 gene. The resulting q value was then used as a cut-off to shortlist candidate target genes. In the AGN193109 experiment, a variance of 0.098 was selected, which gave a q value of 0.623972 for Foxa1 gene; q value was thus set to 0.65 to select candidate target genes. In the DEAB experiment, a variance of 0.053 was selected, which gave a q value of 0.272681 for Foxa1 gene; q value was thus set to 0.30 to select candidate target genes. Original raw data of microarray experiment was deposited in NCBI's GEO and are accessible through GEO Series accession number GSE33955 (http://www.ncbi.nlm.nih.gov/geo/query/acc.cgi?acc=GSE33955).

A list of 403 and 439 unique genes was generated from AGN193109 experiment and DEAB experiment, respectively. As shown in Figure 5.16A, there were 133 overlapping genes, of which 125 genes fulfilled all the three criteria described in Section 5.1, i.e., (i) regulated by AGN193109 and the regulation was abolished or diminished in the presence of exogenous tRA, (ii) regulated by DEAB and the regulation was abolished

or diminished in the presence of exogenous tRA, (iii) the direction of regulation by AGN193109 and by DEAB was the same. Thus, the 125 genes were regarded as candidate targets of endogenous RA/RAR, and designated as group 1 genes. In addition to the group 1 genes, there were 213 genes that fulfilled only criteria (i), designated as group 2 genes, which were candidate genes regulated only by RARs but not by endogenous RA; 266 genes fulfilled only criteria (ii), designated group 3 genes, which were candidate genes regulated only by endogenous RA but independent of RARs.

Of note, group 1 genes appeared to be the minority when all shortlisted genes were overlapped directly (Figure 5.16A). However, when the genes were ranked by fold-changes and only the top 20 and top 10 most regulated genes were overlapped, the intersected genes became the majority (Figure 5.16B and Figure 5.16C).

The top 20 most down- and up-regulated genes within group 1 are listed in Table 5.3 and Table 5.4, respectively; top 10 most down- and up-regulated genes within group 2 are listed in Table 5.5; top 10 most down- and up-regulated genes within group 3 are listed in Table 5.6. The complete lists of intersected genes, genes regulated only by AGN193109, and genes regulated only by DEAB are in Supplementary Table 1, Supplementary Table 2, and Supplementary Table 3, respectively, in the DVD attached.

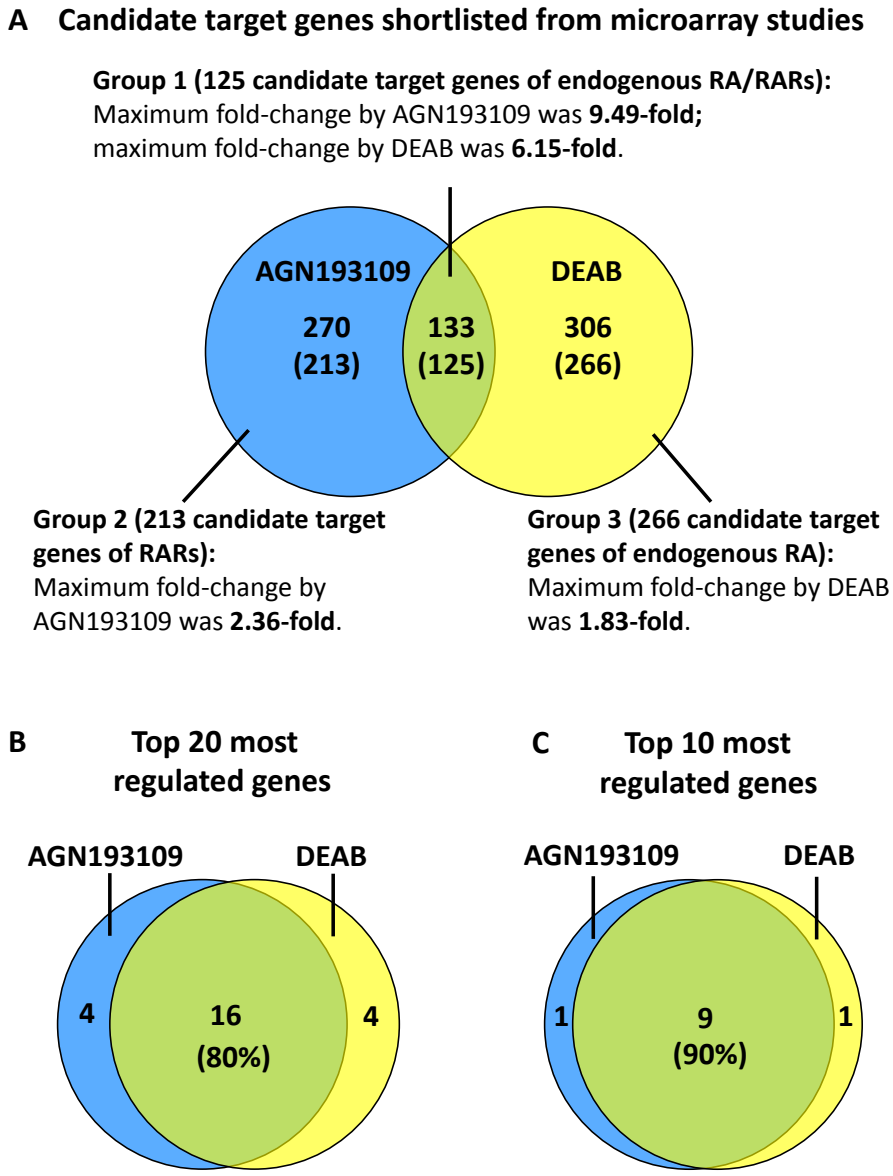


Figure 5.16: Candidate target genes shortlisted from microarray experiments. **A.** A total of 403 and 439 unique genes were shortlisted from AGN193109 experiment and DEAB experiment, respectively. There were 133 intersected genes, of which 125 genes, designated as group 1 genes, were regulated by AGN193109 and DEAB at similar directions, and their regulation was abolished or diminished in the simultaneous presence of exogenous tRA; 270 genes were regulated only by AGN193109, of which regulation of 213 genes, designated as group 2 genes, was abolished or diminished in the simultaneous presence of exogenous tRA; 306 genes were regulated only by DEAB, of which regulation of 266 genes, designated as group 3 genes, was abolished or diminished in the simultaneous presence of exogenous tRA. The fold-changes of group 1 genes were higher than those of group 2 and group 3 genes. When ranked based on fold-changes, 80% of the top 20 most regulated genes (**B**) and 90% of the top 10 most regulated genes were overlapped (**C**).

Table 5.3: Top 20 most down-regulated genes: candidate target genes of endogenous retinoic acid and retinoic acid receptors. Shown here are mean fold-changes of gene expression compared to vehicle control from three experimental groups. Genes were sorted by fold-changes of AGN193109 group compared to vehicle group.

| | Gene Symbol | AGN193109 | AGN193109+tRA | DEAB | DEAB+tRA | Entrez Gene |
|---|---|---|---|---|---|---|
| 1. | Ppbp | -9.49 | -1.53 | -6.15 | +1.85 | 57349 |
| 2. | Dhrs3 | -8.59 | -3.78 | -5.02 | +2.03 | 20148 |
| 3. | Sprr1a | -6.85 | -1.38 | -4.62 | +2.53 | 20753 |
| 4. | Cpm | -5.15 | -1.69 | -2.30 | +1.33 | 70574 |
| 5. | 9930023K05Rik | -4.36 | -1.59 | -2.35 | +1.60 | 226245 |
| 6. | Tns1 | -3.22 | -1.82 | -2.29 | +1.27 | 21961 |
| 7. | Itga2 | -3.22 | -1.16 | -2.56 | +1.25 | 16398 |
| 8. | Klhdc7a | -3.10 | -1.87 | -2.11 | +1.03 | 242721 |
| 9. | Csn3 | -2.91 | -1.91 | -2.18 | +1.18 | 12994 |
| 10. | Sorcs2 | -2.66 | -1.46 | -2.05 | +1.18 | 81840 |
| 11. | Ebf1 | -2.66 | -1.43 | -2.43 | +1.33 | 13591 |
| 12. | Lcn2 | -2.48 | -1.28 | -1.78 | +1.16 | 16819 |
| 13. | 2310007B03Rik | -2.31 | -1.58 | -1.42 | 1.00 | 71874 |
| 14. | Galns | -2.27 | -1.55 | -1.69 | +1.07 | 50917 |
| 15. | Npr3 | -2.21 | -1.03 | -1.99 | +1.52 | 18162 |
| 16. | Muc20 | -2.09 | -1.84 | -2.18 | +1.08 | 224116 |
| 17. | Clca4 | -2.07 | +1.31 | -1.78 | +1.94 | 229927 |
| 18. | Upk3b | -2.05 | -1.50 | -1.47 | +1.07 | 100647 |
| 19. | Slc37a1 | -2.00 | -1.33 | -1.53 | +1.16 | 224674 |
| 20. | Hrsp12 | -1.98 | -1.27 | -1.65 | +1.06 | 15473 |

Table 5.4: Top 20 most up-regulated genes within group 1: candidate target genes of endogenous retinoic acid and retinoic acid receptors. Shown here are mean fold-changes of gene expression compared to vehicle control from three experimental groups. Genes were sorted by fold-changes of AGN193109 compared to vehicle.

| | Gene Symbol | AGN193109 | AGN193109+tRA | DEAB | DEAB+tRA | Entrez Gene |
|---|---|---|---|---|---|---|
| 1. | Anxa8 | +1.73 | -1.10 | +1.43 | -1.54 | 11752 |
| 2. | Ptgs2 | +1.67 | +1.48 | +1.24 | -1.23 | 19225 |
| 3. | Gsdma | +1.61 | -1.01 | +1.39 | -1.33 | 57911 |
| 4. | Cpeb2 | +1.57 | +1.18 | +1.24 | -1.15 | 231207 |
| 5. | Ahnak2 | +1.57 | -1.11 | +1.42 | -1.42 | 100041194 |
| 6. | Casp14 | +1.56 | -1.11 | +1.16 | -1.31 | 12365 |
| 7. | Peg10 | +1.52 | +1.21 | +1.35 | -1.16 | 170676 |
| 8. | Rnf39 | +1.45 | +1.11 | +1.18 | -1.19 | 386454 |
| 9. | Pkp1 | +1.40 | +1.11 | +1.25 | -1.20 | 18772 |
| 10. | Alcam | +1.39 | 1.00 | +1.36 | -1.05 | 11658 |
| 11. | Timp3 | +1.39 | -1.03 | +1.12 | -1.15 | 21859 |
| 12. | Adora1 | +1.38 | +1.15 | +1.27 | -1.08 | 11539 |
| 13. | Car5b | +1.36 | +1.03 | +1.13 | -1.28 | 56078 |
| 14. | Atp6v0a4 /// D630045J12Rik | +1.34 | +1.11 | +1.21 | -1.23 | 140494 /// 330286 |
| 15. | Egr1 | +1.33 | +1.24 | +1.07 | -1.02 | 13653 |
| 16. | Ly6c1 /// Ly6c2 | +1.31 | -1.01 | +1.14 | -1.20 | 17067 /// 100041546 |
| 17. | Cav1 | +1.30 | +1.02 | +1.20 | -1.11 | 12389 |
| 18. | Lama3 | +1.28 | -1.02 | +1.04 | -1.21 | 16774 |
| 19. | Lmna | +1.26 | -1.02 | +1.17 | -1.17 | 16905 |
| 20. | Plxna2 | +1.26 | +1.04 | +1.15 | -1.13 | 18845 |

Table 5.5: Top 10 most up- and down-regulated genes within group 2: candidate target genes of retinoic acid receptors. Shown here are mean fold-changes of gene expression compared to vehicle control from three experimental groups. Genes were sorted by fold-changes of AGN193109 group compared to vehicle group.

| | Gene Symbol | AGN193109 | AGN193109+tRA | Entrez Gene |
|---|---|---|---|---|
| **(I) Top 10 most down-regulated genes** | | | | |
| 1. | G930009F23Rik | -1.83 | -1.30 | 100038726 |
| 2. | Psca | -1.82 | -1.19 | 72373 |
| 3. | Sgpp2 | -1.81 | -1.36 | 433323 |
| 4. | Ly6g | -1.76 | -1.36 | 546644 |
| 5. | Lbp | -1.71 | -1.41 | 16803 |
| 6. | Gpr124 | -1.71 | -1.22 | 78560 |
| 7. | Gm12185 /// Tgtp1 /// Tgtp2 | -1.66 | -1.51 | 620913 /// 21822 /// 100039796 |
| 8. | Mknk2 | -1.63 | -1.49 | 17347 |
| 9. | Alkbh7 | -1.51 | -1.40 | 66400 |
| 10. | Synpo | -1.51 | -1.35 | 104027 |
| **(II) Top 10 most up-regulated genes** | | | | |
| 1. | Areg | +2.36 | +1.28 | 11839 |
| 2. | 1810011O10Rik | +2.07 | +1.58 | 69068 |
| 3. | Etv1 | +1.76 | +1.19 | 14009 |
| 4. | Akr1c19 | +1.73 | -1.36 | 432720 |
| 5. | Spry4 | +1.62 | +1.33 | 24066 |
| 6. | Nr4a1 | +1.60 | +1.27 | 15370 |
| 7. | Etv1 /// Gm5454 | +1.54 | +1.23 | 14009 /// 432800 |
| 8. | Pvr | +1.52 | +1.16 | 52118 |
| 9. | Ankrd22 | +1.50 | +1.01 | 52024 |
| 10. | Dusp6 | +1.46 | +1.26 | 67603 |

Table 5.6: Top 10 most regulated up- and down-genes within group 3: candidate target genes of endogenous retinoic acid. Shown here are mean fold-changes of gene expression compared to vehicle control from three experimental groups. Genes were sorted by fold-changes of DEAB group compared to vehicle group.

| | Gene Symbol | DEAB | DEAB+tRA | Entrez Gene |
|---|---|---|---|---|
| **(I) Top 10 most down-regulated genes** | | | | |
| 1. | Slc16a12 | -1.83 | +1.17 | 240638 |
| 2. | Gabrp | -1.65 | +1.61 | 216643 |
| 3. | Gm8393 | -1.64 | -1.57 | 666972 |
| 4. | Cp | -1.54 | +1.22 | 12870 |
| 5. | 1700011H14Rik | -1.49 | -1.08 | 67082 |
| 6. | Dcdc2a | -1.46 | +1.24 | 195208 |
| 7. | Gstm6 | -1.46 | +1.30 | 14867 |
| 8. | Ifi205 | -1.45 | -1.06 | 226695 |
| 9. | Cpne8 | -1.43 | +1.11 | 66871 |
| 10. | Cxcl10 | -1.43 | +1.02 | 15945 |
| **(II) Top 10 most up-regulated genes** | | | | |
| 1. | Fgfbp1 | +1.48 | -1.32 | 14181 |
| 2. | Gper | +1.45 | -1.22 | 76854 |
| 3. | Ahnak2 | +1.36 | -1.23 | 100041194 |
| 4. | Serpinb5 | +1.32 | -1.60 | 20724 |
| 5. | Mir687 | +1.29 | +1.05 | 751541 |
| 6. | Ramp3 | +1.28 | -1.17 | 56089 |
| 7. | Ctsw | +1.28 | -1.39 | 13041 |
| 8. | Emp1 | +1.25 | -1.04 | 13730 |
| 9. | Klra5 | +1.25 | -1.06 | 16636 |
| 10. | Pdk4 | +1.24 | -1.26 | 27273 |

***Group 1 genes: candidate targets of endogenous RA/RAR***

The number and fold-changes of all group 1 genes are summarised in Figure 5.17. The total number of genes suppressed by both AGN193109 and DEAB were about 3-fold more than those induced by both AGN193109 and DEAB. Of note, there were 19 and 12 genes suppressed by AGN193109 and DEAB by 2-fold or more, respectively, but none were induced by 2-fold or more. It was also noted that AGN193109 had a greater impact on regulation of these genes compared to DEAB.

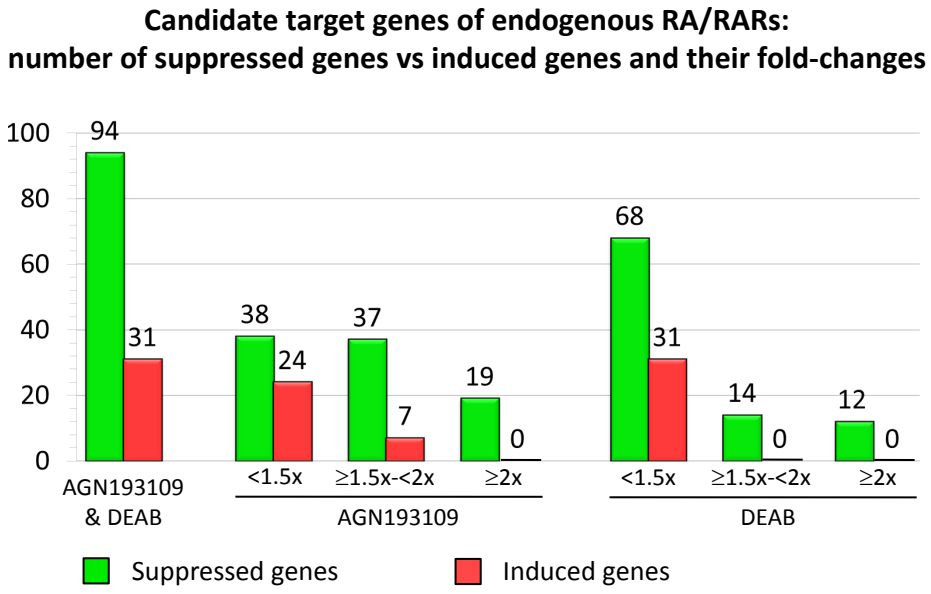


Figure 5.17: Number of candidate target genes of endogenous retinoic acid and retinoic acid receptors and their fold-changes. A total of 94 and 31 genes were down- and up-regulated, respectively, by both AGN193109 and DEAB; regulation of these genes were at least partially abolished in the presence of tRA. Of the 94 down-regulated genes, 38 were down-regulated by AGN193109 by less than 1.5-fold, 37 by more than 1.5-fold but less than 2-fold, and 19 by 2-fold and more; 68 were down-regulated by DEAB by less than 1.5-fold, 14 by more than 1.5-fold but less than 2-fold, and 12 by 2-fold and more. Of the 31 up-regulated genes, 24 were up-regulated by AGN193109 by less than 1.5-fold, 7 by more than 1.5-fold but less than 2-fold, and none by 2-fold and more; none of the genes were up-regulated by DEAB by 1.5-fold and more.

### 5.3.3 Validation of candidate target genes of endogenous RA/RAR

Fold-changes of the no. 20 gene on the top 20 most down-regulated genes (Table 5.3), i.e., Hrsp12 (-1.98-fold by AGN193109 and -1.65-fold by DEAB), are higher than those of the no. 1 gene on the top 20 most up-regulated genes (Table 5.4), i.e., Anxa8 (+1.73-fold by AGN193109 and +1.43-fold by DEAB). Thus, validation of gene expression was focused on the top 20 most down-regulated genes. Five other genes of interest within the down-regulated gene list, which were regulated by at least 1.45-fold by AGN193109, i.e., Tgm2 (-1.97-fold), Tinag (-1.73-fold), Foxj1 (-1.68-fold), Tinagl1 (-1.53-fold), and Dusp1 (-1.45-fold), were also examined.

Results of validation are summarised in Table 5.7 and graphs of fold-changes for individual gene are shown in Appendix B.2. Among the 25 genes examined, Csn3 gene was not amplified. Of the remaining 24 genes, all were significantly down-regulated by AGN193109; suppression of all genes, except Muc20, was at least partially abolished in the simultaneous presence of exogenous tRA. In cells treated with DEAB, all genes were significantly down-regulated, which the regulation was abolished in the simultaneous presence of tRA; suppression of Dusp1 was not statistically significant. Thus, while Csn3, Muc20, and Dusp1 genes required further examination, the remaining 22 genes along with Bmp7 and Foxa1 examined in the pilot study were confirmed as target genes of endogenous RA/RAR. Hence, subsequent analysis was focused on these 24 validated target genes of endogenous RA/RAR.

Table 5.7: Validation of top 20 candidate target genes of endogenous retinoic acid and retinoic acid receptors and five other genes of interest. Shown here are geometric means of fold-change compared to vehicle control and 95% confidence interval in parenthesis. $^{*}$: p<0.05 vs vehicle, $^{**}$: p<0.01 vs vehicle, and $^{***}$: p<0.001 vs vehicle; ^: p<0.05 vs AGN193109, ^^: p<0.01 vs AGN193109, and ^^^: p<0.001 vs AGN193109; $^{+}$: p<0.05 vs DEAB, $^{++}$: p<0.01 vs DEAB, and $^{+++}$: p<0.001 vs DEAB; NA: Not amplified.

| | Gene Symbol | AGN193109 | AGN193109+tRA | DEAB | DEAB+tRA |
|---|---|---|---|---|---|
| **(I) Top 20 most down-regulated genes** | | | | | |
| 1. | Dhrs3 | 0.01 (0.00-0.02) *** | 0.12 (0.05-0.29) ^^^ ** | 0.04 (0.02-0.07) *** | 2.81 (1.53-5.15) +++ ** |
| 2. | Sprr1a | 0.05 (0.02-0.10) *** | 0.60 (0.29-1.25) ^^^ | 0.15 (0.10-0.21) *** | 4.07 (2.80-5.93) +++ *** |
| 3. | Ppbp | 0.07 (0.05-0.09) *** | 0.73 (0.54-0.99) ^^^ * | 0.13 (0.10-0.17) *** | 2.55 (1.96-3.32) +++ *** |
| 4. | 9930023K05Rik | 0.12 (0.10-0.14) *** | 0.63 (0.53-0.75) ^^^ ** | 0.28 (0.18-0.42) *** | 2.05 (1.34-3.14) +++ ** |
| 5. | Cpm | 0.13 (0.07-0.20) *** | 0.47 (0.29-0.75) ^^ * | 0.31 (0.24-0.38) *** | 1.46 (1.17-1.83) +++ ** |
| 6. | Tns1 | 0.13 (0.06-0.27) ** | 0.36 (0.17-0.75) ^ * | 0.31 (0.24-0.41) *** | 1.52 (0.87-2.00) +++ * |
| 7. | Lcn2 | 0.17 (0.14-0.22) *** | 0.70 (0.55-0.87) ^^^ * | 0.26 (0.20-0.35) *** | 1.52 (1.15-1.99) +++ * |
| 8. | Itga2 | 0.19 (0.09-0.37) ** | 0.87 (0.43-1.75) ^^ | 0.27 (0.21-0.34) *** | 1.43 (1.14-1.81) +++ * |
| 9. | Npr3 | 0.20 (0.11-0.38) ** | 0.89 (0.48-1.60) ^^ | 0.34 (0.24-0.49) ** | 2.08 (1.45-2.99) +++ *** |
| 10. | Klhdc7a | 0.21 (0.11-0.38) ** | 0.42 (0.22-0.77) ^ * | 0.34 (0.24-0.47) *** | 1.27 (0.91-1.76) +++ |
| 11. | Sorcs2 | 0.23 (0.10-0.55) ** | 0.67 (0.29-1.59) ^ | 0.34 (0.25-0.46) *** | 1.33 (0.98-1.80) +++ |

| | Gene Symbol | AGN193109 | AGN193109+tRA | DEAB | DEAB+tRA |
|---|---|---|---|---|---|
| 12. | Clca4 | 0.24 (0.15-0.38) *** | 1.58 (0.97-2.54) ^^^ | 0.51 (0.37-0.70) ** | 2.58 (1.87-3.55) +++ ** |
| 13. | 2310007B03Rik | 0.24 (0.18-0.32) *** | 0.53 (0.40-0.70) ^^ ** | 0.59 (0.46-0.75) ** | 1.12 (0.88-1.42) ++ |
| 14. | Muc20 | 0.30 (0.20-0.45) *** | 0.39 (0.26-0.58) ** | 0.35 (0.22-0.58) ** | 1.20 (0.74-1.96) ++ |
| 15. | Upk3b | 0.35 (0.33-0.37) *** | 0.65 (0.62-0.69) ^^^ *** | 0.58 (0.53-0.62) *** | 1.15 (1.06-1.25) +++ ** |
| 16. | Galns | 0.36 (0.30-0.44) *** | 0.64 (0.52-0.76) ^^ ** | 0.48 (0.36-0.64) ** | 1.25 (0.94-1.66) +++ |
| 17. | Slc37a1 | 0.38 (0.21-0.69) ** | 0.75 (0.41-1.38) ^ | 0.61 (0.54-0.70) *** | 1.29 (1.14-1.48) +++ ** |
| 18. | Ebf1 | 0.43 (0.27-0.70) ** | 0.80 (0.49-1.29) ^ | 0.54 (0.42-0.68) ** | 1.54 (1.21-1.94) +++ ** |
| 19. | Hrsp12 | 0.51 (0.40-0.65) ** | 0.79 (0.62-1.01) ^^ | 0.56 (0.46-0.69) ** | 1.18 (0.97-1.44) +++ |
| 20. | Csn3 | NA | NA | NA | NA |
| **(II) Other genes of interest** | | | | | |
| 1. | Tgm2 | 0.35 (0.18-0.68) * | 0.64 (0.33-1.23) | 0.56 (0.45-0.70) ** | 1.19 (0.96-1.50) +++ |
| 2. | Tinag | 0.38 (0.29-0.50) *** | 0.74 (0.57-0.97) ^^ * | 0.61 (0.52-0.71) *** | 1.31 (1.13-1.52) +++ ** |
| 3. | Foxj1 | 0.38 (0.23-0.62) ** | 0.65 (0.40-1.05) ^ | 0.65 (0.56-0.76) ** | 1.21 (1.04-1.40) +++ * |
| 4. | Tinagl1 | 0.45 (0.36-0.56) *** | 0.77 (0.62-0.96) ^^ * | 0.68 (0.60-0.77) *** | 1.26 (1.12-1.43) +++ ** |
| 5. | Dusp1 | 0.46 (0.31-0.68) ** | 0.99 (0.67-1.46) ^^ | 0.68 (0.44-1.04) | 1.58 (1.02-2.42) ++ * |

It was noted that in the presence of DEAB, some of the genes were significantly induced by tRA beyond basal level such as Sprr1a and Drhs3, whereas others such as Hrsp12 and 2310007B03Rik were only marginally induced beyond basal level. In order to determine whether these difference was associated with presence of RARE, a search was performed on the DR5 RARE database of mouse whole genome, based on the (A/G)G(G/T)T(C/G)A motif, published by Lalevee et al. [159]. Based on this database, presence of DR5 RARE in the 24 validated target genes of endogenous RA/RAR is summarised in Table 5.8, at (i) whole gene level and (ii) within 10 kb from transcription start site or from gene end.

While all the 24 genes were validated as target genes of endogenous RA/RAR, not all genes contain DR5 RARE. Among the 17 genes that were significantly down-regulated by DEAB and induced beyond basal level in the simultaneous presence of tRA, 11 contain at least one DR5 RARE at the whole gene level, of which 10 have one DR5 RARE within 10 kb from transcription start site or from gene end. Among the 7 genes that were significantly down-regulated by DEAB but was not induced beyond basal level, five contain at least one DR5 RARE at the whole gene level, of which three have one DR5 RARE within 10 kb from transcription start site or from gene end.

Thus, the presence of DR5 RARE was not the sole indicator of whether the target genes would be induced beyond basal level. In addition, a direct correlation between the presence of DR5 RARE and the magnitude of regulation was lacking. For example, whereas Foxa1 gene contains two DR5 RARE, one of which are within 10 kb from transcription start site/gene ends, it was not significantly induced beyond basal level. On the other hand, Clca4 were significantly induced by more than 2-fold although DR5 RARE was not found in this gene.

Table 5.8: Presence of direct-repeat 5 (DR5) retinoic acid response element (RARE) in validated genes. Genes were sorted by fold-changes, from high to low, of DEAB+tRA compared to vehicle. ^: Geometric means of fold-change compared to vehicle control and 95% confidence interval in parenthesis; §: ±10 kb from transcription start site or from gene end; *: p<0.05 vs vehicle, **: p<0.01 vs vehicle, and ***: p<0.001 vs vehicle.

| | Gene Symbol | DEAB+tRA^ | DR5 RARE (whole gene) | DR5 RARE (±10 kb)§ |
|---|---|---|---|---|
| **(I) Down-regulated genes significantly induced beyond basal level by tRA** | | | | |
| 1. | Sprr1a | 4.07 (2.80-5.93) *** | 1 | 1 |
| 2. | Dhrs3 | 2.81 (1.53-5.15) ** | 6 | 1 |
| 3. | Clca4 | 2.58 (1.87-3.55) ** | 0 | 0 |
| 4. | Ppbp | 2.55 (1.96-3.32) *** | 1 | 1 |
| 5. | Npr3 | 2.08 (1.45-2.99) *** | 3 | 1 |
| 6. | 9930023K05Rik | 2.05 (1.34-3.14) ** | 1 | 1 |
| 7. | Ebf1 | 1.54 (1.21-1.94) ** | 9 | 1 |
| 8. | Lcn2 | 1.52 (1.15-1.99) * | 0 | 0 |
| 9. | Tns1 | 1.52 (0.87-2.00) * | 0 | 0 |
| 10. | Cpm | 1.46 (1.17-1.83) ** | 0 | 0 |
| 11. | Itga2 | 1.43 (1.14-1.81) * | 2 | 1 |
| 12. | Tinag | 1.31 (1.13-1.52) ** | 1 | 0 |
| 13. | Slc37a1 | 1.29 (1.14-1.48) ** | 0 | 0 |
| 14. | Tinagl1 | 1.26 (1.12-1.43) ** | 1 | 1 |
| 15. | Bmp7 | 1.23 (1.08-1.41) * | 4 | 1 |
| 16. | Foxj1 | 1.21 (1.04-1.40) * | 0 | 0 |
| 17. | Upk3b | 1.15 (1.06-1.25) ** | 1 | 1 |
| **(II) Down-regulated genes not significantly induced beyond basal level by tRA** | | | | |
| 1. | Sorcs2 | 1.33 (0.98-1.80) | 11 | 0 |
| 2. | Klhdc7a | 1.27 (0.91-1.76) | 1 | 0 |
| 3. | Galns | 1.25 (0.94-1.66 | 1 | 1 |
| 4. | Tgm2 | 1.19 (0.96-1.50) | 1 | 1 |
| 5. | Hrsp12 | 1.18 (0.97-1.44) | 0 | 0 |
| 6. | 2310007B03Rik | 1.12 (0.88-1.42) | 0 | 0 |
| 7. | Foxa1 | 0.95 (0.66-1.35) | 2 | 1 |

***Gene ontology analysis and transcriptomic database comparison***

Except for a few genes with unknown functions, namely, 9930023K05Rik, Klhdc7a, Sorcs2, and 2310007B03Rik, the validated genes are associated with a broad spectrum of biological processes and molecular functions. The complete list of gene ontologies (last accessed on February 2012) is shown in Supplementary Table 4, saved in the DVD attached.

A search through GEO databases for the expression of the validated genes was performed in order to confirm their presence in native kidney ureteric bud/collecting duct cells. Two GEO series were deemed highly relevant to mIMCD-3 cells: (i) E11.5 mouse ureteric buds and E15.5 mouse medullary collecting duct cells (GEO accession: GSE6290), contributed by GUDMAP (http://www.gudmap.org/) and (ii) inner medullary collecting duct cells derived from 6- and 10-week-old rat kidney (GEO accession: GSE7891), contributed by Uawithya et al. [305]. Transcriptomic profiling of inner medullary collecting duct cells derived from adult mouse kidney was not available on GEO for comparison. There were three biological replicates in each of the database, and a gene is considered present if at least two out of three of the replicates had a "present" call, in at least one probe set. A summary of gene ontologies and GEO database comparison is shown in Table 5.9.

In addition to the RIKEN genes, i.e., 9930023K05Rik and 2310007B03Rik, which are specific only to mouse, four other validated genes, i.e., Itga2, Klhdc7a, Upk3b, and Galns, are also absent from the rat inner medullary collecting duct cell transcriptomic profile. This is due to the fact that the probes on the rat array (Affymetrix® Rat Genome 230 2.0 array) were designed based on the public databases, Unigene and Baylor College of Medicine Human Genome, built in 2002, whereas these genes were only added to the databases after 2003 (personal communication with Affymetrix Application Support Specialist, Ms. K Danielski). Therefore, the expression of these genes in native inner medullary collecting duct cells are undetermined at present.

Table 5.9: Summary of gene ontologies and GEO database comparison. E11.5 UB: embryonic day 11.5 ureteric bud cells from mice (three samples), E15.5 mCD: embryonic day 15.5 medullary collecting duct cells from mice (three samples), rat IMCD: inner medullary collecting duct cells from rat (one sample from 6-week-old and two samples from 10-week-old). +: present, -: absent, ud: undetermined; ˆ: present in 6-week-old sample but absent from 10-week-old sample. Gene ontologies A: retinol metabolism, B: cell-cell, -substrate interaction, C: ureteric bud branching, D: immune/inflammation, E: oxidative stress, F: repair/regeneration, G: ion/solute/water transport and metabolism, H: gene transcription/translation; pink: GeneGO Metacore, yellow: DAVID, green: both GeneGO Metacore and DAVID, blue: additional literature reviews.

| Genes | Native samples | | | Gene ontologies | | | | | | | |
|---|---|---|---|---|---|---|---|---|---|---|---|
| | E11.5 UB | E15.5 mCD | rat IMCD | A | B | C | D | E | F | G | H |
| 1. Dhrs3 | + | + | + | | | | | | | | |
| 2. Sprr1a | + | + | + | | | | | | | | |
| 3. Ppbp | + | + | - | | | | | | | | |
| 4. 9930023K05Rik | - | - | ud | | | | | | | | |
| 5. Cpm | + | + | + | | | | | | | | |
| 6. Tns1 | + | + | + | | | | | | | | |
| 7. Lcn2 | - | - | + | | | | | | | | |
| 8. Itga2 | - | - | ud | | | | | | | | |
| 9. Npr3 | - | + | - | | | | | | | | |
| 10. Klhdc7a | - | + | ud | | | | | | | | |
| 11. Sorcs2 | - | + | + | | | | | | | | |
| 12. Clca4 | - | - | + | | | | | | | | |
| 13. 2310007B03Rik | - | - | ud | | | | | | | | |
| 14. Upk3b | - | + | ud | | | | | | | | |
| 15. Galns | + | + | ud | | | | | | | | |
| 16. Slc37a1 | + | - | + | | | | | | | | |
| 17. Ebf1 | - | + | + | | | | | | | | |
| 18. Hrsp12 | + | + | + | | | | | | | | |
| 19. Tgm2 | + | + | + | | | | | | | | |
| 20. Tinag | + | + | - | | | | | | | | |
| 21. Foxj1 | - | - | - | | | | | | | | |
| 22. Tinagl1 | + | + | + | | | | | | | | |
| 23. Bmp7 | + | + | + | | | | | | | | |
| 24. Foxa1 | - | + | +/-ˆ | | | | | | | | |

## 5.4 Discussions

### 5.4.1 Canonical signalling of retinoids and its candidate target genes

By using two inhibitors that block endogenous RA/RAR signalling at different stages, and by adding exogenous tRA simultaneously to the inhibitors to confirm their specificity of regulation, candidate target genes of endogenous RA/RAR were identified (group 1 genes, Supplementary Table 1). Among the validated genes, some were reported, in original publication or review paper, to be regulated by RA, i.e., Dhrs3 (up-regulated) [40, 78], Sprr1a (down-regulated) [90, 299], Cpm (down-regulated) [153], Itga2 (up-regulated) [87], Ebf1 (up-regulated) [44], Lcn2 (up-regulated) [225], Tgm2 (up-regulated) [12], Bmp7 (up-regulated) [243], and Foxa1 (up-regulated) [12]. Of these known target genes, Ebf1 was induced during or after cell differentiation when RA was added, hence may or may not be a direct target gene of RA. The remaining genes within the group 1 list, i.e., Ppbp, 9930023K05Rik, Tns1, Klhdc7a, Sorcs2, 2310007B03Rik, Galns, Npr3, Clca4, Upk3b, Slc37a1, Hrsp12, Tinag, Foxj1, and Tinagl1 were not reported to be regulated by RA yet. Thus, these genes represent novel target genes of RA/RAR identified in this project.

In addition to the group 1 genes, two additional groups of genes were unveiled, i.e., genes that were regulated only by RARs (group 2 genes, Supplementary Table 2) and genes that were regulated only by endogenous RA (group 3 genes, Supplementary Table 3) (Figure 5.18). The group 2 genes were likely regulated by unliganded RARs or by RARs activated by ligands other than endogenous RA hence perturbation of RAR-mediated signalling by AGN193109 led to a change in gene expression; in the simultaneous presence of exogenous tRA, occupation of RARs by AGN193109 were relieved hence the effect of AGN193109 were abolished or diminished. Group 3 genes were likely regulated by endogenous RA but not via RAR-mediated pathways.

Taken together, the constitutively active RAR-dependent endogenous RA activity observed in mIMCD-3 cells shown in Chapter 4 is indeed playing a role in regulating

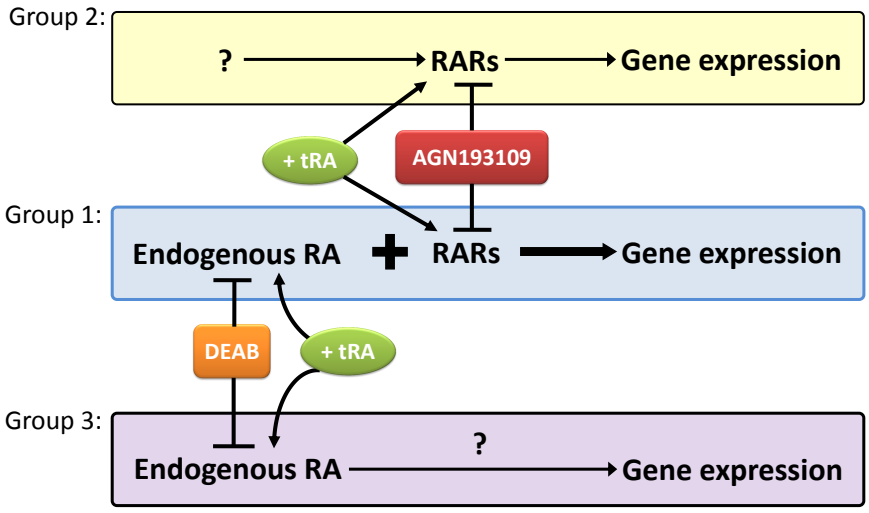


Figure 5.18: Regulation of gene expression by endogenous retinoic acid (RA) and retinoic acid receptors (RARs). While the primary aim was to identify target genes of endogenous RA/RAR as shown in Figure 5.1, three main groups of candidate target genes were identified from microarray studies. Group 1 genes were candidate target genes of endogenous RA/RAR, which their expression was regulated by both AGN193109 and DEAB at similar directions, and the regulation was abolished or diminished in the simultaneous presence of exogenous tRA (blue box); group 2 genes were candidate target genes of RARs, which their expression was not dependent on endogenous RA (yellow box); group 3 genes were candidate target genes of endogenous RA, which their expression was not dependent on RARs (purple box).

transcription of group 1 genes. At the same time, the retinoid system in mIMCD-3 cells is also regulating transcription of group 2 and group 3 genes via non-canonical signalling mechanisms. More importantly, although the number of genes within group 1 were not as many as those within groups 2 and 3, it was clear that the most regulated genes, in terms of their fold-changes, largely fall into the group 1 genes, i.e., regulated by both endogenous RA and RARs (Figure 5.16). This suggests that the canonical signalling activity is more dominant in regulating gene expression. In addition, the most regulated genes were being down-regulated rather than up-regulated (Figure 5.17), suggesting that endogenous RA/RAR signalling plays a primary role as "inducer" to support gene expression rather than as "suppressor" to inhibit gene expression in mIMCD-3 cells.

### 5.4.2 Validation of microarray results

Among the 25 genes selected for RT-qPCR examination, all except Csn3, Muc20, and Dusp1, were validated as target genes of endogenous RA/RAR (Table 5.7). Csn3 gene

was not amplified, perhaps due to the discrepancy between 3'-biased method using oligo-d(T) primers for reverse transcription for qPCR as opposed to the whole-gene cDNA synthesis using random primers in microarray experiment. Muc20 was suppressed by AGN193109 but the suppression was not relieved in the simultaneous presence of exogenous tRA perhaps due to the relatively low tRA dose used (0.2 $\mu$M), which might not be sufficient to compete with AGN193109 for RARs. Dusp1 was significantly suppressed only by AGN193109 but not by DEAB, which might either be due to suboptimal DEAB dose or an insufficient treatment time to deplete the cells of endogenous RA.

The detailed molecular mechanisms involved in regulation of the validated genes by endogenous RA/RAR in not known. Although the presence of DR5 RARE in some of the validated genes might be a potential mechanism, their actual participation remains to be further established. The presence of other yet identified RARE such as the DR1 and DR2 RARE, as well as the possibility of endogenous RA/RAR in modulating stability of gene transcripts might also contributes towards gene expression.

### 5.4.3 Top three most down-regulated genes: Dhrs3, Sprr1a, and Ppbp

***Dhrs3 in retinoid metabolism***

Dhrs3 gene encodes short-chain dehydrogenase/reductase 3 protein, which was first reported in the photoreceptor cells and plays a role in the visual cycle [117]. Dhrs3a, the Dhrs3 ortholog in zebrafish, was reported to constitute a negative feedback mechanism in response to endogenous and exogenous tRA by reducing tRal to tRol in order to restrict tRA biosynthesis [78]. In mIMCD-3 cells, AGN193109 and DEAB treatments resulted in a profound suppression of Dhrs3 mRNA, suggesting that Dhrs3 gene is highly dependent on endogenous RA/RAR. If the negative feedback mechanism of Dhrs3a reported in zebrafish [78] was also true in mIMCD-3 cells, then the marked suppression of Dhrs3 mRNA following perturbation of endogenous RA/RAR signalling might be a mean to increase the availability of tRal and hence tRA biosynthesis, in order to restore tRA level.

Recently, Dhrs3 mouse null mutants have been developed (www.mmrrc.org/catalog/

sds.php?mmrrc_id=32267). It was found that while heterozygotic knockout mutants are viable and fertile, homozygotic knockout leads to pre- and post-natal lethality but the cause of lethality was not described. A detailed investigation on the retinoid profile and the kidney phenotype in Dhrs3 null mutants, e.g., whether there is a higher level of endogenous tRA and presence of RA toxicity, should further complement the existing knowledge on retinoid metabolism in the kidney.

***Sprr1a in collecting duct cell preservation and regeneration***

Sprr1a gene encodes small proline-rich protein 1a, also known as cornifin-A. It is well-known to be expressed in squamous tissues and was associated with tissue keratinisation [299]. However, recent publications had reported its expression and its novel functions in non-keratinising tissues. Specifically, in adult mouse neurons, Sprr1a was found to be dramatically induced in dorsal root ganglions during the regeneration stage after axotomy, and its expression promoted axonal outgrowth in both embryonic and adult neurons culture *in vitro* [29, 287]; in rodent's myocardium, Sprr1a was massively induced in response to biomechanical- and ischemia-induced stress, and its overexpression was found to protect cardiomyocytes from ischemia-induced injury both *in vitro* and *in vivo* [252]; in bleomycin-induced lung fibrosis, carbon monoxide was reported to suppress $\alpha$-smooth muscle actin expression in lung fibroblast, a marker of emerging myofibroblast responsible for excessive generation of extra-cellular matrix, and Sprr1a was proposed to be the key mediator in modulating this effect [340].

In all aforementioned studies, expression of Sprr1a gene was found to be minimum, if any, in healthy or sham-control samples, but was consistently and dramatically up-regulated during the regenerative or repair phases of injuries [29,252,287,340]. The low basal expression of this gene in non-squamous tissues might have lead to its potential roles in repair and regeneration being overlooked in the past. Thus, it is tempting to speculate that Sprr1a might serve as an endogenous defence molecule to protect kidney collecting ducts from damage and to facilitate repair processes during acquired injury.

A higher level of Sprr1a transcript was detected following vitamin A deficiency, which was correlated to squamous metaplasia [299]. On the contrary, disruption of endogenous RA signalling in mIMCD-3 cells had lead to a marked decrease in Sprr1a expression in this study. It is not known whether this discrepancy is due to a cell type-specific activity of RA. Given that embryonic stem cells of Sprr1a knockout are now commercially available (http://www.knockoutmouse.org/martsearch/project/102753), physiological and pathological functions of Sprr1a should be better elucidated soon.

***Ppbp in kidney development and immune/inflammatory response***

Ppbp encodes platelet basic protein that is subjected to a series of N-terminal truncation yielding connective tissue-activating peptide, $\beta$-thromboglobulin, and finally neutrophil-activating peptide 2 that is also known as Cxcl7 [34]. Among these peptides, Cxcl7 is the most potent, acting on a number of target cells, such as neutrophils, mast cells, basophils, and lymphocytes to mediate immune and inflammatory responses, as well as on fibroblasts to stimulate matrix component synthesis and glucose transport [34].

Novel actions of Cxcl7 in mediating kidney development, mediated through its putative receptor, Cxcr2, was recently reported. By performing genomic profiling on metanephric mesenchyme explant stimulated with Cxcl7, Levashova et al. reported an up-regulation of genes associated with angiogenesis and survival, as well as endothelial and mesangial cell marker, with functional evidence of increased tissue invasion; inhibition of Cxcr2 receptor in metanephric mesenchyme explant with chemical reagent led to a reduction in nephron formation, as well as in ureteric bud branching that was deemed a secondary effect following a diminution of metanephric mesenchyme-derived factors [172]. If Cxcl7 is indeed the final product of Ppbp gene in collecting duct cells and in ureteric bud cells, it might represent a novel molecule regulated by endogenous RA in modulation of kidney development.

Emerging publications are pointing towards essential roles of Cxcr2 receptor as an innate defence molecule against bacterial infection in the course of acute pyelonephritis. In experimental urinary tract infection, genetic deletion of Cxcr2 in mice resulted in a delay in neutrophil recruitment, neutrophil retention, prolonged kidney inflammation, epithelial proliferation, and kidney fibrosis [292, 293]. However, whether or not the roles of Cxcr2 reported in the aforementioned studies were mediated by Cxcl7 remains to be further established. In addition, since Ppbp transcript was only detected in the developing ureteric bud cells and medullary collecting duct cells but not in adult rat IMCD cells (Table 5.9), it might be playing a more dominant role during embryonic kidney development. Heterozygotic deletion of Ppbp gene is now commercially available (http://www.velocigene.com/komp/detail/10026), which should facilitate research into the roles of this gene.

### 5.4.4 Potential roles of canonical signalling of endogenous RA/RAR

Gene ontology analysis suggested a broad spectrum of biological processes and molecular functions associated with the genes examined. Certain genes such as Ebf1 and Hrsp12 have rather general functions, e.g., modulating gene transcription and translation. Whereas, functions of several genes such as 9930023K05Rik and 2310007B03Rik are not yet established. Given that the gene ontologies were derived from experimental results involving multiple biological systems, potential functions of these genes in the collecting duct and in the kidney were made by inference, as summarised in Table 5.9. Accordingly, a list of hypotheses on the potential roles of the validated genes are generated and discussed below.

#### *Regulation of kidney development: Ppbp, Tinag, and Bmp7*

Besides Ppbp, there are evidence from *ex vivo* and *in vivo* studies that suggest the involvement of Tinag and Bmp7, which encode tubulointerstitial nephritis antigen and bone morphogenetic protein 7, respectively, in kidney development. Of note, both Tinag and Bmp7 transcripts were detected in native ureteric bud cells and in embryo-

nic medullary collecting duct cells (Table 5.9).

Tubulointerstitial nephritis antigen is an extra-cellular matrix (ECM) protein, which was found in the basement membrane of developing glomeruli and renal tubules [140]. Inhibition of Tinag gene translation in E13 metanephro explants using gene silencing technique did not affect glomerulogenesis but defective tubulogenesis of the nephron and diminished ureteric bud branching was observed, which was speculated to be a result of impaired communication between Tinag and the surrounding ECM protein [140]. The importance of Bmp7 in kidney development was highlighted by kidney development impairment in Bmp7$^{-/-}$ mice particularly at a later stage, i.e., after E14.5 [65, 132], which might be a result of defective control in ureteric bud cell proliferation [251].

While the relationship between Tinag and RA had not been reported, Bmp7 transcriptional activity was reported to be induced by RA [243]. In addition, a global down-regulation of Bmp7 mRNA was found in autopods of RARb$^{-/-}$ / RARg$^{-/-}$ mice [68]. However, Bmp7 mRNA expression was no different in the developing kidney of E14 RAR$\alpha$ / RAR$\beta$2 knockout mice and wild-type mice [204], suggesting metanephric Bmp7 expression to be independent of RAR$\alpha$ and RAR$\beta$2 receptors, at least up to stage E14. Given that kidney development impairment was evident before E14 in RARa$^{-/-}$ / RARb2$^{-/-}$ mice due to a deficiency in Ret, potential role of RA in regulating Bmp7 during later stages of kidney development and its implications remain to be determined.

The crucial involvement of RA in kidney development and the potential involvement of Ppbp, Tinag, and Bmp7 in nephrogenesis suggest them to be novel targets of RA during kidney development [102, 255, 311]. Nonetheless, given that kidney development is a highly dynamic process involving complex crosstalk between the ureteric bud cells and mesenchymal cells, the actual involvement of these genes at various developmental stages and their regulation by RA should be carefully addressed.

***Maintenance of cell integrity and polarity: Tns1, Itga2, Tgm2, and Tinagl1***

Tns1, Itga2, Tgm2, and Tinagl1 are involved in cell-cell and cell-substrate adhesion. Given that cell adhesion represents a central mechanism for maintenance of cell integrity and polarity [115], these genes might be required to ensure survival and to preserve functions of the collecting ducts.

Tns1 encodes Tensin 1 protein that is localised to focal adhesions, the macromolecular assemblies via which cells bind to ECM. Genetic ablation of Tns1 lead to progressive kidney degeneration, characterised by the presence of multiple cysts, irregular epithelial cells, focal interstitial inflammatory infiltrates, and a near complete absence of cortex and medulla in severe cases, all of which were speculated to be resulting from weakening of focal adhesions [179].

Itga2 encodes integrin $\alpha 2$ protein that forms heterodimer with integrin $\beta 1$, and serves as receptor for laminin and collagen [152]. Itga2$^{-/-}$ mice suffered moderate proteinuria, as well as an enhanced glomerular and tubulointerstitial matrix deposition, which was speculated to be due to a failure in cell-matrix interaction [103].

Tgm2 encodes transglutaminase II, which is an enzyme that binds and cross-links a number of ECM protein, thereby stabilising the ECM protein and facilitating cell-adhesion to preserve tissue structure [81]. However, Tgm2 knockout mice was phenotypically normal [53, 222], although impaired would healing associated with altered cytoskeletal dynamics in fibroblasts isolated from Tgm2$^{-/-}$ mice was reported [81].

Tinagl1 encodes tubulointerstitial nephritis antigen-like 1 protein, also known as adrenocortical zonation factor 1, Tin-ag-RP, and lipocalin 7 [175]. Tinagl1 was speculated to serve as a basement membrane protein that facilitates interaction between ECM and cells, as well as to serve as a ligand of integrins to promote cell adhesion [175]. Interestingly, not only the Tinagl1 mRNA was found in IMCD cells, its protein was also

detected with immunostaining in human medullary collecting duct cells [318].

Although cell adhesion is a crucial element in branching morphogenesis [115], Tns1$^{-/-}$, Itga2$^{-/-}$, Tgm2$^{-/-}$ mice did not suffer kidney development impairment, which argue against these genes playing an obligatory role in nephrogenesis. Thus, it is more likely that these genes are acting predominantly at post-natal stages and during adulthood to maintain cell integrity and polarity. Tinagl1-null mutants are not available, hence its functions in kidney development remains unknown.

Loss of cellular integrity and polarity in collecting duct cells of post-natal VAD animals had not been widely reported. However, in mouse offspring restricted to vitamin A supply, thickening of glomerular and tubular basement membrane in the renal cortex was noted [192], which might be due to perturbation of cell-substrate and cell-cell interaction mediated by the aforementioned genes.

***Regulation of cellular response towards stress and modulation of tissue repair: Sprr1a, Cpm, Lcn2, and Bmp7***

Collecting duct cells, particularly those residing in the inner medulla, are encountering immense stress from the hypertonic/hyperosmotic and hypoxic medullary environment [227], with higher chance of bacterial invasion due to their proximity to the lower urinary tract. Besides Sprr1a, genes such as Cpm, Lcn2, and Bmp7 might also be playing a role in the adaptation towards such stress factors and in facilitating repair in the advent of stress-induced cell injury.

Cpm encodes carboxypeptidase M, a plasma membrane bound-enzyme that acts on a wide range of substrates [55]. Although the actual physiological role of Cpm remains poorly understood, it was proposed to play a role in inflammation and defence owing to its potential function in modulating activities of anaphylatoxins, as well as kinins to enhance kinin B1 receptor signalling [55, 337].

Lcn2 encodes lipocalin 2, or better known as neutrophil gelatinase-associated lipocalin, NGAL, which might have dual actions in the kidney [278]. A protective role of Lcn2 against oxidative stress had been reported, by inducing hemeoxygenase-1 (HO-1), a scavenger molecule that clears up harmful oxidant molecule [9], as well as through other HO-1-independent mechanisms [268]. Another well-established role of Lcn2 is its bacteriostatic effect by limiting bacterial invasion through sequestering iron ion crucial for bacterial growth [83]. However, much remains to be learnt with respect to specific roles of Lcn2 in the kidney tubular cells, as a recent report has shown that Lcn2 aggravates renal damage in the advent of chronic kidney injury [309].

Other than playing a role in kidney development, Bmp7 was proposed as a crucial endogenous defence molecule against kidney diseases [72]. Specifically, Bmp7 treatment was found to modulate expression of genes encoding cytokines, chemokines, and hemodynamics in human proximal tubular cells [110], as well as to prevent and reverse kidney fibrosis [334].

The potential involvement of these genes in regulating inflammation, immune response, oxidative stress, and tissue regeneration, fits well with the anti-inflammatory, immunemodulatory, regenerative, and anti-apoptotic roles of RA in kidney. Therefore, it would be of great interest to examine if the aforementioned effects of RA are at least in part mediated by these genes.

***Regulation of renal water homeostasis, chloride transport mechanisms, and stone formation: Npr3, Foxa1, Tgm2, Clca4, and Galns***

Being a member of the natriuretic peptide system, Npr3 is a gene encoding the natriuretic peptide receptor C, which interacts with natriuretic peptides [290]. Natriuretic peptide receptor C was believed to act as a "clearance receptor" to eliminate natriuretic peptides from circulation, thereby counter-balancing the effect of natriuretic peptides on

their regulation of blood pressure and body fluid homeostasis mediated by the other two receptors from the same family [196]. Mice with Npr3 gene deletion had significantly higher urine output coupled with an increased in water intake, which were attributed to a higher level of natriuretic peptides in the glomerular ultra-filtrates leading to a diuretic effect [196].

Genetic deletion of Foxa1, a member of the winged helix family of transcription factors, lead to mild nephrogenic diabetes insipidus without water restriction or water load, characterised by a dehydrated appearance, a reduction in urine osmolality, hydronephrosis, and a lack of response towards vasopressin in concentrating urine [19]. Interestingly, expression of genes encoding several major ion/water transporters and channels in the kidney were not diminished following Foxa1 gene ablation [19], leading to the proposal of Foxa1 as a novel transcription factor that directly regulates renal water homeostasis [79].

A less well-established gene in mediating water homeostasis is Tgm2, which encodes transglutaminase II that was found highly enriched in rat IMCD cells compared to other non-IMCD medullary cells [123, 305]. Given the ability of transglutaminase in mediating endocytosis *in vitro* [174], it was speculated that transglutaminase II might be involved in vasopressin-induced aquaporin 2 trafficking hence facilitating water reabsorption although functional evidence is lacking at this point [123].

Clca4, which encodes chloride channel calcium activated 4, is a chloride secretory channel that is activated by a rise in intracellular $Ca^{+}$ level [180]. While the role of Clca4 in collecting ducts remains to be characterised, transcript of another member within the same family, Clca1, was detected in another mouse inner medullary collecting duct cell line, which was proposed to mediate $Ca^{+}$-dependent $Cl^{-}$ conductance [28].

Galns encodes N-acetylgalactosamine-6-sulfate sulfatase, which is involved in degrada-

tion of keratan sulfate and chondroitin sulfate, two members of the glycosaminoglycans (GAG). GAG such as chondroitin sulfate might play a role in inhibiting stone formation but might also paradoxically promote stone formation, depending on the prevailing conditions such as urine osmolality and presence of other molecules [147]. While mice with Galns gene deletion exhibited higher urinary GAG and an increase in glomerular lysomal storage, stone formation and individual components of GAG were not described [304]. Given the highly complex pathophysiology of stone formation that involves multiple events including cell-crystal interaction and inflammation, whether loss of Galns gene contributes towards modulation of this pathophysiological process requires further investigation.

Although polyuria is rather commonly found in farm animals with vitamin A deficiency, such report in murine models of vitamin A deficiency is lacking. It might be that other factors in rodents are able to compensate for the diminution of RA/RAR signalling in the face of vitamin A deficiency. Perhaps the importance of RA in regulating these genes and its relevance to water balance could be better addressed by subjecting animals to fluid restriction and water load. On the other hand, given the roles of GAG in modulating stone formation, increased incidence of urolithiasis in animals with Vitamin A deficiency might be associated with regulation of galns by endogenous RA/RAR. VAD rats were found to have lower urinary GAG [111] but since activities of GAG in modulation of stone formation is highly complex [147], the potential connection between vitamin A deficiency and urolithiasis requires further investigation.

### 5.4.5 Concluding remarks

A list of endogenous RA/RAR target genes were identified from microarray studies. This supports that the basal constitutive RAR-dependent activity in mIMCD-3 cells is indeed playing a functional role. In fact, the most highly regulated genes were those that their expression was maintained or induced by both endogenous RA and RARs, underscoring the importance of RA canonical signalling as an “inducer” of gene transcription. Among the validated genes, some have not been reported to be regulated by RA before

and hence represent novel target genes of RA/RAR. More importantly, the validated genes are involved in some essential functions of collecting duct principal cells, inner medullary collecting duct cells, and ureteric bud cells, as discussed before. Further studies on genes that their functions are less well-established, e.g., Sorcs2 and Klhdc7a, would uncover other roles of endogenous RA/RAR in the collecting ducts.

Other than target genes of endogenous RA/RAR, the microarray experiments had also unveiled a list of genes potentially regulated by non-canonical signalling of retinoids, i.e., regulated only by RARs and only by endogenous RA. While regulation of these genes remain to be validated, the results had indeed highlighted the complexity or retinoid system in gene expression regulation.

It is worth noting that several well-established target genes of RA, for example Rarb and Cyp26a1 that have more than one functional DR5 RAREs, were not shortlisted in the microarray experiments. This could be explained by the cell type-dependent activity of RA but the treatment length might also have an impact. For instance, these genes might have been regulated at earlier time points but their expression was restored to the basal level at the 24 h time point. Additional examinations at earlier time points,e.g., 4 h or 8 h, should complement the existing profile of endogenous RA/RAR target genes in mIMCD-3 cells.

# Chapter 6

# General Discussion and Future Work

## 6.1 General discussion

It is well-established that endogenous RA and retinoid nuclear receptors are indispensable for kidney development. On the other hand, little is known about the role of endogenous RA and retinoid nuclear receptors in the kidney after birth. In order to address this issue, this project started off by examining reporter activity of RA in the kidney of *RARE-hsp68-lacZ* transgenic mice. Using both X-gal assay and immunostaining technique with carefully optimised and validated antibodies, the reporter signal was found to be predominantly present in ureteric bud-derived collecting ducts in the post-natal and adult mouse kidney.

In the developing kidney of *RARE-hsp68-lacZ* transgenic mice, reporter signal was detected in the ureteric bud trunk and tip, which was shown to be mediated by RARs and by tRA [267]. Thus, it is very likely that the reporter signal observed in the kidney collecting ducts in this project was, at least in part, mediated by endogenous RA and RARs. This deduction also fits well with other reports on the presence of RA [137,139,277,286,328], retinoid nuclear receptors (www.nursa.org/10.1621/datasets.02001), and enzymes involved in RA biosynthesis [4, 7, 57, 58, 118, 177, 232, 335] in the kidney after birth. The

presence of reporter signal in collecting ducts suggests that the endogenous retinoid system, which is an essential component for kidney development, continues to be functional and is constitutively active in the healthy murine kidney. In an attempt to further examine the mediators of reporter transgene activation, immunostaining for RAR$\beta$, RAR$\beta$2, Raldh1, and Raldh3 were performed. However, the results were ambiguous and inconclusive as the sensitivity and specificity of these antibodies were questionable.

While reporter signal was detected in the collecting duct, it remains an observation that requires "loss-of-function" and "gain-of-function" interventions to further confirm it being genuinely mediated by RA and RARs. In order to address this issue, a well-established collecting duct cell line, mImCD-3 cells, were transfected with a RARE reporter plasmid to examine the presence of reporter activity. Exogenous tRA treatment on transfected cells cultured in medium supplemented with normal FBS or with charcoal-stripped FBS resulted in poor induction, if any, of the reporter activity. However, AGN193109 and DEAB treatments resulted in a reduction of reporter activity to about 50% of that of the control group. More importantly, reduction of the reporter activity was abolished in the simultaneous presence of tRA, confirming the specificity of regulation by these chemical reagents in inhibiting retinoid canonical signalling.

The results from reporter assay conducted in mIMCD-3 cells lead to three conclusions. Firstly, a constitutively active RAR-dependent activity was detected. Secondly, the RAR-dependent activity was likely given rise by a cell-autonomous synthesis of endogenous RA. Last but not least, the basal RAR-dependent endogenous RA activity might be so high that renders further induction by exogenous tRA impossible. These conclusions support that the reporter signal observed in the collecting duct of *RARE-hsp68-lacZ* mice, at least in principal cells and inner medullary collecting duct cells, was indeed due to the presence of a constitutively active RAR-dependent endogenous RA activity.

The presence of constitutively active endogenous RA/RAR signalling in the healthy

murine kidney suggests that the retinoid system might be involved in mediating certain signalling events to ensure proper functioning of the kidney. In order to address this issue, microarray experiment was performed to identify potential target genes of endogenous RA/RAR. By employing AGN193109 and DEAB that inhibit retinoic acid signalling at different stages and by adding exogenous tRA simultaneously to examine the reversibility/prevention of the regulation exerted by the chemical inhibitors, a list of specific target genes of endogenous RA/RAR was shortlisted. Among the most highly-regulated target genes of endogenous RA/RAR identified and validated, Dhrs3, Sprr1a, Cpm, Itga2, Ebf1, Lcn2, Tgm2, Bmp7, and Foxa1 were reported by others to be regulated by RA [12, 40, 44, 78, 87, 90, 153, 225, 243, 299]. Whereas, Ppbp, 9930023K05Rik, Tns1, Klhdc7a, Sorcs2, 2310007B03Rik, Galns, Npr3, Clca4, Upk3b, Slc37a1, Hrsp12, Tinag, Foxj1, and Tinagl1 had not been reported to be regulated by RA and hence represent novel target genes of endogenous RA/RAR.

In summary, this project has confirmed the presence of a constitutively active RAR-dependent activity, likely given rise by cell-autonomous synthesis of endogenous RA, in the collecting duct of healthy murine kidney. By performing microarray experiments, genes most dependent on endogenous RA/RAR were shortlisted and validated. Interestingly, the validated genes are involved in biological processes such as kidney development and defence against inflammation and fibrogenesis, which fit well with some of the reported functions of RA and RARs [329]. While renal anomalies such as increased incidence of urolithiasis, renal infection, inflammation, and fibrogenesis, had been associated with vitamin A deficiency in the past, a clear cause-and-effect relationship remains elusive. This project has shed some light on the potential molecular mechanisms, which might provide explanation towards some of these phenomena.

## 6.2 Future work

Before moving on to the next step, it is both prudent and desirable for the findings summarised in this project be further validated and consolidated. Firstly, the reporter

transgene activity of *RARE-hsp68-lacZ* transgenic mice should be further confirmed by characterising the transgene expression, in terms of its sensitivity and specificity towards reporting RAR-dependent activity of RA, at post-natal and adult stages, as discussed in Chapter 3. It would also be of great interest to examine the RA activity using another line of RA reporter mouse, when one becomes available.

One of the issues remain unresolved is the molecular mediators of the reporter signal observed in the *RARE-hsp68-lacZ* reporter mouse model and in the mIMCD-3 cells transfected with RARE-reporter plasmid. In supporting the 3R's principle of Replacement, Refinement, and Reduction, a few pilot studies can be performed on mIMCD-3 cells before *in vivo* experiments are carried out. For example, mIMCD-3 cells can be treated with isotype-selective antagonists or inhibitors, or transfected with siRNA targeting specific retinoid nuclear receptors or enzymes, to get some ideas into potential molecular mediators that gave rise to the reporter activity. Should the activity of RA in intercalated cells be further explored, then a cell model of intercalated cells would first be established in the similar manner as for mIMCD-3 cells, as described in Chapter 4, prior to target gene identification.

Identification and validation of target genes of endogenous RA/RAR in mIMCD-3 cells represent only the first step towards understanding the physiological roles of endogenous RA/RAR in kidney after birth. In the next step, it is imperative to perform further studies focusing on two major aspects. Firstly, the physiological functions of the identified target genes in the collecting duct and in the kidney should be better established as most of them had not been extensively studied in the renal system. Targeted knockout of the validated target genes from the collecting duct, especially the top three most highly-regulated genes, i.e. Drhs3, Sprr1a, Ppbp, at different developmental stages and after birth, should provide valuable information on their specific roles. Detailed molecular mechanisms could be performed on mIMCD-3 cells whenever needed. Secondly, regulation of the identified target genes should be further validated at the protein and

functional level in mIMCD-3 cells. Following that, *in vivo* experiment can be planned, for example by subjecting *RARE-hsp68-lacZ* mice to diet with varied amount of vitamin A to examine the gene expression and to correlate that with the reporter signal as well as with functional defects, if present.

The project could also be further extended to study the role of endogenous retinoid system in renal pathology. For instance, alterations of endogenous RA/RAR activity could be determined after inducing renal diseases in RA reporter mice. Further to that, chemical reagents that diminish or enhance endogenous RA/RAR activity could be administered to the reporter mice, and reporter signal and disease progression could then be monitored. These studies should provide valuable insights on the involvement and alteration of endogenous retinoid system in the advent of renal disease, and the effects of endogenous retinoid system mobilisation on disease progression.

Although the non-canonical signalling of retinoids is not the primary focus of this project, microarray experiments had unveiled a list of genes that their expression was only dependent on RA as well as those dependent only on RARs. Although regulation of these genes has not been validated and their fold-changes are not as dramatic as genes regulated by both RA and RARs, it has highlighted the complexity of retinoid signalling. It would be interesting to further explore in the future, whether the retinoid system is modulating gene expression and the functions of collecting duct cells via both canonical and non-canonical signalling in a coordinated manner.

While retinoids were discovered nearly 100 years ago, much remains to be learnt about their activities and roles in the kidney. It is hoped that this project would serve as a groundwork for further studies, to better understand the roles of endogenous retinoid system in renal physiology and pathology.

# Appendix A

# Plasmid maps

## A.1 pmaxGFP plasmid

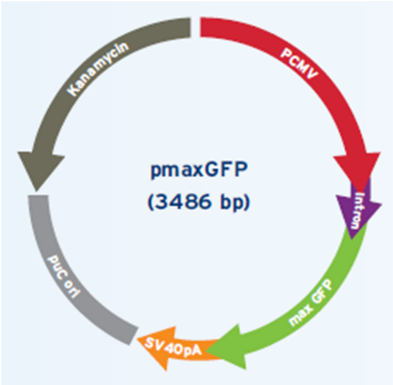


Figure A.1: pmaxGFP plasmid. pmaxGFP plasmid encodes the green fluorescent protein (GFP) from Copepod Pontellina plumata, which expression was driven by the cytomegalovirus promoter (pCMV). Plasmid map is adapted from Amaxa Biosystems.

## A.2 Plasmid maps

### A.2.1 pGL3-RARE-luciferase plasmid

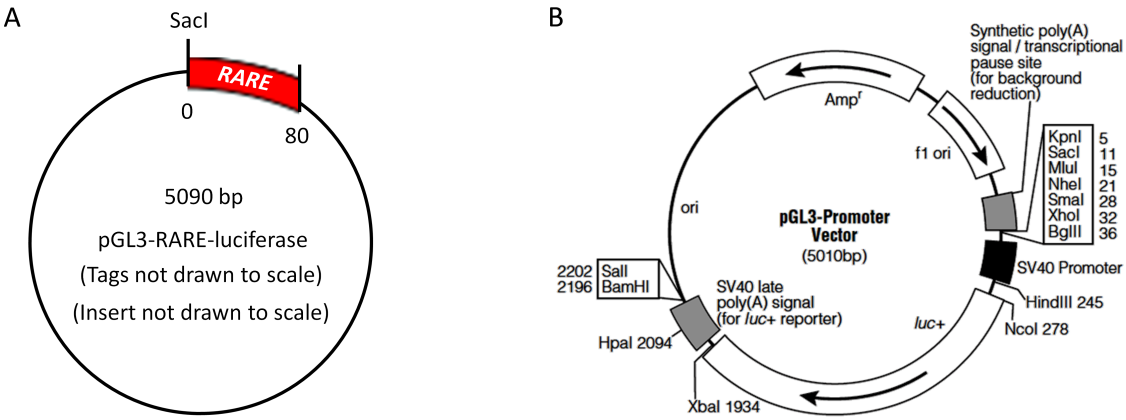


Figure A.2: pGL3-RARE-luciferase plasmid. pGL3-RARE-luciferase contains three copies of RARE that is inserted into the SacI site of the pGL3 luciferase promoter vector (A). In the presence of retinoic acid and endogenous retinoic acid receptors, the plasmid will be activated leading to expression of the $luc^+$ gene driven by simian virus 40 (SV 40) promoter, producing firefly luciferase (B). Plasmid map of pGL3-RARE-luciferase and pGL3 is adapted from Addgene Inc. and Promega UK Ltd., respectively.

### A.2.2 pCI-$\beta$-galactosidase plasmid

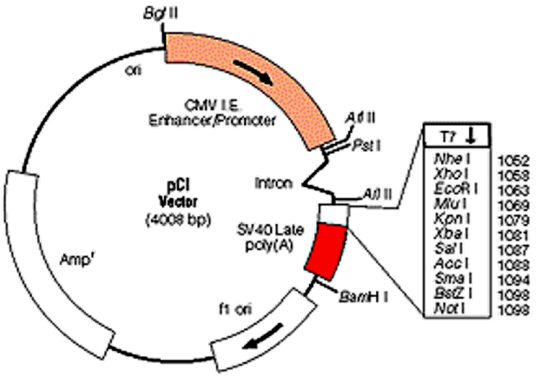


Figure A.3: pCI-$\beta$-galactosidase plasmid. pCI-$\beta$-galactosidase contains the *lacZ* gene construct that is inserted into pCI-vector. Driven by the human cytomegalovirus immediate-early (CMV I.E) enhancer/promoter, $\beta$-galactosidase, a gene product of *lacZ* gene is constitutively expressed upon transfecting into the cells. The plasmid map of pCI-vector is adapted from Promega UK Ltd.

## A.3 Algorithm for image analysis

```
%% Analysis tool: Image processing toolbox version 7.2 Matlab 7.12.0
%% Analyse GFP Image

I = imread('gfp.png');

% Convert to grayscale
gfp = rgb2gray(I);
% Mask the label
gfp(1965:2150,270:655) = 0;
% Resize the images to make them comparable
gfp = imresize(gfp,[500 600]);
% Adjust the contrast
gfp_histeq = adapthisteq(gfp);
% Blob detection
BW = im2bw(gfp_histeq, 0.15);
% Detect boundary
[B,~,N] = bwboundaries(BW);
figure; imshow(BW); hold on;
for k=1:length(B),
    boundary = B{k};
    plot(boundary(:,2),boundary(:,1),'r','LineWidth',2);
end
% Compute area of GFP
areaA = bwarea(BW);

%% Analyse Phase Contrast Image
I2 = imread('phase_contrast.png');
figure; imshow(I2);
% Convert to grayscale
phc = rgb2gray(I2);
% Resize the images to make them comparable
phc = imresize(phc,[500 600]);
% Adjust contrast
phc_histeq = adapthisteq(phc);
% Blob detection
BW2 = ones(size(phc_histeq));
BW2(phc_histeq > 50 & phc_histeq < 170) = 0;
% Mask the label
BW2(425:460,55:140) = 0;
figure; imshow(BW2);
% Compute area of phase contrast
areaB = bwarea(BW2);

%% Compute area ratio
area_ratio = areaA/areaB;

%% For visualisation: Overlay gfp boundary on phase contrast
phc_final = zeros(500,600,3);
phc_final(:,:,1) = 0.5.*BW2 + 0.5*BW;
phc_final(:,:,2) = 0.5.*BW2 + 0.5*BW;
phc_final(:,:,3) = 0.5.*BW2 + 0.5*BW;
figure; imshow(phc_final); hold on;
for k=1:length(B),
    boundary = B{k};
    plot(boundary(:,2),...
        boundary(:,1),'r','LineWidth',2);
end
```

Figure A.4: Matlab algorithm used for image analysis on Green Fluorescent Protein (GFP)-transfected cells.

# Appendix B

# Preliminary experiment and validation of microarray results

## B.1 Preliminary experiments with RT-qPCR

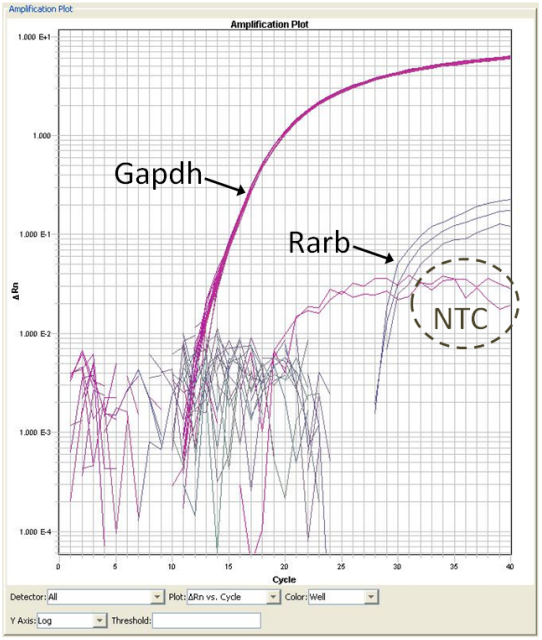


Figure B.1: Amplification plot of Rarb and Gapdh. As opposed to Gapdh gene that is abundantly expressed, expression of Rarb gene was very low, evident by huge gap between technical triplicates from a single sample, which were rather close to the non-template control (NTC) of Gapdh gene.

## B.2 Validation of microarray results with RT-qPCR

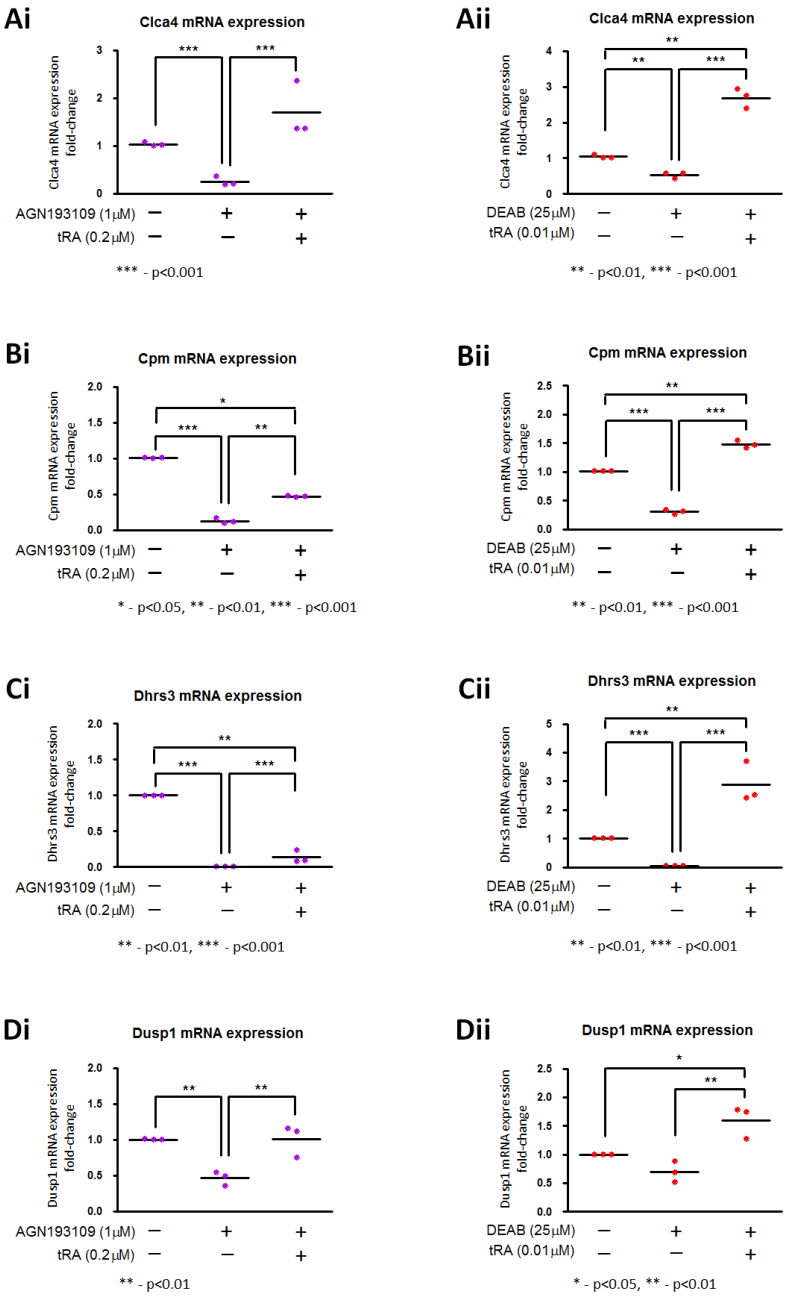


Figure B.2: Regulation of Clca4, Cpm, Dhrs3, and Dusp1 genes by AGN193109 and DEAB with and without all-*trans* retinoic acid (tRA).

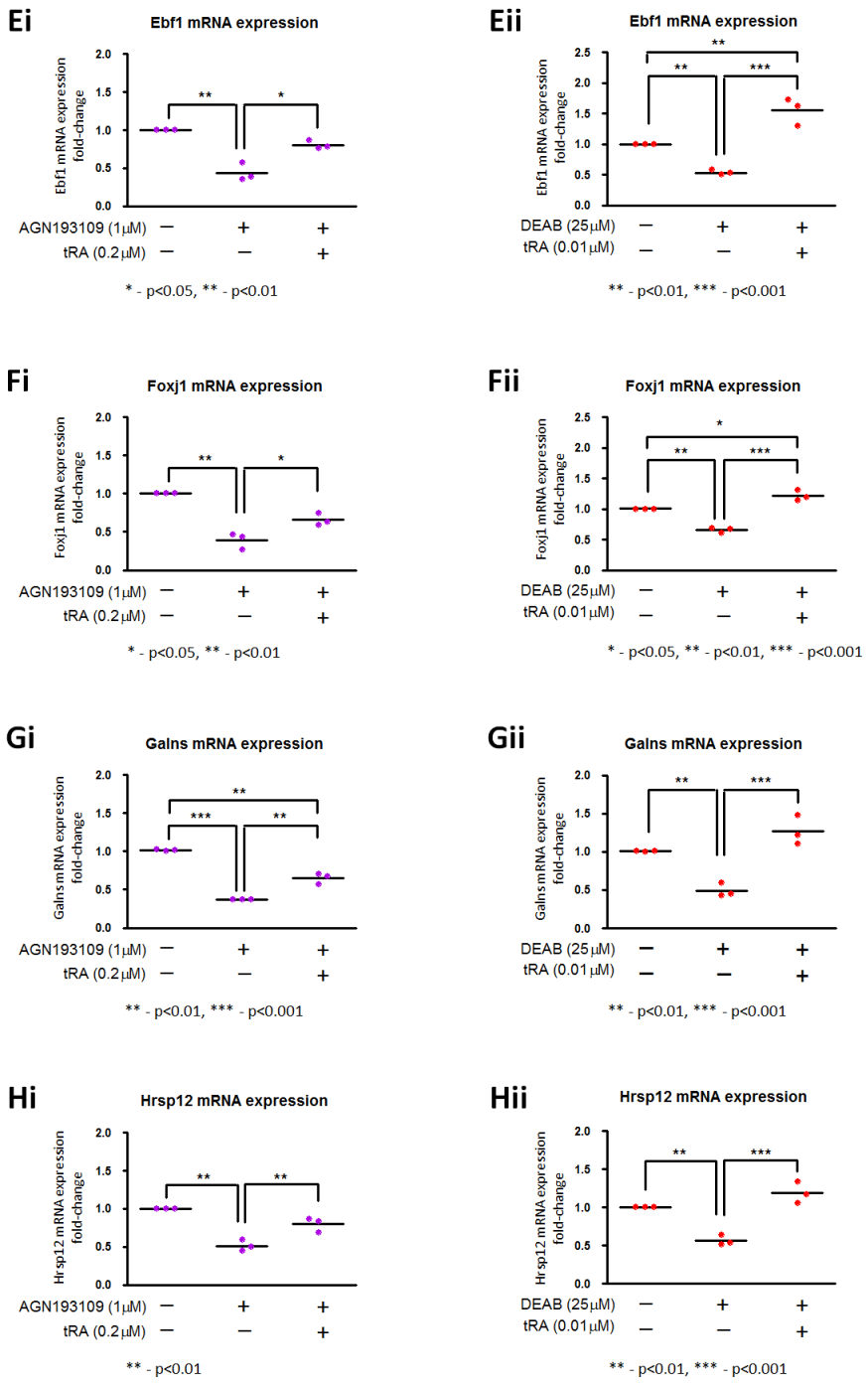


Figure B.3: Regulation of Ebf1, Foxj1, Galns, and Hrsp12 genes by AGN193109 and DEAB with and without all-*trans* retinoic acid (tRA).

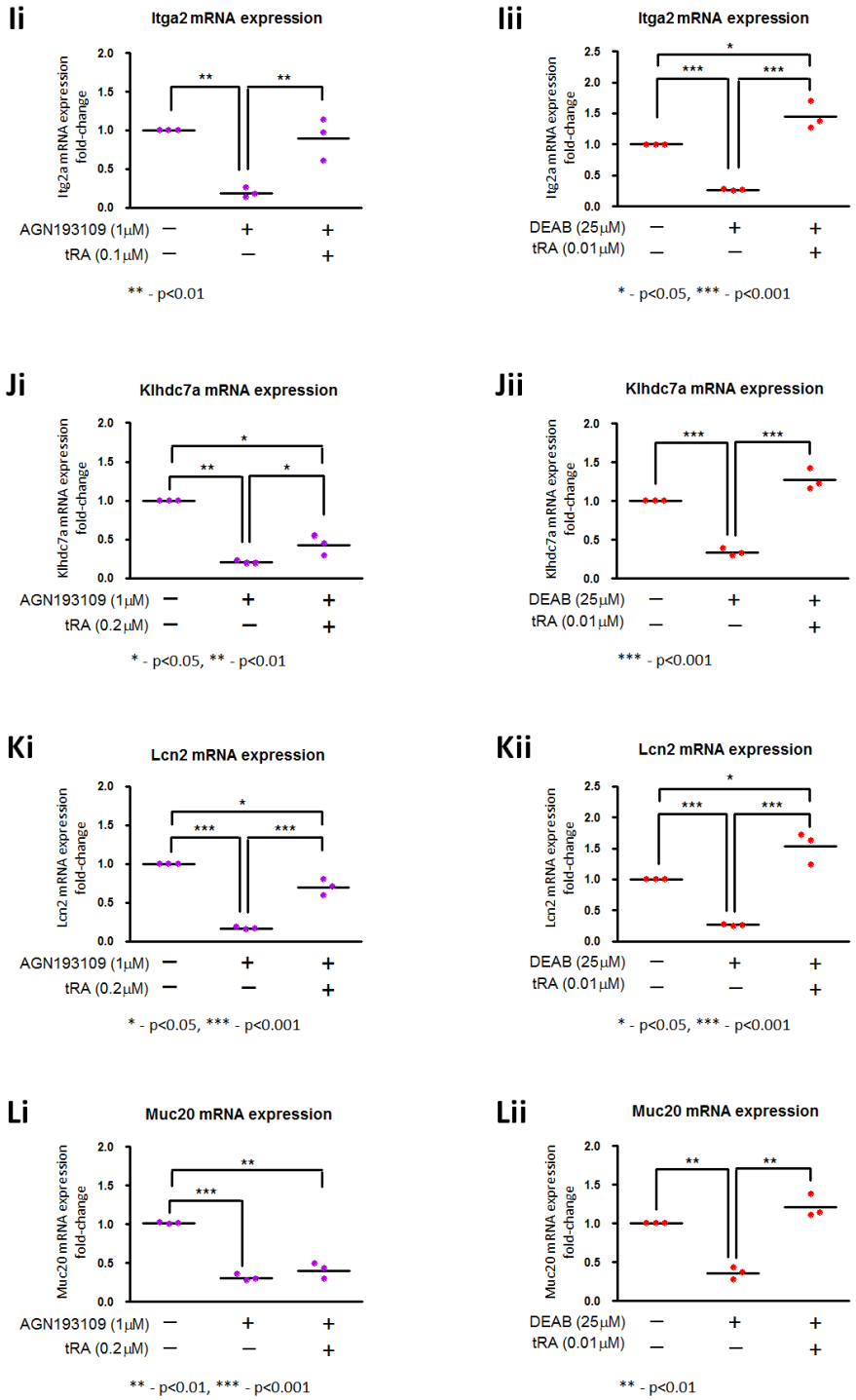


Figure B.4: Regulation of Itga2, Klhdc7a, Lcn2, and Muc20 genes by AGN193109 and DEAB with and without all-*trans* retinoic acid (tRA).

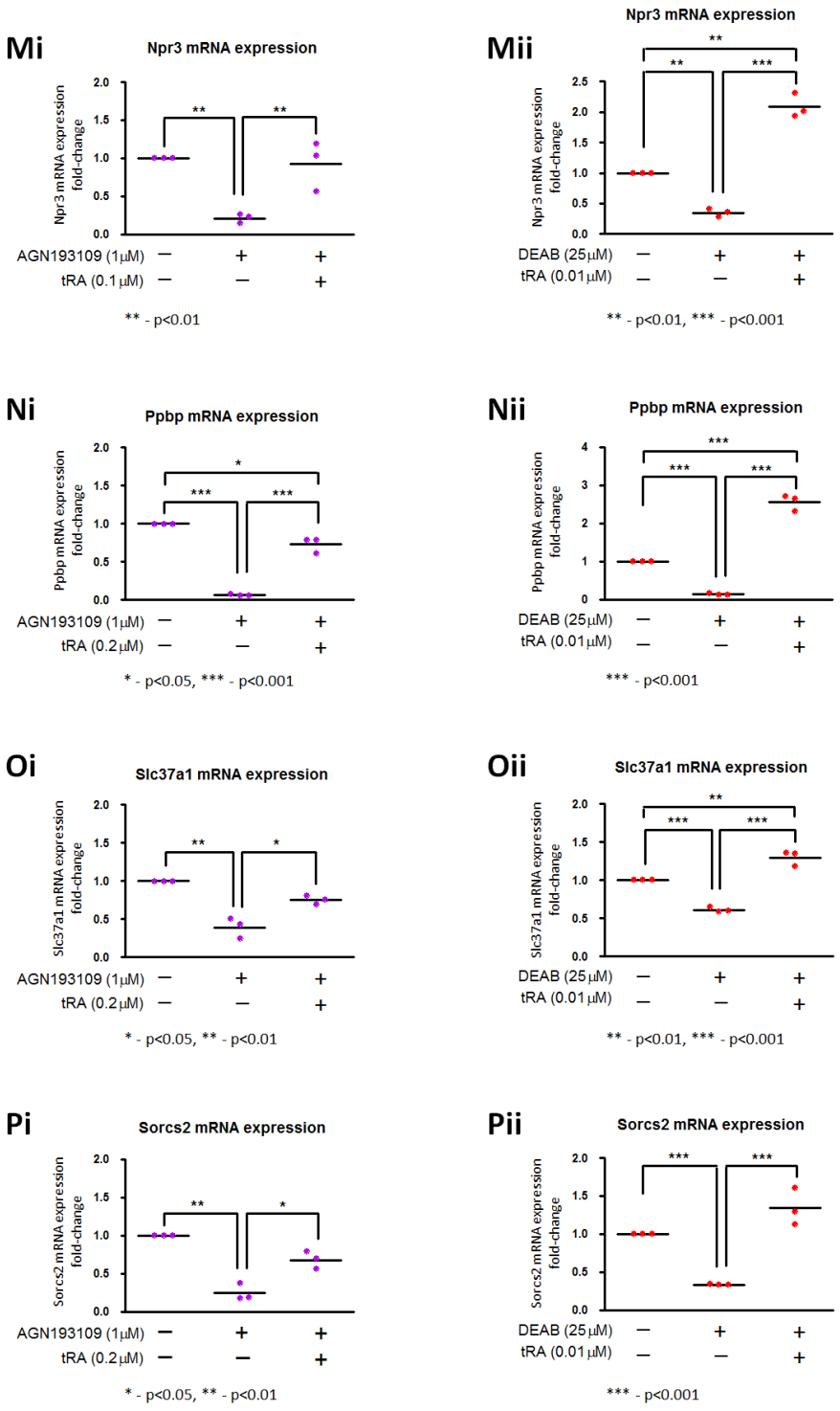


Figure B.5: Regulation of Npr3, Ppbp, Slc37a1, and Sorcs2 genes by AGN193109 and DEAB with and without all-*trans* retinoic acid (tRA).

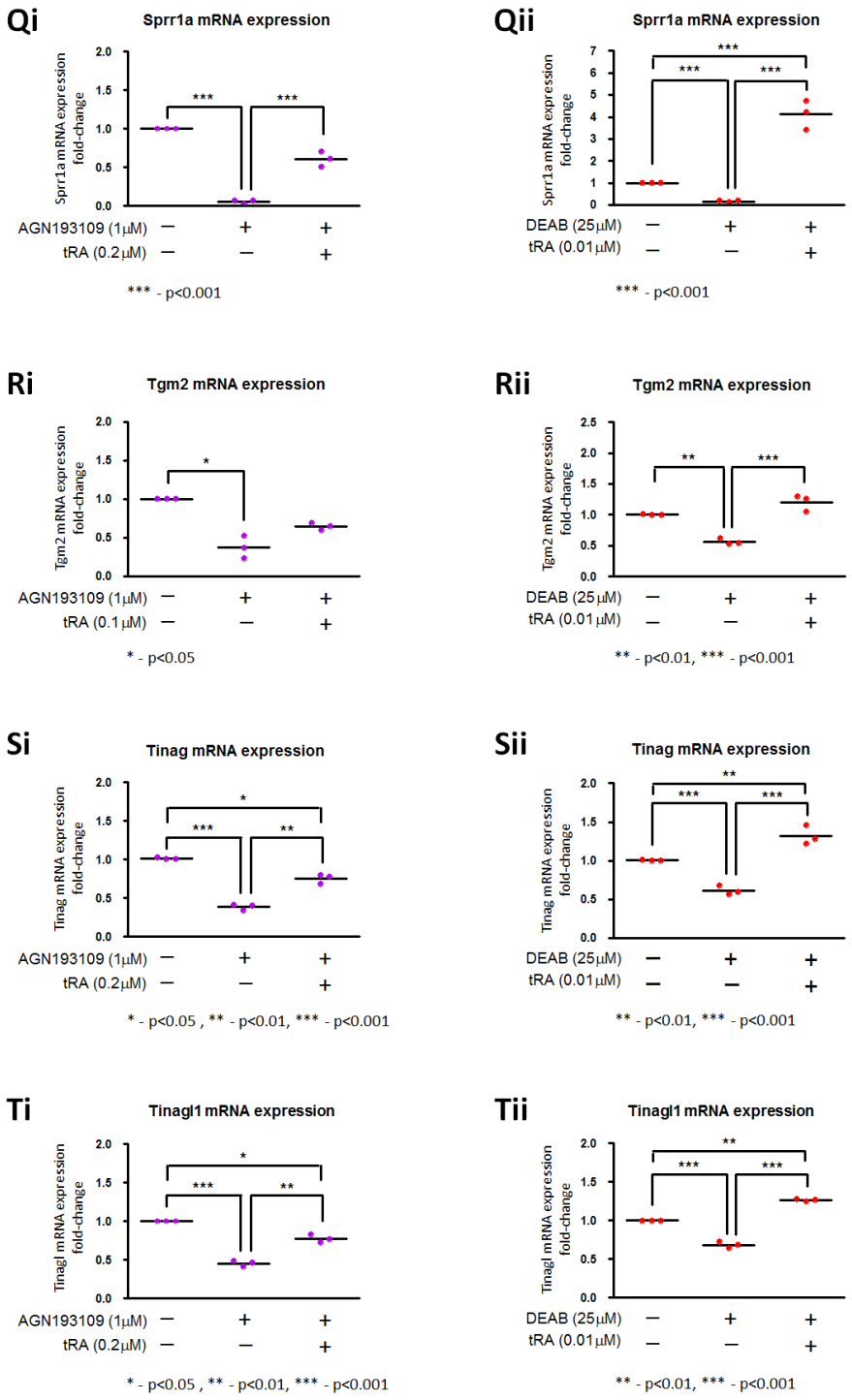


Figure B.6: Regulation of Sprr1a, Tgm2, Tinag, and Tinagl1 genes by AGN193109 and DEAB with and without all-*trans* retinoic acid (tRA).

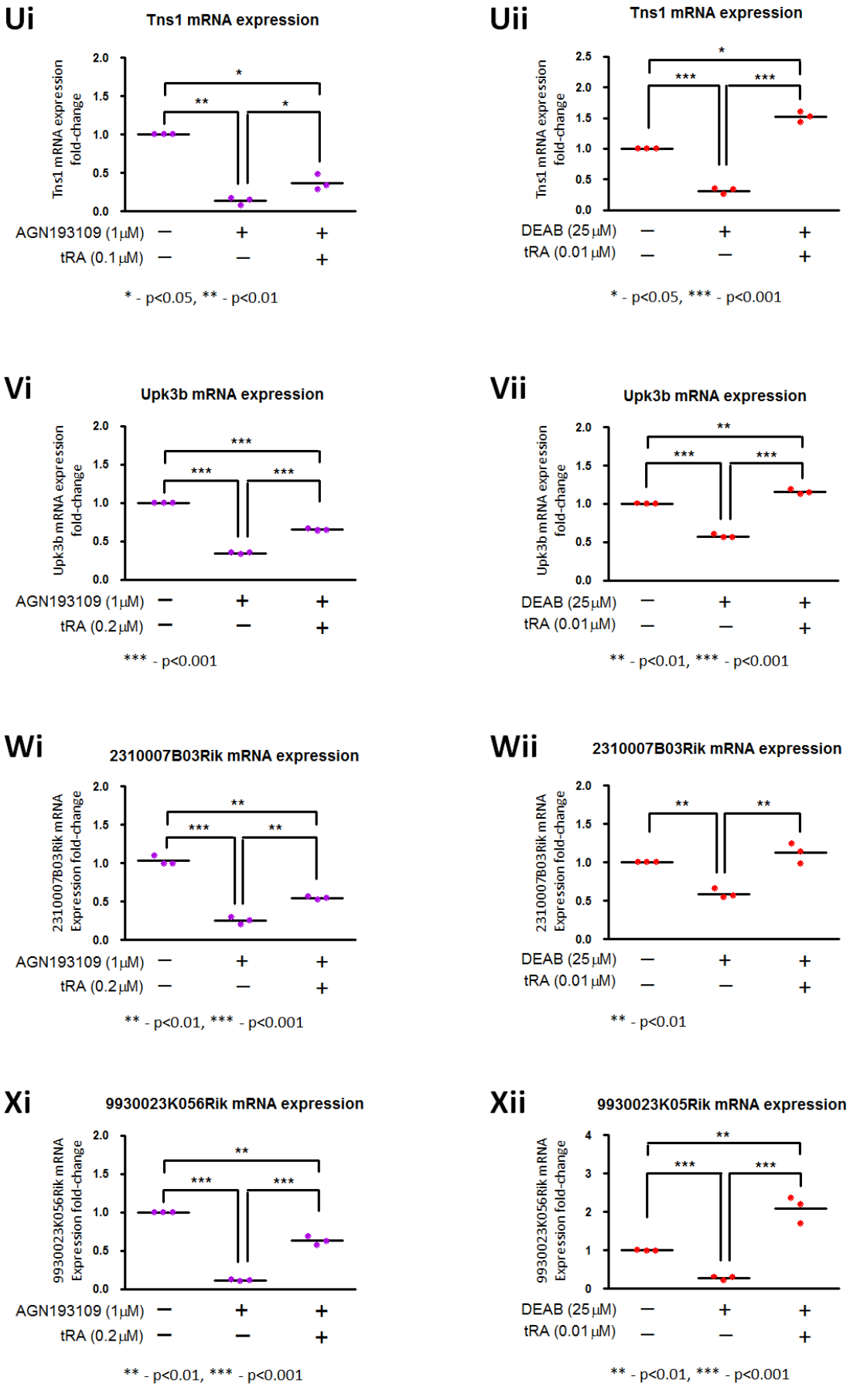


Figure B.7: Regulation of Tns1, Upk3b, 2310007B03Rik, and 9930023K05Rik genes by AGN193109 and DEAB with and without all-*trans* retinoic acid (tRA).

# References

[1] S. Abu-Abed, P. Dollé, D. Metzger, B. Beckett, P. Chambon, and M. Petkovich. The retinoic acid-metabolizing enzyme, CYP26A1, is essential for normal hindbrain patterning, vertebral identity, and development of posterior structures. *Genes Dev*, 15(2):226–240, Jan 2001.

[2] C. C. Achkar, F. Derguini, B. Blumberg, A. Langston, A. A. Levin, J. Speck, R. M. Evans, J. Bolado, K. Nakanishi, J. Buck, and L. J. Gudas. 4-oxoretinol, a new natural ligand and transactivator of the retinoic acid receptors. *Proc Natl Acad Sci U S A*, 93(10):4879–4884, May 1996.

[3] G. Allenby, M. T. Bocquel, M. Saunders, S. Kazmer, J. Speck, M. Rosenberger, A. Lovey, P. Kastner, J. F. Grippo, and P. Chambon. Retinoic acid receptors and retinoid X receptors: interactions with endogenous retinoic acids. *Proc Natl Acad Sci U S A*, 90(1):30–34, 1993.

[4] Y. Alnouti and C. D. Klaassen. Tissue distribution, ontogeny, and regulation of aldehyde dehydrogenase (Aldh) enzymes mRNA by prototypical microsomal enzyme inducers in mice. *Toxicol Sci*, 101(1):51–64, 2008.

[5] L. Altucci, M. D. Leibowitz, K. M. Ogilvie, A. R. de Lera, and H. Gronemeyer. RAR and RXR modulation in cancer and metabolic disease. *Nat Rev Drug Discov*, 6(10):793–810, 2007.

[6] P. M. Amann, S. B. Eichmüller, J. Schmidt, and A. V. Bazhin. Regulation of gene expression by retinoids. *Curr Med Chem*, 18(9):1405–1412, 2011.

[7] H. L. Ang, L. Deltour, M. Zgombić-Knight, M. A. Wagner, and G. Duester. Expression patterns of class I and class IV alcohol dehydrogenase genes in devel-

oping epithelia suggest a role for alcohol dehydrogenase in local retinoic acid synthesis. *Alcohol Clin Exp Res*, 20(6):1050–1064, 1996.

[8] A. Aström, U. Pettersson, P. Chambon, and J. J. Voorhees. Retinoic acid induction of human cellular retinoic acid-binding protein-II gene transcription is mediated by retinoic acid receptor-retinoid X receptor heterodimers bound to one far upstream retinoic acid-responsive element with 5-base pair spacing. *J Biol Chem*, 269(35):22334–22339, 1994.

[9] P. Bahmani, R. Halabian, M. Rouhbakhsh, A. M. Roushandeh, N. Masroori, M. Ebrahimi, A. Samadikuchaksaraei, M. A. Shokrgozar, and M. H. Roudkenar. Neutrophil gelatinase-associated lipocalin induces the expression of heme oxygenase-1 and superoxide dismutase 1, 2. *Cell Stress Chaperones*, 15(4):395–403, 2010.

[10] J. S. Bailey and C. H. Siu. Purification and partial characterization of a novel binding protein for retinoic acid from neonatal rat. *J Biol Chem*, 263(19):9326–9332, 1988.

[11] W. Balkan, M. Colbert, C. Bock, and E. Linney. Transgenic indicator mice for studying activated retinoic acid receptors during development. *Proc Natl Acad Sci U S A*, 89(8):3347–3351, 1992.

[12] J. E. Balmer and R. Blomhoff. Gene expression regulation by retinoic acid. *J Lipid Res*, 43(11):1773–1808, 2002.

[13] J. E. Balmer and R. Blomhoff. A robust characterization of retinoic acid response elements based on a comparison of sites in three species. *J Steroid Biochem Mol Biol*, 96(5):347–354, 2005.

[14] J. H. Barnard, J. C. Collings, A. Whiting, S. A. Przyborski, and T. B. Marder. Synthetic retinoids: structure-activity relationships. *Chemistry*, 15(43):11430–11442, 2009.

[15] M. M. Bashor, D. O. Toft, and F. Chytil. In vitro binding of retinol to rat-tissue components. *Proc Natl Acad Sci U S A*, 70(12):3483–3487, 1973.

[16] J. Bastien and C. Rochette-Egly. Nuclear retinoid receptors and the transcription of retinoid-target genes. *Gene*, 328:1–16, 2004.

[17] E. Batourina, S. Gim, N. Bello, M. Shy, M. Clagett-Dame, S. Srinivas, F. Costantini, and C. Mendelsohn. Vitamin A controls epithelial/mesenchymal interactions through Ret expression. *Nat Genet*, 27(1):74–78, 2001.

[18] D. L. Beaver. Vitamin A deficiency in the germ-free rat. *Am J Pathol*, 38:335–357, 1961.

[19] R. Behr, J. Brestelli, J. T. Fulmer, N. Miyawaki, T. R. Kleyman, and K. H. Kaestner. Mild nephrogenic diabetes insipidus caused by Foxa1 deficiency. *J Biol Chem*, 279(40):41936–41941, 2004.

[20] O. V. Belyaeva, M. P. Johnson, and N. Y. Kedishvili. Kinetic analysis of human enzyme RDH10 defines the characteristics of a physiologically relevant retinol dehydrogenase. *J Biol Chem*, 283(29):20299–20308, 2008.

[21] M. Bens and A. Vandewalle. Cell models for studying renal physiology. *Pflugers Arch*, 457(1):1–15, 2008.

[22] D. C. Berry, H. Jin, A. Majumdar, and N. Noy. Signaling by vitamin A and retinol-binding protein regulates gene expression to inhibit insulin responses. *Proc Natl Acad Sci U S A*, 108(11):4340–4345, 2011.

[23] H. K. Biesalski, J. Frank, S. C. Beck, F. Heinrich, B. Illek, R. Reifen, H. Gollnick, M. W. Seeliger, B. Wissinger, and E. Zrenner. Biochemical but not clinical vitamin A deficiency results from mutations in the gene for retinol binding protein. *Am J Clin Nutr*, 69(5):931–936, 1999.

[24] W. S. Blaner. STRA6, a cell-surface receptor for retinol-binding protein: the plot thickens. *Cell Metab*, 5(3):164–166, 2007.

[25] C. Bloch. Blindness and other diseases in children arising from deficient nutrition (lack of fat-soluble A factor). *Am J Dis Child*, 27:139–148, 1924.

[26] C. E. Bloch. Clinical investigation of xerophthalmia and dystrophy in infants and young children (xerophthalmia et dystrophia alipogenetica). *J Hyg (Lond)*, 19(3):283–304.5, 1921.

[27] R. Blomhoff and H. K. Blomhoff. Overview of retinoid metabolism and function. *J Neurobiol*, 66(7):606–630, 2006.

[28] S. H. Boese, M. Glanville, O. Aziz, M. A. Gray, and N. L. Simmons. $Ca^{2+}$ and cAMP-activated $Cl^-$ conductances mediate $Cl^-$ secretion in a mouse renal inner medullary collecting duct cell line. *J Physiol*, 523 Pt 2:325–338, 2000.

[29] I. E. Bonilla, K. Tanabe, and S. M. Strittmatter. Small proline-rich repeat protein 1A is expressed by axotomized neurons and promotes axonal outgrowth. *J Neurosci*, 22(4):1303–1315, 2002.

[30] M. G. Borland, J. E. Foreman, E. E. Girroir, R. Zolfaghari, A. K. Sharma, S. Amin, F. J. Gonzalez, A. C. Ross, and J. M. Peters. Ligand activation of peroxisome proliferator-activated receptor-beta/delta inhibits cell proliferation in human HaCaT keratinocytes. *Mol Pharmacol*, 74(5):1429–1442, 2008.

[31] P. Bouillet, V. Sapin, C. Chazaud, N. Messaddeq, D. D*é*cimo, P. Doll*é*, and P. Chambon. Developmental expression pattern of Stra6, a retinoic acid-responsive gene encoding a new type of membrane protein. *Mech Dev*, 63(2):173–186, 1997.

[32] J. F. Boylan and L. J. Gudas. The level of CRABP-I expression influences the amounts and types of all-trans-retinoic acid metabolites in F9 teratocarcinoma stem cells. *J Biol Chem*, 267(30):21486–21491, 1992.

[33] N. Brand, M. Petkovich, A. Krust, P. Chambon, H. de Th*é*, A. Marchio, P. Tiollais, and A. Dejean. Identification of a second human retinoic acid receptor. *Nature*, 332(6167):850–853, 1988.

[34] E. Brandt, A. Ludwig, and H.-D. Flad. CTAP-III, $\beta$TG, and NAP-2. DOI:10.1006/rwcy.2000.10005.

[35] N. S. Brown, A. Smart, V. Sharma, M. L. Brinkmeier, L. Greenlee, S. A. Camper, D. R. Jensen, R. H. Eckel, W. Krezel, P. Chambon, and B. R. Haugen. Thyroid hormone resistance and increased metabolic rate in the RXR-gamma-deficient mouse. *J Clin Invest*, 106(1):73–79, 2000.

[36] Y. A. Bulynko and B. W. O'Malley. Nuclear receptor coactivators: structural and functional biochemistry. *Biochemistry*, 50(3):313–328, 2011. Doi: 10.1021/bi101762x.

[37] M. J. Butt, A. F. Tarantal, D. F. Jimenez, and D. G. Matsell. Collecting duct epithelial-mesenchymal transition in fetal urinary tract obstruction. *Kidney Int*, 72(8):936–944, 2007.

[38] Q. Cai, N. I. Dmitrieva, J. D. Ferraris, H. L. Brooks, B. W. van Balkom, and M. Burg. Pax2 expression occurs in renal medullary epithelial cells in vivo and in cell culture, is osmoregulated, and promotes osmotic tolerance. *Proc Natl Acad Sci U S A*, 102(2):503–508, 2005.

[39] G. Capasso. A crucial nephron segment in acid-base and electrolyte transport: the connecting tubule. *Kidney Int*, 70(10):1674–1676, 2006.

[40] F. Cerignoli, X. Guo, B. Cardinali, C. Rinaldi, J. Casaletto, L. Frati, I. Screpanti, L. J. Gudas, A. Gulino, C. J. Thiele, and G. Giannini. retSDR1, a short-chain retinol dehydrogenase/reductase, is retinoic acid-inducible and frequently deleted in human neuroblastoma cell lines. *Cancer Res*, 62(4):1196–1204, 2002.

[41] P. Chambon. A decade of molecular biology of retinoic acid receptors. *FASEB J*, 10(9):940–954, 1996.

[42] C. Chassin, E. Tourneur, M. Bens, and A. Vandewalle. A role for collecting duct epithelial cells in renal antibacterial defences. *Cell Microbiol*, 13(8):1107–1113, 2011.

[43] J. Y. Chen, S. Penco, J. Ostrowski, P. Balaguer, M. Pons, J. E. Starrett, P. Reczek, P. Chambon, and H. Gronemeyer. RAR-specific agonist/antagonists which dissociate transactivation and AP1 transrepression inhibit anchorage-independent cell proliferation. *EMBO J*, 14(6):1187–1197, 1995.

[44] X. Chen, B. L. Esplin, K. P. Garrett, R. S. Welner, C. F. Webb, and P. W. Kincade. Retinoids accelerate B lineage lymphoid differentiation. *J Immunol*, 180(1):138–145, 2008.

[45] D. Choudhary, I. Jansson, J. B. Schenkman, M. Sarfarazi, and I. Stoilov. Comparative expression profiling of 40 mouse cytochrome P450 genes in embryonic and adult tissues. *Arch Biochem Biophys*, 414(1):91–100, 2003.

[46] E. I. Christensen, J. O. Moskaug, H. Vorum, C. Jacobsen, T. E. Gundersen, A. Nykjaer, R. Blomhoff, T. E. Willnow, and S. K. Moestrup. Evidence for an essential role of megalin in transepithelial transport of retinol. *J Am Soc Nephrol*, 10(4):685–695, 1999.

[47] D. M. Cohen, S. R. Gullans, and W. W. Chin. Urea signaling in cultured murine inner medullary collecting duct (mIMCD3) cells involves protein kinase C, inositol 1,4,5-trisphosphate (IP3), and a putative receptor tyrosine kinase. *J Clin Invest*, 97(8):1884–1889, 1996.

[48] S. Q. Cohlan. Congenital anomalies in the rat produced by excessive intake of vitamin A during pregnancy. *Pediatrics*, 13(6):556–567, 1954.

[49] R. A. Coleman, D. C. Wu, J. Liu, and J. B. Wade. Expression of aquaporins in the renal connecting tubule. *Am J Physiol Renal Physiol*, 279(5):F874–F883, 2000.

[50] J. A. Crow and D. E. Ong. Cell-specific immunohistochemical localization of a cellular retinol-binding protein (type two) in the small intestine of rat. *Proc Natl Acad Sci U S A*, 82(14):4707–4711, 1985.

[51] C. Cui, M. A. Wani, D. Wight, J. Kopchick, and P. J. Stambrook. Reporter genes in transgenic mice. *Transgenic Res*, 3(3):182–194, 1994.

[52] D. N. D'Ambrosio, R. D. Clugston, and W. S. Blaner. Vitamin A metabolism: an update. *Nutrients*, 3(1):63–103, 2011.

[53] V. De Laurenzi and G. Melino. Gene disruption of tissue transglutaminase. *Mol Cell Biol*, 21(1):148–155, 2001.

[54] H. de Th*é*, M. M. Vivanco-Ruiz, P. Tiollais, H. Stunnenberg, and A. Dejean. Identification of a retinoic acid responsive element in the retinoic acid receptor beta gene. *Nature*, 343(6254):177–180, 1990.

[55] K. Deiteren, D. Hendriks, S. Scharp*á*, and A. M. Lambeir. Carboxypeptidase M: multiple alliances and unknown partners. *Clin Chim Acta*, 399(1-2):24–39, 2009.

[56] L. Delacroix, E. Moutier, G. Altobelli, S. Legras, O. Poch, M. A. Choukrallah, I. Bertin, B. Jost, and I. Davidson. Cell-specific interaction of retinoic acid receptors with target genes in mouse embryonic fibroblasts and embryonic stem cells. *Mol Cell Biol*, 30(1):231–244, 2010.

[57] L. Deltour, M. H. Foglio, and G. Duester. Impaired retinol utilization in Adh4 alcohol dehydrogenase mutant mice. *Dev Genet*, 25(1):1–10, 1999.

[58] L. Deltour, M. H. Foglio, and G. Duester. Metabolic deficiencies in alcohol dehydrogenase Adh1, Adh3, and Adh4 null mutant mice. Overlapping roles of Adh1 and Adh4 in ethanol clearance and metabolism of retinol to retinoic acid. *J Biol Chem*, 274(24):16796–16801, 1999.

[59] L. Delva, J. N. Bastie, C. Rochette-Egly, R. Kraba, N. Balitrand, G. Despouy, P. Chambon, and C. Chomienne. Physical and functional interactions between cellular retinoic acid binding protein II and the retinoic acid-dependent nuclear complex. *Mol Cell Biol*, 19(10):7158–7167, 1999.

[60] L. A. Denson, A. Bohan, M. A. Held, and J. L. Boyer. Organ-specific alterations in RAR alpha:RXR alpha abundance regulate rat Mrp2 (Abcc2) expression in obstructive cholestasis. *Gastroenterology*, 123(2):599–607, 2002.

[61] P. Dollé, V. Fraulob, J. Gallego-Llamas, J. Vermot, and K. Niederreither. Fate of retinoic acid-activated embryonic cell lineages. *Dev Dyn*, 239(12):3260–3274, 2010.

[62] P. Dollé, E. Ruberte, P. Leroy, G. Morriss-Kay, and P. Chambon. Retinoic acid receptors and cellular retinoid binding proteins. I. A systematic study of their differential pattern of transcription during mouse organogenesis. *Development*, 110(4):1133–1151, 1990.

[63] D. Dong, S. E. Ruuska, D. J. Levinthal, and N. Noy. Distinct roles for cellular retinoic acid-binding proteins I and II in regulating signaling by retinoic acid. *J Biol Chem*, 274(34):23695–23698, 1999.

[64] J. E. Dowling and G. Wald. The biological function of vitamin A acid. *Proc Natl Acad Sci U S A*, 46(5):587–608, 1960.

[65] A. T. Dudley, K. M. Lyons, and E. J. Robertson. A requirement for bone morphogenetic protein-7 during development of the mammalian kidney and eye. *Genes Dev*, 9(22):2795–2807, 1995.

[66] G. Duester. Families of retinoid dehydrogenases regulating vitamin A function: production of visual pigment and retinoic acid. *Eur J Biochem*, 267(14):4315–4324, 2000.

[67] G. Duester. Retinoic acid synthesis and signaling during early organogenesis. *Cell*, 134(6):921–931, 2008.

[68] V. Dupé, N. B. Ghyselinck, V. Thomazy, L. Nagy, P. J. Davies, P. Chambon, and M. Mark. Essential roles of retinoic acid signaling in interdigital apoptosis and control of BMP-7 expression in mouse autopods. *Dev Biol*, 208(1):30–43, 1999.

[69] V. Dupé, N. Matt, J. M. Garnier, P. Chambon, M. Mark, and N. B. Ghyselinck. A newborn lethal defect due to inactivation of retinaldehyde dehydrogenase type 3 is prevented by maternal retinoic acid treatment. *Proc Natl Acad Sci U S A*, 100(24):14036–14041, 2003.

[70] B. Durand, M. Saunders, P. Leroy, M. Leid, and P. Chambon. All-trans and 9-cis retinoic acid induction of CRABPII transcription is mediated by RAR-RXR heterodimers bound to DR1 and DR2 repeated motifs. *Cell*, 71(1):73–85, 1992.

[71] X. E, L. Zhang, J. Lu, P. Tso, W. S. Blaner, M. S. Levin, and E. Li. Increased neonatal mortality in mice lacking cellular retinol-binding protein II. *J Biol Chem*, 277(39):36617–36623, 2002.

[72] A. A. Eddy. Ramping up endogenous defences against chronic kidney disease. *Nephrol Dial Transplant*, 21(5):1174–1177, 2006.

[73] D. Eladari, R. Chambrey, and J. Peti-Peterdi. A new look at electrolyte transport in the distal tubule. *Annu Rev Physiol*, 74:325–349, 2012.

[74] G. Elizondo, J. Corchero, E. Sterneck, and F. J. Gonzalez. Feedback inhibition of the retinaldehyde dehydrogenase gene ALDH1 by retinoic acid through retinoic acid receptor alpha and CCAAT/enhancer-binding protein beta. *J Biol Chem*, 275(50):39747–39753, 2000.

[75] D. I. Eneanya, J. R. Bianchine, D. O. Duran, and B. D. Andresen. The actions of metabolic fate of disulfiram. *Annu Rev Pharmacol Toxicol*, 21:575–596, 1981.

[76] X. Fan, A. Molotkov, S. Manabe, C. M. Donmoyer, L. Deltour, M. H. Foglio, A. E. Cuenca, W. S. Blaner, S. A. Lipton, and G. Duester. Targeted disruption of Aldh1a1 (Raldh1) provides evidence for a complex mechanism of retinoic acid synthesis in the developing retina. *Mol Cell Biol*, 23(13):4637–4648, 2003.

[77] D. Fawcett, P. Pasceri, R. Fraser, M. Colbert, J. Rossant, and V. Giguère. Postaxial polydactyly in forelimbs of CRABP-II mutant mice. *Development*, 121(3):671–679, 1995.

[78] L. Feng, R. E. Hernandez, J. S. Waxman, D. Yelon, and C. B. Moens. Dhrs3a regulates retinoic acid biosynthesis through a feedback inhibition mechanism. *Dev Biol*, 338(1):1–14, 2010.

[79] R. A. Fenton and M. A. Knepper. Mouse models and the urinary concentrating mechanism in the new millennium. *Physiol Rev*, 87(4):1083–1112, 2007.

[80] R. A. Fenton and J. Praetorius. Molecular physiology of the medullary collecting duct. *Comprehensive Physiology*, pages 1031–1056, 2011. DOI: 10.1002/cphy.c100064.

[81] L. Fesus and M. Piacentini. Transglutaminase 2: an enigmatic enzyme with diverse functions. *Trends Biochem Sci*, 27(10):534–539, 2002.

[82] K. E. Finberg, C. A. Wagner, P. A. Stehberger, J. P. Geibel, and R. P. Lifton. Molecular cloning and characterization of Atp6v1b1, the murine vacuolar $H^+$ - ATPase B1-subunit. *Gene*, 318:25–34, 2003.

[83] T. H. Flo, K. D. Smith, S. Sato, D. J. Rodriguez, M. A. Holmes, R. K. Strong, S. Akira, and A. Aderem. Lipocalin 2 mediates an innate immune response to bacterial infection by sequestrating iron. *Nature*, 432(7019):917–921, 2004.

[84] C. Folli, V. Calderone, S. Ottonello, A. Bolchi, G. Zanotti, M. Stoppini, and R. Berni. Identification, retinoid binding, and x-ray analysis of a human retinol-binding protein. *Proc Natl Acad Sci U S A*, 98(7):3710–3715, 2001.

[85] B. M. Forman, K. Umesono, J. Chen, and R. M. Evans. Unique response pathways are established by allosteric interactions among nuclear hormone receptors. *Cell*, 81(4):541–550, 1995.

[86] L. S. Fridericia and E. Holm. Experimental contribution to the study of the relation between night blindness and malnutrition. Influence of deficiency of fat-soluble A-vitamin in the diet on the visual purple in the eyes of rats. *Am J Physiol*, 73:63–78, 1925.

[87] F. E. M. Froeling, C. Feig, C. Chelala, R. Dobson, C. E. Mein, D. A. Tuveson, H. Clevers, I. R. Hart, and H. M. Kocher. Retinoic acid-induced pancreatic stellate cell quiescence reduces paracrine wnt-$\beta$-catenin signaling to slow tumor progression. *Gastroenterology*, 141(4):1486–97, 1497.e1–14, 2011.

[88] C. A. Frolik, A. B. Roberts, T. E. Tavela, P. P. Roller, D. L. Newton, and M. B. Sporn. Isolation and identification of 4-hydroxy- and 4-oxoretinoic acid. In vitro metabolites of all-trans-retinoic acid in hamster trachea and liver. *Biochemistry*, 18(10):2092–2097, 1979.

[89] H. Fujii, T. Sato, S. Kaneko, O. Gotoh, Y. Fujii-Kuriyama, K. Osawa, S. Kato, and H. Hamada. Metabolic inactivation of retinoic acid by a novel P450 differentially expressed in developing mouse embryos. *EMBO J*, 16(14):4163–4173, 1997.

[90] W. Fujimoto, K. W. Marvin, M. D. George, G. Celli, N. Darwiche, L. M. De Luca, and A. M. Jetten. Expression of cornifin in squamous differentiating epithelial tissues, including psoriatic and retinoic acid-treated skin. *J Invest Dermatol*, 101(3):268–274, 1993.

[91] K. Fujiu, I. Manabe, and R. Nagai. Renal collecting duct epithelial cells regulate inflammation in tubulointerstitial damage in mice. *J Clin Invest*, 121(9):3425–3441, 2011.

[92] O. Gallego, F. X. Ruiz, A. Ardèvol, M. Dominguez, R. Alvarez, A. R. de Lera, C. Rovira, J. Farrés, I. Fita, and X. Parés. Structural basis for the high all-trans-retinaldehyde reductase activity of the tumor marker AKR1B10. *Proc Natl Acad Sci U S A*, 104(52):20764–20769, 2007.

[93] M. P. Gaub, Y. Lutz, N. B. Ghyselinck, I. Scheuer, V. Pfister, P. Chambon, and C. Rochette-Egly. Nuclear detection of cellular retinoic acid binding proteins I and II with new antibodies. *J Histochem Cytochem*, 46(10):1103–1111, 1998.

[94] K. Georgas, B. Rumballe, L. Wilkinson, H. S. Chiu, E. Lesieur, T. Gilbert, and M. H. Little. Use of dual section mRNA in situ hybridisation/immunohistochemistry to clarify gene expression patterns during the early stages of nephron development in the embryo and in the mature nephron of the adult mouse kidney. *Histochem Cell Biol*, 130(5):927–942, 2008.

[95] P. Germain, J. Iyer, C. Zechel, and H. Gronemeyer. Co-regulator recruitment and the mechanism of retinoic acid receptor synergy. *Nature*, 415(6868):187–192, 2002.

[96] S. N. Gershoff and R. B. McGandy. The effects of vitamin A-deficient diets containing lactose in producing bladder calculi and tumors in rats. *Am J Clin Nutr*, 34(4):483–489, 1981.

[97] N. B. Ghyselinck, C. Bavik, V. Sapin, M. Mark, D. Bonnier, C. Hindelang, A. Dierich, C. B. Nilsson, H. Hakansson, P. Sauvant, V. Azais-Braesco, M. Frasson, S. Picaud, and P. Chambon. Cellular retinol-binding protein I is essential for vitamin A homeostasis. *EMBO J*, 18(18):4903–4914, 1999.

[98] N. B. Ghyselinck, V. Dup*é*, A. Dierich, N. Messaddeq, J. M. Garnier, C. Rochette-Egly, P. Chambon, and M. Mark. Role of the retinoic acid receptor beta (RARbeta) during mouse development. *Int J Dev Biol*, 41(3):425–447, 1997.

[99] V. Giguère, S. Lyn, P. Yip, C. H. Siu, and S. Amin. Molecular cloning of cDNA encoding a second cellular retinoic acid-binding protein. *Proc Natl Acad Sci U S A*, 87(16):6233–6237, 1990.

[100] V. Giguère, E. S. Ong, P. Segui, and R. M. Evans. Identification of a receptor for the morphogen retinoic acid. *Nature*, 330(6149):624–629, 1987.

[101] M. J. Gijbels, F. van der Ham, A. M. van Bennekum, H. F. Hendriks, and P. J. Roholl. Alterations in cytokeratin expression precede histological changes in epithelia of vitamin A-deficient rats. *Cell Tissue Res*, 268(1):197–203, 1992.

[102] T. Gilbert and C. Merlet-B*é*nichou. Retinoids and nephron mass control. *Pediatr Nephrol*, 14(12):1137–1144, 2000.

[103] R. Girgert, M. Martin, J. Kruegel, N. Miosge, J. Temme, B. Eckes, G.-A. M*ü*ller, and O. Gross. Integrin $\alpha$2-deficient mice provide insights into specific functions of collagen receptors in the kidney. *Fibrogenesis Tissue Repair*, 3:19, 2010.

[104] C. K. Glass and M. G. Rosenfeld. The coregulator exchange in transcriptional functions of nuclear receptors. *Genes Dev*, 14(2):121–141, 2000.

[105] M. Goel and W. P. Schilling. Role of trpc3 channels in atp-induced ca2+ signaling in principal cells of the inner medullary collecting duct. *Am J Physiol Renal Physiol*, 299(1):F225–F233, 2010.

[106] H. Goldblatt and M. Benischek. Vitamin A deficiency and metaplasia. *J Exp Med*, 46(5):699–707, 1927.

[107] M. Gonz*á*lez, L. A. Bagatolli, I. Echabe, J. L. Arrondo, C. E. Argaraña, C. R. Cantor, and G. D. Fidelio. Interaction of biotin with streptavidin. Thermostability and conformational changes upon binding. *J Biol Chem*, 272(17):11288–11294, 1997.

[108] D. W. Goodman, H. S. Huang, and T. Shiratori. Tissue distribution and metabolism of newly absorbed vitamin A in the rat. *J Lipid Res*, 6:390–396, 1965.

[109] P. Gorry, T. Lufkin, A. Dierich, C. Rochette-Egly, D. D*é*cimo, P. Dollé, M. Mark, B. Durand, and P. Chambon. The cellular retinoic acid binding protein I is dispensable. *Proc Natl Acad Sci U S A*, 91(19):9032–9036, 1994.

[110] S. E. Gould, M. Day, S. S. Jones, and H. Dorai. BMP-7 regulates chemokine, cytokine, and hemodynamic gene expression in proximal tubule cells. *Kidney Int*, 61(1):51–60, 2002.

[111] F. Grases, R. Garcia-Gonzalez, C. Genestar, J. J. Torres, and J. G. March. Vitamin A and urolithiasis. *Clin Chim Acta*, 269(2):147–157, 1998.

[112] F. Gr*ü*n, Y. Hirose, S. Kawauchi, T. Ogura, and K. Umesono. Aldehyde dehydrogenase 6, a cytosolic retinaldehyde dehydrogenase prominently expressed in sensory neuroepithelia during development. *J Biol Chem*, 275(52):41210–41218, 2000.

[113] H. N. Green and E. Mellanby. Vitamin A as an anti-infective agent. *Br Med J*, 2(3537):691–696, 1928.

[114] H. Gronemeyer, J. A. Gustafsson, and V. Laudet. Principles for modulation of the nuclear receptor superfamily. *Nat Rev Drug Discov*, 3(11):950–964, 2004.

[115] B. M. Gumbiner. Cell adhesion: the molecular basis of tissue architecture and morphogenesis. *Cell*, 84(3):345–357, 1996.

[116] A. L. Gustafson, M. Donovan, E. Annerwall, L. Dencker, and U. Eriksson. Nuclear import of cellular retinoic acid-binding protein type I in mouse embryonic cells. *Mech Dev*, 58(1-2):27–38, 1996.

[117] F. Haeseleer, J. Huang, L. Lebioda, J. C. Saari, and K. Palczewski. Molecular characterization of a novel short-chain dehydrogenase/reductase that reduces all-trans-retinal. *J Biol Chem*, 273(34):21790–21799, 1998.

[118] R. J. Haselbeck and G. Duester. Regional restriction of alcohol/retinol dehydrogenases along the mouse gastrointestinal epithelium. *Alcohol Clin Exp Res*, 21(8):1484–1490, 1997.

[119] J.-O. H*öö*g and L. J. *Ö*stberg. Mammalian alcohol dehydrogenases - A comparative investigation at gene and protein levels. *Chem Biol Interact*, 191:2–7, 2011.

[120] F. W. Heaton, J. S. Lowe, and R. A. Morton. Aspects of vitamin A deficiency in the rat. *Biochem J*, 67(2):208–215, 1957.

[121] J. Hess, P. Angel, and M. Schorpp-Kistner. AP-1 subunits: quarrel and harmony among siblings. *J Cell Sci*, 117(Pt 25):5965–5973, 2004.

[122] C. Higgins. Production and solution of urinary calculi. *J Am Med Assoc*, 104(15):1296–1299, 1935.

[123] J. D. Hoffert, B. W. M. van Balkom, C.-L. Chou, and M. A. Knepper. Application of difference gel electrophoresis to the identification of inner medullary collecting duct proteins. *Am J Physiol Renal Physiol*, 286(1):F170–F179, 2004.

[124] L. M. Hoffman, K. Garcha, K. Karamboulas, M. F. Cowan, L. M. Drysdale, W. A. Horton, and T. M. Underhill. Bmp action in skeletogenesis involves attenuation of retinoid signaling. *J Cell Biol*, 174(1):101–113, 2006.

[125] D. Hopwood. *Theory and practice of histological techniques*, chapter 5. Churchill Livingstone, 5th edition, 2002.

[126] D. W. Huang, B. T. Sherman, and R. A. Lempicki. Systematic and integrative analysis of large gene lists using DAVID bioinformatics resources. *Nat Protoc*, 4(1):44–57, 2009.

[127] International Union of Pure and Applied Chemistry - International Union of Biochemistry (IUPAC-IUB). Nomenclature of retinoids. Recommendations 1981. *Eur J Biochem*, 129(1):1–5, 1982.

[128] R. A. Irizarry, B. Hobbs, F. Collin, Y. D. Beazer-Barclay, K. J. Antonellis, U. Scherf, and T. P. Speed. Exploration, normalization, and summaries of high density oligonucleotide array probe level data. *Biostatistics*, 4(2):249–264, 2003.

[129] A. Isken, M. Golczak, V. Oberhauser, S. Hunzelmann, W. Driever, Y. Imanishi, K. Palczewski, and J. von Lintig. RBP4 disrupts vitamin A uptake homeostasis in a STRA6-deficient animal model for Matthew-Wood syndrome. *Cell Metab*, 7(3):258–268, 2008.

[130] L. Ivanova, M. J. Butt, and D. G. Matsell. Mesenchymal transition in kidney collecting duct epithelial cells. *Am J Physiol Renal Physiol*, 294(5):F1238–F1248, 2008.

[131] S. Jacobs, D. C. Lie, K. L. DeCicco, Y. Shi, L. M. DeLuca, F. H. Gage, and R. M. Evans. Retinoic acid is required early during adult neurogenesis in the dentate gyrus. *Proc Natl Acad Sci U S A*, 103(10):3902–3907, 2006.

[132] N. Jena, C. Martín-Seisdedos, P. McCue, and C. M. Croce. BMP7 null mutation in mice: developmental defects in skeleton, kidney, and eye. *Exp Cell Res*, 230(1):28–37, 1997.

[133] K. V. John, M. R. Lakshmanan, and H. R. Cama. Preparation, properties and metabolism of 5,6-monoepoxyretinoic acid. *Biochem J*, 103(2):539–543, 1967.

[134] A. T. Johnson, E. S. Klein, S. J. Gillett, L. Wang, T. K. Song, M. E. Pino, and R. A. Chandraratna. Synthesis and characterization of a highly potent and effective antagonist of retinoic acid receptors. *J Med Chem*, 38(24):4764–4767, 1995.

[135] R. K. Kancha and A. Anasuya. Contribution of vitamin A deficiency to calculogenic risk factors of urine: studies in children. *Biochem Med Metab Biol*, 47(1):1–9, 1992.

[136] M. A. Kane, F. V. Bright, and J. L. Napoli. Binding affinities of CRBPI and CRBPII for 9-cis-retinoids. *Biochim Biophys Acta*, 1810(5):514–518, 2011.

[137] M. A. Kane, N. Chen, S. Sparks, and J. L. Napoli. Quantification of endogenous retinoic acid in limited biological samples by LC/MS/MS. *Biochem J*, 388(Pt 1):363–369, 2005.

[138] M. A. Kane, A. E. Folias, A. Pingitore, M. Perri, K. M. Obrochta, C. R. Krois, E. Cione, J. Y. Ryu, and J. L. Napoli. Identification of 9-cis-retinoic acid as a pancreas-specific autacoid that attenuates glucose-stimulated insulin secretion. *Proc Natl Acad Sci U S A*, 107(50):21884–21889, 2010.

[139] M. A. Kane, A. E. Folias, C. Wang, and J. L. Napoli. Quantitative profiling of endogenous retinoic acid in vivo and in vitro by tandem mass spectrometry. *Anal Chem*, 80(5):1702–1708, 2008.

[140] Y. S. Kanwar, A. Kumar, Q. Yang, Y. Tian, J. Wada, N. Kashihara, and E. I. Wallner. Tubulointerstitial nephritis antigen: an extracellular matrix protein that selectively regulates tubulogenesis vs. glomerulogenesis during mammalian renal development. *Proc Natl Acad Sci U S A*, 96(20):11323–11328, 1999.

[141] R. E. Kares, D. C. Manolescu, L. Lakhal-Chaieb, A. Montpetit, Z. Zhang, P. V. Bhat, and P. Goodyer. A human ALDH1A2 gene variant is associated with in-

creased newborn kidney size and serum retinoic acid. *Kidney Int*, 78(1):96–102, 2010.

[142] P. Kastner, J. M. Grondona, M. Mark, A. Gansmuller, M. LeMeur, D. Decimo, J. L. Vonesch, P. Dollé, and P. Chambon. Genetic analysis of RXR alpha developmental function: convergence of RXR and RAR signaling pathways in heart and eye morphogenesis. *Cell*, 78(6):987–1003, 1994.

[143] P. Kastner, M. Mark, N. Ghyselinck, W. Krezel, V. Dupé, J. M. Grondona, and P. Chambon. Genetic evidence that the retinoid signal is transduced by heterodimeric RXR/RAR functional units during mouse development. *Development*, 124(2):313–326, 1997.

[144] P. Kastner, M. Mark, M. Leid, A. Gansmuller, W. Chin, J. M. Grondona, D. Dcimo, W. Krezel, A. Dierich, and P. Chambon. Abnormal spermatogenesis in RXR beta mutant mice. *Genes Dev*, 10(1):80–92, 1996.

[145] P. Kastner, N. Messaddeq, M. Mark, O. Wendling, J. M. Grondona, S. Ward, N. Ghyselinck, and P. Chambon. Vitamin A deficiency and mutations of RXRalpha, RXRbeta and RARalpha lead to early differentiation of embryonic ventricular cardiomyocytes. *Development*, 124(23):4749–4758, 1997.

[146] R. Kawaguchi, J. Yu, J. Honda, J. Hu, J. Whitelegge, P. Ping, P. Wiita, D. Bok, and H. Sun. A membrane receptor for retinol binding protein mediates cellular uptake of vitamin A. *Science*, 315(5813):820–825, 2007.

[147] S. R. Khan and D. J. Kok. Modulators of urinary stone formation. *Front Biosci*, 9:1450–1482, 2004.

[148] Y. H. Kim, J. Kim, A. S. Verkman, and K. M. Madsen. Increased expression of $H^+$-ATPase in inner medullary collecting duct of aquaporin-1-deficient mice. *Am J Physiol Renal Physiol*, 285(3):F550–F557, 2003.

[149] I. Kiss, R. Ruhl, E. Szegezdi, B. Fritzsche, B. Toth, J. Pongracz, T. Perlmann, L. Fesus, and Z. Szondy. Retinoid receptor-activating ligands are produced within

the mouse thymus during postnatal development. *Eur J Immunol*, 38(1):147–155, 2008.

[150] R. Kothary, S. Clapoff, S. Darling, M. D. Perry, L. A. Moran, and J. Rossant. Inducible expression of an hsp68-lacZ hybrid gene in transgenic mice. *Development*, 105(4):707–714, 1989.

[151] J. Kovacikova, C. Winter, D. Loffing-Cueni, J. Loffing, K. E. Finberg, R. P. Lifton, E. Hummler, B. Rossier, and C. A. Wagner. The connecting tubule is the main site of the furosemide-induced urinary acidification by the vacuolar $H^+$-ATPase. *Kidney Int*, 70(10):1706–1716, 2006.

[152] J. A. Kreidberg and J. M. Symons. Integrins in kidney development, function, and disease. *Am J Physiol Renal Physiol*, 279(2):F233–F242, 2000.

[153] M. Kreutz, J. Fritsche, U. Ackermann, S. W. Krause, and R. Andreesen. Retinoic acid inhibits monocyte to macrophage survival and differentiation. *Blood*, 91(12):4796–4802, 1998.

[154] W. Krezel, V. Dup*é*, M. Mark, A. Dierich, P. Kastner, and P. Chambon. RXR gamma null mice are apparently normal and compound RXR alpha$^{+/-}$ / RXR beta$^{-/-}$ / RXR gamma$^{-/-}$ mutant mice are viable. *Proc Natl Acad Sci U S A*, 93(17):9010–9014, 1996.

[155] A. Krust, P. Kastner, M. Petkovich, A. Zelent, and P. Chambon. A third human retinoic acid receptor, hRAR-gamma. *Proc Natl Acad Sci U S A*, 86(14):5310–5314, 1989.

[156] S. Kumar, L. L. Sandell, P. A. Trainor, F. Koentgen, and G. Duester. Alcohol and aldehyde dehydrogenases: retinoid metabolic effects in mouse knockout models. *Biochim Biophys Acta*, 1821(1):198–205, 2012.

[157] S. B. Kurlandsky, M. V. Gamble, R. Ramakrishnan, and W. S. Blaner. Plasma delivery of retinoic acid to tissues in the rat. *J Biol Chem*, 270(30):17850–17857, 1995.

[158] R. Kurokawa, J. DiRenzo, M. Boehm, J. Sugarman, B. Gloss, M. G. Rosenfeld, R. A. Heyman, and C. K. Glass. Regulation of retinoid signalling by receptor polarity and allosteric control of ligand binding. *Nature*, 371(6497):528–531, 1994.

[159] S. Lalev*é*e, Y. N. Anno, A. Chatagnon, E. Samarut, O. Poch, V. Laudet, G. Benoit, O. Lecompte, and C. Rochette-Egly. Genome-wide in silico identification of new conserved and functional retinoic acid receptors response elements (directs repeats separated by 5bp). *J Biol Chem*, 286(38):33322–33334, 2011.

[160] C. Lampron, C. Rochette-Egly, P. Gorry, P. Doll*é*, M. Mark, T. Lufkin, M. LeMeur, and P. Chambon. Mice deficient in cellular retinoic acid binding protein II (CRABPII) or in both CRABPI and CRABPII are essentially normal. *Development*, 121(2):539–548, 1995.

[161] N. Lassen, J. B. Bateman, T. Estey, J. R. Kuszak, D. W. Nees, J. Piatigorsky, G. Duester, B. J. Day, J. Huang, L. M. Hines, and V. Vasiliou. Multiple and additive functions of ALDH3A1 and ALDH1A1: cataract phenotype and ocular oxidative damage in Aldh3a1(-/-)/Aldh1a1(-/-) knock-out mice. *J Biol Chem*, 282(35):25668–25676, 2007.

[162] D. C. Lee, K. W. Chan, and S. Y. Chan. RET receptor tyrosine kinase isoforms in kidney function and disease. *Oncogene*, 21(36):5582–5592, 2002.

[163] M. O. Lee, C. L. Manthey, and N. E. Sladek. Identification of mouse liver aldehyde dehydrogenases that catalyze the oxidation of retinaldehyde to retinoic acid. *Biochem Pharmacol*, 42(6):1279–1285, 1991.

[164] P. Lefebvre, Y. Benomar, and B. Staels. Retinoid X receptors: common heterodimerization partners with distinct functions. *Trends Endocrinol Metab*, 21(11):676–683, 2010.

[165] J. M. Lehmann, X. K. Zhang, and M. Pfahl. RAR gamma 2 expression is regulated

through a retinoic acid response element embedded in Sp1 sites. *Mol Cell Biol*, 12(7):2976–2985, 1992.

[166] Z. Lei, W. Chen, M. Zhang, and J. L. Napoli. Reduction of all-trans-retinal in the mouse liver peroxisome fraction by the short-chain dehydrogenase/reductase RRD: induction by the PPAR alpha ligand clofibrate. *Biochemistry*, 42(14):4190–4196, 2003.

[167] M. Leid, P. Kastner, and P. Chambon. Multiplicity generates diversity in the retinoic acid signalling pathways. *Trends Biochem Sci*, 17(10):427–433, 1992.

[168] M. Leid, P. Kastner, R. Lyons, H. Nakshatri, M. Saunders, T. Zacharewski, J. Y. Chen, A. Staub, J. M. Garnier, and S. Mader. Purification, cloning, and RXR identity of the HeLa cell factor with which RAR or TR heterodimerizes to bind target sequences efficiently. *Cell*, 68(2):377–395, 1992.

[169] M. Leli*è*vre-P*é*gorier, J. Vilar, M. L. Ferrier, E. Moreau, N. Freund, T. Gilbert, and C. Merlet-Merlet-B*é*nichou. Mild vitamin A deficiency leads to inborn nephron deficit in the rat. *Kidney Int*, 54(5):1455–1462, 1998.

[170] M. A. Leo, S. Iida, and C. S. Lieber. Retinoic acid metabolism by a system reconstituted with cytochrome P-450. *Arch Biochem Biophys*, 234(1):305–312, 1984.

[171] P. Leroy, H. Nakshatri, and P. Chambon. Mouse retinoic acid receptor alpha 2 isoform is transcribed from a promoter that contains a retinoic acid response element. *Proc Natl Acad Sci U S A*, 88(22):10138–10142, 1991.

[172] Z. B. Levashova, N. Sharma, O. A. Timofeeva, J. S. Dome, and A. O. Perantoni. ELR$^+$-CXC chemokines and their receptors in early metanephric development. *J Am Soc Nephrol*, 18(8):2359–2370, 2007.

[173] A. A. Levin, L. J. Sturzenbecker, S. Kazmer, T. Bosakowski, C. Huselton, G. Allenby, J. Speck, C. Kratzeisen, M. Rosenberger, and A. Lovey. 9-cis retinoic

acid stereoisomer binds and activates the nuclear receptor RXR alpha. *Nature*, 355(6358):359–361, 1992.

[174] A. Levitzki, M. Willingham, and I. Pastan. Evidence for participation of transglutaminase in receptor-mediated endocytosis. *Proc Natl Acad Sci U S A*, 77(5):2706–2710, 1980.

[175] D. Li, K. Mukai, T. Suzuki, R. Suzuki, S. Yamashita, F. Mitani, and M. Suematsu. Adrenocortical zonation factor 1 is a novel matricellular protein promoting integrin-mediated adhesion of adrenocortical and vascular smooth muscle cells. *FEBS J*, 274(10):2506–2522, 2007.

[176] S. Liebler, B. Uberschar, H. Kubert, S. Brems, A. Schnitger, M. Tsukada, C. C. Zouboulis, E. Ritz, and J. Wagner. The renal retinoid system: time-dependent activation in experimental glomerulonephritis. *Am J Physiol Renal Physiol*, 286(3):F458–F465, 2004.

[177] M. Lin, M. Zhang, M. Abraham, S. M. Smith, and J. L. Napoli. Mouse retinal dehydrogenase 4 (RALDH4), molecular cloning, cellular expression, and activity in 9-cis-retinoic acid biosynthesis in intact cells. *J Biol Chem*, 278(11):9856–9861, 2003.

[178] K. J. Livak and T. D. Schmittgen. Analysis of relative gene expression data using real-time quantitative PCR and the 2(-Delta Delta C(T)) Method. *Methods*, 25(4):402–408, 2001.

[179] S. H. Lo, Q. C. Yu, L. Degenstein, L. B. Chen, and E. Fuchs. Progressive kidney degeneration in mice lacking tensin. *J Cell Biol*, 136(6):1349–1361, 1997.

[180] M. E. Loewen and G. W. Forsyth. Structure and function of CLCA proteins. *Physiol Rev*, 85(3):1061–1092, 2005.

[181] J. Loffing, D. Loffing-Cueni, V. Valderrabano, L. Kl*ä*usli, S. C. Hebert, B. C. Rossier, J. G. Hoenderop, R. J. Bindels, and B. Kaissling. Distribution of trans-

cellular calcium and sodium transport pathways along mouse distal nephron. *Am J Physiol Renal Physiol*, 281(6):F1021–F1027, 2001.

[182] D. Lohnes, P. Kastner, A. Dierich, M. Mark, M. LeMeur, and P. Chambon. Function of retinoic acid receptor gamma in the mouse. *Cell*, 73(4):643–658, 1993.

[183] T. Lufkin, D. Lohnes, M. Mark, A. Dierich, P. Gorry, M. P. Gaub, M. LeMeur, and P. Chambon. High postnatal lethality and testis degeneration in retinoic acid receptor alpha mutant mice. *Proc Natl Acad Sci U S A*, 90(15):7225–7229, 1993.

[184] J. Luo, P. Pasceri, R. A. Conlon, J. Rossant, and V. Giguère. Mice lacking all isoforms of retinoic acid receptor beta develop normally and are susceptible to the teratogenic effects of retinoic acid. *Mech Dev*, 53(1):61–71, 1995.

[185] W. Ma, K. Rogers, B. Zbar, and L. Schmidt. Effects of different fixatives on beta-galactosidase activity. *J Histochem Cytochem*, 50(10):1421–1424, 2002.

[186] G. MacLean, S. Abu-Abed, P. Dollé, A. Tahayato, P. Chambon, and M. Petkovich. Cloning of a novel retinoic-acid metabolizing cytochrome P450, Cyp26B1, and comparative expression analysis with Cyp26A1 during early murine development. *Mech Dev*, 107(1-2):195–201, 2001.

[187] G. MacLean, H. Li, D. Metzger, P. Chambon, and M. Petkovich. Apoptotic extinction of germ cells in testes of Cyp26b1 knockout mice. *Endocrinology*, 148(10):4560–4567, 2007.

[188] K. Maeda, K. T. Uysal, L. Makowski, C. Z. Görgün, G. Atsumi, R. A. Parker, J. Brüning, A. V. Hertzel, D. A. Bernlohr, and G. S. Hotamisligil. Role of the fatty acid binding protein mal1 in obesity and insulin resistance. *Diabetes*, 52(2):300–307, 2003.

[189] L. Mahant and H. D. Eaton. Effect of chronic hypovitaminosis A on water metabolism in the weanling rat. *J Nutr*, 106(12):1817–1826, 1976.

[190] D. J. Mangelsdorf, E. S. Ong, J. A. Dyck, and R. M. Evans. Nuclear receptor that identifies a novel retinoic acid response pathway. *Nature*, 345(6272):224–229, 1990.

[191] D. J. Mangelsdorf, K. Umesono, S. A. Kliewer, U. Borgmeyer, E. S. Ong, and R. M. Evans. A direct repeat in the cellular retinol-binding protein type II gene confers differential regulation by RXR and RAR. *Cell*, 66(3):555–561, 1991.

[192] M. P. Marin, G. Esteban-Pretel, R. Alonso, Y. Sado, T. Barber, J. Renau-Piqueras, and J. Timoneda. Vitamin A deficiency alters the structure and collagen IV composition of rat renal basement membranes. *J Nutr*, 135(4):695–701, 2005.

[193] M. Mark, N. B. Ghyselinck, and P. Chambon. Function of retinoid nuclear receptors: lessons from genetic and pharmacological dissections of the retinoic acid signaling pathway during mouse embryogenesis. *Annu Rev Pharmacol Toxicol*, 46:451–480, 2006.

[194] A. Marlier and T. Gilbert. Expression of retinoic acid-synthesizing and -metabolizing enzymes during nephrogenesis in the rat. *Gene Expr Patterns*, 5(2):179–185, 2004.

[195] M. Masuda, H. Yamamoto, M. Kozai, S. Tanaka, M. Ishiguro, Y. Takei, O. Nakahashi, S. Ikeda, T. Uebanso, Y. Taketani, H. Segawa, K. Miyamoto, and E. Takeda. Regulation of renal sodium-dependent phosphate co-transporter genes (Npt2a and Npt2c) by all-trans-retinoic acid and its receptors. *Biochem J*, 429(3):583–592, 2010.

[196] N. Matsukawa, W. J. Grzesik, N. Takahashi, K. N. Pandey, S. Pang, M. Yamauchi, and O. Smithies. The natriuretic peptide clearance receptor locally modulates the physiological effects of the natriuretic peptide system. *Proc Natl Acad Sci U S A*, 96(13):7403–7408, 1999.

[197] Y. Matsushima, E. Kawachi, H. Tanaka, H. Kagechika, Y. Hashimoto, and K. Shudo. Differentiation-inducing activity of retinoic acid isomers and their oxi-

dized analogs on human promyelocytic leukemia HL-60 cells. *Biochem Biophys Res Commun*, 189(2):1136–1142, 1992.

[198] N. Matt, V. Dupé, J.-M. Garnier, C. Dennefeld, P. Chambon, M. Mark, and N. B. Ghyselinck. Retinoic acid-dependent eye morphogenesis is orchestrated by neural crest cells. *Development*, 132(21):4789–4800, 2005.

[199] N. Matt, C. K. Schmidt, V. Dupé, C. Dennefeld, H. Nau, P. Chambon, M. Mark, and N. B. Ghyselinck. Contribution of cellular retinol-binding protein type 1 to retinol metabolism during mouse development. *Dev Dyn*, 233(1):167–176, 2005.

[200] P. McCaffery, M. O. Lee, M. A. Wagner, N. E. Sladek, and U. C. Dräger. Asymmetrical retinoic acid synthesis in the dorsoventral axis of the retina. *Development*, 115(2):371–382, 1992.

[201] P. T. McCarthy and L. R. Cerecedo. Vitamin A deficiency in the mouse. *J Nutr*, 46(3):361–376, 1952.

[202] A. M. McCormick, K. D. Kroll, and J. L. Napoli. 13-cis-retinoic acid metabolism in vivo. The major tissue metabolites in the rat have the all-trans configuration. *Biochemistry*, 22(16):3933–3940, 1983.

[203] N. J. McKenna and B. W. O'Malley. Combinatorial control of gene expression by nuclear receptors and coregulators. *Cell*, 108(4):465–474, 2002.

[204] C. Mendelsohn, E. Batourina, S. Fung, T. Gilbert, and J. Dodd. Stromal cells mediate retinoid-dependent functions essential for renal development. *Development*, 126(6):1139–1148, 1999.

[205] C. Mendelsohn, S. Larkin, M. Mark, M. LeMeur, J. Clifford, A. Zelent, and P. Chambon. RAR beta isoforms: distinct transcriptional control by retinoic acid and specific spatial patterns of promoter activity during mouse embryonic development. *Mech Dev*, 45(3):227–241, 1994.

[206] C. Mendelsohn, D. Lohnes, D. Decimo, T. Lufkin, M. LeMeur, P. Chambon, and M. Mark. Function of the retinoic acid receptors (RARs) during development (II). Multiple abnormalities at various stages of organogenesis in RAR double mutants. *Development*, 120(10):2749–2771, 1994.

[207] C. Mendelsohn, E. Ruberte, M. LeMeur, G. Morriss-Kay, and P. Chambon. Developmental analysis of the retinoic acid-inducible RAR-beta 2 promoter in transgenic animals. *Development*, 113(3):723–734, 1991.

[208] F. A. Mic, R. J. Haselbeck, A. E. Cuenca, and G. Duester. Novel retinoic acid generating activities in the neural tube and heart identified by conditional rescue of Raldh2 null mutant mice. *Development*, 129(9):2271–2282, 2002.

[209] F. A. Mic, A. Molotkov, D. M. Benbrook, and G. Duester. Retinoid activation of retinoic acid receptor but not retinoid X receptor is sufficient to rescue lethal defect in retinoic acid synthesis. *Proc Natl Acad Sci U S A*, 100(12):7135–7140, 2003.

[210] F. A. Mic, A. Molotkov, X. Fan, A. E. Cuenca, and G. Duester. RALDH3, a retinaldehyde dehydrogenase that generates retinoic acid, is expressed in the ventral retina, otic vesicle and olfactory pit during mouse development. *Mech Dev*, 97(1-2):227–230, 2000.

[211] F. A. Mic, A. Molotkov, N. Molotkova, and G. Duester. Raldh2 expression in optic vesicle generates a retinoic acid signal needed for invagination of retina during optic cup formation. *Dev Dyn*, 231(2):270–277, 2004.

[212] O. Michos. Kidney development: from ureteric bud formation to branching morphogenesis. *Curr Opin Genet Dev*, 19(5):484–490, 2009.

[213] K. D. Miller. *Theory and practice of histological techniques*, chapter 20. Churchill Livingstone, 5th edition, 2002.

[214] A. Molotkov, L. Deltour, M. H. Foglio, A. E. Cuenca, and G. Duester. Distinct retinoid metabolic functions for alcohol dehydrogenase genes Adh1 and Adh4 in

protection against vitamin A toxicity or deficiency revealed in double null mutant mice. *J Biol Chem*, 277(16):13804–13811, 2002.

[215] A. Molotkov, X. Fan, L. Deltour, M. H. Foglio, S. Martras, J. Farrés, X. Parés, and G. Duester. Stimulation of retinoic acid production and growth by ubiquitously expressed alcohol dehydrogenase Adh3. *Proc Natl Acad Sci U S A*, 99(8):5337–5342, 2002.

[216] A. Molotkov, N. Molotkova, and G. Duester. Retinoic acid guides eye morphogenetic movements via paracrine signaling but is unnecessary for retinal dorsoventral patterning. *Development*, 133(10):1901–1910, 2006.

[217] E. Moreau, J. Vilar, M. Lelièvre-Pégorier, C. Merlet-Bénichou, and T. Gilbert. Regulation of c-ret expression by retinoic acid in rat metanephros: implication in nephron mass control. *Am J Physiol*, 275(6 Pt 2):F938–F945, 1998.

[218] J. E. Morley, D. A. Damassa, J. Gordon, A. E. Pekary, and J. M. Hershman. Thyroid function and vitamin A deficiency. *Life Sci*, 22(21):1901–1905, 1978.

[219] J. S. Munday, H. McKinnon, D. Aberdein, M. G. Collett, K. Parton, and K. G. Thompson. Cystitis, pyelonephritis, and urolithiasis in rats accidentally fed a diet deficient in vitamin A. *J Am Assoc Lab Anim Sci*, 48(6):790–794, 2009.

[220] L. D. Nadauld, D. N. Shelton, S. Chidester, H. J. Yost, and D. A. Jones. The zebrafish retinol dehydrogenase, rdh1l, is essential for intestinal development and is regulated by the tumor suppressor adenomatous polyposis coli. *J Biol Chem*, 280(34):30490–30495, 2005.

[221] S. Nagpal, S. Friant, H. Nakshatri, and P. Chambon. RARs and RXRs: evidence for two autonomous transactivation functions (AF-1 and AF-2) and heterodimerization in vivo. *EMBO J*, 12(6):2349–2360, 1993.

[222] N. Nanda, S. E. Iismaa, W. A. Owens, A. Husain, F. Mackay, and R. M. Graham. Targeted inactivation of Gh/tissue transglutaminase II. *J Biol Chem*, 276(23):20673–20678, 2001.

[223] J. L. Napoli. A gene knockout corroborates the integral function of cellular retinol-binding protein in retinoid metabolism. *Nutr Rev*, 58(8):230–236, 2000.

[224] J. L. Napoli. Physiological insights into all-trans-retinoic acid biosynthesis. *Biochim Biophys Acta*, 1821(1):152–167, 2012.

[225] A. M. Nelson, W. Zhao, K. L. Gilliland, A. L. Zaenglein, W. Liu, and D. M. Thiboutot. Neutrophil gelatinase-associated lipocalin mediates 13-cis retinoic acid-induced apoptosis of human sebaceous gland cells. *J Clin Invest*, 118(4):1468–1478, 2008.

[226] D. R. Nelson. A second CYP26 P450 in humans and zebrafish: CYP26B1. *Arch Biochem Biophys*, 371(2):345–347, 1999.

[227] W. Neuhofer and F.-X. Beck. Survival in hostile environments: strategies of renal medullary cells. *Physiology (Bethesda)*, 21:171–180, 2006.

[228] M. E. Newcomer and D. E. Ong. Plasma retinol binding protein: structure and function of the prototypic lipocalin. *Biochim Biophys Acta*, 1482(1-2):57–64, 2000.

[229] R. C. Nicholson, S. Mader, S. Nagpal, M. Leid, C. Rochette-Egly, and P. Chambon. Negative regulation of the rat stromelysin gene promoter by retinoic acid is mediated by an AP1 binding site. *EMBO J*, 9(13):4443–4454, 1990.

[230] K. Niederreither, S. Abu-Abed, B. Schuhbaur, M. Petkovich, P. Chambon, and P. Dollé. Genetic evidence that oxidative derivatives of retinoic acid are not involved in retinoid signaling during mouse development. *Nat Genet*, 31(1):84–88, 2002.

[231] K. Niederreither and P. Dollé. Retinoic acid in development: towards an integrated view. *Nat Rev Genet*, 9(7):541–553, 2008.

[232] K. Niederreither, V. Fraulob, J. M. Garnier, P. Chambon, and P. Dollé. Differential

expression of retinoic acid-synthesizing (RALDH) enzymes during fetal development and organ differentiation in the mouse. *Mech Dev*, 110(1-2):165–171, 2002.

[233] K. Niederreither, P. McCaffery, U. C. Dräger, P. Chambon, and P. Dollé. Restricted expression and retinoic acid-induced downregulation of the retinaldehyde dehydrogenase type 2 (RALDH-2) gene during mouse development. *Mech Dev*, 62(1):67–78, 1997.

[234] K. Niederreither, V. Subbarayan, P. Dollé, and P. Chambon. Embryonic retinoic acid synthesis is essential for early mouse post-implantation development. *Nat Genet*, 21(4):444–448, 1999.

[235] K. Niederreither, J. Vermot, V. Fraulob, P. Chambon, and P. Dollé. Retinaldehyde dehydrogenase 2 (RALDH2)-independent patterns of retinoic acid synthesis in the mouse embryo. *Proc Natl Acad Sci U S A*, 99(25):16111–16116, 2002.

[236] N. Noy. Retinoid-binding proteins: mediators of retinoid action. *Biochem J*, 348 Pt 3:481–495, 2000.

[237] D. E. Ong. A novel retinol-binding protein from rat. Purification and partial characterization. *J Biol Chem*, 259(3):1476–1482, 1984.

[238] D. E. Ong and F. Chytil. Retinoic acid-binding protein in rat tissue. Partial purification and comparison to rat tissue retinol-binding protein. *J Biol Chem*, 250(15):6113–6117, 1975.

[239] T. B. Osborne and L. B. Mendel. The incidence of phosphatic urinary calculi in rats fed on experimental rations. *JAMA*, LXIX:32–33, 1917.

[240] R. Padmanabhan. Retinoic acid-induced caudal regression syndrome in the mouse fetus. *Reprod Toxicol*, 12(2):139–151, 1998.

[241] K. Palczewski. Retinoids for treatment of retinal diseases. *Trends Pharmacol Sci*, 31(6):284–295, 2010.

[242] X. Par*é*s, J. Farr*é*s, N. Kedishvili, and G. Duester. Medium- and short-chain dehydrogenase/reductase gene and protein families: medium-chain and short-chain dehydrogenases/reductases in retinoid metabolism. *Cell Mol Life Sci*, 65(24):3936–3949, 2008.

[243] V. M. Paralkar, W. A. Grasser, A. L. Mansolf, A. P. Baumann, T. A. Owen, S. L. Smock, S. Martinovic, F. Borovecki, S. Vukicevic, H. Z. Ke, and D. D. Thompson. Regulation of BMP-7 expression by retinoic acid and prostaglandin E(2). *J Cell Physiol*, 190(2):207–217, 2002.

[244] F. Pasutto, H. Sticht, G. Hammersen, G. Gillessen-Kaesbach, D. R. Fitzpatrick, G. N*ü*rnberg, F. Brasch, H. Schirmer-Zimmermann, J. L. Tolmie, D. Chitayat, G. Houge, L. Fern*á*ndez-Mart*í*nez, S. Keating, G. Mortier, R. C. Hennekam, A. von der Wense, A. Slavotinek, P. Meinecke, P. Bitoun, C. Becker, P. N*ü*rnberg, A. Reis, and A. Rauch. Mutations in STRA6 cause a broad spectrum of malformations including anophthalmia, congenital heart defects, diaphragmatic hernia, alveolar capillary dysplasia, lung hypoplasia, and mental retardation. *Am J Hum Genet*, 80(3):550–560, 2007.

[245] G. Patrone, A. Puliti, R. Bocciardi, R. Ravazzolo, and G. Romeo. Sequence and characterisation of the RET proto-oncogene 5' flanking region: analysis of retinoic acid responsiveness at the transcriptional level. *FEBS Lett*, 419(1):76–82, 1997.

[246] P. A. Peterson, L. Rask, L. Ostberg, L. Andersson, F. Kamwendo, and H. Pertoft. Studies on the transport and cellular distribution of vitamin A in normal and vitamin A-deficient rats with special reference to the vitamin A-binding plasma protein. *J Biol Chem*, 248(11):4009–4022, 1973.

[247] M. Petkovich, N. J. Brand, A. Krust, and P. Chambon. A human retinoic acid receptor which belongs to the family of nuclear receptors. *Nature*, 330(6147):444–450, 1987.

[248] R. Piantedosi, N. Ghyselinck, W. S. Blaner, and S. Vogel. Cellular retinol-binding protein type III is needed for retinoid incorporation into milk. *J Biol Chem*, 280(25):24286–24292, 2005.

[249] K. Pino-Lagos, M. J. Benson, and R. J. Noelle. Retinoic acid in the immune system. *Ann N Y Acad Sci*, 1143:170–187, 2008.

[250] K. Pino-Lagos, Y. Guo, C. Brown, M. P. Alexander, R. Elgueta, K. A. Bennett, V. De Vries, E. Nowak, R. Blomhoff, S. Sockanathan, R. A. Chandraratna, E. Dmitrovsky, and R. J. Noelle. A retinoic acid-dependent checkpoint in the development of CD4+ T cell-mediated immunity. *J Exp Med*, 208(9):1767–1775, 2011.

[251] T. D. Piscione, T. Phan, and N. D. Rosenblum. BMP7 controls collecting tubule cell proliferation and apoptosis via Smad1-dependent and -independent pathways. *Am J Physiol Renal Physiol*, 280(1):F19–F33, 2001.

[252] S. Pradervand, H. Yasukawa, O. G. Muller, H. Kjekshus, T. Nakamura, T. R. St Amand, T. Yajima, K. Matsumura, H. Duplain, M. Iwatate, S. Woodard, T. Pedrazzini, J. Ross, D. Firsov, B. C. Rossier, M. Hoshijima, and K. R. Chien. Small proline-rich protein 1A is a gp130 pathway- and stress-inducible cardioprotective protein. *EMBO J*, 23(22):4517–4525, 2004.

[253] L. Quadro, W. S. Blaner, D. J. Salchow, S. Vogel, R. Piantedosi, P. Gouras, S. Freeman, M. P. Cosma, V. Colantuoni, and M. E. Gottesman. Impaired retinal function and vitamin A availability in mice lacking retinol-binding protein. *EMBO J*, 18(17):4633–4644, 1999.

[254] L. Quadro, L. Hamberger, M. E. Gottesman, F. Wang, V. Colantuoni, W. S. Blaner, and C. L. Mendelsohn. Pathways of vitamin A delivery to the embryo: insights from a new tunable model of embryonic vitamin A deficiency. *Endocrinology*, 146(10):4479–4490, 2005.

[255] J. Quinlan, F. Kaplan, N. Sweezey, and P. Goodyer. LGL1, a novel branching morphogen in developing kidney, is induced by retinoic acid. *Am J Physiol Renal Physiol*, 293(4):F987–F993, 2007.

[256] K. K. Ratnam, X. Feng, P. Y. Chuang, V. Verma, T.-C. Lu, J. Wang, Y. Jin, E. F. Farias, J. L. Napoli, N. Chen, L. Kaufman, T. Takano, V. D. D'Agati, P. E. Klotman, and J. C. He. Role of the retinoic acid receptor-$\alpha$ in HIV-associated nephropathy. *Kidney Int*, 79(6):624–634, 2011.

[257] M. I. Rauchman, S. K. Nigam, E. Delpire, and S. R. Gullans. An osmotically tolerant inner medullary collecting duct cell line from an SV40 transgenic mouse. *Am J Physiol*, 265(3 Pt 2):F416–F424, 1993.

[258] W. J. Ray, G. Bain, M. Yao, and D. I. Gottlieb. CYP26, a novel mammalian cytochrome P450, is induced by retinoic acid and defines a new family. *J Biol Chem*, 272(30):18702–18708, 1997.

[259] J. J. Repa, K. K. Hanson, and M. Clagett-Dame. All-trans-retinol is a ligand for the retinoic acid receptors. *Proc Natl Acad Sci U S A*, 90(15):7293–7297, 1993.

[260] J. J. Repa, L. A. Plum, P. K. Tadikonda, and M. Clagett-Dame. All-trans 3,4-didehydroretinoic acid equals all-trans retinoic acid in support of chick neuronal development. *FASEB J*, 10(9):1078–1084, 1996.

[261] M. Reynier. Pyrazole inhibition and kinetic studies of ethanol and retinol oxidation catalyzed by rat liver alcohol dehydrogenase. *Acta Chem Scand*, 23(4):1119–1129, 1969.

[262] K. Reynolds, E. Mezey, and A. Zimmer. Activity of the beta-retinoic acid receptor promoter in transgenic mice. *Mech Dev*, 36(1-2):15–29, 1991.

[263] M. Rieck, W. Meissner, S. Ries, S. M*ü*ller-Br*ü*sselbach, and R. M*ü*ller. Ligand-mediated regulation of peroxisome proliferator-activated receptor (PPAR) beta/delta: a comparative analysis of PPAR-selective agonists and all-trans retinoic acid. *Mol Pharmacol*, 74(5):1269–1277, 2008.

[264] C. Rochette-Egly and P. Germain. Dynamic and combinatorial control of gene expression by nuclear retinoic acid receptors (RARs). *Nucl Recept Signal*, 7:e005, 2009.

[265] A. C. Ross and R. Zolfaghari. Cytochrome p450s in the regulation of cellular retinoic acid metabolism. *Annu Rev Nutr*, 31:65–87, 2011.

[266] J. Rossant, R. Zirngibl, D. Cado, M. Shago, and V. Giguère. Expression of a retinoic acid response element-hsplacz transgene defines specific domains of transcriptional activity during mouse embryogenesis. *Genes Dev*, 5(8):1333–1344, 1991.

[267] C. Rosselot, L. Spraggon, I. Chia, E. Batourina, P. Riccio, B. Lu, K. Niederreither, P. Dollé, G. Duester, P. Chambon, F. Costantini, T. Gilbert, A. Molotkov, and C. Mendelsohn. Non-cell-autonomous retinoid signaling is crucial for renal development. *Development*, 137(2):283–292, 2010.

[268] M. H. Roudkenar, R. Halabian, P. Bahmani, A. M. Roushandeh, Y. Kuwahara, and M. Fukumoto. Neutrophil gelatinase-associated lipocalin: a new antioxidant that exerts its cytoprotective effect independent on Heme Oxygenase-1. *Free Radic Res*, 45(7):810–819, 2011.

[269] B. Roy, R. Taneja, and P. Chambon. Synergistic activation of retinoic acid (RA)-responsive genes and induction of embryonal carcinoma cell differentiation by an RA receptor alpha (RAR alpha)-, RAR beta-, or RAR gamma-selective ligand in combination with a retinoid X receptor-specific ligand. *Mol Cell Biol*, 15(12):6481–6487, 1995.

[270] E. Ruberte, V. Friederich, G. Morriss-Kay, and P. Chambon. Differential distribution patterns of CRABP I and CRABP II transcripts during mouse embryogenesis. *Development*, 115(4):973–987, 1992.

[271] F. X. Ruiz, A. Moro, O. Gallego, A. Ardèvol, C. Rovira, J. M. Petrash, X. Parés, and J. Farrés. Human and rodent aldo-keto reductases from the AKR1B subfamily

and their specificity with retinaldehyde. *Chem Biol Interact*, 191(1-3):199–205, 2011.

[272] J. E. Russo, D. Hauguitz, and J. Hilton. Inhibition of mouse cytosolic aldehyde dehydrogenase by 4-(diethylamino)benzaldehyde. *Biochem Pharmacol*, 37(8):1639–1642, 1988.

[273] Y. Sakai, C. Meno, H. Fujii, J. Nishino, H. Shiratori, Y. Saijoh, J. Rossant, and H. Hamada. The retinoic acid-inactivating enzyme CYP26 is essential for establishing an uneven distribution of retinoic acid along the anterio-posterior axis within the mouse embryo. *Genes Dev*, 15(2):213–225, 2001.

[274] L. L. Sandell, B. W. Sanderson, G. Moiseyev, T. Johnson, A. Mushegian, K. Young, J. P. Rey, J. X. Ma, K. Staehling-Hampton, and P. A. Trainor. RDH10 is essential for synthesis of embryonic retinoic acid and is required for limb, craniofacial, and organ development. *Genes Dev*, 21(9):1113–1124, 2007.

[275] B. P. Sani and D. L. Hill. Retinoic acid: a binding protein in chick embryo metatarsal skin. *Biochem Biophys Res Commun*, 61(4):1276–1282, 1974.

[276] R. Schüle, P. Rangarajan, N. Yang, S. Kliewer, L. J. Ransone, J. Bolado, I. M. Verma, and R. M. Evans. Retinoic acid is a negative regulator of AP-1-responsive genes. *Proc Natl Acad Sci U S A*, 88(14):6092–6096, 1991.

[277] C. K. Schmidt, A. Brouwer, and H. Nau. Chromatographic analysis of endogenous retinoids in tissues and serum. *Anal Biochem*, 315(1):36–48, 2003.

[278] K. M. Schmidt-Ott, K. Mori, J. Y. Li, A. Kalandadze, D. J. Cohen, P. Devarajan, and J. Barasch. Dual action of neutrophil gelatinase-associated lipocalin. *J Am Soc Nephrol*, 18(2):407–413, 2007.

[279] A. Schroeder, O. Mueller, S. Stocker, R. Salowsky, M. Leiber, M. Gassmann, S. Lightfoot, W. Menzel, M. Granzow, and T. Ragg. The RIN: an RNA integrity number for assigning integrity values to RNA measurements. *BMC Mol Biol*, 7:3, 2006.

[280] T. T. Schug, D. C. Berry, N. S. Shaw, S. N. Travis, and N. Noy. Opposing effects of retinoic acid on cell growth result from alternate activation of two different nuclear receptors. *Cell*, 129(4):723–733, 2007.

[281] R. D. Semba. Vitamin A as "anti-infective" therapy, 1920-1940. *J Nutr*, 129(4):783–791, 1999.

[282] N. Shaw, M. Elholm, and N. Noy. Retinoic acid is a high affinity selective ligand for the peroxisome proliferator-activated receptor beta/delta. *J Biol Chem*, 278(43):41589–41592, 2003.

[283] D. J. Shin, D. P. Odom, K. B. Scribner, S. Ghoshal, and M. M. McGrane. Retinoid regulation of the phosphoenolpyruvate carboxykinase gene in liver. *Mol Cell Endocrinol*, 195(1-2):39–54, 2002.

[284] W. C. Smith, H. Nakshatri, P. Leroy, J. Rees, and P. Chambon. A retinoic acid response element is present in the mouse cellular retinol binding protein I (mCRBPI) promoter. *EMBO J*, 10(8):2223–2230, 1991.

[285] A. Sproul, S. L. Steele, T. L. Thai, S. Yu, J. D. Klein, J. M. Sands, and P. D. Bell. N-methyl-D-aspartate receptor subunit NR3a expression and function in principal cells of the collecting duct. *Am J Physiol Renal Physiol*, 301(1):F44–F54, 2011.

[286] J. M. Starkey, Y. Zhao, R. G. Sadygov, S. J. Haidacher, W. S. Lejeune, N. Dey, B. A. Luxon, M. A. Kane, J. L. Napoli, L. Denner, and R. G. Tilton. Altered retinoic acid metabolism in diabetic mouse kidney identified by O isotopic labeling and 2D mass spectrometry. *PLoS One*, 5(6):e11095, 2010.

[287] M. L. Starkey, M. Davies, P. K. Yip, L. M. Carter, D. J. N. Wong, S. B. McMahon, and E. J. Bradbury. Expression of the regeneration-associated protein SPRR1A in primary sensory neurons and spinal cord of the adult mouse following peripheral and central injury. *J Comp Neurol*, 513(1):51–68, 2009.

[288] C. Stehlin-Gaon, D. Willmann, D. Zeyer, S. Sanglier, A. V. Dorsselaer, J. P. Renaud, D. Moras, and R. Schüle. All-trans retinoic acid is a ligand for the orphan nuclear receptor ROR beta. *Nat Struct Biol*, 10(10):820–825, 2003.

[289] H. M. Sucov, K. K. Murakami, and R. M. Evans. Characterization of an autoregulated response element in the mouse retinoic acid receptor type beta gene. *Proc Natl Acad Sci U S A*, 87(14):5392–5396, 1990.

[290] S. Suga, K. Nakao, K. Hosoda, M. Mukoyama, Y. Ogawa, G. Shirakami, H. Arai, Y. Saito, Y. Kambayashi, and K. Inouye. Receptor selectivity of natriuretic peptide family, atrial natriuretic peptide, brain natriuretic peptide, and C-type natriuretic peptide. *Endocrinology*, 130(1):229–239, 1992.

[291] A. Suzuki, T. Ito, E. Imai, M. Yamato, H. Iwatani, H. Kawachi, and M. Hori. Retinoids regulate the repairing process of the podocytes in puromycin aminonucleoside-induced nephrotic rats. *J Am Soc Nephrol*, 14(4):981–991, 2003.

[292] M. Svensson, H. Irjala, C. Svanborg, and G. Godaly. Effects of epithelial and neutrophil CXCR2 on innate immunity and resistance to kidney infection. *Kidney Int*, 74(1):81–90, 2008.

[293] M. Svensson, M. Yadav, B. Holmqvist, N. Lutay, C. Svanborg, and G. Godaly. Acute pyelonephritis and renal scarring are caused by dysfunctional innate immunity in mCxcr2 heterozygous mice. *Kidney Int*, 80(10):1064–1072, 2011.

[294] A. Tahayato, P. Dollé, and M. Petkovich. Cyp26C1 encodes a novel retinoic acid-metabolizing enzyme expressed in the hindbrain, inner ear, first branchial arch and tooth buds during murine development. *Gene Expr Patterns*, 3(4):449–454, 2003.

[295] M. Taimi, C. Helvig, J. Wisniewski, H. Ramshaw, J. White, M. Amad, B. Korczak, and M. Petkovich. A novel human cytochrome P450, CYP26C1, in-

volved in metabolism of 9-cis and all-trans isomers of retinoic acid. *J Biol Chem*, 279(1):77–85, 2004.

[296] S. Takase, D. E. Ong, and F. Chytil. Transfer of retinoic acid from its complex with cellular retinoic acid-binding protein to the nucleus. *Arch Biochem Biophys*, 247(2):328–334, 1986.

[297] K. Tamura, K. Ohsugi, and H. Ide. Distribution of retinoids in the chick limb bud: analysis with monoclonal antibody. *Dev Biol*, 140(1):20–26, 1990.

[298] X. H. Tang and L. J. Gudas. Retinoids, retinoic acid receptors, and cancer. *Annu Rev Pathol*, 6:345–364, 2011.

[299] J. Tesfaigzi and D. M. Carlson. Expression, regulation, and function of the SPR family of proteins. A review. *Cell Biochem Biophys*, 30(2):243–265, 1999.

[300] C. Thaller and G. Eichele. Isolation of 3,4-didehydroretinoic acid, a novel morphogenetic signal in the chick wing bud. *Nature*, 345(6278):815–819, 1990.

[301] C. Thaller, C. Hofmann, and G. Eichele. 9-cis-retinoic acid, a potent inducer of digit pattern duplications in the chick wing bud. *Development*, 118(3):957–965, 1993.

[302] M. Theodosiou, V. Laudet, and M. Schubert. From carrot to clinic: an overview of the retinoic acid signaling pathway. *Cell Mol Life Sci*, 67(9):1423–1445, 2010.

[303] J. F. Thompson, L. S. Hayes, and D. B. Lloyd. Modulation of firefly luciferase stability and impact on studies of gene regulation. *Gene*, 103(2):171–177, 1991.

[304] S. Tomatsu, K. O. Orii, C. Vogler, J. Nakayama, B. Levy, J. H. Grubb, M. A. Gutierrez, S. Shim, S. Yamaguchi, T. Nishioka, A. M. Montano, A. Noguchi, T. Orii, N. Kondo, and W. S. Sly. Mouse model of N-acetylgalactosamine-6-sulfate sulfatase deficiency (Galns-/-) produced by targeted disruption of the gene defective in Morquio A disease. *Hum Mol Genet*, 12(24):3349–3358, 2003.

[305] P. Uawithya, T. Pisitkun, B. E. Ruttenberg, and M. A. Knepper. Transcriptional profiling of native inner medullary collecting duct cells from rat kidney. *Physiol Genomics*, 32(2):229–253, 2008.

[306] M. Uehara, K. Yashiro, S. Mamiya, J. Nishino, P. Chambon, P. Doll*é*, and Y. Sakai. CYP26A1 and CYP26C1 cooperatively regulate anterior-posterior patterning of the developing brain and the production of migratory cranial neural crest cells in the mouse. *Dev Biol*, 302(2):399–411, 2007.

[307] E. C. van Leersum. Vitamin A deficiency and urolithiasis. *Br Med J*, 2(3488):873–874, 1927.

[308] P. Venepally, L. G. Reddy, and B. P. Sani. Analysis of the effects of CRABP I expression on the RA-induced transcription mediated by retinoid receptors. *Biochemistry*, 35(31):9974–9982, 1996.

[309] A. Viau, K. El Karoui, D. Laouari, M. Burtin, C. Nguyen, K. Mori, E. Pillebout, T. Berger, T. W. Mak, B. Knebelmann, G. Friedlander, J. Barasch, and F. Terzi. Lipocalin 2 is essential for chronic kidney disease progression in mice and humans. *J Clin Invest*, 120(11):4065–4076, 2010.

[310] J. Vilar, T. Gilbert, E. Moreau, and C. Merlet-B*é*nichou. Metanephros organogenesis is highly stimulated by vitamin A derivatives in organ culture. *Kidney Int*, 49(5):1478–1487, 1996.

[311] J. Vilar, C. Lalou, V. H. Duong, S. Charrin, S. Hardouin, D. Raulais, C. Merlet-B*é*nichou, and M. Leli*è*vre-P*é*gorier. Midkine is involved in kidney development and in its regulation by retinoids. *J Am Soc Nephrol*, 13(3):668–676, 2002.

[312] S. Vogel, C. L. Mendelsohn, J. R. Mertz, R. Piantedosi, C. Waldburger, M. E. Gottesman, and W. S. Blaner. Characterization of a new member of the fatty acid-binding protein family that binds all-trans-retinol. *J Biol Chem*, 276(2):1353–1360, 2001.

[313] S. Vogel, R. Piantedosi, S. M. O'Byrne, Y. Kako, L. Quadro, M. E. Gottesman, I. J. Goldberg, and W. S. Blaner. Retinol-binding protein-deficient mice: biochemical basis for impaired vision. *Biochemistry*, 41(51):15360–15368, 2002.

[314] G. Wald and R. Hubbard. The synthesis of rhodopsin from vitamin A(1). *Proc Natl Acad Sci U S A*, 36(2):92–102, 1950.

[315] D. P. Wallace, M. Christensen, G. Reif, F. Belibi, B. Thrasher, D. Herrell, and J. J. Grantham. Electrolyte and fluid secretion by cultured human inner medullary collecting duct cells. *Am J Physiol Renal Physiol*, 283(6):F1337–F1350, 2002.

[316] K. Webb, Jr, G. Mitchell, Jr, C. O. Little, and G. H. Schmitt. Polyuria in vitamin A-deficient sheep. *J Anim Sci*, 27(6):1657–1662, 1968.

[317] S. Westin, R. Kurokawa, R. T. Nolte, G. B. Wisely, E. M. McInerney, D. W. Rose, M. V. Milburn, M. G. Rosenfeld, and C. K. Glass. Interactions controlling the assembly of nuclear-receptor heterodimers and co-activators. *Nature*, 395(6698):199–202, 1998.

[318] T. Wex, A. Lipyansky, N. C. Brömme, H. Wex, X. Q. Guan, and D. Brömme. TIN-ag-RP, a novel catalytically inactive cathepsin B-related protein with EGF domains, is predominantly expressed in vascular smooth muscle cells. *Biochemistry*, 40(5):1350–1357, 2001.

[319] J. A. White, B. Beckett, S. W. Scherer, J. A. Herbrick, and M. Petkovich. P450RAI (CYP26A1) maps to human chromosome 10q23-q24 and mouse chromosome 19C2-3. *Genomics*, 48(2):270–272, 1998.

[320] J. A. White, B. Beckett-Jones, Y. D. Guo, F. J. Dilworth, J. Bonasoro, G. Jones, and M. Petkovich. cDNA cloning of human retinoic acid-metabolizing enzyme (hP450RAI) identifies a novel family of cytochromes P450. *J Biol Chem*, 272(30):18538–18541, 1997.

[321] J. A. White, H. Ramshaw, M. Taimi, W. Stangle, A. Zhang, S. Everingham, S. Creighton, S. P. Tam, G. Jones, and M. Petkovich. Identification of the hu-

man cytochrome P450, P450RAI-2, which is predominantly expressed in the adult cerebellum and is responsible for all-trans-retinoic acid metabolism. *Proc Natl Acad Sci U S A*, 97(12):6403–6408, 2000.

[322] J. G. Wilson, C. B. Roth, and J. Warkany. An analysis of the syndrome of malformations induced by maternal vitamin A deficiency. Effects of restoration of vitamin A at various times during gestation. *Am J Anat*, 92(2):189–217, 1953.

[323] J. G. Wilson and J. Warkany. Malformations in the genito-urinary tract induced by maternal vitamin A deficiency in the rat. *Am J Anat*, 83(3):357–407, 1948.

[324] C. G. Woelfel, R. Hall, Jr, M. C. Calhoun, J. Rousseau, Jr, H. D. Eaton, S. W. Nielsen, E. J. Kersting, and J. J. Lucas. Volume and osmolality of urine of hypovitaminotic A holstein heifers. *J Dairy Sci*, 48(10):1346–1352, 1965.

[325] S. B. Wolbach and P. R. Howe. Tissue changes following deprivation of fat-soluble A vitamin. *J Exp Med*, 42(6):753–777, 1925.

[326] J. Wolfe and H. Salter. Vitamin A deficiency in the albino mouse. *J Nutr*, 4:185–192, 1931.

[327] Y. F. Wong, J. B. Kopp, C. Roberts, P. J. Scambler, Y. Abe, A. C. Rankin, N. Dutt, B. M. Hendry, and Q. Xu. Endogenous retinoic acid activity in principal cells and intercalated cells of mouse collecting duct system. *PLoS One*, 6(2):e16770, 2011.

[328] Q. Xu, B. M. Hendry, M. Maden, H. Lu, Y. F. Wong, A. C. Rankin, M. Noor, and J. B. Kopp. Kidneys of Alb/TGF-beta(1) transgenic mice are deficient in retinoic acid and exogenous retinoic acid shows dose-dependent toxicity. *Nephron Exp Nephrol*, 114(4):e127–e132, 2010.

[329] Q. Xu, J. Lucio-Cazana, M. Kitamura, X. Ruan, L. G. Fine, and J. T. Norman. Retinoids in nephrology: promises and pitfalls. *Kidney Int*, 66(6):2119–2131, 2004.

[330] H. Yang, K. Chen, X. Zhang, L. Wang, C. Li, H. Tao, and Q. Li. Vitamin A deficiency results in dysregulation of lipid efflux pathway in rat kidney. *Pediatr Nephrol*, 25:1435–1444, 2010.

[331] K. Yashiro, X. Zhao, M. Uehara, K. Yamashita, M. Nishijima, J. Nishino, Y. Saijoh, Y. Sakai, and H. Hamada. Regulation of retinoic acid distribution is required for proximodistal patterning and outgrowth of the developing mouse limb. *Dev Cell*, 6(3):411–422, 2004.

[332] J. Yu, T. J. Carroll, J. Rajagopal, A. Kobayashi, Q. Ren, and A. P. McMahon. A Wnt7b-dependent pathway regulates the orientation of epithelial cell division and establishes the cortico-medullary axis of the mammalian kidney. *Development*, 136(1):161–171, 2009.

[333] V. C. Yu, C. Delsert, B. Andersen, J. M. Holloway, O. V. Devary, A. M. N*ää*r, S. Y. Kim, J. M. Boutin, C. K. Glass, and M. G. Rosenfeld. RXR beta: a coregulator that enhances binding of retinoic acid, thyroid hormone, and vitamin D receptors to their cognate response elements. *Cell*, 67(6):1251–1266, 1991.

[334] M. Zeisberg, J. Hanai, H. Sugimoto, T. Mammoto, D. Charytan, F. Strutz, and R. Kalluri. BMP-7 counteracts TGF-beta1-induced epithelial-to-mesenchymal transition and reverses chronic renal injury. *Nat Med*, 9(7):964–968, 2003.

[335] M. Zhang, W. Chen, S. M. Smith, and J. L. Napoli. Molecular characterization of a mouse short chain dehydrogenase/reductase active with all-trans-retinol in intact cells, mRDH1. *J Biol Chem*, 276(47):44083–44090, 2001.

[336] M. Zhang, P. Hu, C. R. Krois, M. A. Kane, and J. L. Napoli. Altered vitamin A homeostasis and increased size and adiposity in the rdh1-null mouse. *FASEB J*, 21(11):2886–2896, 2007.

[337] X. Zhang, F. Tan, Y. Zhang, and R. A. Skidgel. Carboxypeptidase M and kinin B1 receptors interact to facilitate efficient B1 signaling from B2 agonists. *J Biol Chem*, 283(12):7994–8004, 2008.

[338] Y. Zhang, R. Zolfaghari, and A. C. Ross. Multiple retinoic acid response elements cooperate to enhance the inducibility of CYP26A1 gene expression in liver. *Gene*, 464(1-2):32–43, 2010.

[339] D. Zhao, P. McCaffery, K. J. Ivins, R. L. Neve, P. Hogan, W. W. Chin, and U. C. Dr*ä*ger. Molecular identification of a major retinoic-acid-synthesizing enzyme, a retinaldehyde-specific dehydrogenase. *Eur J Biochem*, 240(1):15–22, 1996.

[340] L. Zheng, Z. Zhou, L. Lin, S. Alber, S. Watkins, N. Kaminski, A. M. K. Choi, and D. Morse. Carbon monoxide modulates alpha-smooth muscle actin and small proline rich-1a expression in fibrosis. *Am J Respir Cell Mol Biol*, 41(1):85–92, 2009.

[341] H. R. Zhou, M. M. Abouzied, and M. H. Zile. Production of a hybridoma cell line secreting retinoic acid-specific monoclonal antibody. *J Immunol Methods*, 138(2):211–223, 1991.

[342] M. Zile, H. F. DeLuca, and H. Ahrens. Vitamin A deficiency and urinary calcium excretion in rats. *J Nutr*, 102(10):1255–1258, 1972.

[343] M. H. Zile, R. J. Emerick, and H. F. DeLuca. Identification of 13-cis retinoic acid in tissue extracts and its biological activity in rats. *Biochim Biophys Acta*, 141(3):639–641, 1967.

[344] C. F. Zizola, G. J. Schwartz, and S. Vogel. Cellular retinol-binding protein type III is a PPARgamma target gene and plays a role in lipid metabolism. *Am J Physiol Endocrinol Metab*, 295(6):E1358–E1368, 2008.